

HIGH BY-PASS RATIO TURBOFAN ENGINES AEROTHERMODYNAMIC  
DESIGN AND OPTIMIZATION

A THESIS SUBMITTED TO  
THE GRADUATE SCHOOL OF NATURAL AND APPLIED SCIENCES  
OF  
MIDDLE EAST TECHNICAL UNIVERSITY

BY

SELÇUK CAN UYSAL

IN PARTIAL FULLFILMENT OF THE REQUIREMENTS  
FOR  
THE DEGREE OF MASTER OF SCIENCE  
IN  
AEROSPACE ENGINEERING

FEBRUARY 2014



Approval of the thesis:

**HIGH BY-PASS RATIO TURBOFAN ENGINES AEROTHERMODYNAMIC DESIGN  
AND OPTIMIZATION**

Submitted by **SELÇUK CAN UYSAL** in partial fulfillment of the requirements for the degree of **Master of Science in Aerospace Engineering Department, Middle East Technical University** by,

Prof. Dr. Canan Özgen

\_\_\_\_\_

Dean, **Graduate School of Natural and Applied Sciences**

Prof. Dr. Ozan Tekinalp

\_\_\_\_\_

Head of Department, **Aerospace Engineering**

Prof. Dr. İ. Sinan Akmandor

\_\_\_\_\_

Supervisor, **Aerospace Engineering Department, METU**

**Examining Committee Members:**

Assoc. Prof. Dr. Sinan Eyi

\_\_\_\_\_

Aerospace Engineering Dept., METU

Prof. Dr. İ. Sinan Akmandor

\_\_\_\_\_

Aerospace Engineering Dept., METU

Assoc. Prof. Dr. Oğuz Uzol

\_\_\_\_\_

Aerospace Engineering Dept., METU

Assoc. Prof. Dr. Dilek Funda Kurtuluş

\_\_\_\_\_

Aerospace Engineering Dept., METU

Asst. Prof. Dr. Sıtkı Uslu

\_\_\_\_\_

Mechanical Engineering Dept., TOBB University

Date: 07.02.2014

**I hereby declare that all information in this document has been obtained and presented in accordance with academic rules and ethical conduct. I also declare that, as required by these rules and conduct, I have fully cited and referenced all material and results that are not original to this work.**

Name, Last Name: Selçuk Can Uysal

Signature:

## **ABSTRACT**

# **HIGH BY-PASS TURBOFAN ENGINES AEROTHERMODYNAMIC DESIGN AND OPTIMIZATION**

Uysal, Selçuk Can

MSc. Department of Aerospace Engineering

Supervisor: Prof.Dr. İ. Sinan Akmandor

February 2014, 224 pages

The first step in Engine Design for an airframe is being the on-design cycle analysis. The results of this analysis are later used in off-design cycle analysis, which gives critical information about the performance of the engine on the whole flight envelope. Both analysis results are later used in turbomachinery component design. In order to accomplish these objectives, an engine design model in MATLAB Simulink® (named as Engine Design Model, EDM) is developed for Separate Flow Turbofan Engines. This engine type is chosen according to its wide usage in Aerospace Industry, but the model can also be extended to the other types of Turbofan and Turbojet Engines. The Engine Design Model uses Variable Specific Heat Model in order to obtain best estimates in thermodynamic parameters throughout the whole cycle. The model use the solution algorithms given in Aircraft Engine Design, 2<sup>nd</sup> Edition [Mattingly, J.D., Heiser W.H., and Pratt, D.T., 2002] for cycle analysis and its verification is made with AEDsys Software, which also uses the same algorithm. The model also includes an aerothermodynamic turbomachinery design section, which uses the outputs from the cycle analysis and its validation is made with engine data of CFM56-5A and GE90-94B engines. The model is then used in an optimization process, which select the best engine according to the constraints determined by the user by using SIMPLEX and gradient descent algorithms.

Keywords: Turbofan Engine Design, Aerothermodynamic Engine Design, On-Design Cycle, Off-Design Cycle, Aerothermodynamic Turbomachinery Design, Optimization in Engine Design

## ÖZ

# YÜKSEK BY-PASS ORANLI TURBOFAN MOTORLARININ AEROTERMODİNAMİK TASARIMI VE OPTİMİZASYONU

Uysal, Selçuk Can

Yüksek Lisans, Havacılık ve Uzay Mühendisliği Bölümü

Tez Yöneticisi: Prof. Dr. İ. Sinan Akmandor

Şubat 2014, 224 Sayfa

Uçak Motoru tasarımındaki ilk adım parametrik döngü analizleridir. Bu analizin sonuçları daha sonra bir uçak motorunun tüm uçuş zarfı boyunca göstereceği performans hakkında bilgi sağlayacak olan performans döngüsü analizlerinde kullanılır. Her iki analiz sonucu en son aşamada turbo makine bileşenleri ön tasarımında kullanılır. Belirtilen bu analizleri gerçekleştirmek amacıyla MATLAB Simulink® kullanılarak ayrı akışlı turbofan motorları için bir motor tasarım aracı (Engine Design Model, EDM olarak isimlendirilmiştir) geliştirilmiştir. Tasarım aracında kullanılan bu motor türü havacılık sanayiindeki yaygın kullanımı nedeniyle seçilmiştir, ancak farklı turbofan ve turbojet motor yapılandırmaları içinde ilgili değişiklikler yapılarak kullanılabilir. EDM aracı hesaplamalarında termodinamik parametrelerin en doğru şekilde kullanılabilmesi için Değişken Özgül Isı modeli kullanılmaktadır. EDM parametrik ve performans döngü analizlerinde Aircraft Engine Design, 2. Baskı [Mattingly, J.D., Heiser W.H., ve Pratt, D.T., 2002] kaynağında verilmiş olan çözüm algoritmalarını kullanmaktadır. Modelin bu bölümlerinin doğrulaması yine aynı kaynak tarafından geliştirilmiş olan AEDsys yazılımı ile yapılmıştır. Model aynı zamanda parametrik döngü sonuçlarını kullanan aerotermodinamik turbo makine bileşen tasarımı bölümü de içermektedir. Modelin bu

bölümünün doğrulaması CFM56-5A ve GE90-94B motorlarına ait gerçek verilerle yapılmıştır. Model doğrulandıktan sonra kullanıcı tarafından belirtilen isteklere göre en iyi motorun seçimini sağlayacak olan bir optimizasyon sürecine sokulmuş ve optimizasyonda SIMPLEX ve Gradient Descent algoritmaları ile çözüm alınmıştır.

Anahtar Kelimeler: Turbofan Motor Tasarımı, Aerotermodinamik Motor Tasarımı, Parametrik Döngü Analizi, Performans Döngü Analizi, Aerotermodinamik Turbomakina Tasarımı, Motor Tasarımında Optimizasyon



## TABLE OF CONTENTS

ABSTRACT.....	iv
ÖZ.....	vi
LIST OF TABLES.....	xi
LIST OF FIGURES.....	xiii
1. INTRODUCTION.....	1
1.1. Jet Engine Development in History.....	1
1.2. Aircraft Engine Design Process .....	3
1.3. Aerothermodynamic Design Tools and the Intention of Developing the Engine DesignModel.....	6
2. LITERATURE REVIEW .....	9
2.1. Parametric Cycle (On-Design) Theory.....	9
2.1.1 Design Tools .....	10
2.1.2 Engine Station Numbering.....	10
2.1.3 Gas Model.....	12
2.1.4 Total Property Ratios of Components.....	12
2.1.5 Mass Flow Rates .....	15
2.1.6 Component Efficiencies .....	17
2.1.7 Parametric Cycle (On-Design) Analysis.....	19
2.2. Performance Cycle (Off-Design) Theory.....	23
2.2.1 Design Tools.....	23
2.2.2 The Mass Flow Parameter .....	25
2.2.3 Performance of Turbines with Coolant Mixers .....	26
2.3. Rotating Component Design Theory.....	32
2.3.1 Fan and Compressor Aerodynamics .....	32
2.3.2 Turbine Aerodynamics.....	43
2.3.3 Structural Considerations .....	52

2.4.	Methodology.....	56
2.4.1	Variable Specific Heat Model .....	56
2.4.2	An Iterative Solution Scheme for Performance Cycle .....	57
2.4.3	Key Points in a Turbomachinery Design Algorithm.....	60
3.	NEW ANALYTICAL TOOLS DEVELOPED FOR HIGH BY-PASS TURBOFAN ENGINES .....	67
3.1	Variable Specific Heat Model and the Flow Property Calculations.....	71
3.1.1	Variable Specific Heat Model .....	71
3.1.2	Flow Property Calculations .....	75
3.2	Parametric Cycle Model .....	78
3.2.1	Inlet .....	82
3.2.2	Diffuser .....	83
3.2.3	Fan.....	84
3.2.4	Low Pressure Compressor .....	85
3.2.5	High Pressure Compressor.....	86
3.2.6	Combustor.....	87
3.2.7	Coolant Mixer 1 .....	89
3.2.8	High Pressure Turbine .....	90
3.2.9	Coolant Mixer 2 .....	91
3.2.10	Low Pressure Turbine .....	92
3.2.11	Primary Exhaust.....	94
3.2.12	Secondary Exhaust.....	95
3.2.13	Final Calculations .....	97
3.3	Performance Cycle Model.....	98
3.3.1	Inlet.....	102
3.3.2	Diffuser.....	102
3.3.3	Initializer .....	103
3.3.4	Pre-Calculations .....	104
3.3.5	Design Loops.....	105
3.4	Turbomachinery Design Model.....	120
3.4.6	Low Pressure Spool.....	123

3.4.7	High Pressure Spool.....	131
4.	VALIDATION .....	141
4.1	Parametric Cycle Model.....	141
4.1.1	Case Specific Tests .....	141
4.1.2	Continuity Tests .....	150
4.2	Performance Cycle Model.....	153
4.2.1	Case Specific Tests .....	154
4.2.2	Continuity Tests .....	162
4.3	Turbomachinery Design Model.....	165
4.3.1	CFM 56-5A Engine.....	165
4.3.2	GE90-94B Engine .....	171
5.	OPTIMIZATION .....	177
5.1	Introduction .....	177
5.2	Optimization Algorithms.....	180
5.2.1	Unconstrained Optimization .....	181
5.2.2	Constrained Optimization .....	183
5.3	Using Optimization in Engine Design.....	184
5.4	Results of an Example Optimization Problem with EDM .....	186
5.4.1	Results of Case 1 .....	189
5.4.2	Results of Case 2.....	193
5.4.3	Results of Case 3.....	196
5.4.4	Results of Case 4.....	199
6.	CONCLUSION AND FUTURE WORK.....	203
	BIBLIOGRAPHY .....	205
	APPENDICES .....	209
	APPENDIX A .....	209
	APPENDIX B.....	213

## LIST OF TABLES

### TABLES

Table 1 Engine Station Numbering and their relevant locations on the real engine .....	12
Table 2 Subscripts used to define engine stations .....	13
Table 3 Subscripts used to define mass flow rates .....	15
Table 4 Engine Performance Variables .....	24
Table 5 The constants for kerosene and air mixture .....	57
Table 6 The list of input parameters for EDM .....	69
Table 7 The list of output parameters of EDM .....	70
Table 8 The list of on-design input parameters for the tests with Mid By-Pass Ratio Generic Engine .....	142
Table 9 On-Design result comparison for Mid By-Pass Ratio Generic Engine .....	143
Table 10 The list of on-design input parameters for the tests with CFM56-5A Engine .....	144
Table 11 On-Design result comparison for CFM56-5A Engine .....	145
Table 12 The list of on-design input parameters for the tests with GE90-94B Engine .....	147
Table 13 On-Design result comparison for GE90-94B Engine .....	149
Table 14 The list of off-design input parameters for the tests with Mid By-Pass Ratio generic engine .....	154
Table 15 Off-Design result comparison for Mid By-Pass Ratio Generic Engine .....	155
Table 16 The list of off-design input parameters for the tests with CFM56-5A Engine .....	157
Table 17 Off-Design result comparison for CFM56-5A Engine .....	157
Table 18 The list of off-design input parameters for the tests with GE90-94B Engine .....	160
Table 19 Off-Design result comparison for GE90-94B Engine .....	160
Table 20 Optimization Example Cases, the active constraints are shown with green and inactive ones are shown with red .....	187
Table 21 Design Variable limits defined for constrained optimization algorithms .....	188
Table 22 Signal constraint values on output parameters .....	188
Table 23 The changes in design variables for each optimization run .....	189
Table 24 The results obtained at each run .....	190
Table 25 The changes in design variables for each optimization run .....	191
Table 26 The results obtained at each run .....	191
Table 27 The changes in design variables for each optimization run .....	192
Table 28 The results obtained at each run .....	192

Table 29 The changes in design variables for each optimization run ..... 193

Table 30 The results obtained at each run..... 193

Table 31 The changes in design variables for each optimization run ..... 194

Table 32 The results obtained at each run..... 194

Table 33 The changes in design variables for each optimization run ..... 195

Table 34 The results obtained at each run..... 195

Table 35 The changes in design variables for each optimization run ..... 196

Table 36 The results obtained at each run..... 196

Table 37 The changes in design variables for each optimization run ..... 197

Table 38 The results obtained at each run..... 197

Table 39 The changes in design variables for each optimization run ..... 198

Table 40 The results obtained at each run..... 198

Table 41 The changes in design variables for each optimization run ..... 199

Table 42 The results obtained at each run..... 200

Table 43 The changes in design variables for each optimization run ..... 200

Table 44 The results obtained at each run..... 201

Table 45 The changes in design variables for each optimization run ..... 201

Table 46 The results obtained at each run..... 202

## LIST OF FIGURES

### FIGURES

Figure 1 Gas Turbine engine design roadmap given by Mattingly J.D. [3].....	4
Figure 2 Preliminary Propulsion Design Sequence by Mattingly J.D. [3].....	5
Figure 3 Low Pressure Turbine disk design roadmap for GE90-115B engine; the method involves FEM and CFD methods that are used iteratively.....	6
Figure 4 Engine Station Numbering shown on a mixed-flow turbofan engine [3].....	11
Figure 5 Airflow paths and the spool designations .....	11
Figure 6 Air and fuel mass flow shown for core engine .....	17
Figure 7 Compressor Stage Nomenclature and angle relations from [3] .....	33
Figure 8 The nomenclature and angular relations given for the airfoil design step in [3] .....	40
Figure 9 Throughflow annulus dimensions for mean-line compressor design [3] .....	41
Figure 10 Typical turbine stage [3] .....	44
Figure 11 The nomenclature used for turbomachinery rotors [3] .....	52
Figure 12 The forces and stresses acting on a rotor airfoil [3].....	53
Figure 13 Disk thickness distributions for different DSF values [3] .....	55
Figure 14 Iterative Solution scheme for high by-pass turbofan engines.....	59
Figure 15 Trends in stage pressure ratio with rotor inlet angle with the variation of inlet Mach number, rotor speed, diffusion factor and solidity .....	61
Figure 16 The trend variation of stage temperature ratio, rotor flow turning angle, rotor degree of reaction and stage exit flow angle with $\alpha_2$ .....	64
Figure 17 The Engine Design Model overview in Simulink Model Window .....	67
Figure 18 The F-AIR1 sub-model for thermodynamic property calculations .....	71
Figure 19 The interior view of the F-AIR1 sub-model .....	72
Figure 20 The F-AIR2 sub-model for thermodynamic property calculations .....	73
Figure 21 The interior view of the F-AIR2 sub-model .....	73
Figure 22 The F-AIR3 sub-model for thermodynamic property calculations .....	74
Figure 23 The interior view of the F-AIR3 sub-model .....	75
Figure 24 The RGCOMPR1 sub-model for the calculation of flow properties .....	76
Figure 25 The interior view of the RGCOMPR1 sub-model .....	77

Figure 26 The RGCOMPR3 sub-model for the calculation of flow properties .....	77
Figure 27 The interior view of the RGCOMPR3 sub-model, the while loop which determines the output parameters is highlighted.....	78
Figure 28 Parametric Cycle Model in the Engine Design Model .....	78
Figure 29 A summarized view of the Parametric Cycle Model.....	79
Figure 30 The interior view of Parametric Cycle Model .....	81
Figure 31 Inlet sub-model for the inlet/diffuser entry cycle calculations .....	82
Figure 32 Interior view of Inlet sub-model .....	83
Figure 33 Diffuser sub-model for the diffuser cycle calculations.....	83
Figure 34 Interior view of Diffuser sub-model .....	84
Figure 35 Fan sub-model for the fan cycle calculations .....	84
Figure 36 Interior view of Fan sub-model .....	85
Figure 37 Low Pressure Compressor sub-model for the Low Pressure Compressor cycle calculations.....	85
Figure 38 Interior view of Low Pressure Compressor sub-model .....	86
Figure 39 High Pressure Compressor sub-model for the High Pressure Compressor cycle calculations.....	87
Figure 40 Interior view of High Pressure Compressor sub-model .....	87
Figure 41 Combustor sub-model for the Combustor cycle calculations.....	88
Figure 42 Interior view of Combustor sub-model.....	88
Figure 43 Coolant Mixer 1 sub-model for the Coolant Mixer 1 cycle calculations .....	89
Figure 44 Interior view of Coolant Mixer 1 sub-model.....	89
Figure 45 High Pressure Turbine sub-model for the High Pressure Turbine cycle calculations.....	90
Figure 46 Interior view of High Pressure Turbine sub-model .....	91
Figure 47 Coolant Mixer 2 sub-model for the Coolant Mixer 2 cycle calculations .....	91
Figure 48 Interior view of Coolant Mixer 2 sub-model.....	92
Figure 49 Low Pressure Turbine sub-model for the Low Pressure Turbine cycle calculations.....	93
Figure 50 Interior view of Low Pressure Turbine sub-model.....	93
Figure 51 Primary Exhaust sub-model for the Primary Exhaust cycle calculations.....	94
Figure 52 Interior view of Primary Exhaust sub-model.....	95
Figure 53 Secondary Exhaust sub-model for the Secondary Exhaust cycle calculations	96
Figure 54 Interior view of Secondary Exhaust sub-model.....	97
Figure 55 Final Calculations sub-model for the on-design cycle calculations .....	98
Figure 56 Interior view of Final Calculations sub-model .....	98
Figure 57 Performance Cycle Model in the Engine Design Model .....	99
Figure 58 A summarized view of the Performance Cycle Model.....	100
Figure 59 The interior view of Performance Cycle Model .....	101
Figure 60 Inlet sub-model for the inlet/diffuser entry off-design calculations .....	102

Figure 61 Diffuser sub-model for the diffuser calculations for off-design .....	103
Figure 62 Initializer sub-model for the initialization of off-design parameters .....	103
Figure 63 The interior view of Initializer sub-model .....	104
Figure 64 Pre-Calculations sub-model for the off-design initial calculations .....	104
Figure 65 The interior view of the Pre-Calculations sub-model .....	105
Figure 66 Design Loops sub-model that includes the Performance Cycle Loops .....	106
Figure 67 Alfa Loop sub-model that perform by-pass ratio calculations .....	107
Figure 68 Interior view of the Alfa Loop sub-model .....	109
Figure 69 TURB sub-model in the Alfa Loop of Performance Cycle Model .....	111
Figure 70 The interior view of the TURB sub-model .....	112
Figure 71 TURBC sub-model in the Alfa Loop of Performance Cycle Model .....	113
Figure 72 The interior view of the TURB sub-model .....	113
Figure 73 <b>m0</b> Loop sub-model that perform mass flow rate and $M_9$ calculations .....	115
Figure 74 Interior view of <b>m0</b> Loop .....	116
Figure 75 Control Loop for the off-design output calculations .....	118
Figure 76 Interior view of the Control Loop .....	119
Figure 77 Turbomachinery Design Model in the Engine Design Model .....	120
Figure 78 A summarized view of the Turbomachinery Design Model .....	122
Figure 79 Interior view of the Turbomachinery Design Model .....	123
Figure 80 Interior view of the Low Pressure Spool .....	124
Figure 81 Model including the Low Pressure Compressor subroutine .....	125
Figure 82 Design algorithm in the Low Pressure Compressor subroutine .....	127
Figure 83 Model including the Low Pressure Turbine subroutine .....	128
Figure 84 Design algorithm in the Low Pressure Turbine subroutine .....	129
Figure 85 Interior view of the High Pressure Spool .....	132
Figure 86 Model including the High Pressure Turbine subroutine .....	133
Figure 87 Design algorithm in the High Pressure Turbine subroutine .....	134
Figure 88 Model including the High Pressure Compressor subroutine .....	137
Figure 89 Design algorithm in the High Pressure Compressor subroutine .....	139
Figure 90 Variation of On-Design Specific Thrust and Thrust Specific Fuel Consumption with respect to By-Pass ratio compared for Engine Design Model (EDM) and AEDsys program (ONX) .....	151
Figure 91 Variation of On-Design Specific Thrust and Thrust Specific Fuel Consumption with respect to High Pressure Compressor pressure ratio compared for Engine Design Model (EDM) and AEDsys program (ONX) .....	152
Figure 92 Variation of On-Design Specific Thrust and Thrust Specific Fuel Consumption with respect to High Pressure Turbine Inlet Temperature compared for Engine Design Model (EDM) and AEDsys program (ONX) .....	153



Figure 93 Variation of Off-Design Mass Flow Rate prediction with respect to flight Mach number compared for Engine Design Model (EDM) and AEDsys program (OFFX).....	162
Figure 94 Variation of Off-Design By-Pass ratio prediction with respect to flight Mach number compared for Engine Design Model (EDM) and AEDsys program (OFFX)...	163
Figure 95 Variation of Specific Thrust with respect to flight Mach number compared for Engine Design Model (EDM) and AEDsys program (OFFX).....	164
Figure 96 Variation of Thrust Specific Fuel Consumption with respect to flight Mach number compared for Engine Design Model (EDM) and AEDsys program (OFFX)...	164
Figure 97 Low Pressure Compressor and Fan dimensional comparison .....	166
Figure 98 High Pressure Compressor dimensional comparison .....	167
Figure 99 High Pressure Turbine dimensional comparison.....	168
Figure 100 Low Pressure Turbine dimensional comparison.....	169
Figure 101 The blade heights are given on the engine map for CFM56-5A Engine .....	170
Figure 102 The wheel speed at mean-line comparison is given for CFM56-5A Engine .....	170
Figure 103 Low Pressure Compressor and Fan dimensional comparison .....	171
Figure 104 High Pressure Compressor dimensional comparison .....	172
Figure 105 High Pressure Turbine dimensional comparison.....	173
Figure 106 Low Pressure Turbine dimensional comparison.....	174
Figure 107 The blade heights are given on the engine map for GE90-94B Engine .....	175
Figure 108 The wheel speed at mean-line comparison is given for GE90-94B Engine	175
Figure 109 The location of the optimization algorithm in a mathematical problem .....	178
Figure 110 The feasible region definition.....	179
Figure 111 The process of direct search method to find the optimum solution $x^*$ .....	181
Figure B 1 The change of design variables with iterations for Case 1 (Gradient Descent Active Set).....	213
Figure B 2 The change of design variables with iterations for Case 1 (Gradient Descent Trust Region Reflective).....	214
Figure B 3 The change of design variables with iterations for Case 1 (SIMPLEX).....	215
Figure B 4 The change of design variables with iterations for Case 2 (Gradient Descent Active Set).....	216
Figure B 5 The change of design variables with iterations for Case 2 (Gradient Descent Trust Region Reflective).....	217
Figure B 6 The change of design variables with iterations for Case 2 (SIMPLEX).....	218
Figure B 7 The change of design variables with iterations for Case 3 (Gradient Descent Active Set).....	219

Figure B 8 The change of design variables with iterations for Case 3 (Gradient Descent Trust Region Reflective) ..... 220  
Figure B 9 The change of design variables with iterations for Case 3 (SIMPLEX)..... 221  
Figure B 10 The change of design variables with iterations for Case 4 (Gradient Descent Active Set)..... 222  
Figure B 11 The change of design variables with iterations for Case 4 (Gradient Descent Trust Region Reflective) ..... 223  
Figure B 12 The change of design variables with iterations for Case 4 (SIMPLEX)... 224

## CHAPTER 1

### INTRODUCTION

#### 1.1. Jet Engine Development in History

From the first flight of Wright Brothers in 1903, until the end of Second World War the common type of engine that powered the flight was the piston-propeller engine. This engine type was a natural starting point because of its resemblance to the ones used by the automobile industry. After the attainment to the performance limit of propeller engines in the late 1930s by the industry, jet propulsion came into life because it had the potential of reaching greater flight speeds. In 1950s, jet engine powered aircrafts were available to transgress the sonic speed. At the end of 1950s, commercial applications of turbojet engines were started with Comet, Caravelle and Boeing 707 (von Ohain [1]). Due to their high fuel consumption and noise emissions turbojet engines were replaced with turbofan engines in the late 1960s (Bräunling W.J.G. [2]). With the introduction of high by-pass turbofan engines, wide body aircraft types came into existence because of the higher fuel efficiency and reliability provided by this new type of engine.

The idea of airbreathing jet engines was born through several patents by Lorin and M. Guillaume in the beginning of the 20<sup>th</sup> century. However, these were never implemented. In 1903, Ægidius Elling patented the gas turbine idea (Patent Number 1766886) and produced a prototype in Norway which produced 11hp power. In 1930, Sir Frank Whittle from United Kingdom also patented the turbojet engine idea and was able to produce a prototype engine in 1937 at the Power Jets Ltd. Company. The bench tests of the engines were so successful that the British Air Ministry started right away a development program of an experimental aircraft (Gloster E28/29) that would use this

type of engine. After the satisfactory demonstration tests with W1X engine, several British aircraft engine corporations and specifically Rolls-Royce started to develop turbojet engines. During the demonstrations with aircrafts powered with turbojet engines, US Army also found this new type of engine promising and decided that related technology should be immediately transferred to USA. Through a special agreement between the US Secretary of War and British Air Commission General Electric from USA produced a similar engine named as GE 1-A (W2B). The by-pass turbofan engine idea was also patented by Sir Frank Whittle during the research for reducing the fuel consumption of recent turbojets. (Patent Number 2404334)

Around the same decades in the development of turbojet engines in United Kingdom, early turbojet type engine developments were running in Germany by von Ohain. The research was carried on by a special team in Ernst Heinkel Flugzeugwerke AG (Heinkel). The prototype turbojet engine, which was produced in 1937, was used Hydrogen as fuel together with radial turbomachinery component. After completing the bench tests and reaching an equivalent horsepower per square-meter of  $1000 \text{ hp/m}^2$ , flight test engine were decided to be built by the same company for the prototype aircraft He-178. The prototype engine was reshaped to fit into the aircraft and named as He.S3. In 1939, He-178 aircraft had the first flight, which is also being the first turbojet powered aircraft flight in the world. Due to the success and the high speed level reached by this aircraft, German aircraft engine companies Junkers and BMW made a cooperation with Heinkel and developed more advanced turbojet engines (Jumo004B and BMW003) which are using axial flow compressors and turbines. Jumo004B engine was used in a more advanced German fighter aircraft, He-162, and the developments in turbojet engines continued until the end of the Second World War. (Von Ohain [1])

According to von Ohain [1], from this early development stages up to today's technology level the following advancements in engine technology played a major role:

- Research on combustion processes, increasing the specific mass flow through combustors and reducing the pressure drop and reaching nearly 99% combustion efficiency

- Minimization of the excitations coming from vibrations and associated fatigue phenomenon
- Improvement of the structural design and structural materials
- Increasing the turbine temperature capability by improving air cooling effectiveness, and increasing the turbine polytropic efficiency
- Advanced controllable thrust nozzles and their interactions with the aircraft
- Advancements in control systems

During the researches on increasing the overall efficiency of the early turbojets, it was found out that there was a direct connection of performance and efficiency with increase in compressor pressure ratio. Because of this fact, the overall compressor pressure ratio of turbojet and turbofan engines was continuously increased from 1930s up to-date. By the introduction of variable stator blades it was possible to reach higher compression ratios while reducing flow instabilities. With the increased stage pressure loadings, the engine lengths, frontal areas and weight per power output were reduced. Continuous improvements in turbomachinery technology were also vital in the advancement of airbreathing engines.

The evolution of airbreathing engines are still in progress and improvements that are aiming to satisfy higher flight speeds with higher component efficiencies are also researched in the near future. By the introduction of more advanced materials, it is possible to obtain higher efficiencies with lower fuel consumption and lighter structures.

## **1.2. Aircraft Engine Design Process**

The aircraft engine design process starts with a Request for Proposal (RFP) from the customer, and the design constraints are determined according to this list of requirements. Although the steps in design process may differ from one company to another, depending on their proper experience, testing capabilities and expertise a sample roadmap is given by Mattingly (2002) [3] and simplified in Figure 1 to explain the general trend in the industry.

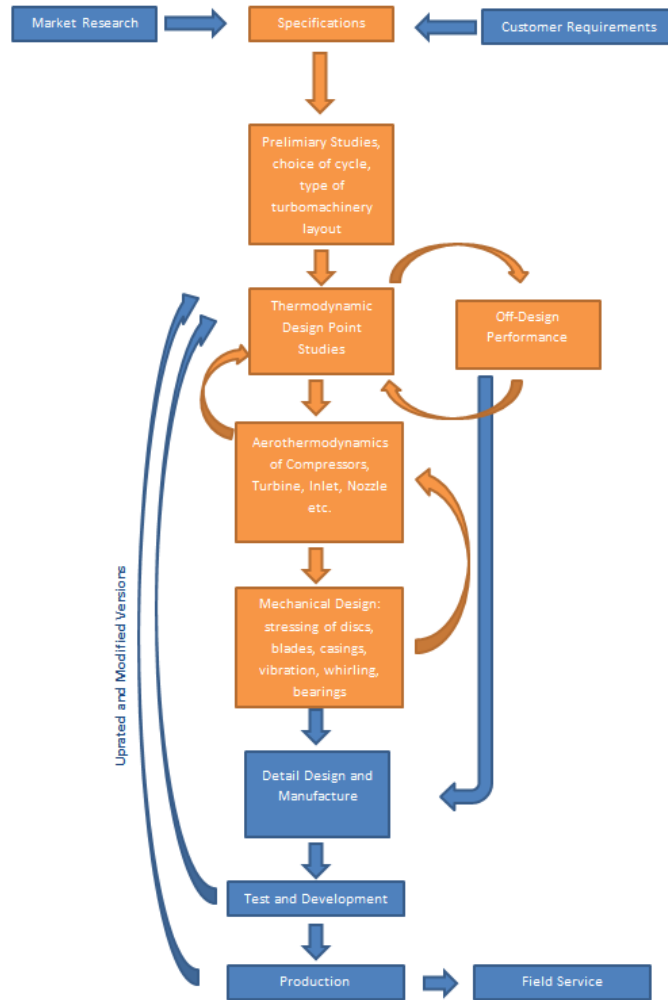


**Figure 1** Gas Turbine engine design roadmap given by Mattingly J.D. [3]

The design phase highlighted with orange color in Figure 1 is further detailed in Figure 2 as follows.

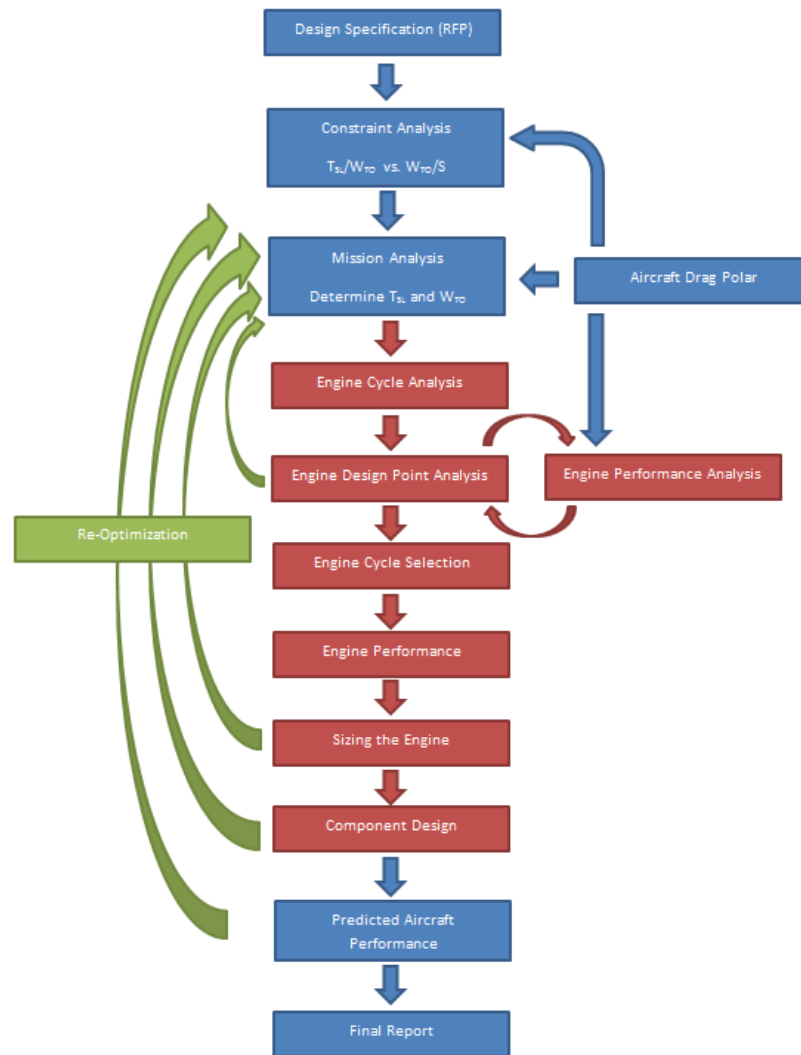


**Figure 2** Preliminary Propulsion Design Sequence by Mattingly J.D. [3]

The cycle analysis sections involve thermodynamics calculations whereas; the component design phase involves the velocity triangle calculations and extended CFD analysis in blade aerodynamic design and Finite Elements Methods in blade structural design. Aerothermodynamic design is the first step and starting point of advanced component design phases. The exact sizing and determination of the component geometries are obtained after an iterative loop including aerothermodynamic design, aerodynamic design and structural design phases. Design process of Low Pressure Turbine blade design of GE90-115B turbofan engine is outlined by Horibe, K. et al (2004) [4] and shown in Figure 3 as an example.

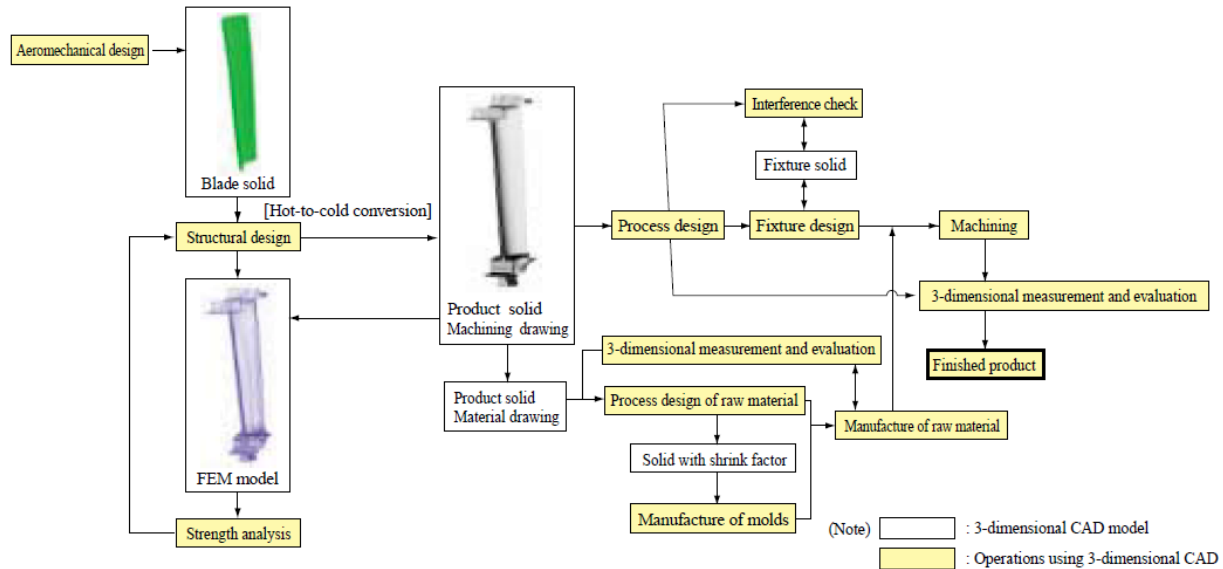


**Figure 3** Low Pressure Turbine disk design roadmap for GE90-115B engine; the method involves FEM and CFD methods that are used iteratively

In this thesis, Engine Design Point, Engine Performance Analysis, Engine Sizing and Component Design phases of the roadmap is introduced in Figure 2. Only aerothermodynamic design is considered in the component design of the engine.

### 1.3. Aerothermodynamic Design Tools and the Intention of Developing the Engine Design Model

A new gas turbine engine design generally starts with the aerothermodynamic cycle analysis. The turbomachinery design starts after the cycle analysis is completed. These three design sections are repeated and end once the specifications determined by the Request for Proposal are met. The aerothermodynamic design can be summed up to three main phases as follows:

- Parametric (or On-Design) Cycle Analysis
- Performance (or Off-Design) Cycle Analysis
- Turbomachinery Design

In the aero-propulsion industry, there are several other aerothermodynamic analysis tools that are used frequently: AEDsys Software by Mattingly, Heiser and Pratt [3], GASTURB by GasTurb GmbH, T-AXI by Mark G. Turner, Ali Merchant, and Dario



Bruna. There are also several design software that are developed by engine manufacturer companies as well. As stated by Liew K.H. [5], such programs are not available to be used by the third party recipients and the commercially available software allows only applications to specific type of engines. In order to analyze different types of engine configurations, and cycles, use different fuels, and/or design different turbomachinery components a new engine design software is developed.

The engine design loop, repeatedly calls on-design, off-design and turbomachinery design subsections. Also the design process requires lower execution times, and high conversion speeds. Such criteria can be attained by coding for speed and convergence optimization. Different coding languages may require different optimization methods and those may be sometimes too complex to be applied by a standard programmer. In addition to the expertise in programming, dealing with the compiler and builder errors in an engine design algorithm may cause the loss of focus from the design methodology itself.

For the sake of eliminating these possible disadvantages, MATLAB Simulink® (Simulink) tool is used as platform to the engine design algorithm. The ease of setting and modifying the subcomponents provide efficiency and speed in error handling. Such coding environment also allows for expanding a design algorithm for a specific type of engine to another one. Besides, the Optimization Toolbox of MATLAB® (MATLAB) encompasses different built-in optimization techniques (Genetic Algorithms, Gradient Descent or SIMPLEX) and are readily used without making modifications to the verified Simulink model.

Engine Design Model (EDM) is developed for separate flow turbofan engines. The model consists of sub-models which are named after the following three main aerothermodynamic engine design processes: Parametric Cycle, Performance Cycle, and Turbomachinery Design. Each sub-model performs calculations and the required engine design parameters are obtained at the end. The cycle algorithms are mostly based on the algorithms steps explained in Aircraft Engine Design by Mattingly et al (1987) [6]. The

turbomachinery design algorithm steps are based on the design requirements and methods also given in Aircraft Engine Design by Mattingly et al (1987) [6], Axial Flow Turbines by Horlock J.H. (1966) [7], Axial Flow Compressors by Horlock J.H. (1973) [8], Korpela J.H. (2011) [9] and Dixon S.L. et al (2010) [10], and the validation and/or benchmarking of the results are made with the AEDsys Software [3] and real engine data respectively.

## CHAPTER 2

### LITERATURE REVIEW

The theory needed to develop the Parametric Cycle, and Performance Cycle sections of the Engine Design Model are used from the theory given in [3] without any modifications. Therefore Sections 2.1 and 2.2 gives a rewording in order to show the equations used in the relevant parts of EDM. Most of the theory used in Turbomachinery Design section of EDM is based on the theory given in [6] and Section 2.3 gives a rewording as for the cycle design section, in order to present the equations used in the relevant parts of EDM.

#### **2.1. Parametric Cycle (On-Design) Theory**

The object of parametric cycle analysis is to obtain the performance parameters (primarily specific thrust and thrust specific fuel consumption) in terms of:

1. Design limitations (such as maximum allowable turbine inlet temperature and attainable component efficiencies), the flight conditions (the ambient pressure, temperature and Mach Number)
2. Design choices (such as compressor pressure ratio, fan pressure ratio, by-pass ratio and theta break).

The relatively simple aerothermodynamic analysis is achieved by treating each stream as 1D perfect gas flow, and by representing non-ideal component behavior through realistic efficiencies.

### 2.1.1 Design Tools

The uninstalled engine thrust ( $F$ ) and the uninstalled thrust specific fuel consumption ( $S$ ) is the primary measures of the engine's overall performance. The uninstalled thrust for a single exhaust stream engine can be written as:

$$F = \frac{1}{g_c} m_9 V_9 - m_0 V_0 + A_9(P_9 - P_0) \quad (1)$$

In the Equation (1), Station 0 indicates the far upstream of the engine and Station 9 indicates the engine exit. The term  $g_c$  is a unit dependent constant and if the units of  $m$  is slug/s and  $V$  is in ft/s it is equal to 1. It is also equal to 1 in SI Unit System, and 32.174 lbm-ft/(lbf-s<sup>2</sup>) in the British Engineering System.

The uninstalled thrust specific fuel consumption ( $S$ ) is given by Equation (2).

$$S = \frac{m_f}{F} \quad (2)$$

In the Equation (2),  $m_f$  represents the total fuel flow rate to the main combustor of an engine.

### 2.1.2 Engine Station Numbering

A generalized turbofan engine schematic is shown in Figure 4 and the indicated station numbers are in accordance with Aerospace Recommended Practice (ARP) 755A and will be used throughout the thesis.

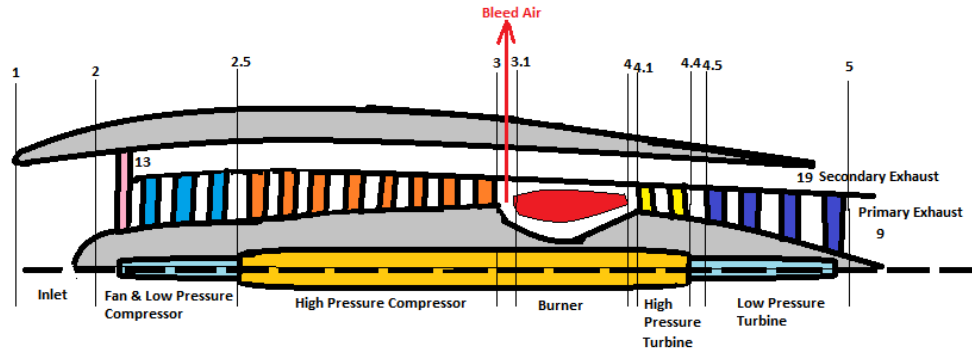


**Figure 4** Engine Station Numbering shown on a mixed-flow turbofan engine [3]

Blade and turbine cooling airflows and the spool naming are shown in Figure 5.

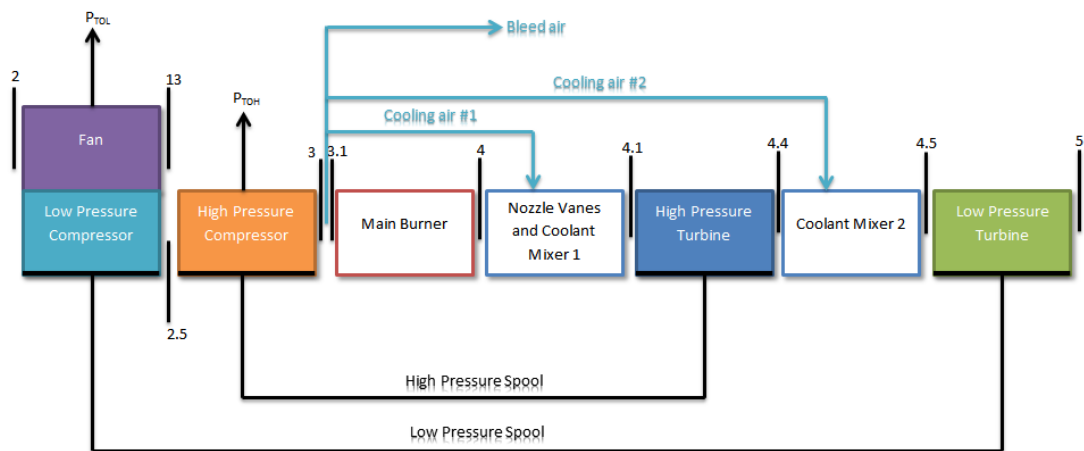


**Figure 5** Airflow paths and the spool designations

The station numbering of aerothermodynamic analysis and their corresponding locations on the real engines is given in Table 1.

**Table 1** Engine Station Numbering and their relevant locations on the real engine

<b>Engine Station Number</b>	<b>The location on the engine</b>
<b>0</b>	Far upstream/free stream
<b>1</b>	Inlet/Diffuser entry
<b>2</b>	Inlet/Diffuser exit, Fan entry
<b>13</b>	Fan exit
<b>2.5</b>	Low Pressure Compressor exit, High Pressure Compressor entry
<b>3</b>	High Pressure Compressor exit
<b>3.1</b>	Combustor entry
<b>4</b>	Combustor exit, Nozzle vanes entry, modeled Coolant Mixer 1 entry, High Pressure Turbine entry for $\pi_{tH}$ definition
<b>4.1</b>	Nozzle vanes exit, Coolant Mixer 1 exit, High Pressure Turbine entry for $\pi_{tH}$ definition
<b>4.4</b>	High Pressure Turbine exit, modeled Coolant Mixer 2 entry
<b>4.5</b>	Coolant Mixer 2 exit, Low Pressure Turbine entry
<b>5</b>	Low Pressure Turbine exit
<b>6</b>	Core Stream Mixer entry
<b>16</b>	Fan by-pass stream Mixer entry
<b>6A</b>	Mixer exit, Afterburner entry
<b>7</b>	Afterburner exit, Exhaust nozzle entry
<b>8</b>	Exhaust Nozzle throat
<b>9</b>	Exhaust Nozzle exit

### 2.1.3 Gas Model

The air and combustion gases are modeled as perfect gases in thermodynamic equilibrium. As such, gas model includes the variation of specific heat at constant pressure,  $c_p$  with temperature.

### 2.1.4 Total Property Ratios of Components

The ratio of total (isentropic stagnation) pressures is denoted by  $\pi$  and its definition is given in Equation (3).

$$\pi_i = \frac{\text{total pressure leaving component } i}{\text{total pressure entering component } i} \quad (3)$$

The ratio of total temperatures (adiabatic stagnation) is denoted by  $\tau_i$  and its definition is given in Equation (4).

$$\tau_i = \frac{\text{total temperature leaving component } i}{\text{total temperature entering component } i} \quad (4)$$

Moreover, the  $\pi$  and  $\tau$  of each component will be identified with the subscripts given in Table 2.

**Table 2** Subscripts used to define engine stations

Subscript	Definition	Engine Station
<b>b</b>	Combustor	3.1 → 4
<b>c</b>	Compressor	2 → 3
<b>cH</b>	High Pressure Compressor	2.5 → 3
<b>cL</b>	Low Pressure Compressor	2 → 2.5
<b>d</b>	Diffuser/Inlet	0 → 2
<b>f</b>	Fan	2 → 13
-	Fan Duct	13 → 16
<b>m1</b>	Coolant Mixer 1	4 → 4.1
<b>m2</b>	Coolant Mixer 2	4.4 → 4.5
<b>n</b>	Exhaust Nozzle	7 → 9
<b>t</b>	Turbine	4 → 5
<b>tH</b>	High Pressure Turbine	4 → 4.5
<b>tL</b>	Low Pressure Turbine	4.5 → 5

The isentropic relations used in the parametric cycle analysis are given in Equations (5) and (6).

$$\frac{T_{t0}}{T_0} = 1 + \frac{\gamma-1}{2} M_0^2 \quad (5)$$

$$\frac{P_{t0}}{P_0} = 1 + \frac{\gamma-1}{2} M_0^2 \quad \gamma/(\gamma-1) \quad (6)$$

The component pressure and temperature ratios are given in Equations (7) to (29) with the following assumptions in Fan Duct and High Pressure Compressor exit respectively:

- I.  $P_{t13} = P_{t16}$
- II.  $P_{t3} = P_{t3.1}$

- Diffuser (Station 0 to Station 2)

$$\pi_d = \frac{P_{t2}}{P_{t0}} \quad (7) \quad \tau_d = \frac{T_{t2}}{T_{t0}} = 1 \quad (8)$$

- Fan (Station 2 to Station 13)

$$\pi_f = \frac{P_{t13}}{P_{t2}} \quad (9) \quad \tau_f = \frac{T_{t13}}{T_{t2}} \quad (10)$$

- Low Pressure Compressor (Station 2 to Station 2.5)

$$\pi_{cL} = \frac{P_{t2.5}}{P_{t2}} \quad (11) \quad \tau_{cL} = \frac{T_{t2.5}}{T_{t2}} \quad (12)$$

- High Pressure Compressor (Station 2.5 to Station 3)

$$\pi_{cH} = \frac{P_{t3}}{P_{t2.5}} \quad (13) \quad \tau_{cH} = \frac{T_{t3}}{T_{t2.5}} \quad (14)$$

- Compressor (Station 2 to Station 3)

$$\pi_c = \pi_{cL}\pi_{cH} = \frac{P_{t3}}{P_{t2}} \quad (15) \quad \tau_c = \tau_{cL}\tau_{cH} = \frac{T_{t3}}{T_{t2}} \quad (16)$$

- Combustor (Station 3.1/3 to Station 4)

$$\pi_b = \frac{P_{t4}}{P_{t3.1}} = \frac{P_{t4}}{P_{t3}} \quad (17) \quad \tau_b = \frac{c_{p4}T_{t4}}{c_{p3.1}T_{t3.1}} = \frac{c_{p4}T_{t4}}{c_{p3}T_{t3}} \quad (18)$$

- Coolant Mixer 1 (Station 4 to Station 4.1)

$$\pi_{m1} = \frac{P_{t4.1}}{P_{t4}} \quad (19) \quad \tau_{m1} = \frac{T_{t4.1}}{T_{t4}} \quad (20)$$

- High Pressure Turbine (Station 4.1 to Station 4.4)

$$\pi_{tH} = \frac{P_{t4.4}}{P_{t4}} \quad (21) \quad \tau_{tH} = \frac{T_{t4.4}}{T_{t4.1}} \quad (22)$$

- Coolant Mixer 2 (Station 4.4 to Station 4.5)

$$\pi_{m2} = \frac{P_{t4.5}}{P_{t4.4}} = 1 \quad (23) \quad \tau_{m2} = \frac{T_{t4.5}}{T_{t4.4}} \quad (24)$$

- Low Pressure Turbine (Station 4.5 to Station 5)

$$\pi_{tL} = \frac{P_{t5}}{P_{t4.5}} \quad (25) \quad \tau_{tL} = \frac{T_{t5}}{T_{t4.5}} \quad (26)$$

- Exhaust Nozzle (Station 7 to Station 9)

$$\pi_n = \frac{P_{t9}}{P_{t7}} \quad (27) \quad \tau_n = \frac{T_{t9}}{T_{t7}} = 1 \quad (28)$$

- Other parameters

$$\tau_\lambda = \frac{c_{p4}T_{t4}}{c_{p0}T_{t0}} \quad (29)$$



### 2.1.5 Mass Flow Rates

The symbol  $m$  is used for the mass flow rate with a subscript location described in Table 3.

**Table 3** Subscripts used to define mass flow rates

Subscript	Definition
<b>b</b>	Bleed air
<b>c</b>	Core airflow through the engine
<b>c1</b>	Cooling air for High Pressure Turbine nozzle vanes
<b>c2</b>	Cooling air for remainder of High Pressure Turbine
<b>F</b>	Fan airflow through the by-pass duct
<b>f</b>	Fuel flow to main combustor

In engine cycle analysis, it is often most effective to cast the calculations into dimensionless mass flow ratios. The most useful of these are given as follows:

- By-Pass Ratio ( $\alpha$ )

$$\alpha = \frac{\text{by-pass flow}}{\text{core flow}} = \frac{m_F}{m_c} \quad (30)$$

- Bleed air fraction ( $\beta$ )

$$\beta = \frac{\text{bleed flow}}{\text{core flow}} = \frac{m_b}{m_c} \quad (31)$$

- Cooling air fractions ( $\epsilon_1$  and  $\epsilon_2$ )

$$\epsilon_1 = \frac{m_{c1}}{m_c} \quad (32)$$

$$\epsilon_2 = \frac{m_{c2}}{m_c} \quad (33)$$

- Combustor fuel/air ratio ( $f$ )

$$f = \frac{\text{burner fuel flow}}{\text{burner inlet airflow}} = \frac{m_f}{m_{3,1}} \quad (34)$$

- Overall fuel to air ratio ( $f_o$ )

$$f_o = \frac{\text{total fuel flow}}{\text{engine inlet airflow}} = \frac{m_f + m_{f_{AB}}}{m_c + m_F} \quad (35)$$

- Fuel to air ratio at Station 4.1 ( $f_{4,1}$ )

$$f_{4,1} = \frac{f}{1 + f + \frac{\varepsilon_1}{1 - \beta - \varepsilon_1 - \varepsilon_2}} \quad (36)$$

- Fuel to air ratio at Station 4.5 ( $f_{4,5}$ )

$$f_{4,5} = \frac{f}{1 + f + \frac{\varepsilon_1 + \varepsilon_2}{1 - \beta - \varepsilon_1 - \varepsilon_2}} \quad (37)$$

The mass flow rates at different engine sections and their relationships to the mass flow ratio definitions given in Equations (30) to (37) are formulated below in Equations (38) to (43).

$$m_0 = m_c + m_F = (1 + \alpha)m_c \quad (38)$$

$$m_3 = m_c \quad (39)$$

$$m_{3,1} = m_c - m_c\beta - m_c\varepsilon_1 - m_c\varepsilon_2 \quad (40)$$

$$m_4 = m_c(1 - \beta - \varepsilon_1 - \varepsilon_2)(1 + f) \quad (41)$$

$$m_{4,1} = m_{4,4} = m_c \frac{1 - \beta - \varepsilon_1 - \varepsilon_2}{1 + f} + \varepsilon_1 \quad (42)$$

$$m_{4,5} = m_5 = m_c \frac{1 - \beta - \varepsilon_1 - \varepsilon_2}{1 + f} + \varepsilon_1 + \varepsilon_2 \quad (43)$$

Cooling air is drawn off from the compressor exit (Station 3). A portion of this cooling air ( $m_{c1} = m_c\varepsilon_1$ ) is used to cool the High Pressure Turbine nozzle inlet guide vanes. The remainder ( $m_{c2} = m_c\varepsilon_2$ ) is used to cool the High Pressure Turbine rotor. In the cycle calculations, the cooling airflows  $m_{c1}$  and  $m_{c2}$  are modeled as being introduced and fully mixed in Coolant Mixer 1 and Coolant Mixer 2 sections respectively. No total pressure loss is assumed at Coolant Mixer 2. No cooling air is drawn for Low Pressure

Turbine. The coolant air modeling and other core engine mass flow rates are shown on Figure 6.

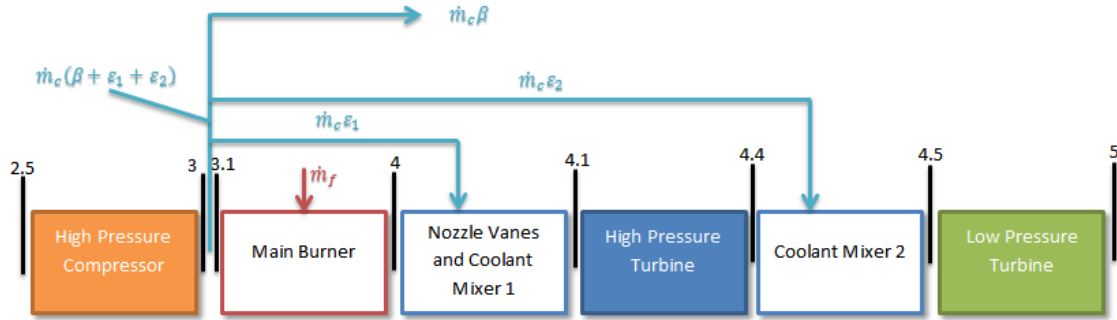


**Figure 6** Air and fuel mass flow shown for core engine

## 2.1.6 Component Efficiencies

### 2.1.6.1 Rotating Components

For the rotating turbomachinery components it is very convenient to relate pressure ratios ( $\pi$ ) to their temperature ratios ( $\tau$ ) through efficiency definitions. As such losses or real effects are accounted for. Two such efficiencies are commonly employed;”  $\eta$ ” corresponding to the overall pressure and temperature ratios, and “ $e$ ” corresponding to polytropic process where  $\pi$  and  $\tau$  are infinitesimally close to 1.

The subscript “i” is used to represent isentropic exit state in the overall efficiency ( $\eta$ ). The actual pressure ratios are written in terms of polytropic efficiencies and the overall efficiency definitions are given in Equations (44) to (53).

- Fan (Stations 2 to 13)

$$\pi_f = \frac{P_{t13}}{P_{t2}} e_f = \frac{T_{t13}}{T_{t2}} \frac{e_f \gamma}{\gamma - 1} \quad (44)$$

$$\eta_f = \frac{\frac{T_{t13i} - 1}{T_{t2}}}{\tau_f - 1} \quad (45)$$

- Low Pressure Compressor (Stations 2 to 2.5)

$$\pi_{cL} = \frac{P_{t2.5}}{P_{t2}} e_{cL} = \frac{T_{t2.5}}{T_{t2}} \frac{e_{cL} \gamma}{\gamma - 1} \quad (46)$$

$$\eta_{cL} = \frac{\frac{T_{t2.5i} - 1}{T_{t2}}}{\tau_{cL} - 1} \quad (47)$$

- High Pressure Compressor (Stations 2.5 to 3)

$$\pi_{cH} = \frac{P_{t3}}{P_{t2.5}} e_{cH} = \frac{T_{t3}}{T_{t2.5}} \frac{e_{cH} \gamma}{\gamma - 1} \quad (48)$$

$$\eta_{cH} = \frac{\frac{T_{t3i} - 1}{T_{t2.5}}}{\tau_{cH} - 1} \quad (49)$$

- High Pressure Turbine (Stations 4.1 to 4.4)

$$\pi_{tH} = \frac{P_{t4.4}}{P_{t4.1}} 1/e_{tH} = \frac{T_{t4.4}}{T_{t4.1}} \frac{\gamma}{e_{tH}(\gamma - 1)} \quad (50)$$

$$\eta_{tH} = \frac{1 - \frac{T_{t4.4}}{T_{t4.1}}}{1 - \frac{T_{t4.4i}}{T_{t4.1}}} \quad (51)$$

- Low Pressure Turbine (Stations 4.5 to 5)

$$\pi_{tL} = \frac{P_{t5}}{P_{t4.5}} 1/e_{tL} = \frac{T_{t5}}{T_{t4.5}} \frac{\gamma}{e_{tL}(\gamma - 1)} \quad (52)$$

$$\eta_{tL} = \frac{1 - \frac{T_{t5}}{T_{t4.5}}}{1 - \frac{T_{t5i}}{T_{t4.5}}} \quad (53)$$

### 2.1.6.2 Combustion Components

For those components in which combustion take place, combustion efficiency is used to characterize the degree to which extent the chemical reactions is completed. The efficiencies are based upon the ratio of the actual thermal energy rise to the maximum possible thermal energy increase as represented by the lower heating value of the fuel ( $h_{PR}$ ). Thus, the efficiencies are represented as:

$$\eta_b = \frac{m_4 c_{p4} T_{t4} - m_{3.1} c_{p3.1} T_{t3.1}}{m_f h_{PR}} \quad (54)$$

### 2.1.6.3 Power Transmission Components

For those components that merely transmit mechanical power by means of shafts, gears, etc., a simple definition of mechanical efficiency is used to account for losses due to windage, bearing friction, and seal drag. In such cases the overall efficiency component

$\eta_m$  is defined for power transmission components and  $\eta_{mH}$ ,  $\eta_{mL}$ ,  $\eta_{mPH}$  and  $\eta_{mPL}$  refer to the High Pressure Turbine shaft, Low Pressure Turbine shaft, and power takeoffs from the High Pressure Turbine shaft and Low Pressure Turbine shaft respectively. This type of overall efficiency is defined as:

$$\eta_m = \frac{\text{mechanical power output}}{\text{mechanical power input}} \quad (55)$$

### 2.1.7 Parametric Cycle (On-Design) Analysis

The parametric cycle analysis is based on the following assumptions:

- 1) The flow is, on the average, steady
- 2) The flow is 1D at the entry and the exit of each component and at each axial station
- 3) The fluid behaves as a perfect gas with constant molecular weight across the diffuser, fan, turbine and connecting ducts.
- 4) The total pressure ratio of the diffuser or inlet is defined as follows:

$$\frac{P_{t2}}{P_{t0}} = \frac{P_{t2}}{P_{t0 \max}} \eta_{Rspec}$$

$\frac{P_{t2}}{P_{t0 \max}}$  = Total Pressure Ratio caused only by wall friction effects

$$\eta_{Rspec} = \begin{cases} 1 & \text{for } M_0 \leq 1 \\ 1 - 0.075 M_0 - 1^{1.35} & \text{for } 1 < M_0 \leq 5 \\ \frac{800}{M_0^4 + 935} & \text{for } M_0 > 5 \end{cases}$$

- 5) The Fan and Low Pressure Compressor are driven by the Low-Pressure Turbine, and they also provide mechanical power for accessories,  $P_{TOL}$ .
- 6) The High Pressure Compressor receives air directly from the Low Pressure Compressor and is driven by the High Pressure Turbine, and they also provide mechanical power for accessories,  $P_{TOH}$ .
- 7) High pressure bleed air and turbine cooling air are removed between Stations 3 and 3.1.

- 8) The flow in the by-pass duct (from Station 13 to 16) is isentropic.
- 9) The effect of cooling on turbine efficiency is accounted for by a reduction of  $e_{tH}$  due to,  $m_{c1}$  and  $m_{c2}$ .

In this thesis, only equations needed to be used in the parametric cycle analysis of dual spool turbofan engines are introduced.

### 2.1.7.1 Uninstalled Thrust ( $F/m_0$ ):

The general uninstalled thrust equation is rearranged into the following non-dimensional form given in Equation (56).

$$\frac{Fg_c}{m_0 a_0} = 1 + f_0 + \frac{\beta}{1+\alpha} \frac{V_9}{a_0} - M_0 + 1 + f_0 - \frac{\beta}{1+\alpha} \frac{R_9}{R_0} \frac{T_9}{T_0} \frac{1 - \frac{P_0}{P_9}}{\frac{V_9}{a_0} \gamma_0} \quad (56)$$

When the nozzle exit area is chosen for ideal expansion and maximum uninstalled specific thrust then  $P_0=P_9$  and the last term in Equation (56) vanishes. Otherwise  $P_0/P_9 \neq 1$  is a design input, and Equation (56) is non-dimensional uninstalled specific thrust depending largely upon the velocity ratio  $\frac{V_9}{a_0}$  and the overall static temperature ratio  $\frac{T_9}{T_0}$ .

### 2.1.7.2 Velocity Ratio ( $\frac{V_9}{a_0}$ ):

From the enthalpy equation  $h_t = h + \frac{V^2}{2g_c}$  a relationship can be written between the enthalpy and speed ratio as:

$$\frac{V_9}{V_0}^2 = M_0^2 \frac{h_{t9} - h_9}{h_{t0} - h_0} \quad (57)$$

Since  $\frac{h_{t9}}{h_9}$  is proportional with  $\frac{T_{t9}}{T_9}$  and using the isentropic relations given in Equations (5) and (6), the total to static pressure ratio  $\frac{P_{t9}}{P_9}$  can be used in Equation (57) to give the velocity for a calorically perfect gas as:

$$\frac{V_9}{a_0} = M_0 \frac{\tau_\lambda \tau_{m1} \tau_{tH} \tau_{m2} \tau_{tL}}{\tau_r - 1} \left[ 1 - \frac{P_{t9}}{P_9} \frac{\gamma_t - 1}{\gamma_t} \right]^{1/2} \quad (58)$$

### 2.1.7.3 Overall Static Temperature Ratio ( $\frac{T_9}{T_0}$ ):

The static temperature ratio  $\frac{T_9}{T_0}$  directly follows using the reduced pressure<sup>†</sup> at Station 9 to obtain the corresponding temperature. For the case of a calorically perfect gas, the static temperature ratio is given directly by Equation (59).

$$\frac{T_9}{T_0} = \frac{c_{pc}}{c_{pt}} \frac{\tau_\lambda \tau_{m1} \tau_{tH} \tau_{m2} \tau_{tL}}{\frac{P_{t9}}{P_9} \gamma_t^{-1} / \gamma_t} \quad (59)$$

### 2.1.7.4 Combustor Fuel to Air Ratio ( $f$ ):

Applying the definition of combustor efficiency given in Equation (54) and using the definition of fuel to air ratio given in Equation (34) yields the combustor fuel to air ratio equation given in Equation (60).

$$f = \frac{\frac{c_{p4} T_{t4}}{c_{p0} T_{t0}} \frac{T_{t0} T_{t2.5} T_{t3}}{T_0 T_{t2} T_{t2.5}}}{\frac{h_{PR} \eta_b}{c_{pc} T_0} \frac{c_{p4} T_{t4}}{c_{p0} T_{t0}}} \quad (60)$$

### 2.1.7.5 Coolant Mixer Temperature Ratios ( $\tau_{m1}$ , $\tau_{m2}$ ):

The 1<sup>st</sup> Law energy balance of the mixing process from Station 4 to 4.1 yields the relation for Coolant Mixer 1 given as:

$$\tau_{m1} = \frac{1 - \beta - \varepsilon_1 - \varepsilon_2}{1 - \beta - \varepsilon_1 - \varepsilon_2} \frac{1 + f + \varepsilon_1}{1 + f + \varepsilon_1} \frac{\tau_r \tau_{cL} \tau_{cH}}{\tau_\lambda} \quad (61)$$

Likewise, the 1<sup>st</sup> Law energy balance of the mixing process from Station 4.4 to 4.5 gives the relation for Coolant Mixer 2 given as:

$$\tau_{m2} = \frac{1 - \beta - \varepsilon_1 - \varepsilon_2}{1 - \beta - \varepsilon_1 - \varepsilon_2} \frac{1 + f + \varepsilon_1 + \varepsilon_2}{1 + f + \varepsilon_1} \frac{\tau_r \tau_{cL} \tau_{cH}}{\tau_\lambda \tau_{m1} \tau_{tH}} \quad (62)$$

### 2.1.7.6 High Pressure Turbine Temperature Ratio ( $\tau_{tH}$ ):

A power balance on the high pressure spool is:

$$m_{4.1} h_{t4.1} - h_{t4.4} \eta_{mH} = m_c h_{t3} - h_{t2.5} + \frac{P_{TOH}}{\eta_{mPH}} \quad (63)$$

By using Equation (63), the High Pressure Turbine Total Temperature ratio is found as:

$$\tau_{tH} = 1 - \frac{\tau_r \tau_{cL} \tau_{cH} - 1 + (1 + \alpha) \frac{P_{TOH}}{\eta_{mPH} m_0 h_0}}{\eta_{mH} \tau_\lambda \frac{1 - \beta - \varepsilon_1 - \varepsilon_2}{1 + f + \varepsilon_1} \frac{\tau_r \tau_{cL} \tau_{cH}}{\tau_\lambda}} \quad (64)$$

### 2.1.7.7 Low Pressure Turbine Temperature Ratio ( $\tau_{tL}$ ):

A power balance on the low pressure spool is:

$$m_{4.5} h_{t4.5} - h_{t5} \eta_{mL} = m_c h_{t2.5} - h_{t2} + m_F h_{t13} - h_{t2} + \frac{P_{TOL}}{\eta_{mPL}} \quad (65)$$

By using Equation (65), the Low Pressure Turbine Total Temperature ratio is found as:

$$\tau_{tL} = 1 - \frac{\tau_r \tau_{cL}^{-1} + \alpha(\tau_f - 1) + (1 + \alpha) \frac{P_{TOL}}{\eta_{mPL} m_0 h_0}}{\eta_{mH} \tau_\lambda \tau_{tH} \quad 1 - \beta - \varepsilon_1 - \varepsilon_2 \quad 1 + f + \varepsilon_1 + \frac{\varepsilon_2}{\tau_{tH}} \frac{\tau_r \tau_{cL} \tau_{cH}}{\tau_\lambda}} \quad (66)$$

### 2.1.7.8 Uninstalled Thrust Specific Fuel Consumption (S):

Equation (2) can be rearranged into the following forms for the uninstalled thrust specific fuel consumption:

$$S = \frac{m_f}{F} = \frac{m_f/m_0}{F/m_0} = \frac{f_0}{F/m_0} \quad (67)$$

The input for this equation is given in Equations (56), (35), and (60).

### 2.1.7.9 Propulsive, Thermal and Overall Efficiencies ( $\eta_p$ , $\eta_{th}$ , $\eta_o$ ):

The propulsive efficiency (the ratio of thrust power to the rate of kinetic energy generation of the engine gas flow), the thermal efficiency (the ratio of the rate of kinetic energy generation of the engine gas flow plus shaft takeoff power to the rate at which thermal energy is made available by the fuel), and overall efficiency (the ratio of the thrust power to the rate at which thermal energy is made available by the fuel) are included in parametric cycle calculations. For the general case the propulsive, thermal and overall efficiency relations are given in Equations (68), (69) and (70) respectively.

[3]

$$\eta_p = \frac{2 \frac{F g_c}{m_0 V_0}}{1 + f_0 - \frac{\beta}{1 + \alpha} \frac{V_9^2}{V_0^2} - 1} \quad (68)$$

$$\eta_{th} = \frac{\frac{V_0^2}{2 g_c} \quad 1 + f_0 - \frac{\beta}{1 + \alpha} \frac{V_9^2}{V_0^2} - 1 + \frac{P_{TOL} + P_{TOH}}{m_0}}{f_0 h_{PR}} \quad (69)$$



$$\eta_o = \frac{V_o(F/m_o)}{f_o h_{PR}} = \frac{V_o}{h_{PR}} \frac{1}{S} \quad (70)$$

## 2.2. Performance Cycle (Off-Design) Theory

The parametric cycle analysis showed how reference point (on-design point) engine performance was determined. This made it possible to examine sensitivity of engine specific performance (specific thrust and thrust specific fuel consumption) to the input variables.

The object of performance cycle analysis is to determine the engine's performance over its operating envelope. Thus, it is possible to focus in on the most promising designs and to ultimately find the engine that has the best balanced performance over the whole mission spectrum.

Performance analysis differs significantly from the parametric analysis. In parametric cycle analysis, all of the design choices (including the flight conditions) are free to be selected by the designer, and the engine performance characteristics per unit mass flow are determined for each selected set of choices. In contrast, in performance cycle analysis, the design choices mostly frozen, and the performance of this engine is now extended to all possible operating conditions.

### 2.2.1 Design Tools

The performance of a selected high by-pass turbofan engine is desired at any flight conditions, throttle settings and nozzle settings. It is assumed that a parametric cycle analysis has been performed for the reference point engine having known "reference conditions". The reference conditions will be denoted by subscript "R" for the engine ( $S_R, (F/m_o)_R$  etc.), overall performance also for each engine component ( $\tau_{fR}, \pi_{fR}$ , etc.) and for the flight conditions ( $M_{OR}, P_{OR}, T_{OR}$  etc.).

In the parametric cycle analysis, all of the relevant equations constitute 10 independent equations for finding values of these 10 dependent component performance variables namely,  $\tau_f, \tau_{cL}, \tau_{cH}, f, \tau_{m1}, \tau_{tH}, \pi_{tH}, \tau_{m2}, \tau_{tL}$ , and  $\pi_{tL}$ . Given are values of the independent quantities consisting of flight conditions, aircraft system parameters, and design choices.

As a result, the engine reference point performance in terms of  $(F/m_0)$ ,  $S$ ,  $\eta_p$ , and  $\eta_{th}$  is readily found.

Similarly, to find the engine performance, the operational performance values of the 16 dependent variables are listed in Table 4 must be determined through 16 independent equations.

**Table 4** Engine Performance Variables

Component	Independent Variable	Constant/ Known Quantity	Dependent Variable
Engine	$M_0, P_0, T_0$	$\beta$	$m_0, \alpha$
Diffuser	-	$\pi_d$	-
Fan	-	$\eta_f$	$\pi_f, \tau_f$
Low Pressure Compressor	-	$\eta_{cL}$	$\pi_{cL}, \tau_{cL}$
High Pressure Compressor	-	$\eta_{cH}$	$\pi_{cH}, \tau_{cH}$
Combustor	$T_{t4}$	$\pi_b$	$f$
Coolant Mixer 1	-	$\varepsilon_1$	$\tau_{m1}$
High Pressure Turbine	-	$\eta_{tH}, M_4$	$\pi_{tH}, \tau_{tH}$
Coolant Mixer 2	-	$\varepsilon_2$	$\tau_{m2}$
Low Pressure Turbine	-	$\eta_{tL}, M_{4.5}$	$\pi_{tL}, \tau_{tL}$
Exhaust Nozzle	$P_0/P_9$	$\pi_n$	$M_9$
<b>Total Number</b>	6	-	16

Because performance analysis is an indirect problem, the solution of the 16 performance equations is an iterative process. Once the values of the 16 dependent variables are found, the engine performance in terms of  $f, (F/m_0)$ ,  $S$ ,  $\eta_p$ , and  $\eta_{th}$  follows immediately from Equations (60), (56), (67), (68) and (69) respectively.

Table 4 assumes that constant  $\pi_b$  and  $\pi_n$  and  $\tau_d, \pi_{m2}$  and  $\tau_n$  are equal to 1 and  $\pi_{m1}$  is contained in  $\pi_{tH}$ . In addition, it should be noted that due to the consideration of power extraction in the analysis, a preliminary guess for  $m_0$  is required to start the performance analyses.

In addition to the assumptions summarized in the Parametric Cycle Section (Section 2.1), the following list of assumptions is needed in performance analysis.

- 1) The flow areas are constant at stations 4 and 4.5.
- 2) The flow is choked at High Pressure Turbine entrance nozzles (choking area 4), at the Low Pressure Turbine entrance nozzles (choking area 4.5) and at the exhaust nozzle.
- 3) The component efficiencies ( $\eta_f$ ,  $\eta_{cL}$ ,  $\eta_{cH}$ ,  $\eta_b$ ,  $\eta_{tH}$ ,  $\eta_{tL}$ ,  $\eta_{mL}$ ,  $\eta_{mH}$ ,  $\eta_{mPL}$ , and  $\eta_{mPH}$ ) and total pressure ratios ( $\pi_b$  and  $\pi_n$ ) do not change from their design values.
- 4) Bleed air and cooling air fractions are constant. Power takeoffs are constant.
- 5) The air and combustion gases are perfect gases.
- 6) The exit area  $A_9$  of the exhaust nozzle is adjustable so that the pressure ratio  $\frac{P_0}{P_9}$  can be set to a predetermined value, mainly  $\frac{P_0}{P_9} = 1$
- 7) The area at each engine station is constant

### 2.2.2 The Mass Flow Parameter

The functional relations for engine cycle analysis are based on the application of mass, energy, momentum, and entropy considerations to the 1D steady flow of a perfect gas at an engine reference or off-design steady state operating point.

The Mass Flow Parameter (MFP) is defined as the grouping  $m \sqrt{T_t}/P_t A$ , that can be written as in Equation (71).

$$MFP = \frac{\dot{m} \sqrt{T_t}}{P_t A} \quad (71)$$

The static to total pressure and temperature ratios are functions of the total temperature of the gas, chemical equilibrium properties, and the Mach number; then MFP can also be expressed by the equivalent formula given in Equation (72).

$$MFP = M \sqrt{\frac{\gamma g_c P}{R P_t}} \sqrt{\frac{T_t}{T}} \quad (72)$$

In the solution algorithm of Performance Cycle given in Appendix F of Mattingly J.D. et al. [6], a subroutine named as RGCOMPR is used to perform calculations of the Mass Flow Parameter for different engine stations.

### 2.2.3 Performance of Turbines with Coolant Mixers

The first step in determining the performance of the entire engine at conditions away from the reference point is to analyze the behavior of the high and low pressure turbines. Because of the choked entry conditions of the turbines and the dependency of low pressure turbine exit conditions to mixer entry conditions or nozzle entry conditions narrow the range of operation of turbines and this gives a straightforward method of solution. The remainder of the engine performance analysis starts after this step because the turbines, in conjunction with the throttle setting (i.e.  $T_{t4}$ ), provide the power for the fan and compressors and controls the mass flows at these components.

The performance of a turbine ( $\pi_t$  and  $\tau_t$ ) at off design is primarily determined by the efficiency and mass conservation relationships. Oates G.C [11] shows that when a cooled turbine with variable specific heats is modeled,  $\pi_{tH}$  and  $\tau_{tH}$  vary only slightly with engine operating condition.

Consider a high pressure turbine with cooling air fractions  $\varepsilon_1$  and  $\varepsilon_2$ . Let the nozzle throat stations just downstream of stations 4 and 4.5 be denoted by 4' and 4.5' respectively. Then with a choked flow at 4' and 4.5' and assuming  $P_{t4}=P_{t4'}$  and  $P_{t4.5}=P_{t4.5'}$ , a relation given in Equation (73) can be obtained to calculate the high pressure turbine pressure ratio with a variable specific heat model.

$$\frac{\pi_{tH}}{\sqrt{T_{t4.5}/T_{t4}}} = \left\{ 1 + \frac{\varepsilon_1 + \varepsilon_2}{(1 - \beta - \varepsilon_1 - \varepsilon_2)(1 + f)} \right\} \frac{A_{4'}}{A_{4.5'}} \frac{MFP(M_{4'}, T_{t4'}, f)}{MFP(M_{4.5'}, T_{t4.5'}, f_{4.5})} \quad (73)$$

The right hand side of Equation (73) is essentially constant for the assumptions of this analysis (Section 2.2.1), namely  $\frac{A_{4'}}{A_{4.5'}} = \text{constant}$ ,  $M_{4'} = 1$ ,  $M_{4.5'} = 1$  and constant bleed and cooling air fractions.

$$f_{4.5} = \frac{f}{1+f+\frac{\varepsilon_1+\varepsilon_2}{(1-\beta-\varepsilon_1-\varepsilon_2)}} \quad (74)$$

Since  $f_{4.5}$  is dependent only on  $f$  as in Equation (74), then for a specific value of  $T_{t4}$  and  $f$  Equation (73) can be used to determine  $\pi_{tH}$  for an assumed value of  $T_{t4.5}$ . Furthermore, for given values of  $T_{t4}$ ,  $f$ ,  $\pi_{tH}$  and  $\eta_{tH}$  the resultant turbine exit temperature ( $T_{t4.5}$ ) can be calculated by the following procedure:

- 1) By using the total enthalpies at states  $t4.1$  ( $h_{t4.1}$ ) and  $t4$  ( $h_{t4}$ ), the relation for the Coolant Mixer 1 temperature ratio and fuel to air ratio at Station 4.1 can be found as in Equation (75) and (76) respectively.

$$\tau_{m1} = \frac{1-\beta-\varepsilon_1-\varepsilon_2}{1-\beta-\varepsilon_1-\varepsilon_2} \frac{1+f+\varepsilon_1\tau_r\tau_{cL}\tau_{cH}/\tau_\lambda}{1+f+\varepsilon_1} \quad (75)$$

$$f_{4.1} = \frac{f}{1+f+\frac{\varepsilon_1}{(1-\beta-\varepsilon_1-\varepsilon_2)}} \quad (76)$$

- 2) With state  $t4.1$  known and using  $\pi_{tH}$ , the total pressure at state 4.4i can be found as in Equation (77).

$$P_{rt4.4i} = \pi_{tH} P_{rt4.1} \quad (77)$$

- 3) With the found total pressure at state 4.4i from Equation (77), and noting that  $f_{4.4}=f_{4.1}$  total enthalpy at state 4.4i ( $h_{t4.4i}$ ) can be found using the subroutine FAIR<sup>†</sup>. Then the total enthalpy ratio of the ideal turbine can be found as in Equation (78).

$$\tau_{tHi} = \frac{c_{pt4.4} T_{t4.4i}}{c_{pt4.1} T_{t4.1}} \quad (78)$$

- 4) Assuming that the high pressure turbine has constant efficiency, high pressure turbine temperature ratio can be found as in Equation (79).

$$\tau_{tH} = 1 - \eta_{tH} (1 - \tau_{tHi}) \quad (79)$$

<sup>†</sup> FAIR is a subroutine that is used in Mattingly J.D. et al. [3] for the variable specific heat model calculations. It is given in 3 different methods of which the first method inputs only the temperature and fuel-to air ratio, second method takes enthalpy and fuel to air ratio and the third method takes relative pressure and fuel-to air ratio as input.

5) With the total temperature ratio of Coolant Mixer 2 with Equation (80) and  $f_{4.5}$  with Equation (74) the total enthalpy at Station 4.5 can be calculated by using Equation (81).

$$\tau_{m2} = \frac{1-\beta-\varepsilon_1-\varepsilon_2}{1-\beta-\varepsilon_1-\varepsilon_2} \frac{1+f+\varepsilon_1+\varepsilon_2}{1+f+\varepsilon_1+\varepsilon_2} \frac{\tau_r\tau_{cL}\tau_{cH}/(\tau_\lambda\tau_{m1}\tau_{tH})}{1+f+\varepsilon_1+\varepsilon_2} \quad (80)$$

$$h_{t4.5} = h_{t4}\tau_{m1}\tau_{tH}\tau_{m2} \quad (81)$$

6) With  $h_{t4.5}$  and  $f_{4.5}$  are known,  $T_{t4.5}$  can be found directly by using the subroutine FAIR.

Equations (73), (75), (76), (77), (78), (79), (80) and (81) forms a system of equations that determine the high pressure turbine performance parameters  $\pi_{tH}$  and  $\tau_{tH}$  and should be solved in an iterative way. This system of equations are programmed into the cooled turbine subroutine named TURBC in Mattingly J.D. et al. [3] and it solves this system

by first assuming an initial value of  $T_{t4.5}$  and use Equation (73) to find  $\pi_{tH}$ . By using this value of  $\pi_{tH}$ , the procedure described above gives a new value of  $T_{t4.5}$ . This new value is input into Equation (73) and calculations are repeated until the successive values are within 0.01. A similar, but simpler set of equations can be solved for the uncooled low pressure turbine. Rewriting Equation (73) for the low pressure turbine gives the relation for low pressure turbine pressure ratio as in Equation (82).

$$\frac{\pi_{tL}}{\sqrt{T_{t5}/T_{t4.5}}} = \frac{A_{4.5}}{A_5} \frac{MFP(M_{4.5}, T_{t4.5}, f_{4.5})}{MFP(M_5, T_{t5}, f_{4.5})} \quad (82)$$

For a specific value of  $T_{t4.5}$ ,  $f_{4.5}$  and  $M_5$ , Equation (82) can be used to determine the low pressure turbine pressure ratio. Along with the high pressure turbine case, with the given values of  $T_{t4.5}$ ,  $f_{4.5}$ ,  $\pi_{tL}$ ,  $\eta_{tL}$  and  $M_5$  the resultant turbine exit temperature ( $T_{t5}$ ) can be found with a system of equations. The procedure is given as follows:

1) By using the reduced pressure at the state t4.5 ( $P_{t4.5}$ ) and turbine total pressure ratio  $\pi_{tL}$ , the reduced pressure can be found at the ideal exit state t5i ( $P_{t5i}$ ) as in Equation (83).

$$P_{rt5i} = \pi_{tL} P_{rt4.5} \quad (83)$$

- 2) With  $P_{rt5i}$ ,  $h_{t5i}$  can be found using the subroutine FAIR. Then the total temperature ratio of the ideal low pressure turbine can be found as in Equation (84).

$$\tau_{tLi} = \frac{h_{t5i}}{h_{t4.5}} \quad (84)$$

- 3) Assuming that the low pressure turbine has constant efficiency Equation (84) can be solved to obtain the total temperature ratio of the low pressure turbine as in Equation (85).

$$\tau_{tL} = 1 - \eta_{tL}(1 - \tau_{tLi}) \quad (85)$$

- 4)  $T_{t5}$  can be found by using subroutine FAIR.

Equations (82), (83), (84) and (85) form a system of equations that determine the low pressure turbine performance parameters  $\pi_{tL}$  and  $\tau_{tL}$  and should be solved in an iterative way. This system of equations are programmed into the uncooled turbine subroutine named TURB in Mattingly J.D. et al. [3] and it solves this system by first assuming an initial value of  $T_{t5}$  and use Equation (82) to find  $\pi_{tL}$ . By using this value of  $\pi_{tL}$ , the procedure described above gives a new value of  $T_{t5}$ . Then this new value is input into Equation (83) and calculations are repeated until the successive values are within 0.01.

## 2.2.4 Component Performance Analysis

The performance of the high by-pass turbofan engine can now be analyzed using the assumptions in Section 2.2.1 and the technique used for low and high pressure turbines in the Section 2.2.3. The aim is to obtain 16 independent equations required to determine the dependent performance variables. The values of  $\pi_{tH}$ ,  $\tau_{tH}$ ,  $\tau_{m1}$ ,  $\tau_{m2}$ ,  $T_{t4.5}$ ,  $\pi_{tL}$ ,  $\tau_{tL}$  and  $T_{t5}$  are calculated in the previous section and therefore they will be treated as known values in this section.

### 2.2.4.1 Fan and Low Pressure Compressor

Equation (66) from the parametric cycle analysis can be rearranged and rewritten by considering the ratio of the enthalpy rise across the fan to the enthalpy rise across the

low pressure compressor is constant, since they are on the same shaft. By using referencing, this ratio can be written as in Equation (86).

$$\frac{h_{t13}-h_{t2}}{h_{t2.5}-h_{t2}} = \frac{\tau_f-1}{\tau_{cL}-1} = \frac{(\tau_f-1)_R}{(\tau_{cL}-1)_R} \quad (86)$$

Therefore,  $\tau_f$  and  $\tau_{cL}$  can be found with the Equations (87) and (88) respectively.

$$\tau_f = 1 + \frac{1-\tau_{tL} \eta_{mL} \quad 1-\beta-\varepsilon_1-\varepsilon_2 \quad 1+f \frac{\tau_\lambda \tau_{tH}}{\tau_r} + \varepsilon_1 \tau_{tH} + \varepsilon_2 \quad \tau_{cL} \tau_{cH} \quad \frac{(1+\alpha) P_{TOL}}{\tau_r \eta_{mPL} m_0 h_0}}{\frac{(\tau_{cL}-1)_R}{(\tau_f-1)_R} + \alpha} \quad (87)$$

$$\tau_{cL} = 1 + (\tau_f - 1) \frac{(\tau_{cL}-1)_R}{(\tau_f-1)_R} + \alpha \quad (88)$$

From the definition of fan efficiency and using the subroutine FAIR to find the reduced pressure  $P_{rt13i}$  from the enthalpy at state t13i ( $h_{t13i}$ ), the fan pressure ratio can be calculated by Equation (89).

$$\pi_f = \frac{P_{rt13i}}{P_{rt2}} \quad (89)$$

Alike with the fan pressure ratio, using the definition of Low Pressure Compressor efficiency and using the subroutine FAIR to find the reduced pressure  $P_{rt2.5i}$  from the enthalpy at state 2.5i ( $h_{t2.5i}$ ), the Low Pressure Compressor pressure ratio can be calculated by Equation (90).

$$\pi_{cL} = \frac{P_{rt2.5i}}{P_{rt2}} \quad (90)$$

#### 2.2.4.2 High Pressure Compressor

The high pressure spool power balance of Equation (64) can be rearranged to yield the relation given in Equation (91) to calculate the High Pressure Compressor temperature ratio for performance cycle analysis.

$$\tau_{cH} = \frac{1+ \quad 1-\tau_{tH} \quad \eta_{mH} \quad 1-\beta-\varepsilon_1-\varepsilon_2 \quad 1+f \frac{\tau_\lambda}{\tau_r \tau_{cL}} \quad \frac{(1+\alpha) P_{TOL}}{\tau_r \tau_{cL} \eta_{mPH} m_0 h_0}}{1-\varepsilon_1 \quad 1-\tau_{tH} \quad \eta_{mH}} \quad (91)$$



From the definition of High Pressure Compressor efficiency and using the subroutine FAIR to find the reduced pressure  $P_{rt3i}$  from the enthalpy at state t3i ( $h_{t3i}$ ), the High Pressure Compressor pressure ratio can be calculated by Equation (92).

$$\pi_{cH} = \frac{P_{rt3i}}{P_{rt2.5}} \quad (92)$$

#### 2.2.4.3 Engine By-Pass Ratio ( $\alpha$ )

An expression for the engine by-pass ratio ( $\alpha$ ) follows directly from its definition given in Equation (30) and  $m_F$  and  $m_C$  can be rewritten in terms of the Mass Flow Parameters and area ratios as in Equations (93) and (94) respectively.

$$\dot{m}_F = \frac{P_0 \pi_r \pi_d \pi_f \pi_{nf} A_{19}}{\sqrt{T_{t13}}} MFP_{19} \quad (93)$$

$$\dot{m}_C = \frac{P_0 \pi_r \pi_d \pi_{cL} \pi_{cH} \pi_b A_4}{(1-\beta-\varepsilon_1-\varepsilon_2)(1+f)\sqrt{T_{t4}}} MFP_4 \quad (94)$$

By using Equations (93) and (94), the relation for the engine by-pass ratio is obtained as in Equation (95).

$$\alpha = \frac{(1-\beta-\varepsilon_1-\varepsilon_2)(1+f)}{\pi_{cL} \pi_{cH} \pi_b / (\pi_f \pi_{nf})} \sqrt{\frac{T_{t4}}{T_{t13}}} \frac{MFP_{19} A_{19}}{MFP_4 A_4} \quad (95)$$

#### 2.2.4.4 Engine Mass Flow Rate ( $m_0$ )

Conservation of mass and the definition of the by-pass ratio ( $\alpha$ ) yield the relation that can be used for calculating the engine mass flow rate given in Equation (96).

$$\dot{m}_0 = \frac{P_0 \pi_r \pi_d \pi_{cL} \pi_{cH} \pi_b}{(1-\beta-\varepsilon_1-\varepsilon_2)(1+f)} \frac{A_4}{\sqrt{T_{t4}}} MFP_4 \quad (96)$$

#### 2.2.4.5 Mach Number at Station 9 and 19 ( $M_9$ and $M_{19}$ )

The Mach number at Station 9 depends on the pressure ratio  $\frac{P_{t9}}{P_9}$  given in Equation (97) and the compressible flow subroutine RGCOMPR<sup>†</sup> is input this total to static pressure ratio in combination with the fuel to air ratio at the Low Pressure Turbine exit and the Mach Number at Station 9 as output. [3]

$$\frac{P_{t9}}{P_9} = \frac{P_0}{P_9} \pi_r \pi_d \pi_{cL} \pi_{cH} \pi_b \pi_{tH} \pi_{tL} \pi_n \quad (97)$$

For the by-pass airstream, the pressure ratio is given by Equation (98).

$$\frac{P_{t19}}{P_{19}} = \frac{P_0}{P_{19}} \pi_r \pi_d \pi_f \pi_{nf} \quad (98)$$

### 2.3. Rotating Component Design Theory

#### 2.3.1 Fan and Compressor Aerodynamics

The design methodology that will be discussed in this section is valid only for axial flow, constant axial velocity, repeating stage and repeating row mean-line design. The basic building block of the aerodynamic design of axial flow compressors is the cascade, an endlessly repeating array of airfoils that contains stationary (stator) and rotating (rotor) airfoils. The velocity triangles and angle relations of a compressor stage are given in Figure 7.

<sup>†</sup>RGCOMPR is a subroutine used in Mattingly J.D. et al. [3] that includes compressible flow functions. It has 5 different methods and every method calculates the Mach Number, Total to Static Temperature and Pressure Ratios, and the Mass Flow Parameter. The methods differ from each other by the input set or the input Mach Number range.

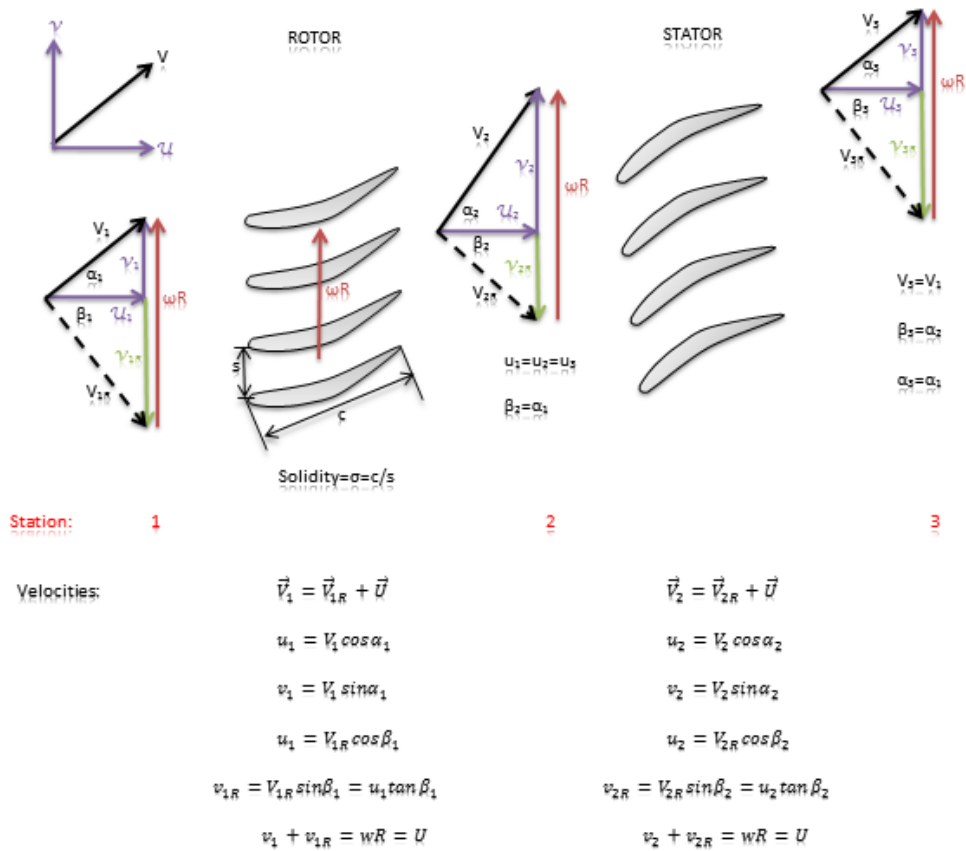


**Figure 7** Compressor Stage Nomenclature and angle relations from [3]

Each cascade passage acts as a small diffuser and is said to be well designed or behaved when it provides a large static pressure rise without incurring unacceptable total pressure losses and/or flow instabilities caused by shockwaves and/or boundary layer separation. The aim of the compressor design is to find the cascade parameters and airfoil contours that make this happen.

After finding a satisfactory airfoil cascade, next step is to place it in a series with a rotor that is made up of the same airfoils in mirror image about the axial location, which are moving at a speed that maintains the original relative inlet flow angle. A compressor stage (that is stator plus rotor) is generated from a cascade, and likewise placing similar stages in series can create a multi-stage compressor [3]. In compressors, the cascade has

stator at the front and rotor at the end, whereas in turbines the cascade has the rotor at the front and the stator at the end. [2]

A commonly employed measure of the degree of difficulty when designing a successful compressor cascades or airfoil rows; is the “diffusion factor”, which is expressed empirically as in Equation (99).

$$D \cong 1 - \frac{V_e}{V_i} + \frac{v_i - v_e}{2\sigma V_i} \quad (99)$$

The subscripts “i” and “e” in Equation (99) correspond to inlet and exit of the cascade, respectively. The diffusion factor is an analytical measure directly related to the size of the adverse pressure gradient to be encountered by the boundary layer on the suction surface of the cascade airfoil. It is therefore a measure of the danger of the boundary layer separation an unacceptable losses or flow instability.

The goal of a good design is to have high aerodynamic efficiency at large values of D because that allows the number of stages (that is lower  $V_e/V_i$ ), and/or airfoils (that is lower  $\sigma$ ) to be reduced. D is generally taken around 0.5 in recent technology level.

### 2.3.1.1 Flow Field Geometry Design

According to Horlock J.H. [8], there exist no precise rules for the design of axial flow compressors as for every design problem and it is essentially a trial and error process. However, some preliminary design methods are given in Mattingly J.D. et al. [6] and Horlock J.H. [8] that may serve as the basis of an axial flow compressor design algorithm.

The assumptions for the method suggested by Mattingly J.D. et al [3] are given as follows:

- Repeating row/repeating airfoil cascade geometry will be used. That is  $\alpha_1 = \beta_2 = \alpha_3$ ,  $\beta_1 = \alpha_2 = \beta_3$  (refer to Figure 8)
- 2 Dimensional flow through the cascades; that is no property variation or velocity component normal to the flow exists
- Constant axial velocity ( $u_1 = u_2 = u_3$ )

- Stage Polytropic Efficiency ( $e_c$ ) completely represents the stage losses
- Constant mean radius
- Calorically Perfect Gas with constant  $\gamma_c$  and  $R_c$ .

The diffusion factor ( $D$ ), cascade inlet flow Mach number ( $M_1$ ), specific heat ratio for compressor  $\gamma_c$  and polytropic efficiency ( $e_c$ ) are the inputs of this analysis. The analysis should include the following considerations:

1) *Conservation of Mass*: The conservation of mass law produces the relation given in Equation (100) for the stage.

$$m = \rho_1 u_1 A_1 = \rho_2 u_2 A_2 = \rho_3 u_3 A_3 \quad \text{or} \quad \rho_1 A_1 = \rho_2 A_2 = \rho_3 A_3 \quad (100)$$

2) *Repeating Row Constraint*: Since  $\beta_2 = \alpha_1$  then the relative velocity component of rotor in the vertical direction will be as in Equation (101)

$$v_{2R} = v_1 = wr - v_2 \quad (101)$$

Incidentally since  $\beta_3 = \alpha_2$ , then the relative velocity component at the stator exit in the vertical direction is equal to the velocity component at the rotor exit in the vertical direction ( $v_{3R} = v_2$ ) and then by using Equation (100) it can be found that the velocity conditions at the stage exit are identical to those at the stage entrance as stated in Equation (102).

$$v_3 = v_1 \quad (102)$$

3) *Diffusion Factor*: When the diffusion factor relation given in Equation (99) is written for both rotor and stator separately, because of the repeating row constraint it can be found that they are equal for both sides and they need to be evaluated only once for the entire stage. Therefore rearranging Equation (99) and solving for  $\alpha_2$  gives a relationship that can be used to determine the value of  $\alpha_2$  with known solidity, diffusion factor and  $\alpha_1$  angle. This relation is given in Equation (103).

$$\cos(\alpha_2) = \frac{2\sigma(1-D)\Gamma + \sqrt{\Gamma^2 + 1 - 4\sigma^2(1-D)^2}}{\Gamma^2 + 1}$$

$$\Gamma \cong \frac{2\sigma + \sin(\alpha_1)}{\cos(\alpha_1)} \quad (103)$$

There is a unique value of  $\alpha_2$  that corresponds to the chosen value of the diffusion factor (D), and solidity ( $\sigma$ ) for each  $\alpha_1$ . Thus, the entire flow field geometry is dictated by those choices.

4) *Degree of Reaction ( ${}^\circ R_c$ )*: It is defined as the ratio of static temperature rise of rotor to the stage temperature rise of the stage. It is another type of measure of a successful compressor design together with the diffusion factor (D). The mathematical expression of this term is given in Equation (104).

$${}^\circ R_c = \frac{T_2 - T_1}{T_3 - T_1} \quad (104)$$

For a perfect gas with constant density, the degree of reaction is equal to the ratio of static pressures. In the general case, it is desirable to have  ${}^\circ R_c$  in the vicinity of 0.5 for the compressors because the stator and rotor rows will then share the burden of the stage static temperature rise and neither will benefit at the expense of the other. This is an alternative way to avoid excessively large values of diffusion factors [3]. Horlock J.H. [8] states that according to the experimental studies, optimum stage efficiency may occur in higher degrees of reactions (around 0.6). Therefore the upper limit of the degree of reaction may be set higher than 0.5 in the design algorithms.

5) *Stage Total Temperature Increase/Rise ( $\Delta T_t$ ) and Total Temperature Ratio ( $\tau_s$ )*: By using the Euler pump and turbine equation with constant radius together with Equation (101) yields the relation for the Total Temperature Increase given in Equation (105).

$$\frac{\Delta T_t}{\frac{V_1^2}{c_p g_c}} = \frac{\cos^2(\alpha_1)}{\cos^2(\alpha_2)} - 1 \quad (105)$$

Since  $V^2 = M^2 \gamma R g_c T$  and using Equation (5) to convert total temperatures in Equation (105) to static temperatures, the relation for Stage Total Temperature Ratio is obtained as in Equation (106).

$$\tau_S \cong \frac{T_{t3}}{T_{t1}} = \frac{\gamma-1}{1+\frac{\gamma-1}{2}M_1^2} \frac{\cos^2 \alpha_1}{\cos^2 \alpha_2} - 1 + 1 \quad (106)$$

For a given flow geometry, the stage total temperature rise is proportional to  $T_{t1}$  and  $M_1$  [3]. Stage Total Temperature rise determine the number of stages of the compressor at the beginning of the turbomachinery design, and the total temperature ratio should satisfy the cycle analysis result in order to have an appropriate design.

- 6) *Stage Pressure Ratio ( $\pi_S$ )*: A primary objective of a compressor blade is to produce a rise in static pressure as well as a deflection of the flow angle. [10] A relevant performance parameter is therefore the static pressure rise per stage. The relation for stage pressure ratio for calorically perfect gases is given in Equation (107).

$$\pi_S = \frac{P_{t3}}{P_{t1}} = \frac{T_{t3}}{T_{t1}}^{\gamma_{ec}/(\gamma-1)} = \tau_S^{\gamma_{ec}/(\gamma-1)} \quad (107)$$

- 7) *Stage Efficiency ( $\eta_S$ )*: It is defined as the ratio of total temperature difference of an ideal (irreversible) compressor stage to actual total temperature difference.[8] The relation for stage efficiency is given in Equation (108a).

$$\eta_S = \frac{T_{t3i}-T_{t1}}{T_{t3}-T_{t1}} = \frac{\pi_S^{(\gamma-1)/\gamma}}{\tau_S-1} = \frac{\tau_S^{ec}-1}{\tau_S-1} \quad (108a)$$

Another expression including the loss coefficient ( $\xi$ ), which is an indicator of total pressure loss per cascade airfoil, and the cascade angles is given in Equation (108b).

$$\eta_s = \frac{(1-\xi) \left[ \frac{1}{(\cos(\alpha_1))^2} - \frac{1}{(\cos(\alpha_2))^2} \right]}{\frac{1}{(\cos(\alpha_1))^2} - \frac{1}{(\cos(\alpha_2))^2}} \quad (108b)$$

- 8) *Stage Exit Mach Number ( $M_3$ )*: The Mach Number gradually decreases as the flow progresses through the compressor causing compressibility effects to become less important. This situation is a result driven by using Equation (109).

$$\frac{M_3}{M_1} = \sqrt{\frac{T_3}{T_1}} = \sqrt{\frac{1}{\tau_s \left[ 1 + \frac{(\gamma-1)}{2} M_1^2 \right] - \frac{(\gamma-1)}{2} M_1^2}} \leq 1 \quad (109)$$

Since  $\frac{T_3}{T_1} < 1$ , then  $\frac{M_3}{M_1} < 1$  therefore the Stage Exit Mach Number should always be less than the inlet Mach number and this situation should be checked during the design.

- 9) *Wheel Speed to Inlet Velocity Ratio ( $wR/V_1$ ):* One of the most important trigonometric relationships (given in Equation (110)) is that between the wheel speed ( $wR$ ) and the total cascade entrance velocity ( $V_1$ ) because the latter is usually known and the former puts constraints to the materials and structures that should be used in the compressor which may difficult to satisfy.

$$\frac{wR}{V_1} = \cos(\alpha_1)(\tan \alpha_1 + \tan \alpha_2) \quad (110)$$

- 10) *Inlet Relative Mach Number ( $M_{1R}$ ):* Excessively high inlet relative Mach numbers may cause the compressor to surge or stall, therefore inlet Mach number should be chosen carefully. In order to make a proper choice, the relation given in Equation (111) can be used.

$$\frac{M_{1R}}{M_1} = \frac{\cos(\alpha_1)}{\cos(\alpha_2)} \quad (111)$$

Since  $\alpha_2 > \alpha_1$ , then by using Equation (111) it can be found that  $M_{1R} > M_1$ , therefore this is another condition that must be checked during the turbomachinery design. [3]

- 11) *Flow Coefficient ( $\Phi$ ):* In compressible flow machines, the flow coefficient ( $\Phi$ ) is an important parameter for design and analysis. It is defined as the ratio of the average meridional velocity to the mean blade speed as given in Equation (112). As the flow coefficient increases, the flow turning required reduces. Hence, the diffusion through the blades is found to reduce as flow coefficient increases. Higher values of flow coefficient correspond to smaller diameter machines for a fixed mass flow rate. However, very high flow coefficients may cause compressors to have higher relative inlet Mach numbers that causes losses from choking and shock waves. [10]



Therefore a typical value for compressor design suggested by Dixon et al. [10] is between 0.4 and 0.8.

$$\phi = \frac{c_m}{U} = \frac{m}{\rho_1 A_1 U_1} = 2(1 - \circ R_c - \psi * \tan \alpha_1 ) \quad (112)$$

In Equation (112),  $\psi$  indicates the Stage Loading Coefficient.

12) *Stage Loading Coefficient ( $\psi$ )*: The stage loading is related with the total enthalpy rise through the stage. It is therefore related with the flow geometry as well. The relation for stage loading ( $\psi$ ) is given in Equation (113).

$$\psi = \frac{h_{03} - h_{01}}{U^2} = \phi(\tan \alpha_2 - \tan(\alpha_1)) \quad (113)$$

The choice of stage loading at the compressor design point is critical. Too low stage loading will lead to an excessive number of compressor stages to achieve a required pressure ratio. A value of too high stage loading will limit the operating range of the compressor and increase the number of airfoils needed to remove the risk of flow separation. For these reasons the stage loading for compressors are typically limited around 0.4, but in more advanced compressor designs (especially the high pressure compressor designs) may have higher stage loadings. [10]

The behavior of every imaginable repeating row compressor stage with given values of diffusion factor, inlet Mach number, specific heat ratio, solidity, and polytropic efficiency can be computed with the 12 design points given previously are considered. This is done by selecting any initial value for  $\alpha_1$ , stage loading and flow coefficient. The rest of the process is to follow the sequence of equations expressed as functional relationships shown below.

$$\alpha_2 = f(D, \sigma, \alpha_1) \quad \text{Equation (103)}$$

$$\Delta\alpha = \alpha_2 - \alpha_1$$

$$\tau_s = f(M_1, \gamma, \alpha_1, \alpha_2) \quad \text{Equation (106)}$$

$$\pi_s = f(\tau_s, \gamma, e_c) \quad \text{Equation (107)}$$

$$wR V_1 = f(\alpha_1, \alpha_2) \quad \text{Equation (110)}$$

$$M_{1R} M_1 = f(\alpha_1, \alpha_2) \quad \text{Equation (111)}$$

It should be noted that only  $\tau_s$  and  $\pi_s$  depend upon  $M_1$  and that the process may be repeated to cover the entire range of reasonable values of  $\alpha_1$ .

### 2.3.1.2 Airfoil Geometry

After the repeating row compressor stage flow field geometry has been selected, the following step is to design the physical airfoils that will make it happen. The necessary nomenclature and angle definitions for airfoil design are shown in Figure 8.

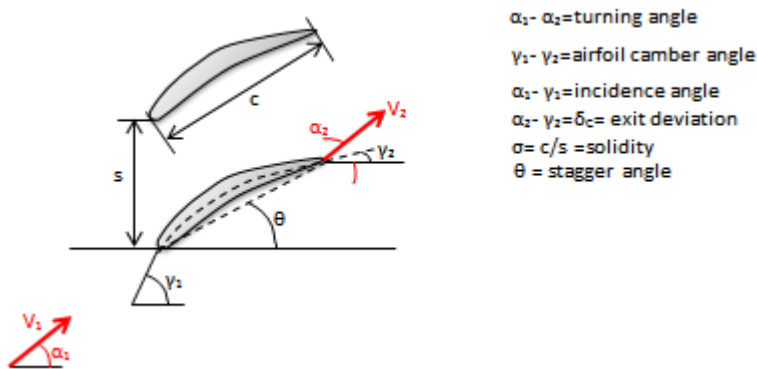


**Figure 8** The nomenclature and angular relations given for the airfoil design step in [3]

A useful method for determining the metal angles  $\gamma_1$  and  $\gamma_2$  at the design point is to take  $\gamma_1 = \alpha_1$  and using the Carter's Rule given in Equation (114) [3].

$$\delta_c = \frac{\gamma_1 - \gamma_2}{4\sqrt{\sigma}} \quad (114)$$

$$\gamma_2 = \alpha_2 - \delta_c$$

A useful relation between the solidity and Stage Loading and Flow Coefficient is given in Equation (115) by Korpela [9].

$$c/s = \frac{1.5\psi}{1.55\phi - \psi} \quad (115)$$

### 2.3.1.3 Flow path Dimensions

The necessary design inputs for a satisfactory sketch of the fan and compressor flow path is obtained in the previous steps explained in previous chapters. An entire compressor may now be created by placing a sufficient number “n” of repeating row stages in succession so that  $n \Delta T_{t \text{ stage}} \geq \Delta T_{t \text{ compressor}}$  to maintain the same values of  $V_1$  and  $\alpha_1$  for every stage at the mean radius. The flow path design nomenclature and necessary relations are given in Figure 9.

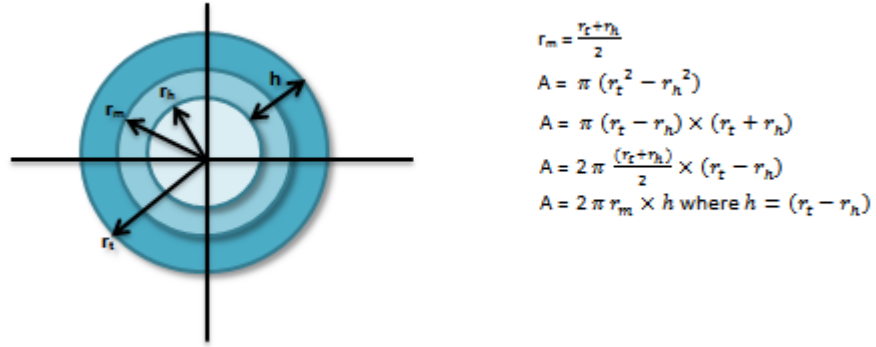


**Figure 9** Throughflow annulus dimensions for mean-line compressor design [3]

By using Equation (100) and Equation (116), a realistic estimation of the ratio of the compressor inlet area to exit area  $A_2/A_3$  can be made.

$$\frac{A_2}{A_3} = \frac{\rho_3}{\rho_2} \cong \frac{\rho_{t3}}{\rho_{t2}} = \frac{P_{t3} T_{t2}}{P_{t2} T_{t3}} = \frac{T_{t3}}{T_{t2}} \frac{\gamma e_c}{\gamma - 1} \frac{T_{t2}}{T_{t3}} = \frac{T_{t3}}{T_{t2}} \frac{1 - \gamma}{\gamma - 1} \frac{1 - e_c}{\gamma - 1} = 1 + \frac{n \Delta T_t}{T_{t2}} \frac{1 - \gamma}{\gamma - 1} \frac{1 - e_c}{\gamma - 1} = \frac{P_{t3}}{P_{t2}} \frac{1 - \gamma(1 - e_c)}{\gamma e_c} \quad (116)$$

Equation (116) reveals that the throughflow area “A” diminishes continuously and rapidly from the front of the compressor to the back. This is the origin of the typical shrinking shape of the compressor annulus, and the reason for very small heights of the airfoils at the final stages. Because the design analysis in Section 2.3.1.2 provides total temperatures, total pressures and Mach numbers for any station “i”, the mass flow

parameter affords the most direct means of determining the throughflow area given in Equation (117).

$$A_i = \frac{\dot{m} \sqrt{T_{ti}}}{MFP \cos(\alpha_i) P_{ti}} \quad (117)$$

The throughflow area can be calculated by using Equation (117) and the mean radius is tied to the required rotor speed at the mean radius  $\omega_{rm}$ .

Blade axial widths ( $W_r$  and  $W_s$ ) of a stage can be calculated for a selected chord-to-height ratio  $((c/h)_r$  and  $(c/h)_s$ ) for the rotor and stator blades, and the blade stagger angle at the rotor hub ( $\theta_{rh}$ ) and the stator tip ( $\theta_{st}$ ) as given in Equation (118).

$$W_r = \frac{h_1 + h_2}{2} \left( \frac{c}{h} \right)_r \cos(\theta_{rh})$$

$$W_s = \frac{h_2 + h_3}{2} \left( \frac{c}{h} \right)_s \cos(\theta_{st}) \quad (118)$$

The spacing between the blade rows can be estimated as one-quarter of the width of the preceding row. [3]

#### 2.3.1.4 Radial Variation of Flow Geometry

In some applications, the compressor, fan and turbine airfoils are twisted from hub to tip. The reason is the inevitable fact that the rotating airfoils subject to solid body motion and therefore have a rotational speed that increases linearly with radius. If an amount of work on the fluid passing through a stage that is independent of radius is made, the Euler pump and turbine equations reveal that less change in tangential velocity (or “turning” the flow) will be required as the radius increases. In addition, the static pressure must increase with radius in order to maintain the radial equilibrium because of the tangential velocity or “swirling” of the flow. All of the airfoil and flow properties must therefore vary with radius. There are three types of swirl distributions are considered and they are given as follows:

- Free Vortex Swirl Distribution

- Exponential Swirl Distribution
- 1<sup>st</sup> Power Swirl Distribution

The swirl distributions affect the degree of reaction of the compressor and the free vortex swirl distribution yields minimum flow property changes in the radius from the mean-line design. However, depending on the design choices, other types of swirl distributions can also be selected. [3]

### **2.3.2 Turbine Aerodynamics**

The design methodology that will be discussed in this section is valid only for constant axial velocity, adiabatic, selected inlet Mach number and mean-line stage design. The design of turbines is different from that of compressors for a number of reasons including the following:

- The turbine stage entrance stator (i.e. inlet guide vanes or nozzle) should be choked and all other stator and rotor airfoil rows should not be choked.
- The density of the working fluid changes dramatically, so that compressibility or Mach number effects must be included.
- The turbine generates rather than absorbs power.
- High inlet temperatures require that heat transfer and cooling must also be considered.
- There are no wide-ranging rules for choosing turbine flow and airfoil geometries such as the compressor diffusion factor.

A typical turbine stage and its velocity diagrams are shown in Figure 10.

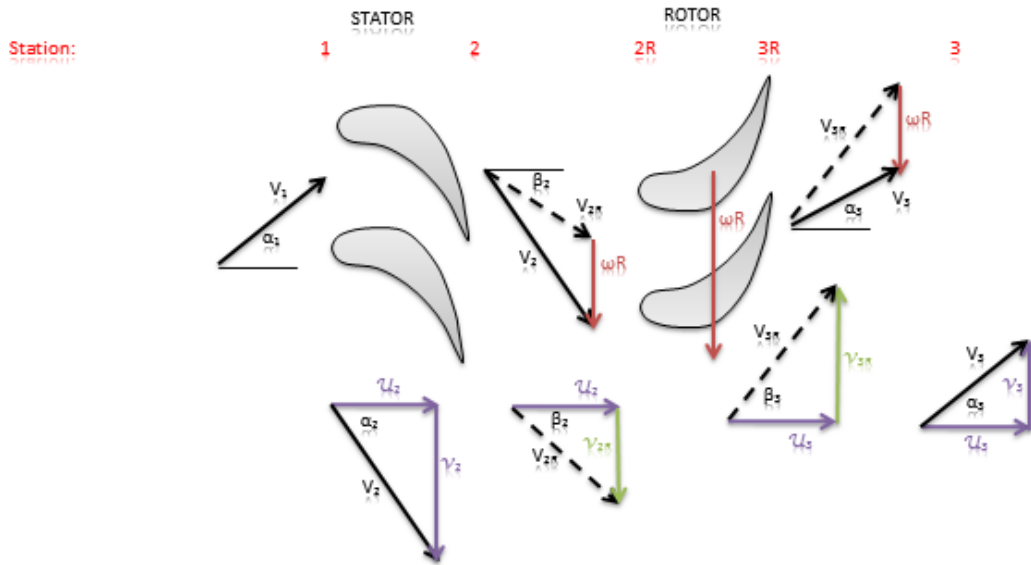


**Figure 10** Velocity triangles, angle definitions and nomenclature are shown on a typical turbine stage [3]

The Euler Turbine Equation gives the energy per unit mass flow exchanged between the rotor and the fluid for constant radius in Equation (119).

$$h_{t2} - h_{t3} = c_{pt} T_{t2} - T_{t3} = \frac{\omega R}{g_c} (v_2 + v_3) \quad (119)$$

As can be seen from the velocity triangles shown in Figure 12, because of the large angle  $\alpha_2$  at the stator (nozzle) exit and the large turning possible in the rotor the value of  $v_3$  is often positive (positive  $\alpha_3$ ). As a result, the two swirl velocity terms on the right hand side of Equation (119) add, giving larger power output. Because of the compressibility effects, the rotor degree of reaction  ${}^{\circ}R_t$  has a definition that is more suitable to turbines, which is the rotor static enthalpy drop divided by the stage total enthalpy drop. Degree of Reaction for turbines is given in Equation (120) for calorically perfect gases.

$${}^{\circ}R_t = \frac{h_2 - h_3}{h_{t2} - h_{t3}} = \frac{T_2 - T_3}{T_{t2} - T_{t3}} \quad (120)$$

The static pressure drop is roughly proportional to the static temperature drop, and that the stator degree of reaction is approximately the difference between the rotor degree of reaction and 1.

### 2.3.2.1 Flow Field Geometry Design

According to Horlock J.D. [7], as for the compressors, there are no precise rules for the design of a turbine can be formulated. The steps in a preliminary design are introduced both in Mattingly et al. [6] and Horlock J.D. [7], but it should be emphasized that the described methods is but one of many that could be used.

The assumptions for the method described in Mattingly et al. [3] are listed as follows:

- Stator exit Mach number ( $M_2$ ) and rotor exit relative Mach number ( $M_{3R}$ ) are fixed
- 2D Flow across the turbine (that is no property variation or velocity component normal to the flow)
- Constant axial velocity ( $u_1=u_2=u_3$ )
- Constant mean radius
- Adiabatic flow in the stator and rotor
- Calorically perfect gas with constant  $\gamma_t$  and  $R_t$

The following reductions introduced in Equation (121) are used throughout the analysis.

$$V' = \sqrt{g_c c_{pt} T_{t1}}$$

$$\Omega = \frac{\omega R}{V'} \quad (121)$$

This approach cannot be used to design a series of stages as it was for the compressors because the effect of steadily decreasing static temperatures, when combined with constant velocities, would eventually lead to supersonic velocities everywhere, contradicting one of the central design constraints. Thus, this method is primarily used to reveal the capabilities of individual turbine stages.

The analysis should include the following considerations in the given order since they are chained together with an unknown determined in the previous relation.

1) *Total Velocity at Station 2 ( $V_2/V'$ )*: The total velocity at the stator exit is given in Equation (122).

$$\frac{V_2}{V'} = \sqrt{\frac{(\gamma_t - 1)M_2^2}{1 + \frac{(\gamma_t - 1)}{2}M_2^2}} \quad (122)$$

2) *Stage Axial Velocity ( $u/V'$ )*: The stage axial velocity depends on the stator angle  $\alpha_2$  and stator exit velocity  $V_2$  as shown in Equation (123)

$$\frac{u}{V'} = \frac{V_2}{V'} \cos(\alpha_2) \quad (123)$$

3) *Tangential Velocity at Station 2 ( $v_2/V'$ )*: The tangential velocity at the stator exit is the sine component of the stator exit velocity as given in Equation (124).

$$\frac{v_2}{V'} = \frac{V_2}{V'} \sin(\alpha_2) \quad (124)$$

4) *Rotor Relative Tangential Velocity at Station 2 ( $v_{2R}/V'$ )*: This is the relative velocity of the tangential velocity at the stator exit, with respect to rotor. The relation is obtained by applying the relative velocity theorem between stator and rotor and given in Equation (125).

$$\frac{v_{2R}}{V'} = \frac{v_2}{V'} - \Omega \quad (125)$$

5) *Rotor Relative Flow Angle at Station 2 ( $\beta_2$ )*: The rotor relative flow angle is obtained by applying the tangent theorem to the triangle formed by rotor relative tangential velocity at stator exit and stage axial velocity components. The angle is found by the inverse tangent operation. The relation is given in Equation (126).



$$\tan(\beta_2) = \frac{v_{2R}/V'}{u/V'} \quad (126)$$

6) *Rotor Relative Total Temperature ( $T_{t2R}/T_{t1}$ ):* The rotor relative total temperature is the temperature rise obtained in the rotor. It is given in Equation (127).

$$\frac{T_{t2R}}{T_{t1}} = 1 + \Omega^2 \left( \frac{1}{2} - \frac{v_2/V'}{\Omega} \right) \quad (127)$$

7) *Rotor Relative Flow Angle at Station 3 ( $\beta_3$ ):* The rotor relative flow angle at the stage exit is obtained by applying the relation given in Equation (128). The angle is found by the inverse tangent operation.

$$\tan(\beta_3) = \sqrt{\frac{T_{t2R}/T_{t1}}{(u/V')^2} \frac{(Y_t - 1)M_{3R}^2}{1 + \frac{(Y_t - 1)}{2} M_{3R}^2} - 1} \quad (128)$$

8) *Rotor Flow Turning Angle:* This is the sum of the rotor relative flow angle at the rotor inlet and exit as shown in Equation (129).

$$\vartheta = \beta_2 + \beta_3 \quad (129)$$

9) *Tangential Velocity at Station 3 ( $v_3/V'$ ):* The rotor exit tangential velocity is given in Equation (130).

$$\frac{v_3}{V'} = \frac{u}{V'} \tan(\beta_3) - \Omega \quad (130)$$

10) *Stage Exit Flow Angle ( $\alpha_3$ ):* The stage exit flow angle, or exhaust swirl angle defined by Horlock J.D. [7], is a parameter that must be controlled in order to prevent high rotation between adjacent stages which may cause losses. It can be found with

applying tangent theorem in the triangle formed by the stage axial velocity and the tangential velocity at the rotor exit. The relation for stage exit flow angle is given in Equation (131).

$$\tan(\alpha_3) = \frac{v_3/V'}{u/V'} \quad (131)$$

- 11) *Static Temperature at Station 3 ( $T_3/T_{t1}$ )*: The static temperature at the rotor exit is the ratio of the rotor relative total temperature to the total to static temperature ratio at Station 3R (refer to Figure 12) as given in Equation (132).

$$\frac{T_3}{T_{t1}} = \frac{T_{t2R}/T_{t1}}{1 + \frac{(\gamma_t - 1)}{2} M_{3R}^2} \quad (132)$$

- 12) *Rotor Exit Relative Mach Number ( $M_{2R}$ )*: The relative Mach number at the rotor exit should always be less than 1 in order to prevent the separation of the suction boundary layer across the rotor that is caused by high degree of reaction requiring designs. This parameter can be calculated by using Equation (133).

$$M_{2R} = M_1 \sqrt{\frac{1 - \frac{(\omega r)^2}{2g_c C_{pt} T_{t1}} \left(1 + \frac{2}{(\gamma_t - 1) M_1^2}\right) \{4(1 - \theta_{R_t})^2 - 1\}}{1 - \left(1 + \frac{\gamma_t - 1}{2} M_1^2\right) (1 - \tau_s) \theta_{R_t}}} \quad (133)$$

Equation (133) also shows that for avoiding reaching supersonic Mach number in turbine rotor blades, the degree of reaction should be less than 0.5.

- 13) *Stage Temperature Ratio ( $\tau_s$ )*: The total temperature rise across the turbine stage can be found by using Equation (134).

$$\tau_{tS} = \frac{T_{t3}}{T_{t1}} = \frac{T_3}{T_{t1}} + \left(\frac{u}{V'}\right)^2 \frac{(1 + \tan^2(\alpha_3))}{2}$$

(134)

- 14) *Stator Exit Flow Angle ( $\alpha_1$ ):* The flow angle at the stator exit (at Station 1 of the cascade) can be found by using Equation (135).

$$\sin(\alpha_1) = (1 - \tau_S) \sqrt{\left\{1 + \frac{2}{(\gamma_t - 1)M_1^2}\right\} \frac{g_c C_{pt} T_{t1}}{2(\omega r)^2}}$$

(135)

- 15) *Rotor Degree of Reaction ( ${}^\circ R_t$ ):* The rotor degree of reaction can also be calculated by using the difference between the stator exit and rotor exit relative velocities and the stage temperature ratio as given in Equation (136). This is another important control parameter for the turbine design as for the compressors.

$${}^\circ R_t = \frac{v_{3R}^2 - v_{2R}^2}{2(1 - \tau_S)V'^2}$$

(136)

- 16) *Stage Loading Coefficient ( $\psi$ ):* It is defined as the ratio of the stagnation enthalpy change through a stage to the square of the blade speed. The stage loading coefficient for an adiabatic turbine is given in Equation (137). High stage loading implies large flow turning and leads to highly “skewed” velocity triangles to achieve this turning. Since the stage loading is a non-dimensional measure of the work extraction per stage, a high stage loading is desirable because it means fewer stages are needed to produce a required work output [10].

$$\psi = \frac{g_c C_{pt} \Delta T_t}{(\omega R)^2}$$

(137)

$\Psi$  is generally between 1.4 and 2, however Horlock J.D. [7] states that it may be as high as 3 for advanced multi-stage turbines accepting high exit swirl angles (up to 40°).

17) *Stage Pressure Ratio* ( $\pi_{tS}$ ): After determining the turbine stage temperature ratio  $\tau_{tS}$ , the flow field and airfoil characteristics, stage pressure ratio can be calculated by using the formula given in Equation (138) for the calorically perfect gases.

$$\Pi_{tS} = \tau_{tS}^{\gamma_t / (\gamma_t - 1) e_s} \quad (138)$$

18) *Stage Efficiency* ( $\eta_{tS}$ ): The stage efficiency can be calculated by using the stage temperature and pressure ratios as given in Equation (139).

$$\eta_{tS} = \frac{1 - \tau_{tS}}{1 - \Pi_{tS}^{(\gamma_t - 1) / \gamma_t}} \quad (139)$$

By using the above relations, it is possible to design a turbine stage analysis algorithm [3].

### 2.3.2.2 Airfoil Geometry

The situation in unchoked turbines is similar to that in compressors except that the deviations are markedly smaller owing to the thinner boundary layers. The necessary nomenclature and angle definitions are the same with the compressor airfoils and they were given in Figure 10. The exit deviation angle is defined for turbines as in Equation (140).

$$\delta_t = \frac{\gamma_1 - \gamma_2}{8\sqrt{\sigma}} \quad (140)$$

When the turbine airfoil cascade exit Mach number is near 1, the deviation is usually negligible because the cascade passage is similar to a nozzle. [3]

### 2.3.2.3 Flow Path Dimensions

The flow path dimension calculations and the nomenclature presented in Section 2.3.1.3 are also applicable to turbines. Therefore, Figure 11 will be used in the turbine flow path dimension calculations.

### 2.3.2.4 Radial Variations

The discussion on compressor radial variation given in Section 2.3.1.4 is also applicable to turbines. However, because the mass flow rate per annulus area is higher in turbines than compressors, turbine airfoils are correspondingly shorter. Therefore little radial variation of aerodynamic properties from hub to tip is obtained except possibly in the last few stages of the Low Pressure Turbine. If the aerodynamic design of these stages were chosen as free vortex, then the rotor degree of reaction would be the same as for compressors but the sign of the pressure change is reversed. [3]

### 2.3.2.5 Turbine Cooling

The gas temperatures in modern turbines are high enough to damage all of the recent available materials used in turbines unless they are protected by cooling air. The undesirable heat may be carried or convected away by air flowing within the airfoils or prevented from reaching the airfoils by means of an unbroken external blanket of air. The cooling effectiveness is usually defined as in Equation (141).

$$\phi = \frac{T_g - T_m}{T_g - T_c} \quad (141)$$

In equation (141),  $T_g$  is the main-stream gas temperature,  $T_m$  is the average metal temperature, and  $T_c$  is the cooling air temperature. It should be noted that the cooling air temperature  $T_c$  can be less than the compressor discharge temperature  $T_{13}$  if the fluid is taken from an earlier compressor stage.  $\phi$  must lie between 0 and 1, the values which are closer to 1 indicates better cooling technology.

### 2.3.3 Structural Considerations

The effect of structural considerations acts as the same on both compressor and turbine. Turbomachinery rotor nomenclature in Mattingly et al. [6] will be used in this section and the developed algorithm, and it is shown in Figure 11.

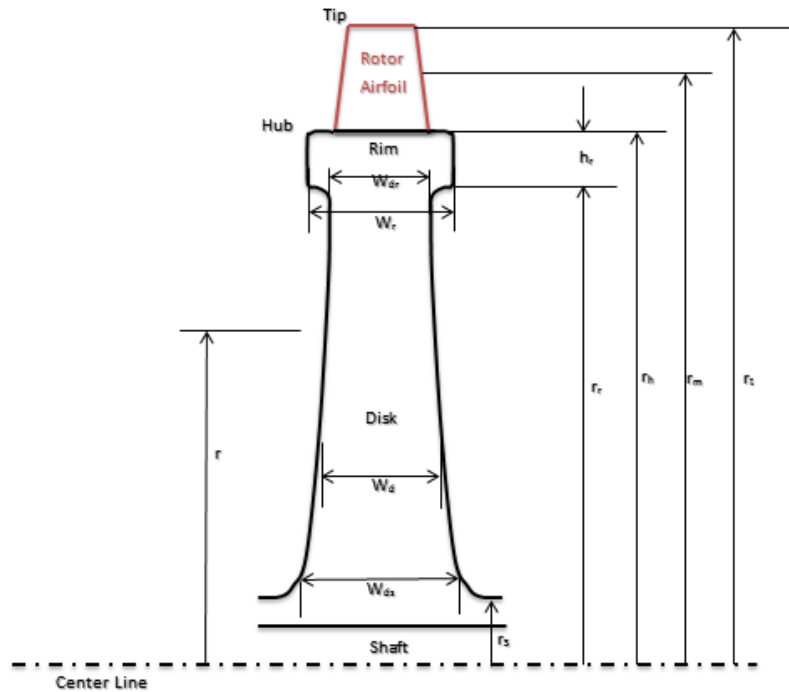


**Figure 11** The nomenclature used for turbomachinery rotors [3]

#### 2.3.3.1 Rotor Airfoil Centrifugal Stress ( $\sigma_c$ )

Because each cross sectional area of the rotor airfoil must restrain the centrifugal force on all of the material beyond its own radial location, the hub or base of the airfoil must experience the greatest force. The forces and stress distributions on a rotor blade is shown in Figure 12.

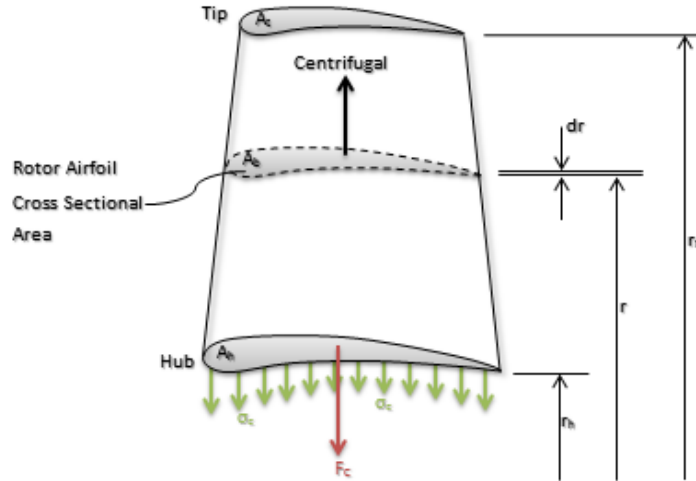


**Figure 12** The forces and stresses acting on a rotor airfoil [3]

The airfoil cross sectional area usually tapers down or diminishes with increasing radius, which has a reducing effect on the principle tensile stress on the rotor blade. If this taper is linear, then an average tensile stress, which can be applied directly in any situation, can be expressed as in Equation (142).

$$\sigma_c = \frac{\rho \omega^2 A}{4\pi} \left( 1 + \frac{A_t}{A_h} \right) \quad (142)$$

In general the ratio  $\frac{A_t}{A_h}$  is in between 0.8 and 1.0, and the area (A) in equation (144) is the flow path annulus area which is given by  $\pi(r_t^2 - r_h^2)$  as shown in Figure 11.

In Equation (142),  $\rho$  indicates the density of the material that the rotor is made from. According to Mattingly et al. [6] common rotor materials are Aluminum Alloy, Titanium Alloy, Wrought Nickel Alloy, High Strength Nickel Alloy or Single Crystal Super-Alloy. [3]

### 2.3.3.2 AN<sup>2</sup> Value

AN<sup>2</sup> represents a measure for the allowable airfoil material specific strength. Its definition is given in Equation (143) and its unit is “m<sup>2</sup>rpm<sup>2</sup>”.

$$AN^2 = \frac{2.323}{\pi(1 + A_t/A_h)} \frac{\sigma_c}{\rho} \quad (143)$$

The accepted practice is to use Equation (143) to calculate the allowable  $AN^2$  using material properties ( $\sigma_c/\rho$ ), and to compare that with the value actually required by the engine rotating parts. If the required  $AN^2$  exceeds the allowable  $AN^2$ , a superior material must be found or the flow path design must be changed. [3]

### 2.3.3.3 Disk of Uniform Stress

The rotating airfoils are inserted into slots which are called as “rims”, that maintain their circular motion. The disk supports and positions the rim while connecting it to the shaft. Its thickness is equal to the rim web thickness at the inside edge of the rim and generally grows as the radius decreases due to the accumulating centrifugal force that must be resisted. The most efficient way to use available disk materials is to design the disk for constant radial and circumferential stress. Because the rim and disk are one continuous piece of material, the design stress would be the same throughout.

Applying radial equilibrium to the infinitesimal element of the disk and taking the necessary integration will give the relation to calculate the disk thickness as shown in Equation (144).

$$\frac{W_d}{W_{dr}} = e^{\frac{\rho(\omega r_r)^2}{2\sigma_d} \left[1 - \left(\frac{r}{r_r}\right)^2\right]} \quad (144)$$

The disk thickness grows exponentially in proportion to  $(\omega r_r)^2$  which is the square of the rim velocity of the disk. [3]

### 2.3.3.4 Allowable Wheel Speed

The first term of the exponent in Equation (146) is named as Disk Shape Factor (DSF) and defined as in Equation (145).



$$DSF = \frac{\rho(\omega r_r)^2}{2\sigma_d} \quad (145)$$

The disk thickness distributions are obtained for different DSF values from 1 to 4, and the disk thicknesses in Figure 13. High DSF are used in radial compressor and turbines, whereas low DSF are common in axial compressors and turbines. [2]

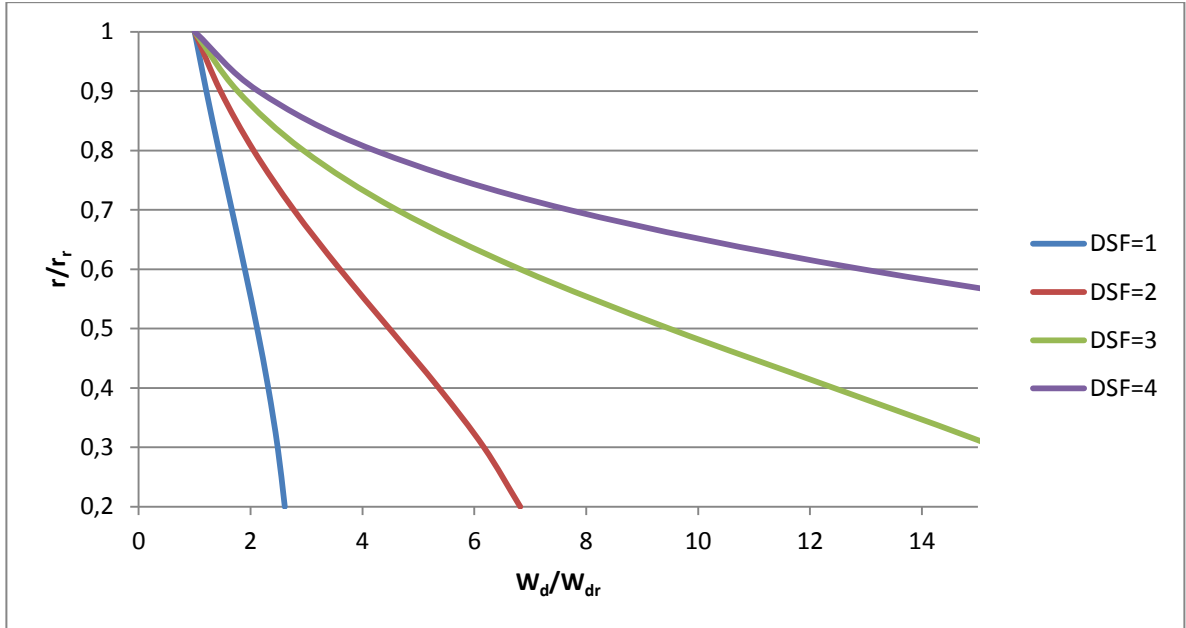


**Figure 13** Disk thickness distributions for different DSF values [3]

According to Figure 13, the maximum allowable value of DSF is not much more than 2 therefore the allowable wheel speed is defined as in Equation (146).

$$[\omega r_r]_{max} \cong \sqrt{\frac{4\sigma_d}{\rho}} \quad (146)$$

Allowable wheel speed is a surrogate for the allowable disk material specific strength. Because the annulus area  $A$  is largest on the low pressure spool and particularly for the first fan stage of High By-Pass ratio engines, the rotational speed  $\omega$  will most likely be limited by allowable blade centrifugal stress. Conversely on the high pressure spool,

where the annulus flow area is considerably smaller but the temperatures are higher, the rotational speed will most likely be limited by allowable wheel speed. [3]

## 2.4. Methodology

### 2.4.1 Variable Specific Heat Model

For the sake of reflecting the changes on thermodynamic parameters such as temperature, reduced pressure, enthalpy, heat capacity, gas constant and the speed of sound to temperature and pressure ratio calculations precisely, Variable Specific Heat Model is used throughout the cycle.

An efficient method is developed by Guha A. [12] in order to estimate the thermodynamic properties of combustion products including kerosene. The formulization given in [12] for the gas constant, specific heat at constant pressure and the specific heat ratio of air and kerosene mixture given in Equation (147), (148) and (149) respectively.

$$\frac{R_{combust}}{R_{air}} = \frac{1 + \aleph f}{1 + f} \quad (147)$$

$$\frac{c_{p,combust}}{c_{p,air}} = \frac{1 + f(\beth_0 + \beth_1 T - \beth_2/T^2)}{1 + f} \quad (148)$$

$$\gamma_{combust} = \frac{c_{p,combust}}{c_{p,combust} - R_{combust}} \quad (149)$$

The formulae given in Equations (147), (148) and (149) are valid not only for kerosene, but also for diesel, gasoline, natural gas, octane, propane, methane, and benzene. Only the constants  $\aleph$ , and  $\beth$  are changed for different types of fuels. These constants are given in Table 5 for the kerosene fuel.

**Table 5** The constants for kerosene and air mixture

$\kappa$	$\gamma_0$	$\gamma_1$	$\gamma_2$
1.016	2.465	$3.129 \cdot 10^{-4}$	$7.721 \cdot 10^{-4}$

For the three thermodynamic properties of air and kerosene mixture, the Engine Design Model uses the formulation in [12]. As can be seen from the equations (147) through (149), these formulas include thermodynamic properties of pure air. The thermodynamic properties of pure air are tabulated in Moran M.J. et al. [13] for different temperatures and can be used for the operational temperature range valid for a high by-pass turbofan engine. These values are also used in the cycle analysis of the engine parts before the combustor.

In addition to the three thermodynamic properties given above, the enthalpy and reduced pressure are also needed in cycle analysis calculations. These two properties of air and kerosene mixture are tabulated in Mattingly et al. [1] with respect to fuel to air ratio and temperature of the mixture. These two properties of pure air are also given by tables in [13] and these tables can be used for the operational temperature ranges of a high by-pass turbofan engine.

#### **2.4.2 An Iterative Solution Scheme for Performance Cycle**

As a consequence of having 16 dependent variables and 16 equations in the performance analysis, there are many different ways that the off-design cycle analysis equations can be ordered to obtain a solution. Mattingly J.D. et al. [3] suggest that the engine by-pass ratio ( $\alpha$ ), and the engine mass flow rate ( $m_0$ ) should be the preferred iteration variables for a high by-pass turbofan engine. Successful solution of the off-design performance depends on the convergence of these iteration variables. To begin a solution, initial estimates to these iteration variables should be made and they are suggested to be taken equal to their reference point values initially as in Equation (150) and (151).

$$m_0 = m_{0R} \quad (150)$$

$$\alpha = \alpha_R \quad (151)$$

An example flowchart is given in Figure 14 for high by-pass ratio turbofan engines. This figure is obtained by modifying the figure given for mixed turbofan engine by Mattingly et al. [3].

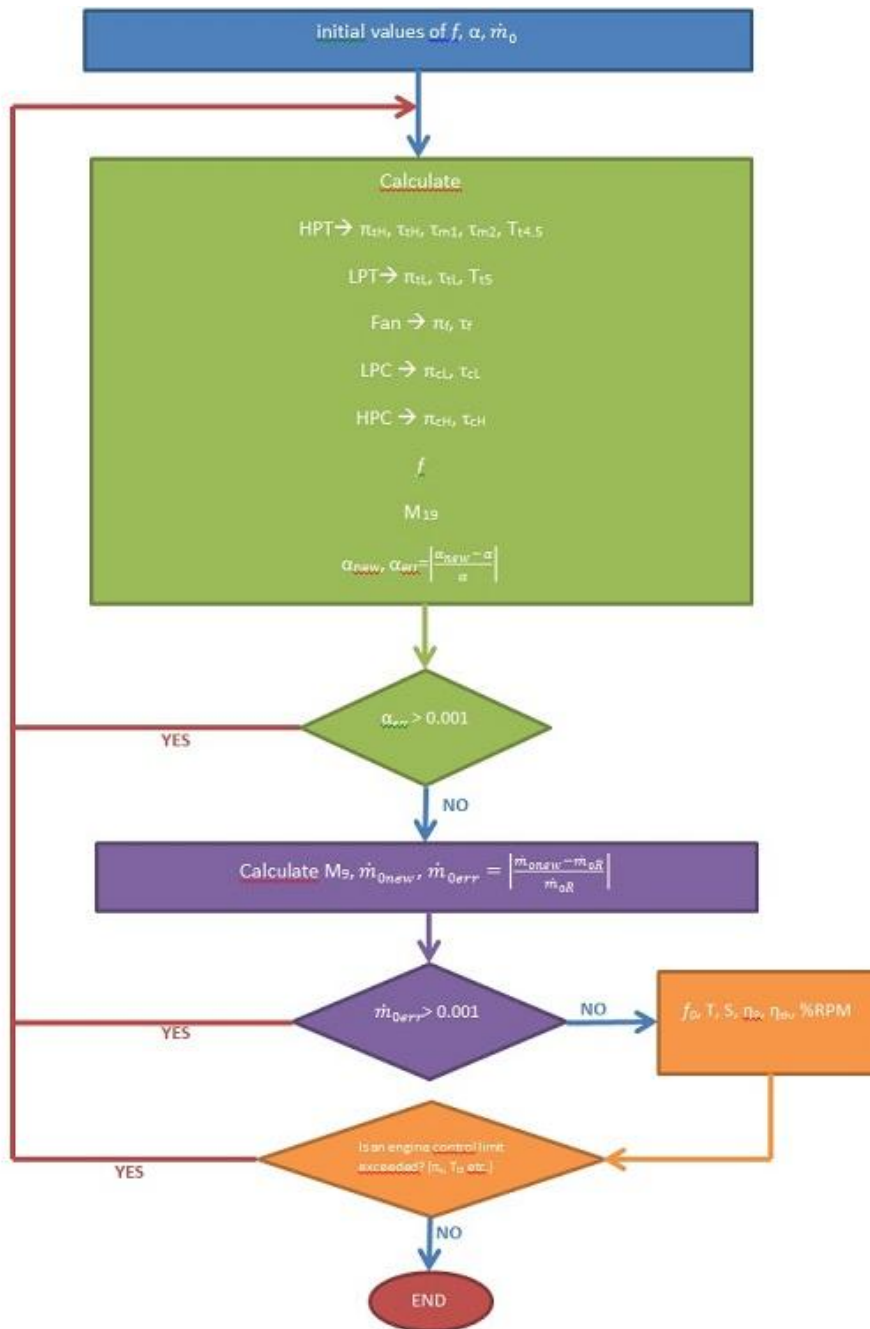


**Figure 14** Iterative Solution scheme for high by-pass turbofan engines

It should be noted that each equation given in Figure 14 can be solved, in principle, in the order listed for given initial estimates of the two component performance variables  $\alpha$  and  $m_0$ . As the solution progresses, these estimates are compared with their newly computed values and iterated if necessary until satisfactory convergence is obtained.

The first six quantities of the solution sequence ( $\pi_{tH}$ ,  $\tau_{tH}$ ,  $\tau_{m1}$ ,  $\tau_{m2}$ ,  $\pi_{tL}$  and  $\tau_{tL}$ ) can be determined by the iterative methods presented in Section 2.2.3. The fuel to air ratios  $f_{4.1}$  and  $f_{4.5}$  at Stations 4.1 and 4.5 respectively are required to solve the system of equations for variable specific heats. [3]

### **2.4.3 Key Points in a Turbomachinery Design Algorithm**

#### **2.4.3.1 Considerations in Compressor Design**

The most direct way to increase the stage pressure ratio ( $\pi_s$ ) is to increase  $M_1$  (or  $V_1$ ); that in order to operate at higher values of  $\alpha_1$  and  $\pi_s$  higher values of  $\omega R$  is required. The inlet Mach number ( $M_1$ ) must be less than 0.7 in order to avoid supersonic relative flow into the rotor. For a given constant degree of aerodynamic and mechanical difficulty (that is  $M_1$ ,  $V_1$  and  $\omega R$  or  $^{wR}V_1$  is fixed) increasing either diffusion factor ( $D$ ) or solidity ( $\sigma$ ) allows greater  $\pi_s$  and therefore the possibility of fewer stages. The analysis shown that; the effect of a change in diffusion factor always favors over the effect of the change in solidity. [3] These comments are shown graphically in Figure 15 that is a summary of numerical graphs obtained by Mattingly et al. [3], which shows the relation between  $\alpha_1$  and  $\pi_s$  with the change of different design parameters.

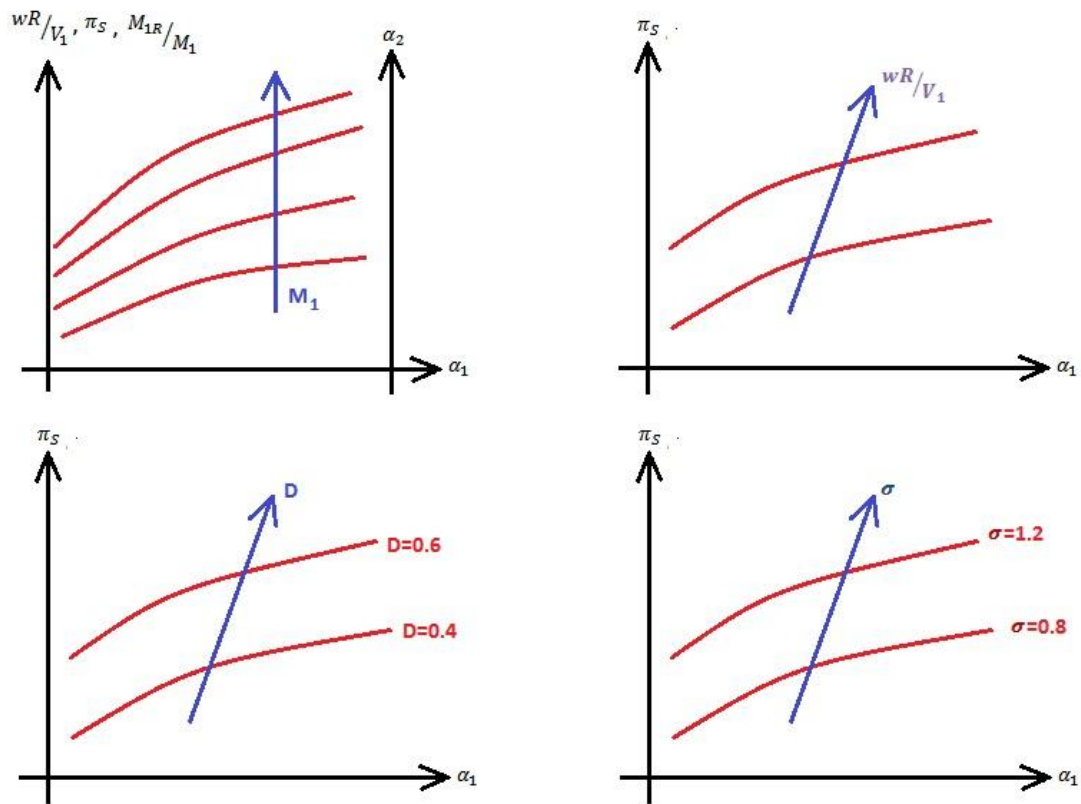


**Figure 15** Trends in stage pressure ratio with rotor inlet angle with the variation of inlet Mach number, rotor speed, diffusion factor and solidity

### 2.4.3.2 Considerations in Turbine Design

According to Mattingly et al. [3], the following points should be considered in the turbine design:

- Two different types of turbine stages must be considered, namely those having choked or unchoked stators. The former are required as the entrance stages for every turbine and will be represented in the analyses by  $M_2=1.1$ . The latter are required for all other turbine stages and will be represented with  $M_2=0.9$ .

- Higher values of rotor relative exit Mach numbers ( $M_{3R}$ ) always improve stage performance, provided that some margin to avoid rotor choking exists. Consequently,  $M_{3R}$  is set to 0.9 generally as maximum.
- The open literature strongly suggests that the best performance is obtained when  $60^\circ < \alpha_2 < 75^\circ$ . The open literature also concludes that larger values of  $\Omega$  are better, the upper limit being presently in the range  $0.2 < \Omega < 0.3$ . Every measure of aerodynamic thermodynamic performance for choked and unchoked stages is improved by increasing  $\Omega$ .

The engine cycle selection process presented in the preceding chapters determines High Pressure Turbine Inlet Temperature ( $T_{t4}$ ). The goal of the turbine design is to accomplish the desired work extraction with the minimum number of stages, which is equivalent to finding the minimum practical value of stage temperature ratio ( $\tau_{ts}$ ). Stage temperature ratio diminishes as  $\alpha_2$  increases and smaller values of stage temperature ratio are obtained for choked stators than unchoked ones as can be seen in Figure 13.

The smallest amount of boundary layer separation, even if the reattachment flows in the rotor airfoils is disastrous for turbines because the large local Mach numbers and dynamic pressures cause unacceptable aerodynamic (drag) losses. Unfortunately, as can be seen from Figure 13, the tendency to increasing  $\alpha_2$  causes a rapid increase in the rotor flow turning angle. This high flow turning causes boundary layer separation, especially when the average Mach numbers is near sonic and shock waves can arise.

A good design choice is to define rotor airfoil profiles that do not separate for flow turning angles ( $\beta_2 + \beta_3$ ) up to  $120^\circ$ - $130^\circ$  provided that the rotor degree of reaction is at least 0.20. These criteria are met as long as  $\alpha_2$  does not exceed approximately  $70^\circ$ , depending on the exact value of  $\Omega$ .

The stage exit flow angle or swirl, which should be kept small whether or not another stage follows. In the former case, a small  $\alpha_3$  reduces the total flow turning for the



succeeding inlet stator. In the latter case, the need for turbine exit guide vanes and their accompanying diffusion losses is reduced or avoided.

According to the discussions given after the turbine design analysis by Horlock J.D. [7], for the turbines larger axial velocities lead to smaller annulus areas and lower centrifugal stress. The centrifugal stress virtually fixes the nozzle angle. With the fixed nozzle angle, a compromise made between reaction, swirl, disc stresses and weight. Increasing the reaction lowers the Mach number relative to the blade but raises the disc stresses and blade root temperature. Increasing the exit swirl decreases the disc stresses but increases the Mach number relative to blade and the blade root temperature. The agreement of the turbine designers is that  $\alpha_3$  should not exceed  $40^\circ$ . The results presented in Figure 13 show that meeting this criterion depends strongly on both  $\alpha_2$  and  $\Omega$  as well as whether the stage is choked or unchoked.

These comments are shown graphically in Figure 16 that is a summary of numerical graphs obtained by Mattingly et al. [3], which shows the relation between  $\alpha_2$  and stage temperature ratio, rotor flow turning angle, rotor degree of reaction and stage exit flow angle.

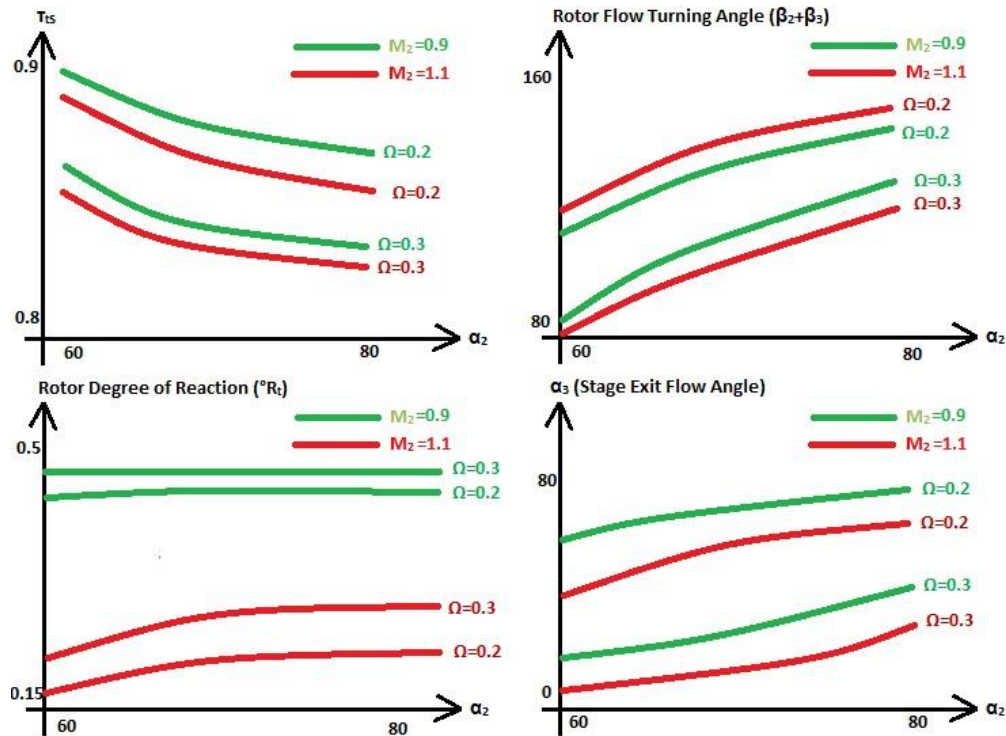


**Figure 16** The trend variation of stage temperature ratio, rotor flow turning angle, rotor degree of reaction and stage exit flow angle with  $\alpha_2$

Designing the Low Pressure Turbine to rotate in the opposite direction can accommodate large amounts of exit swirl from the High Pressure Turbine. The so called counter-rotating Low Pressure Turbine will thus require an inlet guide vane with little turning, or perhaps no inlet guide vanes at all. Modern turbines use this principle to avoid high swirl angles between the turbines.

Because the individual turbine stator and rotor airfoils are heavy and expensive, especially cooled airfoils require advanced materials, elaborate manufacturing processes and intricate internal flow passages, it is important to reduce their number to the extent possible. The Zweifel Coefficient ( $\zeta$ ) provides a reliable and straightforward method for making an initial estimate of the minimum solidity and number of required airfoils. According to its mathematical definition, in order to obtain an ideal pressure distribution

across the airfoil,  $\zeta$  should be unity. Rotor solidity decreases rapidly as  $\alpha_2$  is increased for both choked and unchoked stages, therefore the designers are suggested to select higher values of  $\alpha_2$  in order to reduce the number of rotor airfoils.

The dimensionless stage axial velocity given in Equation (123) is an indicator of the throughflow area that will be required by the stage and hence of the height of the airfoils and the rotor centrifugal stress. The stage axial velocity diminishes rapidly as  $\alpha_2$  increases for both choked and unchoked stages and is independent of  $\Omega$ . The designers are suggested to choose values of  $\alpha_2 < 70^\circ$  in order to increase the stage axial velocity and thus obtain shorter, lighter airfoils and rotor blades that have lower centrifugal stresses.

High Pressure Turbine Inlet Temperature ( $T_{t4}$ ), cooling airflow and Low Pressure Turbine Stage Loading Coefficient ( $\psi_{tL}$ ) are the key parameters that increases the overall pressure ratio (i.e. the thermal efficiency) and the by-pass ratio (i.e. the propulsive efficiency) and thus greatly reduce the specific fuel consumption (i.e. the overall efficiency).

#### **2.4.3.3 Effect of Structural Design Parameters**

Due to the desire of high rotor blade speeds, since they reduce the required number of compressor and turbine stages, the iterations between  $AN^2$  and  $\omega r$  design criteria becomes the basis for many important design choices.

In the case of high by-pass turbofan engines, the rotational speed of the low pressure or fan spool is dominated by the allowable value of  $AN^2$  for fan blades, and the fact that annulus area  $A$  is fixed in advance by cycle computations. Thus, the fan designers should work at the maximum resulting value of  $N$  (number of blades) and places the fan hub at the largest possible radius. The latter will be determined by other factors such as the largest reasonable fan tip radius and or the minimum acceptable fan blade aspect ratio. This choice provides the low pressure turbine the highest allowable value of  $N$ .

The blade hubs for the Low Pressure Turbine are also placed at the largest possible radius, the limitation usually being either the largest possible blade-tip radius or radial displacement from the High Pressure Turbine exit.

In the case of high pressure spool, the rotational speed is often determined by the allowable value of  $\omega r$  for the first turbine disk. Thus, the turbine is designed at the minimum reasonable value of hub radius. The latter will be determined by other factors such as the minimum radius required for the internal functions of the engine (for example shafts, bearings, cooling flows, and lubricant flows) or the largest reasonable radial displacement from the High Pressure Compressor exit or the Low Pressure Turbine entrance. This choice provides the High Pressure Compressor, the highest allowable value of  $\omega$ . The blade hubs of the High Pressure Compressor are placed at the largest possible radius, the limitation usually being the allowable value of  $(\omega r)$  for the compressor disks, the height of the rear airfoils or radial displacement from the High Pressure Turbine entrance. [3]

## CHAPTER 3

### NEW ANALYTICAL TOOLS DEVELOPED FOR HIGH BY-PASS TURBOFAN ENGINES

Concerning to perform cycle computations and aerothermodynamic turbomachinery design at the same time, the Engine Design Model (EDM) was developed by using MATLAB ® Simulink. The aim of developing this model was to make cycle calculations for a user defined scenario and use these results directly to obtain a relevant turbomachinery design. In addition, by using the Optimization Toolbox of MATLAB ®, it can be used to give the user an engine configuration that meets the design constraints optimally.

The model consists of three sub-models which are named after their intention in the calculations of the Engine Design Process. EDM takes inputs via an input m-file that can be edited out of the model and outputs its results as workspace variables. The EDM is shown in Figure 17.

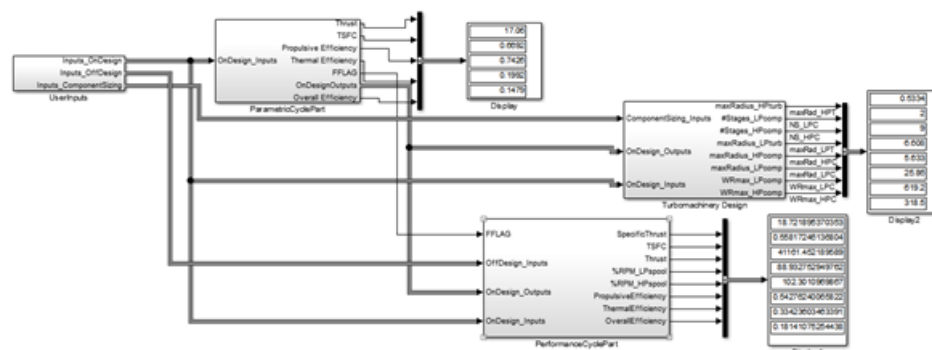


**Figure 17** The Engine Design Model overview in Simulink Model Window

The definitions of the blocks shown in Figure 17 are as follows:

- 1) *UserInputs*: Takes the user inputs from the input m-file and distribute them to the relevant blocks which they are required from
- 2) *ParametricCyclePart*: It performs the on-design cycle calculations given in Section 2.1.
- 3) *PerformanceCyclePart*: It performs the off-design cycle calculations given in Section 2.2.
- 4) *Turbomachinery Design*: It includes turbomachinery design algorithms for High and Low Pressure Compressors and Turbines which are using the design concepts introduced in Section 2.3.

The name of the input m-file is given to the model from the Model Properties→Callbacks→Initialization Functions directive, since the input file is defined as an initialization function of the model. An example input m-file is given in Appendix A. The input file contains inputs for the parametric cycle, performance cycle and turbomachinery design which are given in Table 6.

**Table 6** The list of input parameters for EDM

<b>Parametric Cycle Inputs</b>	
<b>Flight Conditions</b>	$M_0, P_0, T_0, CTOL, CTOH$
<b>Fuel Properties</b>	$h_{PR}$
<b>Bleed Air and Coolant Air Ratios</b>	$\beta, \varepsilon_1, \varepsilon_2$
<b>Pressure Ratios</b>	$\Pi_b, \Pi_{dMAX}, \Pi_n, \Pi_f, \Pi_{nF}, \Pi_{cL}, \Pi_c$
<b>Polytropic Efficiencies</b>	$\eta_f, \eta_{cL}, \eta_{cH}, \eta_{tH}, \eta_{tL}$
<b>Component Efficiencies</b>	$\eta_b, \eta_{mL}, \eta_{mH}, \eta_{mPL}, \eta_{mPH}$
<b>Others</b>	$\alpha, T_{t4}, m_0$
<b>Performance Cycle Inputs</b>	
<b>Flight Conditions</b>	$M_0, P_0, T_0, CTOL, CTOH, PTOL, PTOH$
<b>Fuel Properties</b>	$h_{PR}$
<b>Bleed Air and Coolant Air Ratios</b>	$\beta, \varepsilon_1, \varepsilon_2$
<b>Pressure Ratios</b>	$\Pi_b, \Pi_{dMAX}, \Pi_n, \Pi_f, \Pi_{nF}$
<b>Polytropic Efficiencies</b>	$\eta_f, \eta_{cL}, \eta_{cH}, \eta_{tH}, \eta_{tL}$
<b>Component Efficiencies</b>	$\eta_b, \eta_{mL}, \eta_{mH}, \eta_{mPL}, \eta_{mPH}$
<b>Limiting Conditions</b>	$T_{t4}, \Pi_{c(max)}$
<b>Turbomachinery Design</b>	
<b>Blade Material Densities</b>	$\rho_{cH}, \rho_{cL}, \rho_{tH}, \rho_{tL}$
<b>Tensile Stresses of Blade Materials</b>	$\sigma_{c, cH}, \sigma_{c, cL}, \sigma_{c, tH}, \sigma_{c, tL}$
<b>Tensile Stresses of Disk Materials</b>	$\sigma_{D, tH}, \sigma_{D, tL}$
<b>Aerodynamic Design Parameters</b>	$D, \text{Loss Coefficient}$
<b>Polytropic Efficiencies</b>	$\eta_{tH}, \eta_{tL}$

The outputs of the EDM are shown to the user by using Display blocks but they can also be recorded to mat-files. The current display in Figure 17 contains the displays of the output variables that are chosen to be used in optimization process. Aside from the displayed ones, the whole output set of the EDM is given in Table 7.

**Table 7** The list of output parameters of EDM

<b>Parametric Cycle Outputs</b>	
<b>Thrust</b>	$F/m_0$
<b>Thrust Specific Fuel Consumption</b>	S
<b>Propulsive Efficiency</b>	$\eta_p$
<b>Thermal Efficiency</b>	$\eta_{th}$
<b>Overall Efficiency</b>	$\eta_o$
<b>Speeds at the Nozzles</b>	$V_9, V_{19}$
<b>Component Behavior</b>	$T_f, T_{cL}, T_{cH}, T_{tH}, T_{tL}, T_\lambda, f, \eta_f, \eta_{cL}, \eta_{cH}, \eta_{tH}, \eta_{tL}, M_9, P_{t9}/P_9, P_9/P_0, T_9/T_0, M_{19}, P_{t19}/P_{19}, P_{19}/P_0, T_{19}/T_0$
<b>Performance Cycle Outputs</b>	
<b>Thrust</b>	F
<b>Mass Flow Rate</b>	$\dot{m}_0$
<b>Thrust Specific Fuel Consumption</b>	S
<b>Efficiencies</b>	$\eta_p, \eta_{th}, \eta_o$
<b>Fuel to Air Ratio</b>	$f_o$
<b>Overall Performance</b>	$V_9/a_0, V_{19}/a_0, \alpha, P_{t9}/P_9, P_9/P_0, T_9/T_0, P_{t19}/P_{19}, P_{19}/P_0, T_{19}/T_0$
<b>Component Behavior</b>	$\Pi_f, \Pi_{cL}, \Pi_{cH}, \Pi_{tH}, \Pi_{tL}, T_f, T_{cL}, T_{cH}, T_{tH}, T_{tL}, T_\lambda, f, M_9, M_{19}$
<b>Turbomachinery Design</b>	
<b>Number of Stages</b>	$NS_{cL}, NS_{cH}, NS_{tH}, NS_{tL}$
<b>Blade Height (for each stage)</b>	$r_{tip}-r_{hub}$
<b>Flow Path Areas (for each stage)</b>	A
<b>Shaft Rotational Speeds</b>	$\omega$
<b>Blade Tangential Speeds (at mean radius)</b>	$\omega r_{m(LP\ Spool)}, \omega r_{m(HP\ Spool)}$

The number of outputs can be increased or decreased according to the user needs. The given list is determined so as to include parameters that will be used in the optimization to find the optimal engine in the design input range defined by the user.



### 3.1 Variable Specific Heat Model and the Flow Property Calculations

#### 3.1.1 Variable Specific Heat Model

By using the aforementioned tables and the calculation methodology for the thermodynamic properties in Section 2.4.1, thermodynamic property calculators are developed for the Engine Design Model. The property calculators take two types of input parameters, in which the first one is fixed and being the fuel to air ratio and the second one is variable. The second input parameter may be temperature, enthalpy or reduced pressure and the calculators differ according to this second input type and named as F-AIR1, F-AIR2 and F-AIR3 respectively.

##### 3.1.1.1 F-AIR1

This sub-model takes fuel to air ratio ( $f$ ) and temperature ( $T$ ) of the air or air and kerosene mixture and gives the values of enthalpy ( $h$ ), reduced pressure ( $P_r$ ), specific heat at constant pressure ( $C_p$ ), gas constant ( $R$ ), specific heat ratio ( $\gamma$ ), and the speed of sound ( $a$ ). The block is shown in Figure 18.

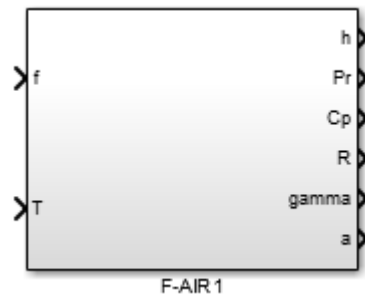


**Figure 18** The F-AIR1 sub-model for thermodynamic property calculations

The interior view of F-AIR1 is shown in Figure 19. The tabulated thermodynamic properties are put into single and two dimensional lookup tables, which are available to make linear interpolations.

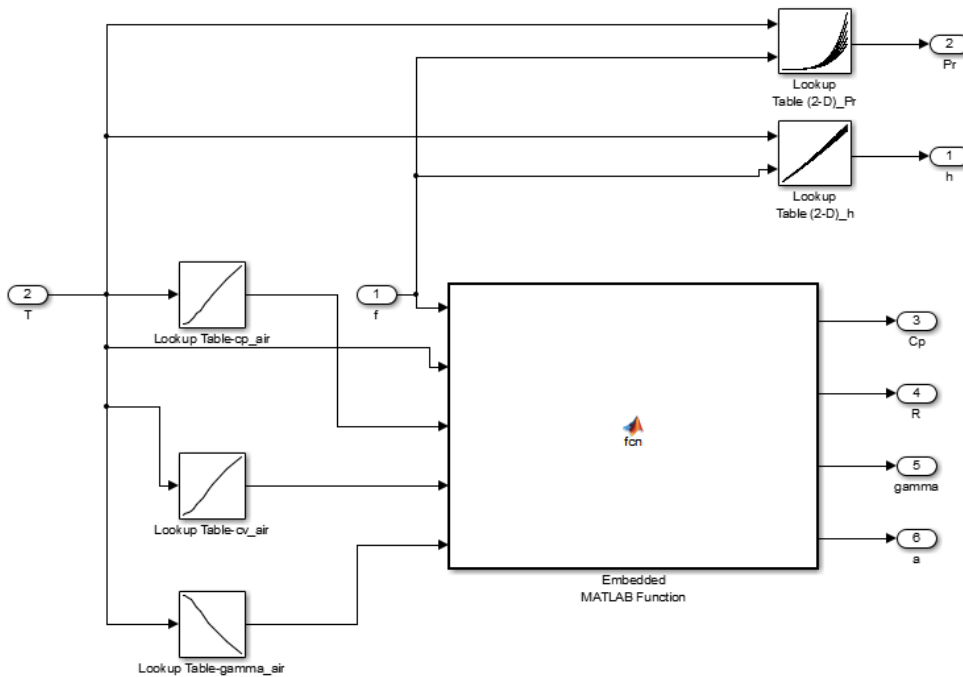


**Figure 19** The interior view of the F-AIR1 sub-model

The formulization given in Equations (147) through (149) is coded in the Embedded MATLAB function shown in Figure 19.

### 3.1.1.2 F-AIR2

This sub-model takes fuel to air ratio ( $f$ ) and enthalpy ( $h$ ) of the air or air and kerosene mixture and gives the values of temperature ( $T$ ), reduced pressure ( $P_r$ ), specific heat at constant pressure ( $C_p$ ), gas constant ( $R$ ), specific heat ratio ( $\gamma$ ), and the speed of sound ( $a$ ). The block is shown in Figure 20.

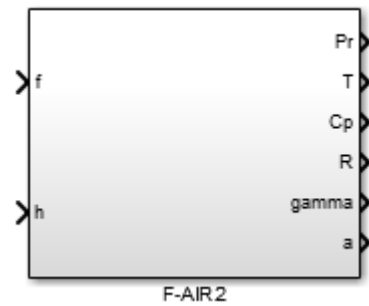


**Figure 20** The F-AIR2 sub-model for thermodynamic property calculations

The interior view of F-AIR2 is shown in Figure 21. The tabulated thermodynamic properties are put into single and two dimensional lookup tables. This sub-model includes an additional subroutine, which is highlighted in Figure 21, for determining the temperature from enthalpy and fuel to air ratio by using enthalpy property tables inversely with linear interpolation.

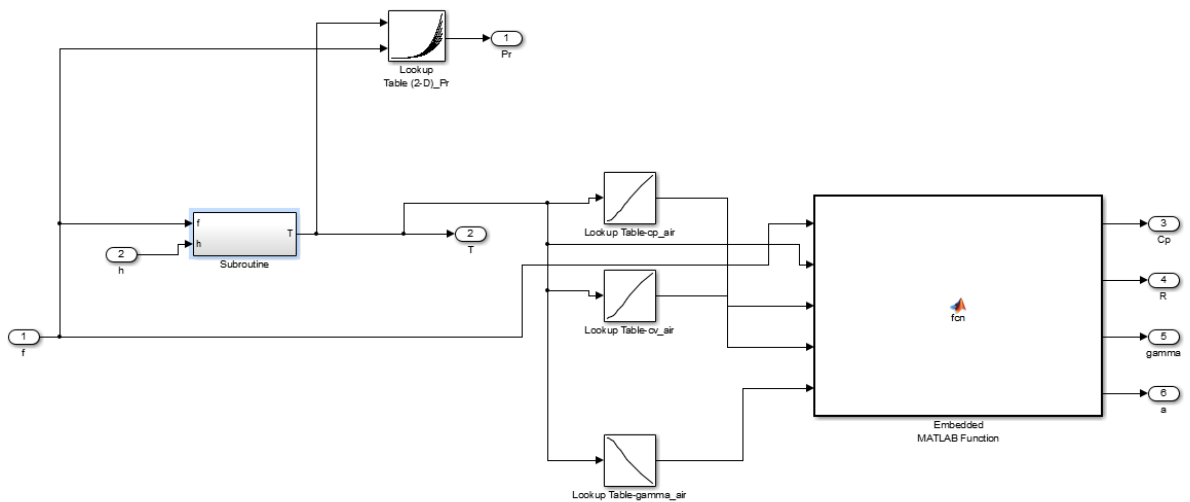


**Figure 21** The interior view of the F-AIR2 sub-model

The formulization given in Equations (147) through (149) is coded in the Embedded MATLAB function shown in Figure 21.

### 3.1.1.3 F-AIR3

This sub-model takes fuel to air ratio ( $f$ ) and reduced pressure ( $Pr$ ) of the air or air and kerosene mixture and gives the values of temperature ( $T$ ), enthalpy ( $h$ ), specific heat at constant pressure ( $C_p$ ), gas constant ( $R$ ), specific heat ratio ( $\gamma$ ), and the speed of sound ( $a$ ). The block is shown in Figure 22.

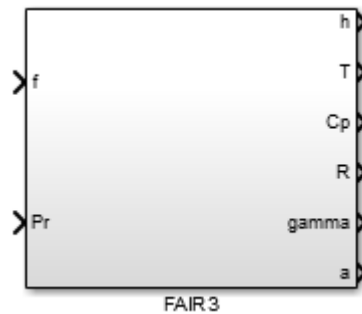


**Figure 22** The F-AIR3 sub-model for thermodynamic property calculations

The interior view of F-AIR3 is shown in Figure 23. The tabulated thermodynamic properties are put into single and two dimensional lookup tables. This sub-model includes an additional subroutine as in F-AIR2, which is highlighted in Figure 23, for determining the temperature from reduced pressure and fuel to air ratio by using reduced pressure property tables inversely with linear interpolation.

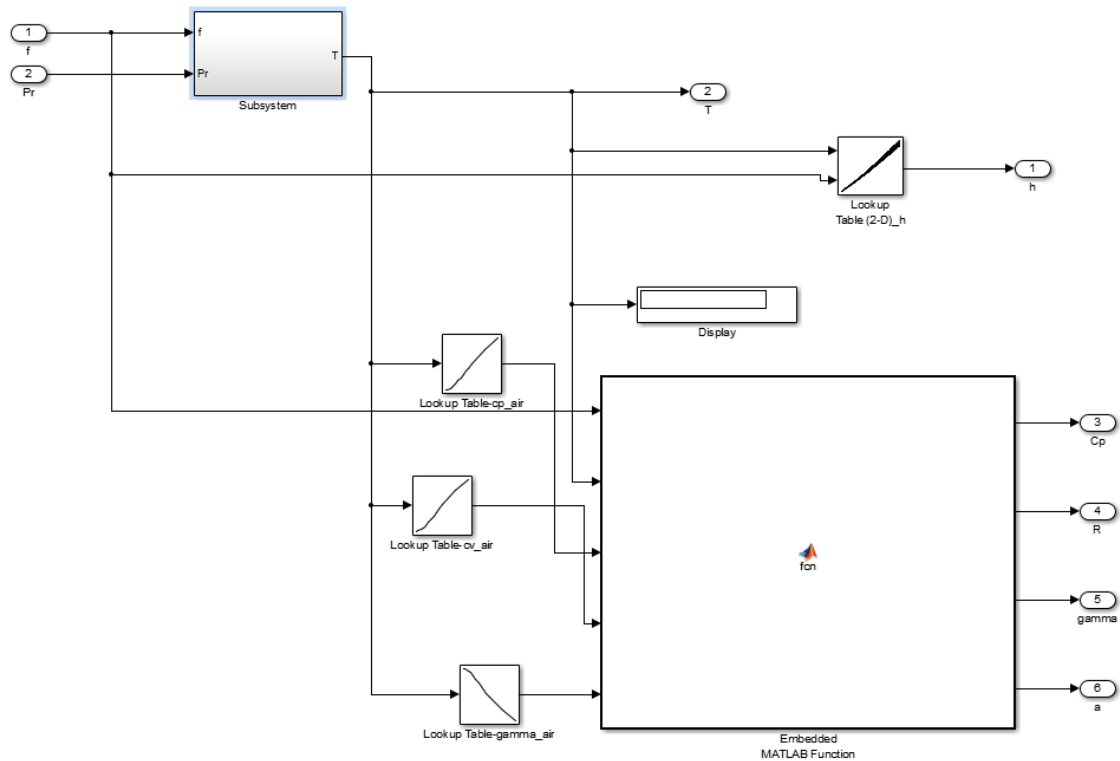


**Figure 23** The interior view of the F-AIR3 sub-model

The formulation given in Equations (147) through (149) is coded in the Embedded MATLAB function shown in Figure 23.

### 3.1.2 Flow Property Calculations

The mass flow parameter, total static temperature and pressure ratios are used in order to obtain the flow properties of an engine section, needed during the cycle analysis. In order to perform these calculations during the cycle analysis, an algorithm named as RGCOMPR based on the NASA Glenn thermochemical data and the Gordon-McBride equilibrium algorithm is given in Appendix F of [3]. The inputs of this subroutine are the total temperature ( $T_t$ ), fuel to air ratio ( $f$ ), and one of the following inputs being the Mach Number ( $M$ ), total to static temperature ratio ( $T_t/T$ ), total to static pressure ratio ( $P_t/P$ ) or Mass Flow Parameter (MFP). According to the known input type, this subroutine has different cases and it outputs the following outputs being the Mach

Number ( $M$ ), total to static temperature ratio ( $T_t/T$ ), total to static pressure ratio ( $P_t/P$ ) or Mass Flow Parameter (MFP). The outputs differ according to the input cases, for instance if the Mass Flow Parameter is the input, the output parameters are the Mach Number ( $M$ ), total to static temperature ratio ( $T_t/T$ ), total to static pressure ratio ( $P_t/P$ ).

The cycle analysis algorithms given for the high by-pass turbofan engine given in Mattingly et al. [3] uses the known input Mach number and total to static pressure ratio cases of RGCOMPR. Therefore only these two cases are modelled and named as RGCOMPR1 and RGCOMPR3 respectively. These blocks uses F-AIR sub-models presented in Section 3.1.1 to obtain the thermodynamic properties and Equation (72) to calculate the Mass Flow Parameter (MFP).

### 3.1.2.1 RGCOMPR1

This sub-model takes total temperature ( $T_t$ ), fuel to air ratio ( $f$ ) and Mach Number ( $M$ ) as inputs and calculates total to static temperature ratio ( $T_t/T$ ), total to static pressure ratio ( $P_t/P$ ) and Mass Flow Parameter (MFP). The block is shown in Figure 24.

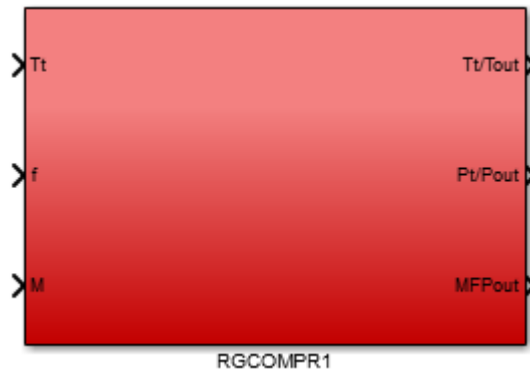


**Figure 24** The RGCOMPR1 sub-model for the calculation of flow properties

The interior view of RGCOMPR1 is given in Figure 25. This sub-model is a while iterator block which stops iterations when the difference between the predicted flow speed and the input flow speed is less than  $10^{-5}$ . This tolerance is determined according to the algorithm given for RGCOMPR in [3].

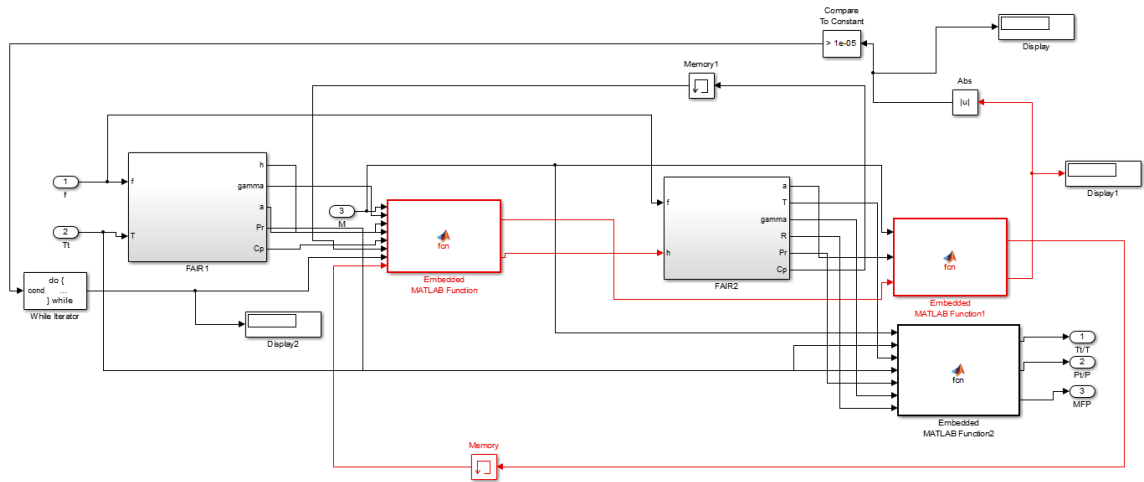


**Figure 25** The interior view of the RGCOMPR1 sub-model

### 3.1.2.2 RGCOMPR3

This sub-model takes total temperature ( $T_t$ ), fuel to air ratio ( $f$ ) and total to static pressure ratio ( $P_t/P$ ) as inputs and calculates total to static temperature ratio ( $T_t/T$ ), Mach Number ( $M$ ) and Mass Flow Parameter ( $MFP$ ). The block is shown in Figure 26.

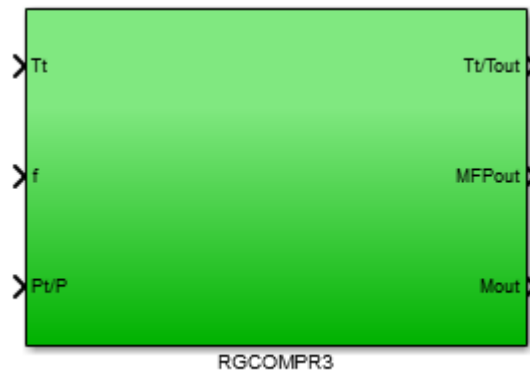


**Figure 26** The RGCOMPR3 sub-model for the calculation of flow properties

The interior view of RGCOMPR3 is given in Figure 26. This sub-model includes the while iterator block in RGCOMPR1 and stop iterations when the difference between the predicted flow speed and the flow speed determined from the total to static pressure ratio

is less than  $10^{-5}$ . This tolerance is determined according to the algorithm given for RGCMPR in [3].

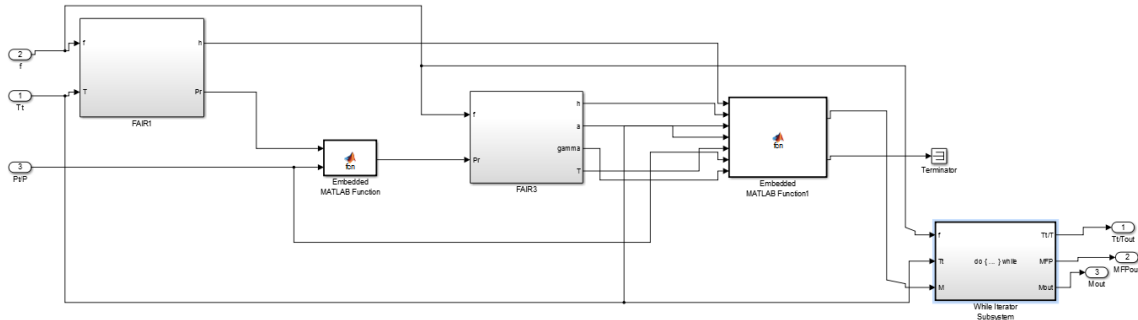


**Figure 27** The interior view of the RGCMPR3 sub-model, the while loop which determines the output parameters is highlighted

### 3.2 Parametric Cycle Model

The intention of the parametric cycle model is to perform the on-design cycle analysis calculations presented in Section 2.1 for the high by-pass ratio turbofan engines. The model based on the algorithm given in Appendix J of [3]. The Parametric Cycle Model is shown in Figure 28.

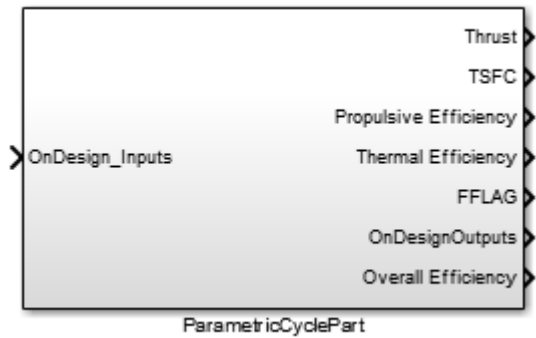


**Figure 28** Parametric Cycle Model in the Engine Design Model

The Parametric Cycle Model takes the On-Design input parameters listed in Table 5 and outputs the on-design output parameters listed in Table 6 and a finish flag (FFLAG) in



order to indicate the performance cycle model that the on-design calculations are completed and off-design calculations can be initiated.

The Parametric Cycle Model includes 10 sub-models that are calculating the aerothermodynamic properties of 10 different engine sections such as temperature and pressure ratios and component efficiencies. The sub-models are named after their respective engine stations and their work sequence is set according to the engine station numbering given in Figure 4. The model is outlined in Figure 29.

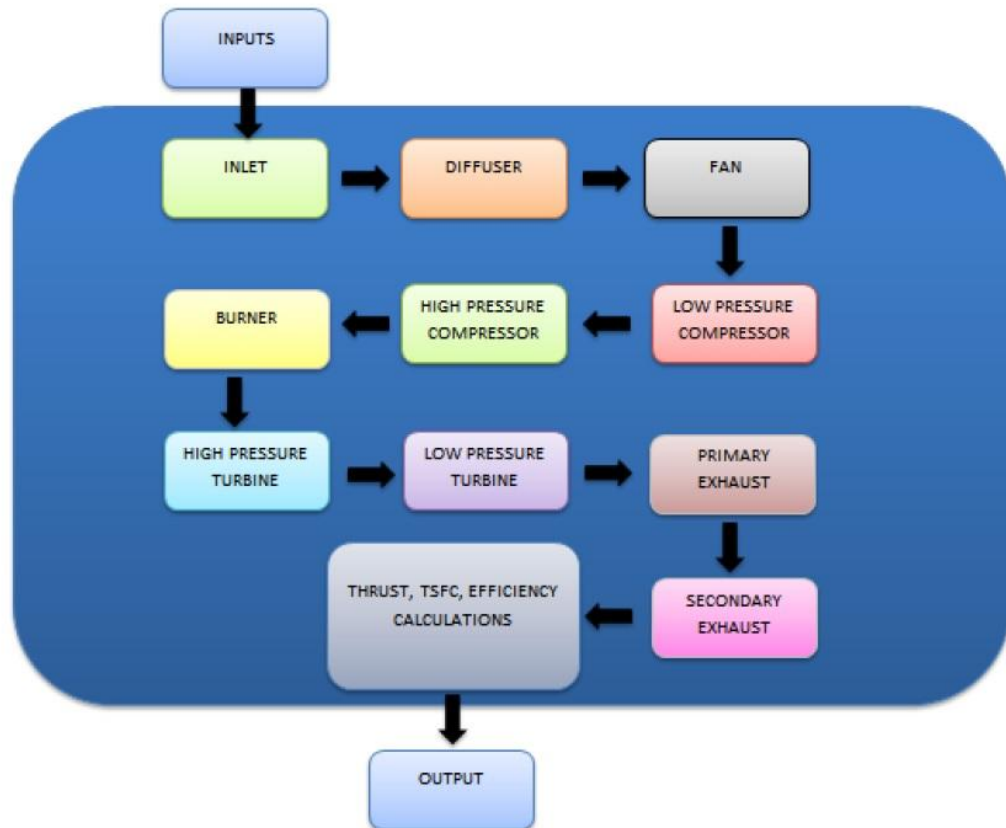


**Figure 29** A summarized view of the Parametric Cycle Model

The execution sequence of the Parametric Cycle Model is given as follows:

- 1) Inlet
- 2) Diffuser

- 3) Fan
- 4) Low Pressure Compressor
- 5) High Pressure Compressor
- 6) Combustor
- 7) Coolant Mixer 1
- 8) High Pressure Turbine
- 9) Coolant Mixer 2
- 10) Low Pressure Turbine
- 11) Primary Exhaust
- 12) Secondary Exhaust

This sequence is controlled by “if-action” blocks which inputs the finish flag signal (FFLAG) from the previous block and enables the execution of the following block. The interior view of the Parametric Cycle Model is given in Figure 30.

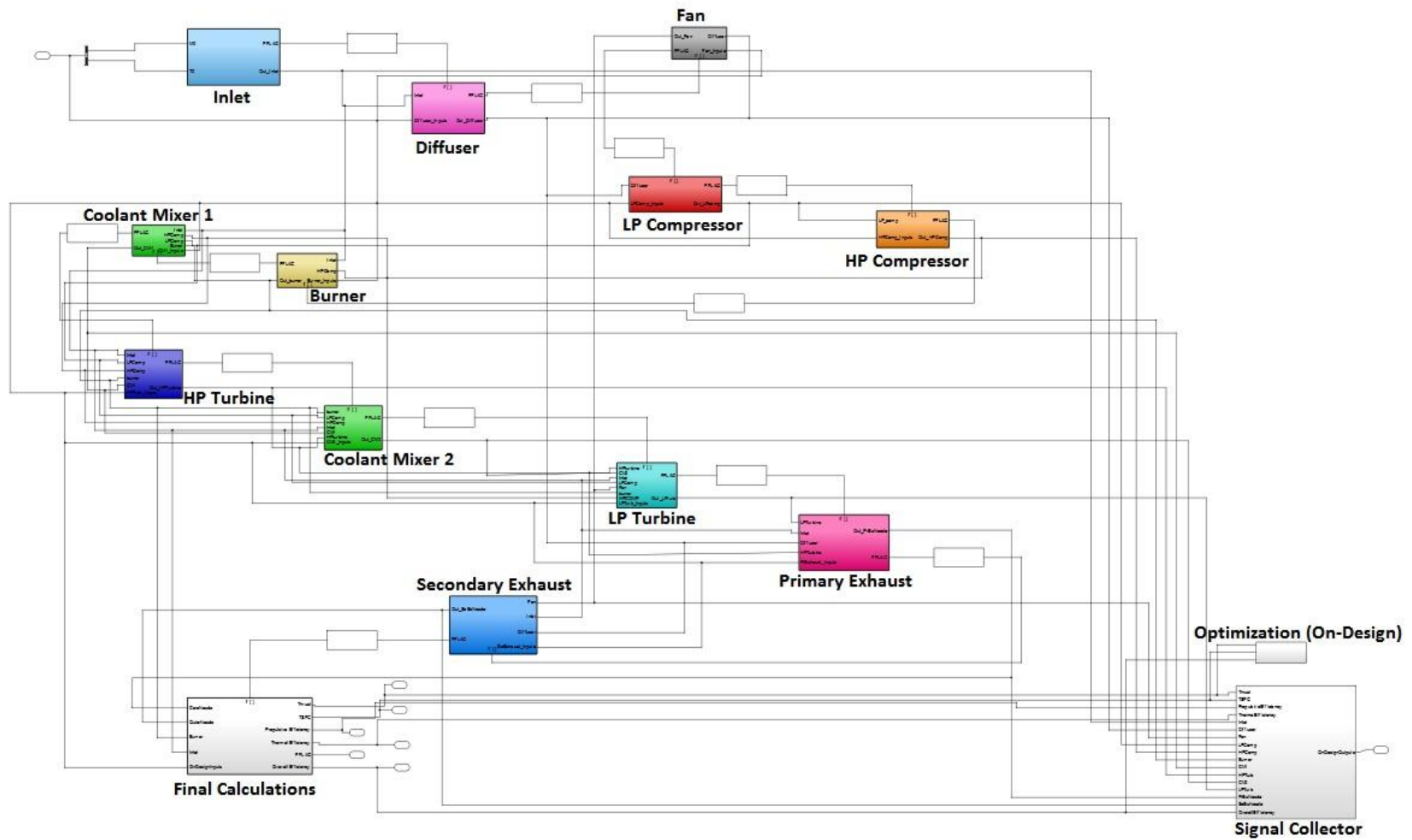
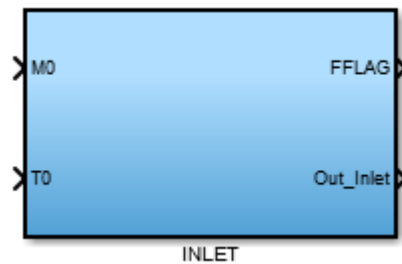


Figure 30 The interior view of Parametric Cycle Model

An optimization block is added for the introduction of the optimization signal constraints on the predetermined on-design output parameters to the Simulink Optimization Toolbox. The Signal Collector block is put in order to multiplex the on-design output signals by using bus creators in order to expurgate the needed signals from the Performance Cycle and Turbomachinery Design models easier. The sub-models used in cycle analysis calculations are explained hereinafter.

### 3.2.1 Inlet

This sub-model is responsible for the calculations of inlet/diffuser entry pressure ratios ( $\pi_r$ ), temperature ratios ( $\tau_r$ ) and  $\eta_{Rspec}$ . It takes only the inlet Mach number and Temperature from the on-design input set as inputs. The block is shown in Figure 31.



**Figure 31** Inlet sub-model for the inlet/diffuser entry cycle calculations

The Inlet sub-model uses F-AIR1 and F-AIR2 blocks to obtain the thermodynamic properties of inlet conditions and uses the relations given in Assumption 4 of Section 2.1.7 to calculate the pressure ratio and the  $\eta_{Rspec}$ . The interior view of Inlet sub-model is given in Figure 32.

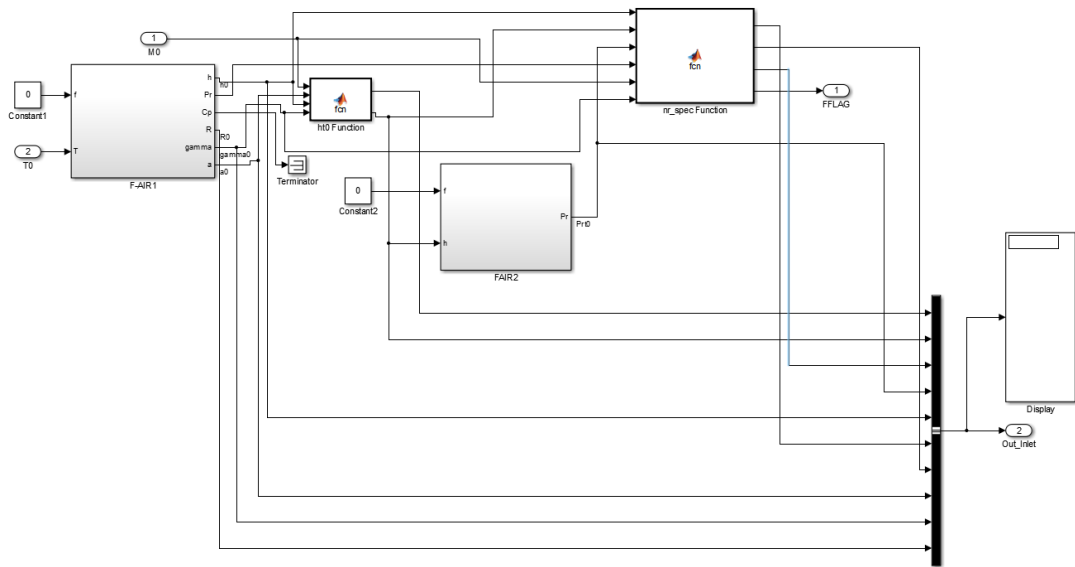


**Figure 32** Interior view of Inlet sub-model

In Figure 32, the ht0 Function calculates the total enthalpy for the inlet and nr\_spec Function is responsible for the calculations of the pressure ratio and  $\eta_{Rspec}$ .

### 3.2.2 Diffuser

This sub-model calculates total enthalpy of diffuser, total reduced pressure and the diffuser pressure ratio ( $\pi_d$ ). It takes  $\pi_{dMAX}$  value from on-design input set and  $\eta_{Rspec}$ , inlet thermodynamic properties from the Inlet sub-model. The block is shown in Figure 33.

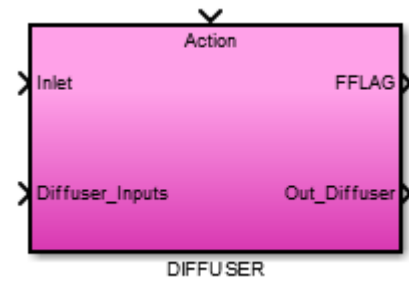


**Figure 33** Diffuser sub-model for the diffuser cycle calculations

The Diffuser sub-model uses Equation (7) to find the diffuser pressure ratio and the interior view of the model is given in Figure 34.

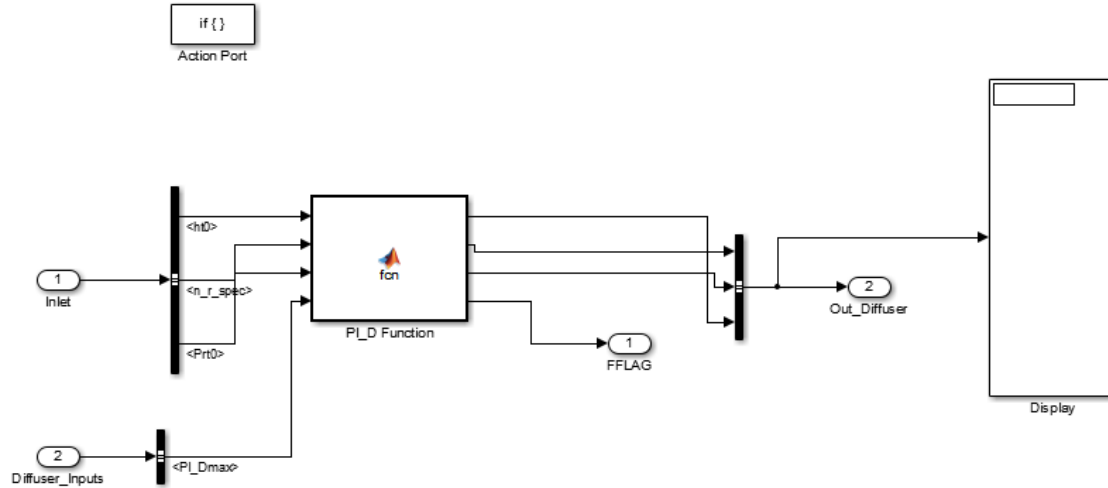


**Figure 34** Interior view of Diffuser sub-model

In Figure 34, the PI\_D Function given in Figure 34 is responsible for the calculations of diffuser pressure ratio.

### 3.2.3 Fan

This sub-model calculates fan total thermodynamic properties, fan efficiency and the fan temperature ratio ( $\tau_f$ ). It takes  $\pi_f$  and  $\eta_f$  value from on-design input set and diffuser thermodynamic properties from the Diffuser sub-model. The block is shown in Figure 35.

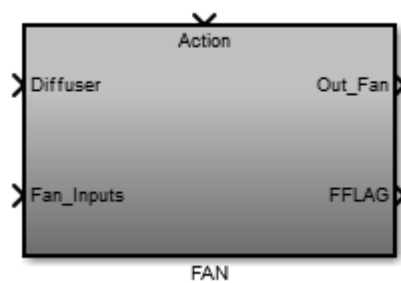


**Figure 35** Fan sub-model for the fan cycle calculations

Fan sub-model uses Equation (10) for calculating the fan temperature ratio and Equation (45) to calculate the fan component efficiency. The interior view of the model is given in Figure 36.

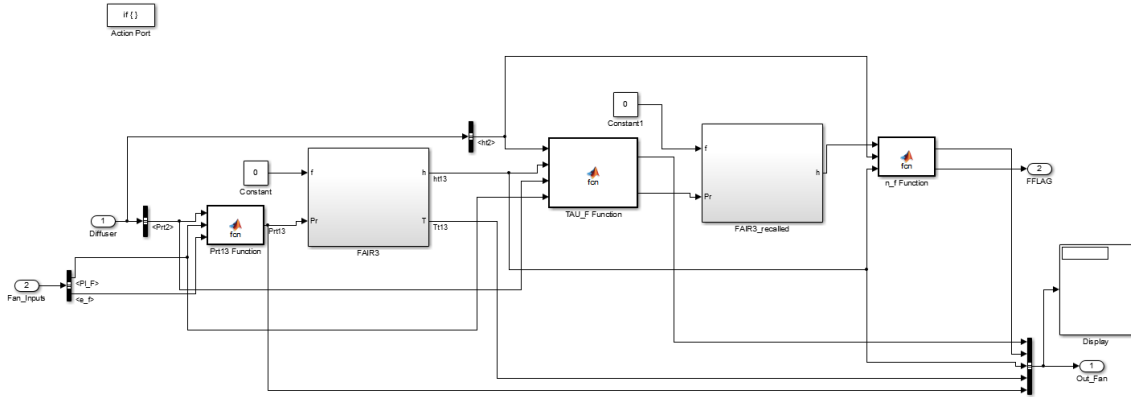


**Figure 36** Interior view of Fan sub-model

In Figure 36, the Pr13 Function calculates the fan total reduced pressure, TAU\_F Function calculates the fan temperature ratio and n\_f Function calculates the component efficiency.

### 3.2.4 Low Pressure Compressor

This sub-model calculates Low Pressure Compressor total thermodynamic properties, Mass Flow Parameter at the Low Pressure Compressor, Low Pressure Compressor efficiency and the Low Pressure Compressor temperature ratio ( $\tau_{cL}$ ). It takes  $\pi_{cL}$  and Polytropic Efficiency  $e_{cL}$  value from on-design input set and diffuser thermodynamic properties from the Diffuser sub-model. The block is shown in Figure 37.

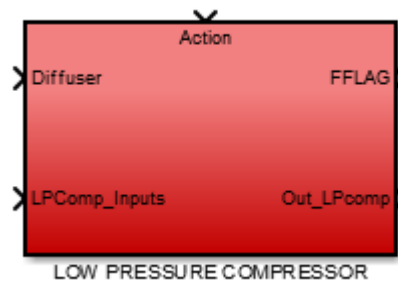


**Figure 37** Low Pressure Compressor sub-model for the Low Pressure Compressor cycle calculations

Low Pressure Compressor sub-model uses Equation (12) for calculating the Low Pressure Compressor temperature ratio and Equation (47) to calculate the Low Pressure Compressor component efficiency. RGCOMPR1 is used to calculate the Mass Flow

Parameter for the Low Pressure Compressor component design at the Turbomachinery Design Model. The interior view of the model is given in Figure 38.

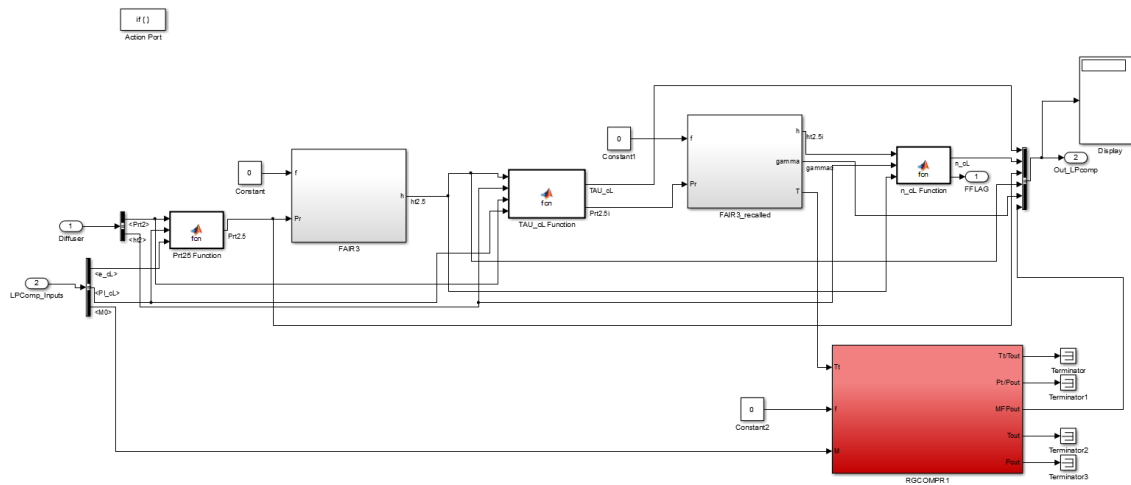


**Figure 38** Interior view of Low Pressure Compressor sub-model

In Figure 38, the Prt25 Function calculates the Low Pressure Compressor total reduced pressure, TAU\_cL Function calculates the Low Pressure Compressor temperature ratio and n\_f Function calculates the component efficiency.

### 3.2.5 High Pressure Compressor

This sub-model calculates High Pressure Compressor total thermodynamic properties, Mass Flow Parameter at the High Pressure Compressor, High Pressure Compressor efficiency and the High Pressure Compressor temperature ratio ( $\tau_{CH}$ ). It takes  $\pi_{cH}$  and Polytopic Efficiency  $e_{cH}$  value from on-design input set and Low Pressure Compressor thermodynamic properties from the Low Pressure Compressor sub-model. The block is shown in Figure 39.



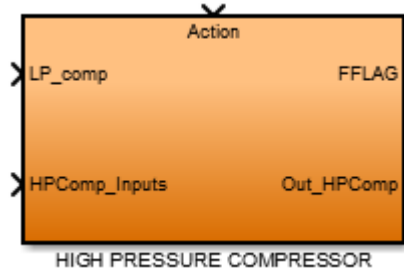


**Figure 39** High Pressure Compressor sub-model for the High Pressure Compressor cycle calculations

High Pressure Compressor sub-model uses Equation (14) for calculating the High Pressure Compressor temperature ratio and Equation (49) to calculate the High Pressure Compressor component efficiency. RGCOMPR1 is used to calculate the Mass Flow Parameter for the High Pressure Compressor component design at the Turbomachinery Design Model. The interior view of the model is given in Figure 40.

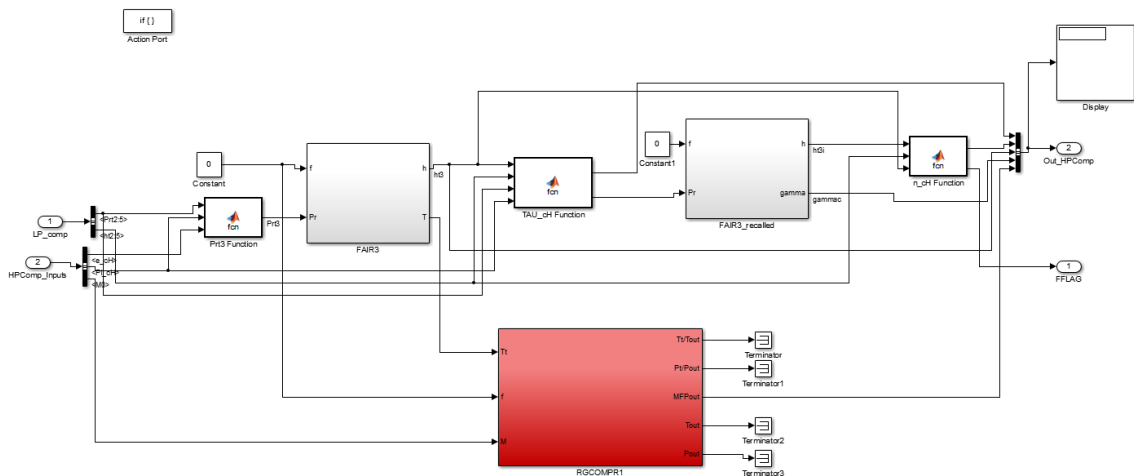


**Figure 40** Interior view of High Pressure Compressor sub-model

In Figure 40, the Prt3 Function calculates the High Pressure Compressor total reduced pressure, TAU\_cH Function calculates the High Pressure Compressor temperature ratio and n\_cH Function calculates the component efficiency.

### 3.2.6 Combustor

The Combustor sub-model calculates fuel to air ratio,  $\tau_\lambda$ , total enthalpy at combustor exit, and Mass Flow Parameter. It takes thermodynamic properties from the Inlet and High Pressure Compressor, Total Temperature at High Pressure Turbine entry ( $T_{14}$ ), total

mass flow rate, by-pass ratio and bleed air fractions from the on-design input set. This sub-model is shown in Figure 41.

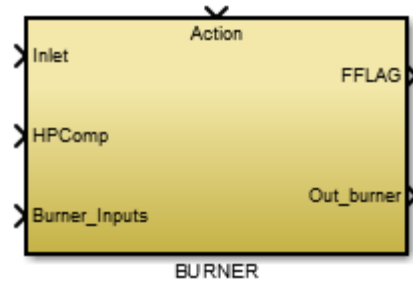


**Figure 41** Combustor sub-model for the Combustor cycle calculations

Combustor sub-model uses Equation (60) to calculate the fuel to air ratio, Equation (29) to calculate  $\tau_\lambda$ , F-AIR blocks to calculate the thermodynamic parameters and RGCOMPR1 block to calculate Mass Flow Parameter. The interior view of the model is given in Figure 42.

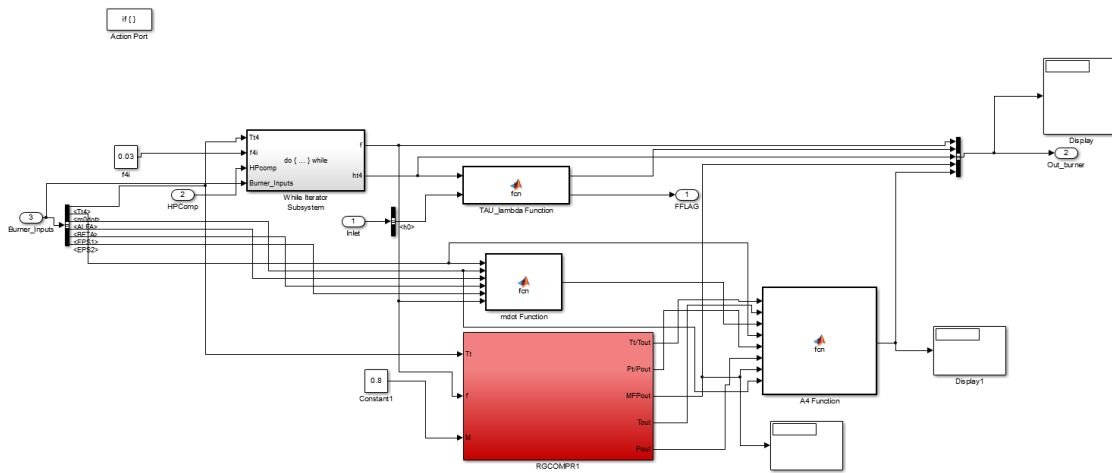


**Figure 42** Interior view of Combustor sub-model

In Figure 42, the While Iterator Subsystem calculates the fuel to air ratio with an iterative process which stops iterations when the calculated fuel to air ratio change between two iteration steps is less than  $10^{-6}$ . This method of solution complies with the method given in Appendix F of [3]. The TAU\_lambda Function calculates the  $\tau_\lambda$ , mdot Function calculates the mass flow rate at the combustor ( $m_4$ ) and A4 Function calculates the flow area at the combustor exit for the Performance Cycle model.

### 3.2.7 Coolant Mixer 1

This sub-model calculates the Coolant Mixer 1 temperature ratio. It takes inlet temperature ratio from Inlet sub-model, temperature ratios of Low and High Pressure Compressors from the Low and High Pressure Compressor sub-models respectively, and fuel to air ratio and  $\tau_\lambda$  from the Combustor sub-model. It takes only the bleed air fractions from the on-design input set. This sub-model is shown in Figure 43.

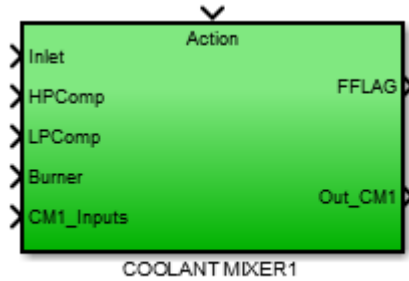


**Figure 43** Coolant Mixer 1 sub-model for the Coolant Mixer 1 cycle calculations

Coolant Mixer 1 sub-model uses Equation (61) to calculate the Coolant Mixer 1 temperature ratio. The interior view of the model is given in Figure 44.

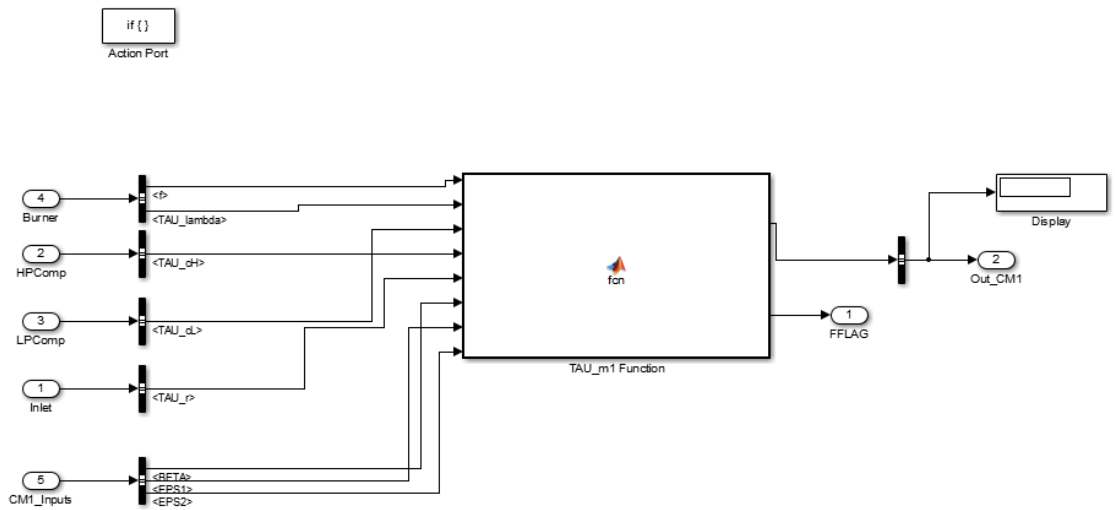


**Figure 44** Interior view of Coolant Mixer 1 sub-model

In Figure 44, TAU\_m1 Function calculates the Coolant Mixer 1 temperature ratio.

### 3.2.8 High Pressure Turbine

The High Pressure Turbine sub-model calculates the High Pressure Turbine pressure ratio, fuel to air ratio at Station 4.1, High Pressure Turbine temperature ratio, component efficiency, Mass Flow Parameter, and thermodynamic properties for the High Pressure Turbine. The inputs of this sub-model are inlet temperature ratio from the Inlet sub-model, Low and High Pressure Compressor temperature ratios from the Low and High Pressure Compressor sub-models respectively, fuel to air ratio, total enthalpy at combustor exit and  $\tau_\lambda$  from the Combustor sub-model and by-pass ratio, bleed air fractions, Polytropic Efficiency  $e_{tH}$ , High Pressure Turbine Shaft Efficiency, Power Take-off efficiency from the High Pressure Turbine shaft and CTOH value from the on-design input set. This sub-model is shown in Figure 45.

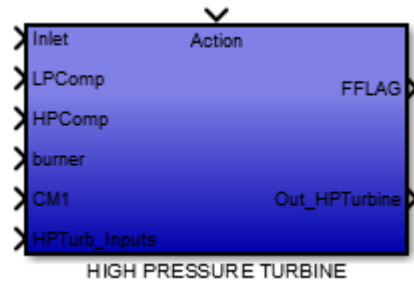


**Figure 45** High Pressure Turbine sub-model for the High Pressure Turbine cycle calculations

This sub-model uses Equation (64) to calculate the High Pressure Turbine temperature ratio, Equation (36) to calculate the fuel to air ratio at Station 4.1, Equation (50) for High Pressure Turbine pressure ratio and Equation (51) to calculate the component efficiency. It uses F-AIR blocks to calculate intermediate thermodynamic properties for necessary calculations and RGCOMPR1 to calculate Mass Flow Parameter for the component design calculations at Turbomachinery Design model. The interior view of the model is given in Figure 46.

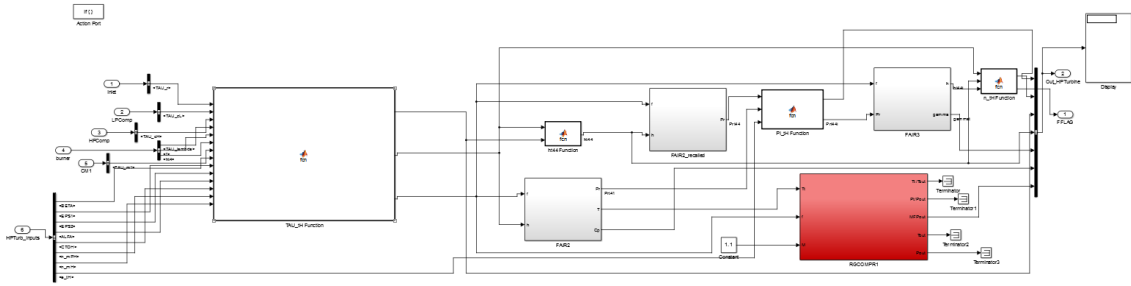


**Figure 46** Interior view of High Pressure Turbine sub-model

In Figure 46, TAU\_tH Function calculates the High Pressure Turbine temperature ratio and fuel to air ratio at Station 4.1, the ht44 Function calculates total enthalpy at Station 4.4, PI\_tH Function calculates High Pressure Turbine pressure ratio, and n\_tH Function calculates the component efficiency.

### 3.2.9 Coolant Mixer 2

This sub-model calculates the Coolant Mixer 2 temperature ratio. It takes inlet temperature ratio from Inlet sub-model, temperature ratios of Low and High Pressure Compressors from the Low and High Pressure Compressor sub-models respectively, fuel to air ratio and  $\tau_\lambda$  from the Combustor sub-model, Coolant Mixer 1 temperature ratio from the Coolant Mixer 1 sub-model, and High Pressure Turbine temperature ratio from the High Pressure Turbine sub-model. It takes only the bleed air fractions from the on-design input set. This sub-model is shown in Figure 47.

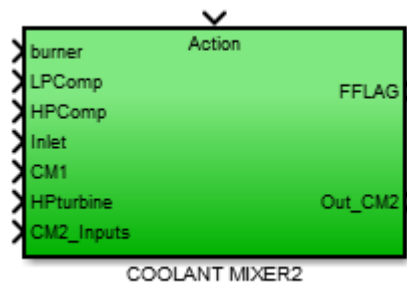


**Figure 47** Coolant Mixer 2 sub-model for the Coolant Mixer 2 cycle calculations

Coolant Mixer 2 sub-model uses Equation (62) to calculate the Coolant Mixer 2 temperature ratio. The interior view of the model is given in Figure 48.

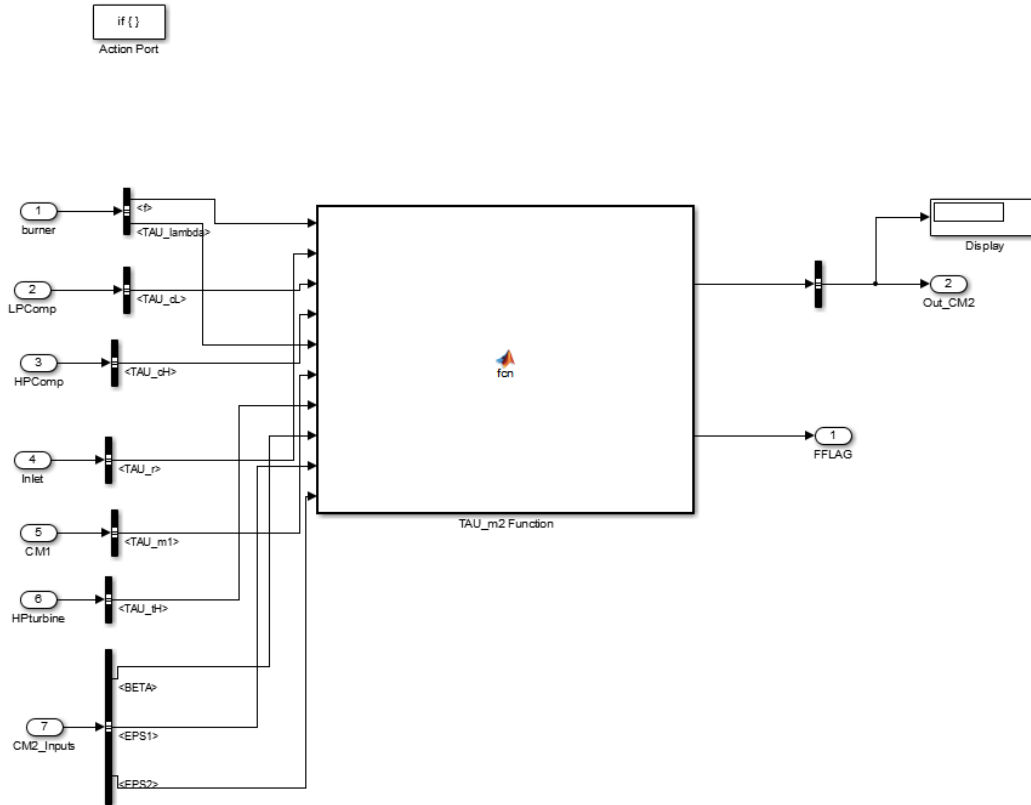


**Figure 48** Interior view of Coolant Mixer 2 sub-model

In Figure 48, TAU\_m2 Function calculates the Coolant Mixer 2 temperature ratio.

### 3.2.10 Low Pressure Turbine

The Low Pressure Turbine sub-model calculates the Low Pressure Turbine pressure ratio, fuel to air ratio at Station 4.5, Low Pressure Turbine temperature ratio, component efficiency, Mass Flow Parameter, and thermodynamic properties for the Low Pressure Turbine. The inputs of this sub-model are inlet temperature ratio from the Inlet sub-model, Low and High Pressure Compressor temperature ratios from the Low and High Pressure Compressor sub-models respectively, fuel to air ratio and  $\tau_\lambda$  from the Combustor sub-model and by-pass ratio, Fan temperature ratio from the Fan sub-model, High Pressure Turbine temperature and pressure ratios and High Pressure Turbine exit total enthalpy from High Pressure Turbine sub-model, and Coolant Mixer 2 temperature ratio from the Coolant Mixer 2 sub-model. It takes bleed air fractions, by-pass ratio, Polytropic Efficiency  $e_{tL}$ , Low Pressure Turbine Shaft Efficiency, Power Take-off

efficiency from the Low Pressure Turbine shaft and CTOL value from the on-design input set. This sub-model is shown in Figure 49.

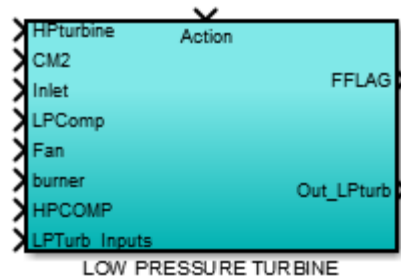


**Figure 49** Low Pressure Turbine sub-model for the Low Pressure Turbine cycle calculations

This sub-model uses Equation (66) to calculate the Low Pressure Turbine temperature ratio, Equation (37) to calculate the fuel to air ratio at Station 4.5, Equation (52) for Low Pressure Turbine pressure ratio and Equation (53) to calculate the component efficiency. It uses F-AIR blocks to calculate intermediate thermodynamic properties for necessary calculations and RGCMPR1 to calculate Mass Flow Parameter for the component design calculations at Turbomachinery Design model. The interior view of the model is given in Figure 50.

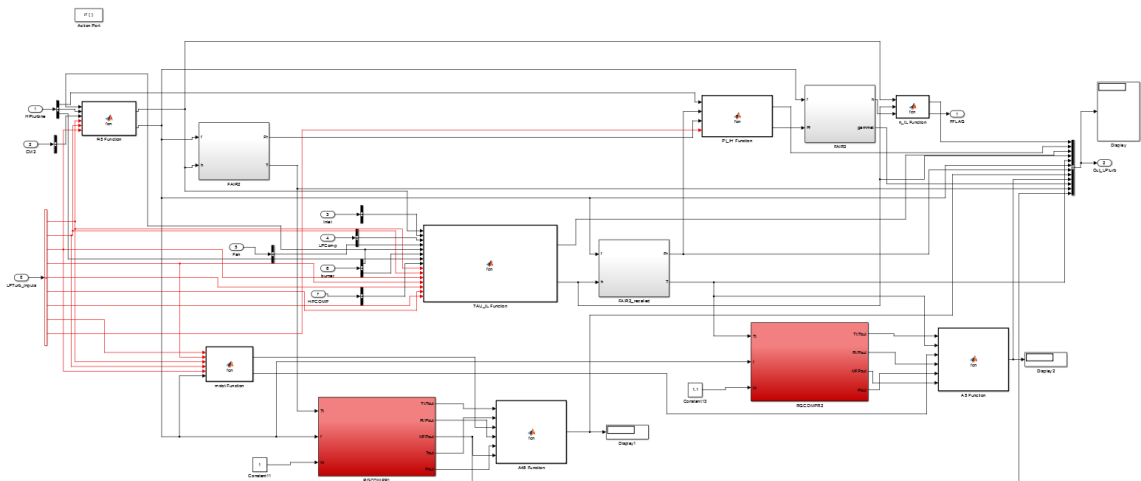


**Figure 50** Interior view of Low Pressure Turbine sub-model

In Figure 50, mdot Function calculates the mass flow rate at Low Pressure Turbine entry, f45 Function calculates the fuel to air ratio at Station 4.5, TAU\_tH Function calculates the High Pressure Turbine temperature ratio and total enthalpy at Station 5,

PI\_tH Function calculates High Pressure Turbine pressure ratio, n\_tH Function calculates the component efficiency, A45 Function calculates the flow area at Station 4.5, and A5 Function calculates the flow area at Station 5 for Performance Cycle computations.

### 3.2.11 Primary Exhaust

Primary Exhaust sub-model calculates the primary stream Mach number,  $\frac{P_0}{P_9}$ , primary stream flow speed, temperature and gas constant. It takes Inlet pressure ratio from Inlet sub-model, Diffuser pressure ratio from Diffuser sub-model, High Pressure Turbine Pressure Ratio from High Pressure Turbine sub-model and Low Pressure Turbine pressure ratio, fuel to air ratio at Station 4.5 and Low Pressure Turbine exit total thermodynamic properties from the Low Pressure Turbine sub-model. Primary Exhaust sub-model takes Low and High Pressure compressor pressure ratios, combustor pressure ratio and nozzle pressure ratio from the on-design input set. This sub-model is shown in Figure 51.

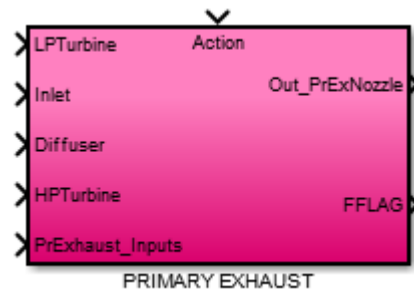


**Figure 51** Primary Exhaust sub-model for the Primary Exhaust cycle calculations

Primary Exhaust sub-model uses a subroutine to find the primary stream Mach number and  $\frac{P_0}{P_9}$ . In this subroutine total to static pressure ratio at the primary exhaust is compared with the ratio  $\frac{P_{t9}}{P_0}$ . If the latter is smaller than the first one the Mach number at primary exhaust is calculated by using Equation (6) at Station 9 and  $\frac{P_0}{P_9}$  is calculated by dividing the total to static pressure ratio at the primary exhaust to the



$P_{t9} / P_0$ , else  $P_0 / P_9$  is taken as unity and total to static pressure ratio at the primary exhaust is equal to  $P_{t9} / P_0$ . The Mach number is calculated by using the total to static pressure ratio at the primary exhaust in Equation (6). This methodology complies with the method given in Appendix J of [3]. The interior view of the model is given in Figure 52.

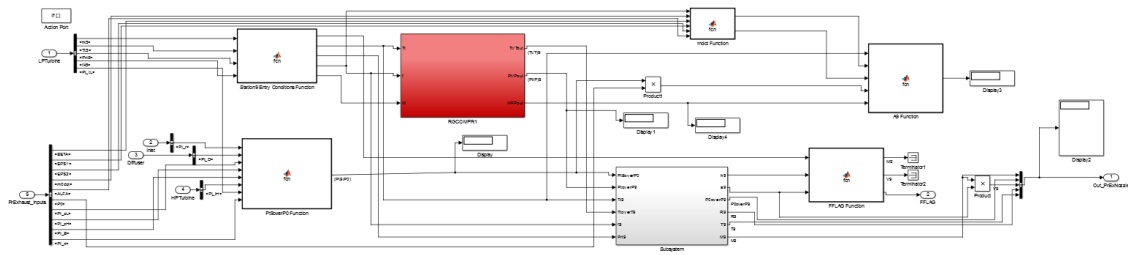


**Figure 52** Interior view of Primary Exhaust sub-model

In Figure 52, the Subroutine performs calculations of the primary exhaust Mach number and  $P_0 / P_9$  with the aforementioned methodology. The Station9 Entry Conditions Function initializes the thermodynamic states of Station 9, Pt9overP0 Function calculates the pressure ratio  $P_{t9} / P_0$ , and FFLAG Function sets the FFLAG value to indicate that the calculations of this sub-model is finished. RGCOMP1 block is used to find total property ratios at Station 9.

### 3.2.12 Secondary Exhaust

Secondary Exhaust sub-model calculates the secondary stream Mach number,  $P_0 / P_{19}$ , secondary stream flow speed, temperature and gas constant and Secondary Exhaust flow area. It takes Inlet pressure ratio from Inlet sub-model, Fan total thermodynamic properties from Fan sub-model, Diffuser pressure ratio from Diffuser sub-model. Secondary Exhaust sub-model takes Fan and Fan nozzle pressure ratios, ambient

pressure, by-pass ratio and total mass flow rate from the on-design input set. This sub-model is shown in Figure 53.

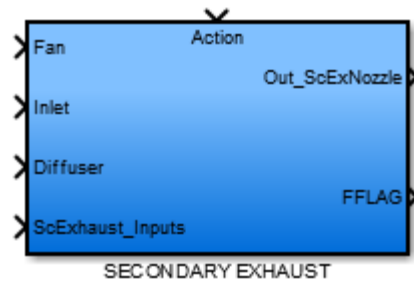


**Figure 53** Secondary Exhaust sub-model for the Secondary Exhaust cycle calculations

Secondary Exhaust sub-model uses a similar subroutine with Primary Exhaust to find the secondary stream Mach number and  $\frac{P_0}{P_{19}}$ . In this subroutine total to static pressure ratio at the secondary exhaust is compared with the ratio  $\frac{P_{t19}}{P_0}$ . If the latter is smaller than the first one the Mach number at secondary exhaust is calculated by using Equation (6) at Station 19 and  $\frac{P_0}{P_{19}}$  is calculated by dividing the total to static pressure ratio at the secondary exhaust to the  $\frac{P_{t19}}{P_0}$ , else  $\frac{P_0}{P_{19}}$  is taken as unity and total to static pressure ratio at the secondary exhaust is equal to  $\frac{P_{t19}}{P_0}$ . The Mach number is calculated by using the total to static pressure ratio at the secondary exhaust in Equation (6). This methodology complies with the method given in Appendix J of [3]. The interior view of the model is given in Figure 54.

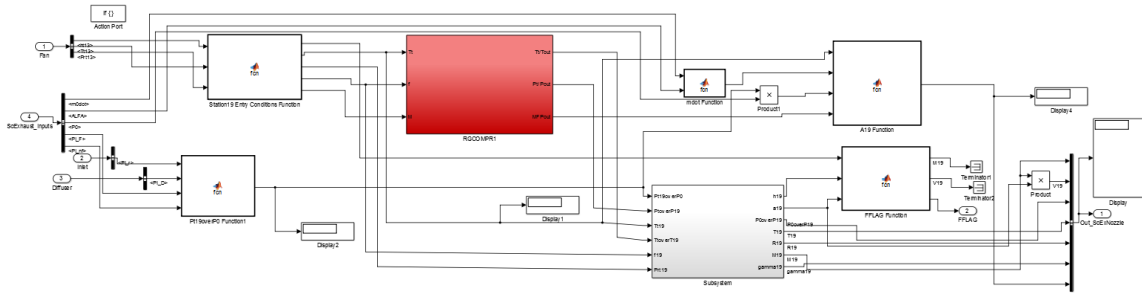


**Figure 54** Interior view of Secondary Exhaust sub-model

In Figure 54, the Subsystem performs calculations of the primary exhaust Mach number and  $P_0$   $P_{19}$  with the aforementioned methodology. The Station19 Entry Conditions Function initializes the thermodynamic states of Station 19, Pt19overP0 Function calculates the pressure ratio  $P_{t19}$   $P_0$ , FFLAG Function sets the FFLAG value to indicate that the calculations of this sub-model is finished, and A19 Function calculates the flow area at the Secondary Exhaust for Performance Cycle model. RGCOMP1 block is used to find total property ratios at Station 19.

### 3.2.13 Final Calculations

This sub-model calculates the on-design cycle main outputs such as Specific Thrust, Thrust Specific Fuel Consumption, Propulsive, Thermal and Overall Efficiencies. The on-design cycle calculations finish with these calculations and an indicator of this situation is sent by FFLAG output parameter to the Engine Design Model. This sub-model takes inlet thermodynamic properties from Inlet sub-model, fuel to air ratio from the Combustor sub-model, primary exhaust flow speed, and thermodynamic properties from Primary Exhaust sub-model and secondary exhaust flow speed and thermodynamic properties from Secondary Exhaust sub-model. It takes by-pass ratio, bleed air fractions, fuel heating value, ambient temperature, and CTOL and CTOH coefficients from the on-design input set. This sub-model is shown in Figure 55.

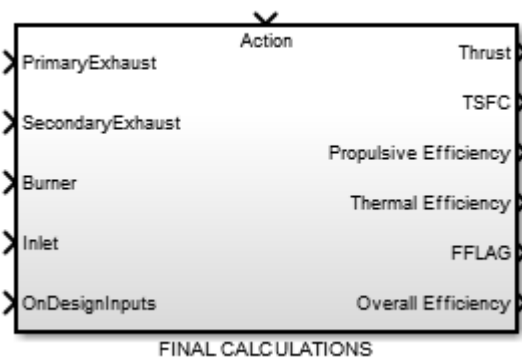


**Figure 55** Final Calculations sub-model for the on-design cycle calculations

Final Calculations sub-model uses Equation (56) for Specific Thrust calculation, Equation (67) for Thrust Specific Fuel Consumption, and Equations (68), (69) and (70) for the Propulsive, Thermal and Overall Efficiency calculations respectively. The interior view of the model is given in Figure 56.

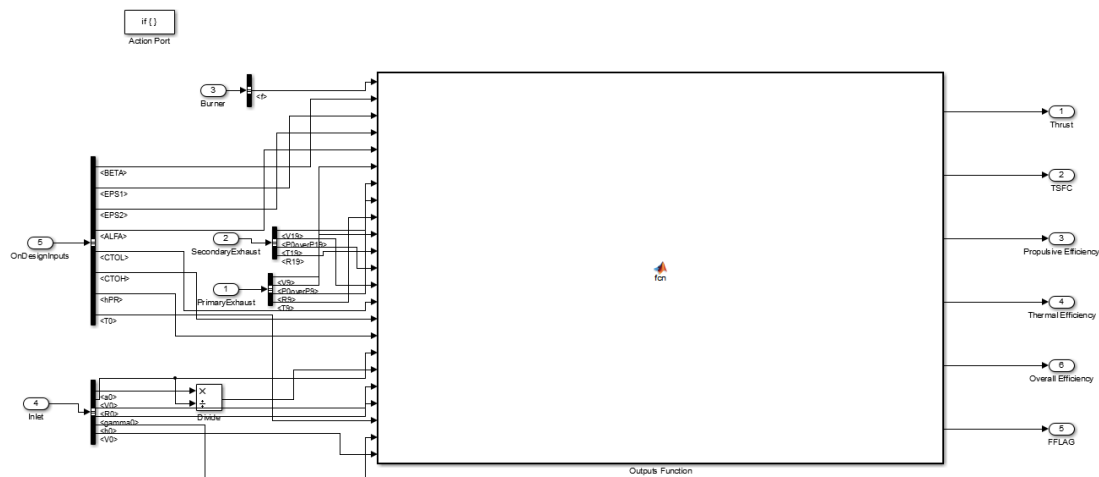


**Figure 56** Interior view of Final Calculations sub-model

In Figure 56, Outputs Function calculates the Specific Thrust, Thrust Specific Fuel Consumption, Propulsive, Thermal and Overall Efficiencies.

### 3.3 Performance Cycle Model

Performance Cycle Model calculates the off-design performance of the engine used in the on-design analysis by using the off-design analysis equations introduced in Section

2.2. The calculation methodology is based on the algorithm given in Appendix J of [3] for high by-pass turbofan engines. The model view in Simulink is shown in Figure 57.

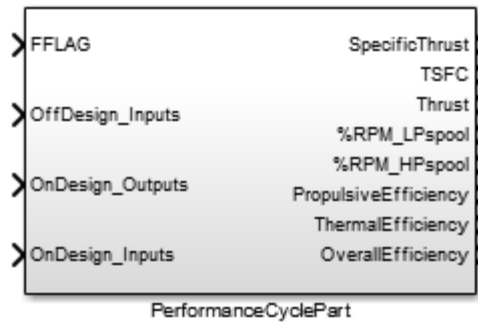


**Figure 57** Performance Cycle Model in the Engine Design Model

The Performance Cycle Model starts execution after the Parametric Cycle model sends it its finalizing signal (FFLAG). In addition to the on-design cycle outputs, the Performance Cycle Model takes the Off-Design input parameters listed in Table 5 and outputs the off-design output parameters listed in Table 6.

The Performance Cycle Model includes 3 nested while iterator loops, the first two are being the design loops and the latter one is the control loop. The design loops are named after the main decision parameter used in it. The inner while loop determines the by-pass ratio and the outer while loop determines the mass flow rate. The outermost while loop controls the control criteria ( $T_{t4}$  and  $\pi_{Cmax}$ ) and gives end of execution command if these criteria are met. The ranges of control criteria are determined by the user via input m-file. After the convergence of the design loops and the control loop, off-design cycle results are calculated. The “if-action” blocks are used similarly with the Parametric Cycle Model, in order to control the execution sequence. The model is outlined in Figure 58.

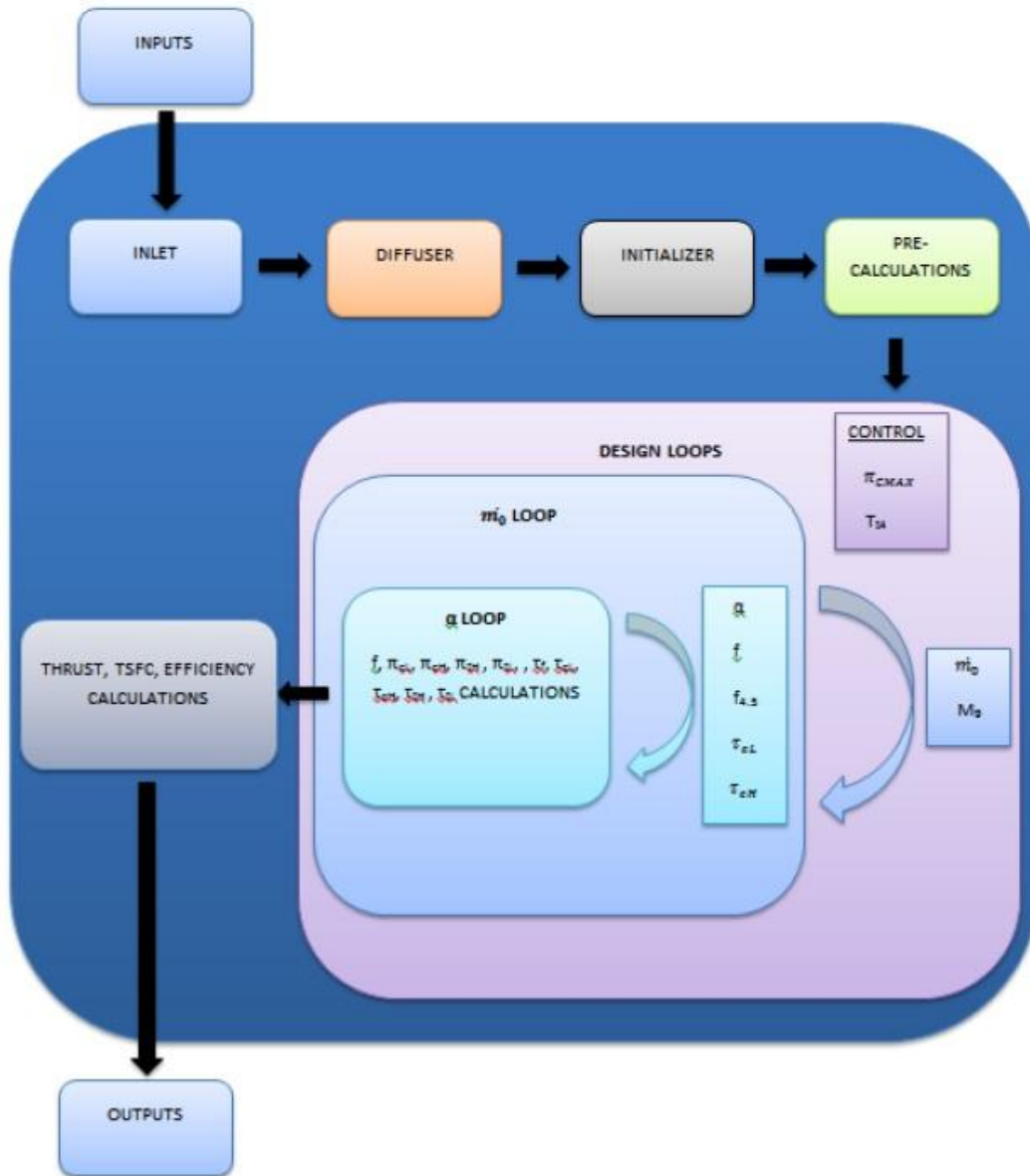


**Figure 58** A summarized view of the Performance Cycle Model

The Performance Cycle Model usually needs more execution time and computational power when compared to the Parametric Cycle and Turbomachinery Design models. The convergence criterion of design loops comply with the method given in performance cycle calculation algorithm in Appendix J of [3]. The interior view of the Parametric Cycle Model is given in Figure 59.

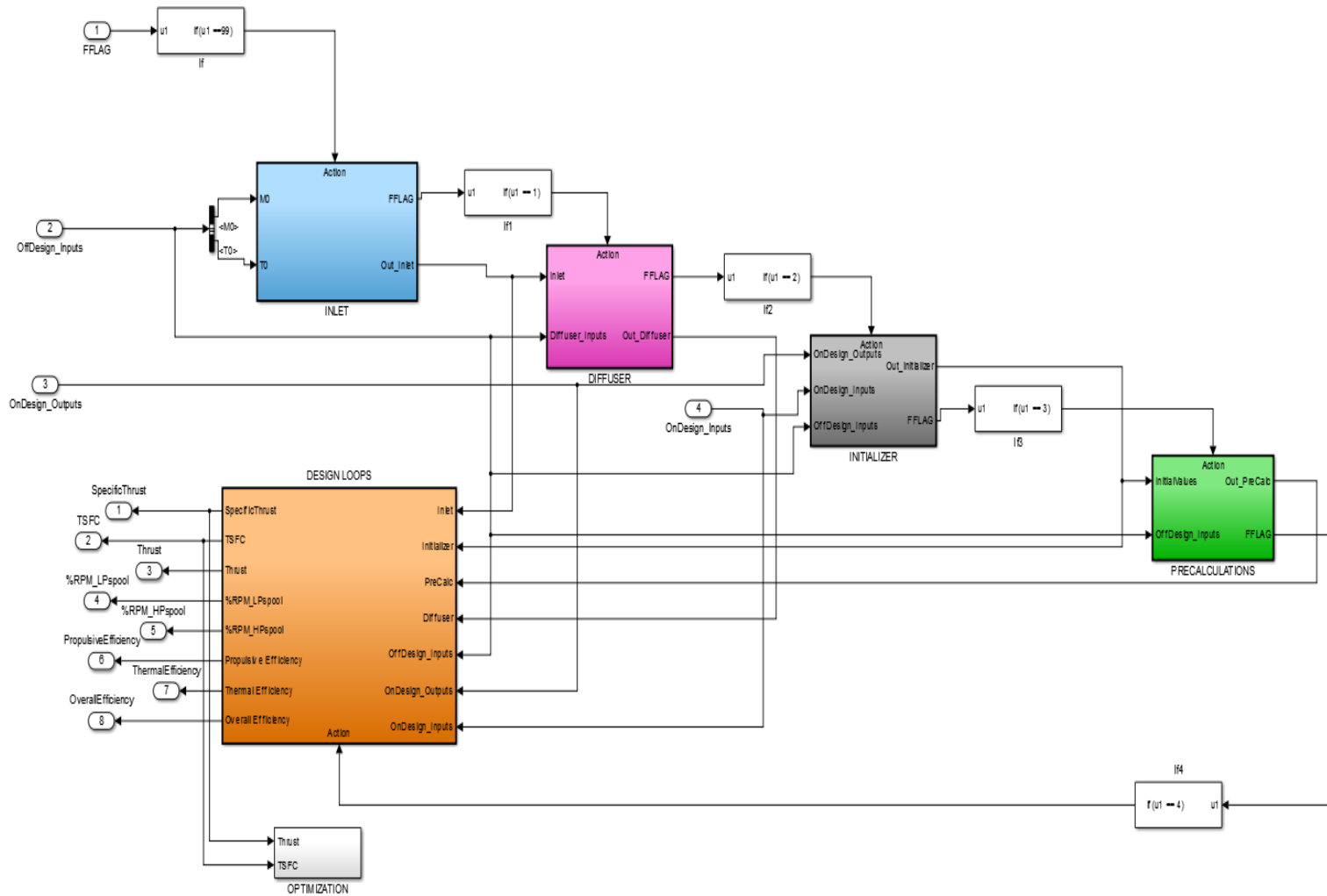
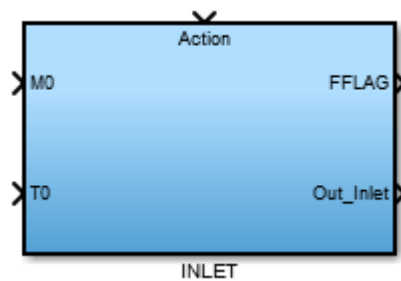


Figure 59 The interior view of Performance Cycle Model

As for the Parametric Cycle model, an Optimization block is added to the model containing the signal constraints needed by the Optimization Toolbox of Simulink. The sub-models used in cycle analysis calculations are explained hereinafter.

### 3.3.1 Inlet

The Inlet sub-model in the Performance Cycle Model is identical with the Inlet sub-model used in Parametric Cycle model. The intention of the block is the same and it takes only the inlet Mach number and Temperature from the off-design input set as inputs. The block is shown in Figure 60.



**Figure 60** Inlet sub-model for the inlet/diffuser entry off-design calculations

The Inlet sub-model uses F-AIR1 and F-AIR2 blocks to obtain the thermodynamic properties of inlet conditions and uses the relations given in Assumption 4 of Section 2.1.7 to calculate the pressure ratio and the  $\eta_{Rspec}$ . The interior view of the model is the same with the given view in Figure 32.

### 3.3.2 Diffuser

The Diffuser sub-model in the Performance Cycle Model is identical with the Diffuser sub-model used in Parametric Cycle model. The outputs of the block are also same and it takes  $\pi_{dMAX}$  value from off-design input set and  $\eta_{Rspec}$ , inlet thermodynamic properties from the Inlet sub-model. The block is shown in Figure 61.



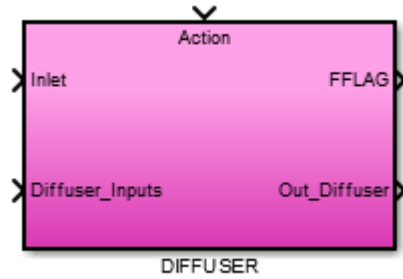


**Figure 61** Diffuser sub-model for the diffuser calculations for off-design

The Diffuser sub-model uses Equation (7) to find the diffuser pressure ratio and the interior view of the model is the same with the given view in Figure 34.

### 3.3.3 Initializer

The Initializer block passes the output parameters from the Parametric Cycle Model (on-design) to the relevant variables in the Performance Cycle Model. It takes on-design temperature ratios (Fan, Compressors, Combustor, Turbines and Coolant Mixers), exhaust Mach numbers and fuel to air ratio from the on-design results, on-design input pressure ratios of Fan and Compressors and by-pass ratio from on-design inputs, and High Pressure Turbine entry temperature ( $T_{t4}$ ) from the off-design inputs. The block is shown in Figure 62.

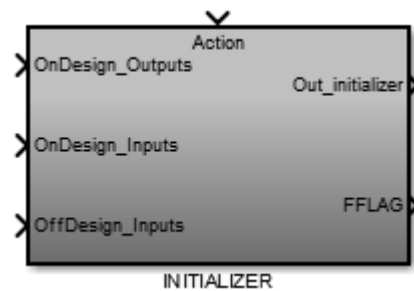


**Figure 62** Initializer sub-model for the initialization of off-design parameters

The initial values and reference values of some off-design parameters during the off-design cycle calculations are taken from this sub-model. The interior view of the sub-model is shown in Figure 63.

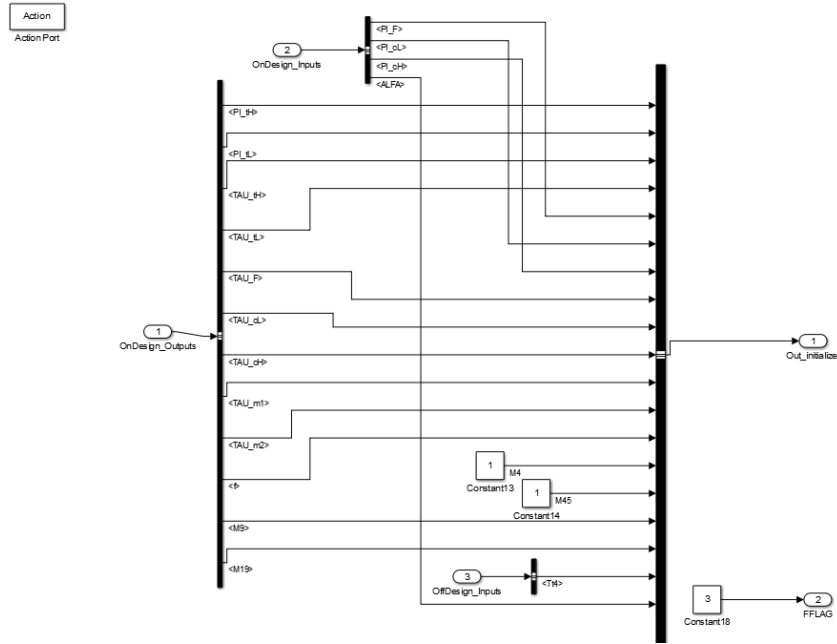


**Figure 63** The interior view of Initializer sub-model

### 3.3.4 Pre-Calculations

Pre-Calculations sub-model performs initial fuel to air ratio at Station 4.5 ( $f_{4.5}$ ), total temperature (for states 5i and 4.5i) and enthalpy calculations (for Station 5) before starting the calculations in the off-design cycle loops. It takes on-design fuel to air ratio, Coolant Mixer temperature ratios and High and Low Pressure Turbines initial temperature ratios from the Initializer block, and High Pressure Turbine entry temperature and bleed air fractions from the off-design input set. The block is shown in Figure 64.

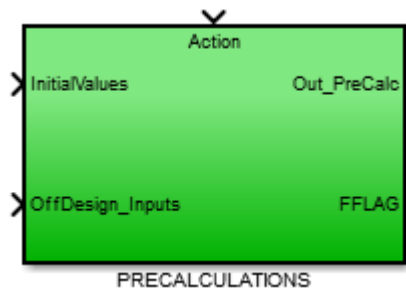


**Figure 64** Pre-Calculations sub-model for the off-design initial calculations

Equation (74) is used in the calculation of fuel to air ratio at Station 4.5 and total thermodynamic properties are calculated by using F-AIR blocks. The interior view of the model is given in Figure 65.

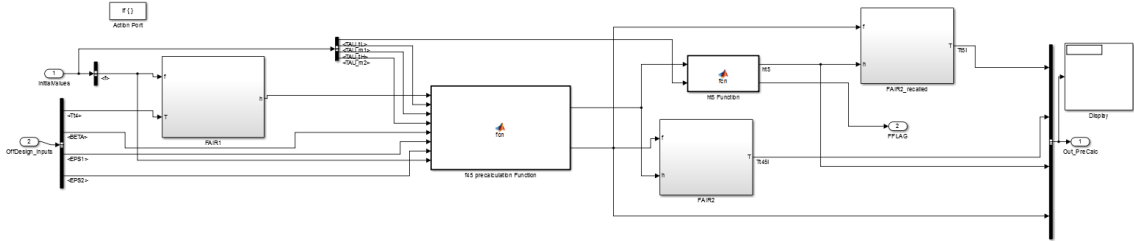


**Figure 65** The interior view of the Pre-Calculations sub-model

In Figure 65, the f45 precalculation Function calculates the fuel to air ratio and total enthalpy at Station 4.5 and the ht5 Function calculates the total enthalpy at Station 5.

### 3.3.5 Design Loops

This sub-model includes the performance cycle control loop,  $\mathbf{m}_0$  and  $\alpha$  design loops. The loop structures are designed according to the solution theory in Section 2.2 and the methodology given in Appendix J of [3]. Design Loops sub-model gives Specific Thrust, Thrust Specific Fuel Consumption, Thrust, %RPM at Low Pressure Spool, %RPM at High Pressure Spool, Propulsive Efficiency, Thermal Efficiency and Overall Efficiency as outputs. Inlet, Diffuser, Initializer, Pre-Calculations sub-model outputs and Parametric Cycle results, Parametric Cycle input set and Performance Cycle input set are the inputs of the sub-model to perform the necessary off-design cycle calculations. The sub-model is shown in Figure 66.

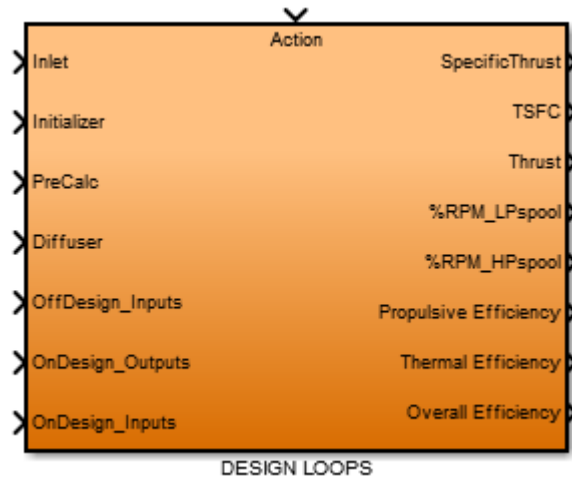


**Figure 66** Design Loops sub-model that includes the Performance Cycle Loops

The execution sequence of the loop structure starts from the innermost loop and ends with the outermost loop. For the off-design calculations, the loop that determines the by-pass ratio ( $\alpha$  loop) should be converged first. Then with the fixed by-pass ratio, the calculation of the mass flow rate begins. If the loop that determines the mass flow rate ( $m_0$  loop) does not converge, than a new by-pass ratio is calculated by  $\alpha$  loop. This procedure is repeated until the convergence of the  $m_0$  loop. With the fixed values of by-pass ratio and mass flow rates and relevant component design parameters, the control loop checks whether the control criteria is satisfied or not. If it is satisfied then the off-design calculations are finished with the calculation of the off-design output parameters, else the whole procedure starts with a new High Pressure Turbine Inlet Temperature value. The sub-models that perform this cyclic calculation procedure are explained in the following sections starting from the innermost one to the outer ones.

### 3.3.5.1 Alfa Loop

This while-iterator sub-model calculates the by-pass ratio, the High Pressure Turbine pressure and temperature ratio, Low Pressure Turbine pressure and temperature ratio,  $\tau_\lambda$ , Low Pressure Compressor pressure and temperature ratio, High Pressure Compressor pressure and temperature ratio, Fan temperature ratio, fuel to air ratio, fuel to air ratio at Station 4.5, and Secondary Exhaust flow speed and thermodynamic properties.

It takes inlet thermodynamic properties and inlet pressure and temperature ratio from the Inlet sub-model, diffuser pressure ratio from the Diffuser sub-model, reference values from the Initializer sub-model, initial estimates of fuel to air ratio at Station 4.5 and total temperature at Station 4.5 from the Pre-Calculations sub-model, High Pressure Turbine Inlet Temperature, Primary Exhaust flow Mach number, and total mass flow rate. The flow areas calculated for Stations 4, 4.5, 5 and 19 are taken from the on-design outputs. Alfa Loop sub-model is shown in Figure 67.

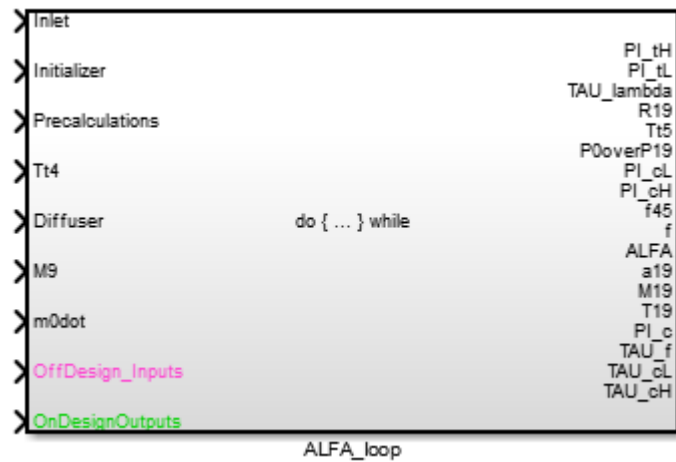


**Figure 67** Alfa Loop sub-model that perform by-pass ratio calculations

The High Pressure Turbine Inlet Temperature, Primary Exhaust flow Mach number, and total mass flow rate comes from the outer loops and are taken equal to the reference (on-design) values at the first run. Then these values are modified according to the convergence of the design loops. Two special sub-models are developed, which are named as TURB and TURBC, for the Low and High Pressure Turbine cyclic off-design calculations presented in Section 2.2.3. The interior view of the sub-model is shown in Figure 67.

The off-design by-pass ratio calculations start with the turbine calculations and finish with the new by-pass ratio calculation. The convergence of the Alfa loop is determined by the criterion suggested by Mattingly et al. [3] and given in Equation (152).

$$Err = \left| \frac{\alpha - \alpha_{new}}{\alpha_R} \right| < 0.001 \quad (152)$$

In Equation (152),  $\alpha$  is the by-pass ratio from the previous iteration,  $\alpha_{new}$  is the by-pass ratio calculated at the recent iteration and  $\alpha_R$  is the reference by-pass ratio which is the on-design by-pass ratio. If the convergence criterion in Equation (152) is satisfied, the by-pass ratio calculations are completed.

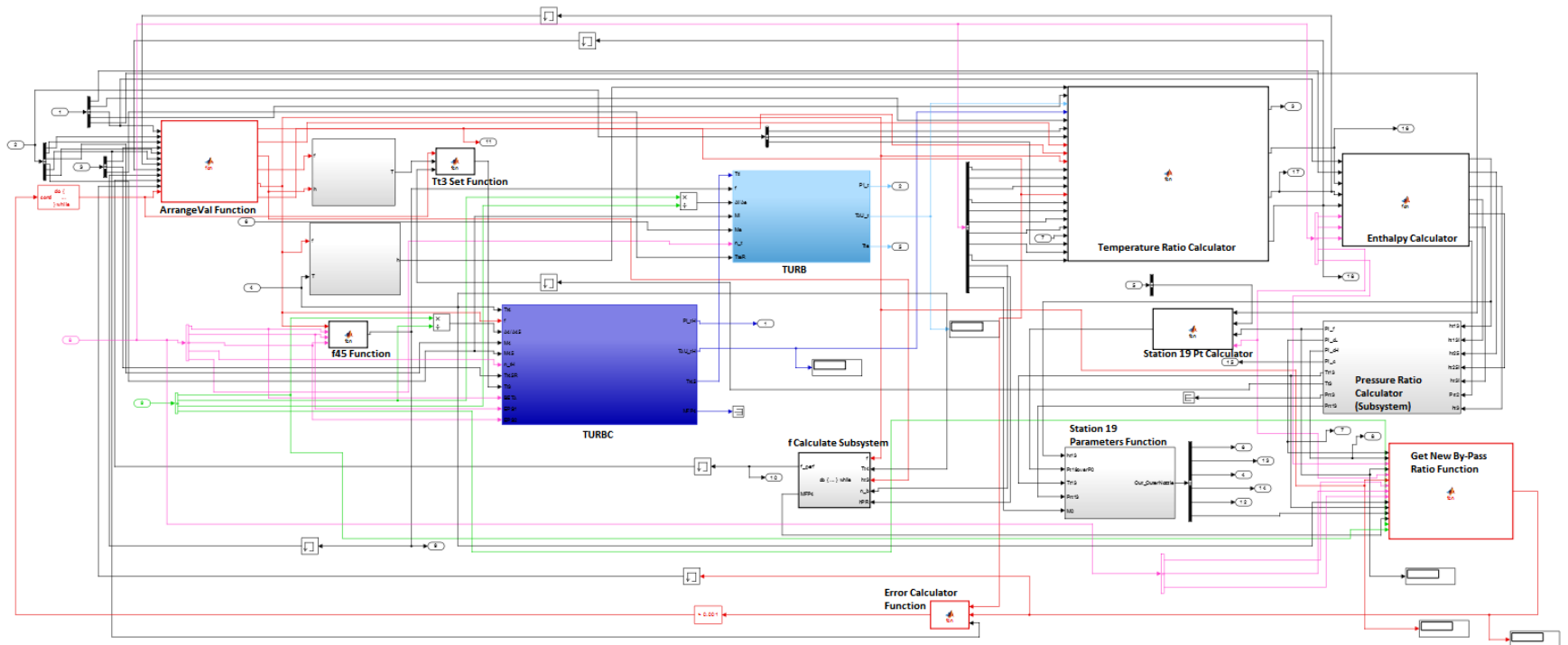


**Figure 68** Interior view of the Alfa Loop sub-model, off-design input signals are highlighted with pink, on-design output signals are highlighted with green, TURB function outputs are highlighted with light blue, TURBC function outputs are highlighted with dark blue and the loop signals and the functions calculating them are highlighted with red

In Figure 68, the ArrangeVal Function sends the values of fuel to air ratio at Station 4.5, fuel to air ratio, by-pass ratio, and temperature ratio of Low and High Pressure Compressor to the thermodynamic property calculations for Station 3. If the loop is run for the first time, it sends the initial conditions of these values, for the later runs it sends the calculated values from the previous loop. Tt3 Set Function is a special version of ArrangeVal Function, which sends the initial condition on  $T_{t3}$  for the first run and sends the calculated  $T_{t3}$  value at the later runs.

The f45 Function calculates the recent fuel to air ratio at Station 4.5 with the new parameters by using Equation (74). The Temperature Ratio Calculator function calculates the  $\tau_\lambda$  value by using Equation (29), Fan temperature ratio by using Equation (87), Low Pressure Compressor temperature ratio by using Equation (88), and High Pressure Compressor temperature ratio by using Equation (91).

The Enthalpy Calculator Function calculates the total enthalpies at fan entry (Station 13), high pressure compressor entry (Station 2.5), high pressure compressor exit (Station 3) and total enthalpies of isentropic processes at these stations for the calculation of pressure ratios of Fan, Low and High Pressure Compressors at Pressure Ratio Calculator Subsystem.

Pressure Ratio Calculator Subsystem includes F-AIR blocks to apply equations (89), (90) and (92) for the calculations of pressure ratios of Fan, Low Pressure Compressor and High Pressure Compressor respectively. The Station19 Pt Calculator function calculates  $\frac{P_{t19}}{P_0}$  by using Equation (98) in order to be used in the Station 19 Calculator

Subsystem which calculates the primary exhaust Mach number and  $\frac{P_0}{P_{19}}$  and identical to the Subsystem in Section 3.2.12.

The Get New By-Pass Ratio Function calculates the new by-pass ratio by using Equation (95) with the new calculated off-design parameters. Its output is used in Error Calculator Function, where the value of the error given in Equation (152) is computed.



The f-calculate subsystem computes the fuel to air ratio of the off-design cycle and the Mass Flow Parameter at Station 4 in an iterative scheme. It uses a comparison criterion similar to the one given in Equation (152). It ends iterations if the difference between the fuel-to air ratios of two adjacent iterations is less than 0.0001. The respective Mass Flow Parameter is calculated by using RGCOMPR1 block.

### 3.3.5.1.1 TURB

TURB subroutine calculates the Low Pressure Compressor pressure ratio, temperature ratio and Low Pressure Turbine exit temperature with an iterative process. It takes fuel to air ratio at Station 4.5, Low Pressure Turbine Inlet Temperature, flow Mach number, Low Pressure Turbine inlet to exit area ratio, primary exhaust Mach number, Low Pressure Turbine component efficiency and reference (on-design) Turbine exit temperature. These input parameters are taken from the reference values at the first run, but they are updated during the succeeding runs and calculated in the Alfa loop. The sub-model in the Performance Cycle model is given in Figure 69.

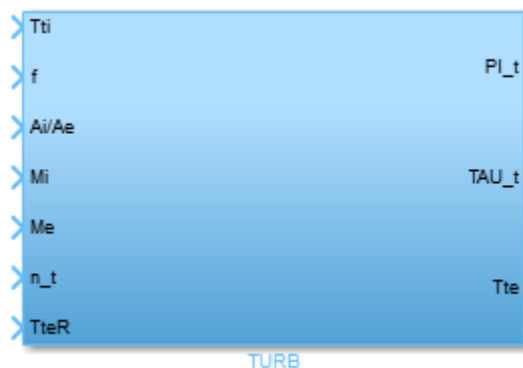


**Figure 69** TURB sub-model in the Alfa Loop of Performance Cycle Model

The interior view of the sub-model is given in Figure 70. This sub-model is developed from the TURB algorithm given in Appendix F of Mattingly et al. [3]. The algorithm of this subroutine is explained in Section 2.2.3.

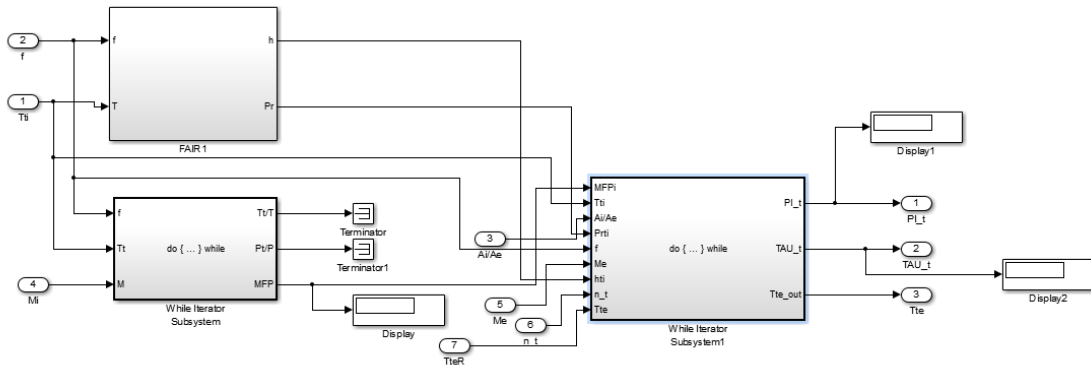


**Figure 70** The interior view of the TURB sub-model

In Figure 70, F-AIR1 block calculates the enthalpy and reduced pressure at the Low Pressure Turbine inlet (Station 4.5) and the While Iterator Subsystem calculates the Mass Flow Parameter at Station 4.5 for the Low Pressure Turbine design algorithm by using the same while iterator block used in RGCMPR1. The While Iterator Subsystem 1 calculates the Low Pressure Turbine pressure ratio by using Equation (82). Equation (85) is used for the calculation of the Low Pressure Turbine temperature ratio and the total enthalpies of the States 5i and 4.5 used in Equation (84) to find the ideal temperature ratio is calculated by the F-AIR blocks. Low Pressure Turbine exit temperature is found by using F-AIR2 block with  $f_{4.5}$  and total enthalpy at Station 5. The whole process (Steps 1, 2, 3 and 4 in Section 2.2.3) is repeated in a while loop until the difference between two Low Pressure Turbine exit temperatures calculated from two adjacent loop runs is less than 0.0001.

### 3.3.5.1.2 TURBC

TURBC subroutine calculates the High Pressure Compressor pressure ratio, temperature ratio and High Pressure Turbine exit temperature with an iterative process. It takes fuel to air ratio, High Pressure Turbine Inlet Temperature, flow Mach number at Station 4, High Pressure Turbine inlet to exit area ratio from on-design outputs, flow Mach number at Station 4.5, bleed air ratios, Combustor inlet total temperature, High Pressure Turbine component efficiency and reference (on-design) High Pressure Turbine exit temperature. These input parameters are taken from the reference values at the first run, but they are

updated during the succeeding runs and calculated in the Alfa loop. The sub-model in the Performance Cycle model is given in Figure 71.

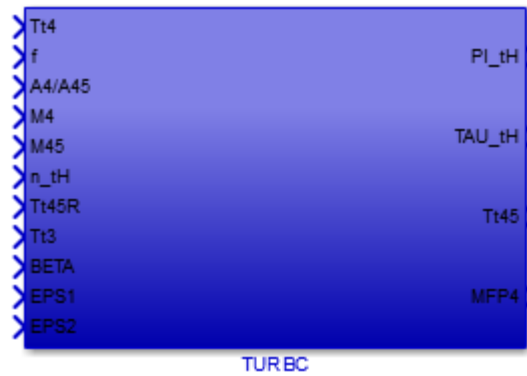


**Figure 71** TURBC sub-model in the Alfa Loop of Performance Cycle Model

The interior view of the sub-model is given in Figure 72. This sub-model is developed from the TURBC algorithm given in Appendix F of Mattingly et al. [3]. The algorithm of this subroutine is explained in Section 2.2.3.

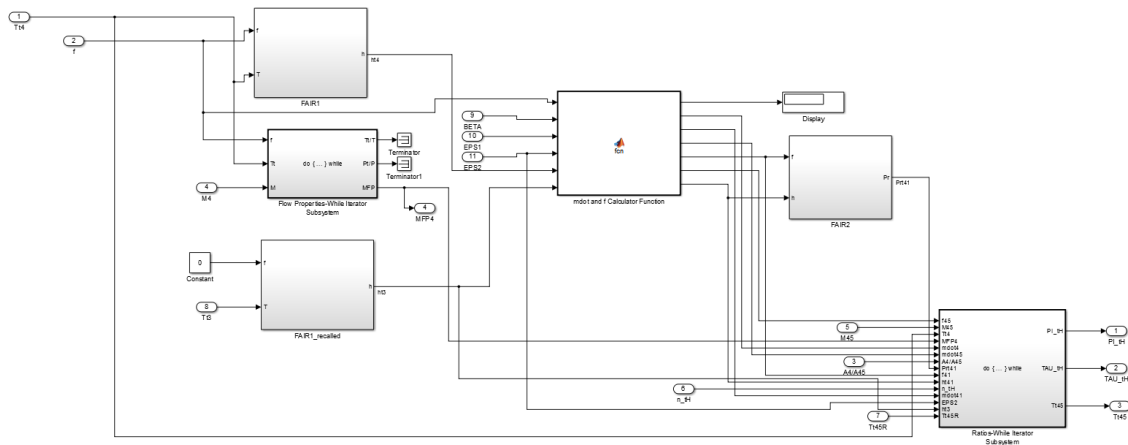


**Figure 72** The interior view of the TURBC sub-model

In Figure 72, F-AIR1 blocks are used to calculate the total enthalpies at Stations 3 and 4, which are used in the calculation of the total enthalpy at Station 4.1 together with the bleed air fractions. The Flow Properties-While Iterator Subsystem is the same while loop algorithm used in the RGCOMP1 block to find the Mass Flow Rate at Section 4. The

$\dot{m}$  and  $f$  Calculator function calculates the mass flow rates at Stations 4, 4.1 and 4.5 and fuel to air ratios at Stations 4.1 and 4.5.

The Ratios-While Iterator Subsystem calculates the High Pressure Turbine pressure ratio, temperature ratio and total temperature at Station 4.5 with an iterative scheme. It is the application of the method given in Section 2.2.3 for High Pressure Turbines. It calculates the High Pressure Turbine pressure ratio by using Equation (73). Equation (79) is used for the calculation of the High Pressure Turbine temperature ratio and the total enthalpies of the States 4.4i and 4.1 used in Equation (78) to find the ideal temperature ratio is calculated by the F-AIR blocks. Total temperature at Station 4.5 is found by using F-AIR2 block with  $f$  and total enthalpy at Station 4.5. The whole process (Steps 1, 2, 3, 4, 5 and 6 in Section 2.2.3) is repeated in a while loop until the difference between two  $T_{t4.5}$  values calculated from two adjacent loop runs is less than 0.0001.

### 3.3.5.2 $m_0$ Loop

This loop determines the off-design total mass flow rate and Primary Exhaust Mach number ( $M_9$ ) by calculating  $\frac{P_{t9}}{P_0}$  from the component pressure ratios, which are calculated in Alfa Loop.  $m_0$  Loop takes inlet pressure ratio from the Inlet sub-model, initial value of Primary Exhaust Mach from the Initializer sub-model, Diffuser pressure ratio from the Diffuser sub-model, ambient pressure and temperature, Combustor pressure ratio and nozzle pressure ratio from the off-design input set and Inlet and Diffuser reference pressure ratio and Mass Flow Parameter at the Combustor from the Parametric Cycle outputs. It also sends the outputs of Alfa Loop to the relevant calculations in the control loop.  $m_0$  Loop sub-model is shown in Figure 73.

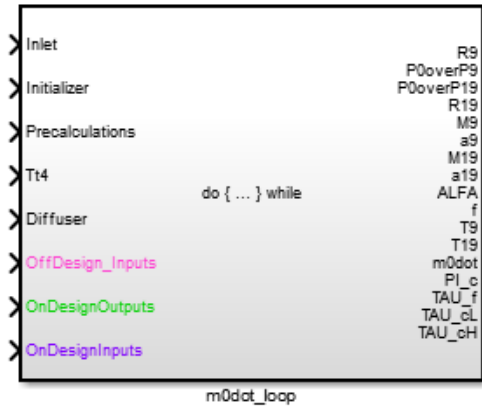


**Figure 73**  $m_0$  Loop sub-model that perform mass flow rate and  $M_9$  calculations

$m_0$  Loop transmits some of the input signals to the Alfa Loop and output signals from the Alfa Loop to the relevant calculations in the Control Loop. As being the outer loop in the design, it calls Alfa Loop with new  $M_9$  and  $m_0$  values if the stopping criterion is not satisfied. As for the Alfa Loop, the convergence criterion suggested by Mattingly et al. [3] uses the difference between the new calculated  $m_0$  with the one calculated in the previous loop and the reference value. The convergence criterion is given in Equation (153).

$$Err = \left| \frac{\dot{m}_{0,new} - \dot{m}_0}{\dot{m}_{0,R}} \right| < 0.001 \quad (153)$$

In Equation (153)  $m_0$  is the total mass flow rate from the previous iteration,  $m_{0,new}$  is the total mass flow rate calculated at the recent iteration and  $m_{0,R}$  is the reference mass flow rate which is the on-design mass flow rate. If the convergence criterion in Equation (153) is satisfied, the iterations end. The interior view of the  $m_0$  Loop is shown in Figure 74.



In Figure 74, Pt9overP0 Function calculates  $\frac{P_{t9}}{P_0}$  by using Equation (97). RGCOMPR3

block uses this value together with the Low Pressure Turbine exit temperature and fuel to air ratio to calculate the Mass Flow Parameter at Station 9. The Mass Flow Parameter and the Total to Static Temperature ratio at Station 9 are then used in Subsystem 1 to calculate  $\frac{P_0}{P_9}$  and  $M_9$ . Subsystem 1 uses the same subroutine with the one introduced in Section 3.2.11 for  $M_9$  calculation which is based on the algorithm given in Appendix J of Mattingly et al. [3]. The static temperature at Station 9, which is another output of Subroutine 1, is then used in F-AIR1 block to calculate the gas constant and speed of sound at Station 9 which are later be used in Thrust calculations.

RGCOMPR1 is used to calculate Mass Flow Parameter at Station 4, which will be used in total mass flow rate for off-design calculations. The m0dot Calculator Function calculates the total mass flow rate by using Equation (96). The newly calculated mass flow rate is then compared by using the criteria given in Equation (153) in Error Calculator Function. If the criterion is not satisfied, the whole loop runs again with the newly calculated mass flow rate and Primary Exhaust Mach number ( $M_9$ ). For the first run the m0dot Set Function and M9 Set Function sends the reference values of mass flow rate and  $M_9$  respectively, whereas for the later runs it sends the newly calculated mass flow rate and  $M_9$  to the relevant calculations.

### 3.3.5.3 Control Loop

The Control Loop is the outermost loop in the Performance Cycle calculation method. The intention of this loop is to control whether the calculated values of the High Pressure Turbine inlet total temperature ( $T_{t4}$ ) and compressor pressure ratio ( $\pi_C$ ) from the design loops satisfy the limits put by the user in off-design input set or not.

It takes inlet flow conditions, thermodynamic properties and Inlet pressure ratio from the Inlet sub-model, on-design Fan, Low Pressure Compressor and High Pressure Compressor temperature ratio and  $T_{t4}$  values from the Initializer sub-model, off-design ambient pressure and temperature, inlet Mach number, fuel heating value, bleed air fractions and CTOL and CTOH values from the off-design input set, Inlet temperature

ratio and inlet enthalpy values from the on-design outputs. This loop calculates all of the Performance Cycle outputs which are Specific Thrust, Thrust, Thrust Specific Fuel Consumption, Propulsive Thermal and Overall Efficiencies, and Low and High Pressure Spool %RPM values. The Control Loop is shown in Figure 75.

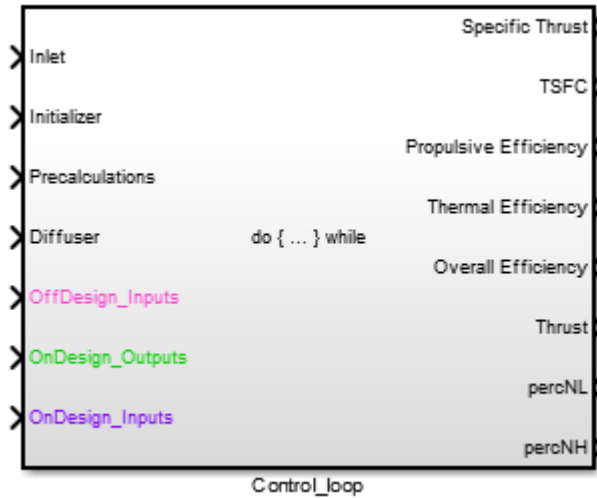


**Figure 75** Control Loop for the off-design output calculations

The value of  $T_{14}$  is taken equal to the off-design input value at the first run. This value is updated (reduced) if the control on compressor pressure ratio is not satisfied, it is reduced until the compressor pressure ratio criterion is satisfied. The compressor pressure ratio input by the user through the off-design input set is defined as the maximum attainable value by compressors and should always be lower than or equal to this value in order to finalize the off-design calculations.

Control Loop transmits the Inlet, Diffuser, Initializer, Pre-Calculations, Off-Design Input set, On-Design results, and some of the On-Design Inputs to the inner loops and takes the outputs of the design loops to calculate the off-design results. The interior view of the model is given in Figure 76.

The Low and High Pressure Spool %RPM values represent the variations in engine spool rotational speeds with respect to their respective on-design values. These variations can be obtained from the Equations (154) and (155) respectively, which are given in Mattingly et al. [3].



$$\%N_L = \sqrt{\frac{h_{t0} \tau_{cL} - 1}{h_{t0,R} \tau_{cL,R} - 1}} \quad (154)$$

$$\%N_H = \sqrt{\frac{h_{t0} \tau_{cL} \tau_{cH} - 1}{h_{t0,R} \tau_{cL,R} \tau_{cH,R} - 1}} \quad (155)$$

In Figure 76, in the first run the Tt4 Set Function sends the  $T_{t4}$  value from the off-design input set and  $m_0$  Loop initiates. After the convergence of the  $m_0$  Loop, the f0 Calculator Function takes the Combustor fuel to air ratio and by-pass ratio from the  $m_0$  Loop and bleed air fractions from the off-design inputs to calculate the overall fuel to air ratio by using Equation (35). After the calculation of the overall fuel to air ratio, the required input set for the Off-Design Results Function is completed for the calculations of off-design output set.

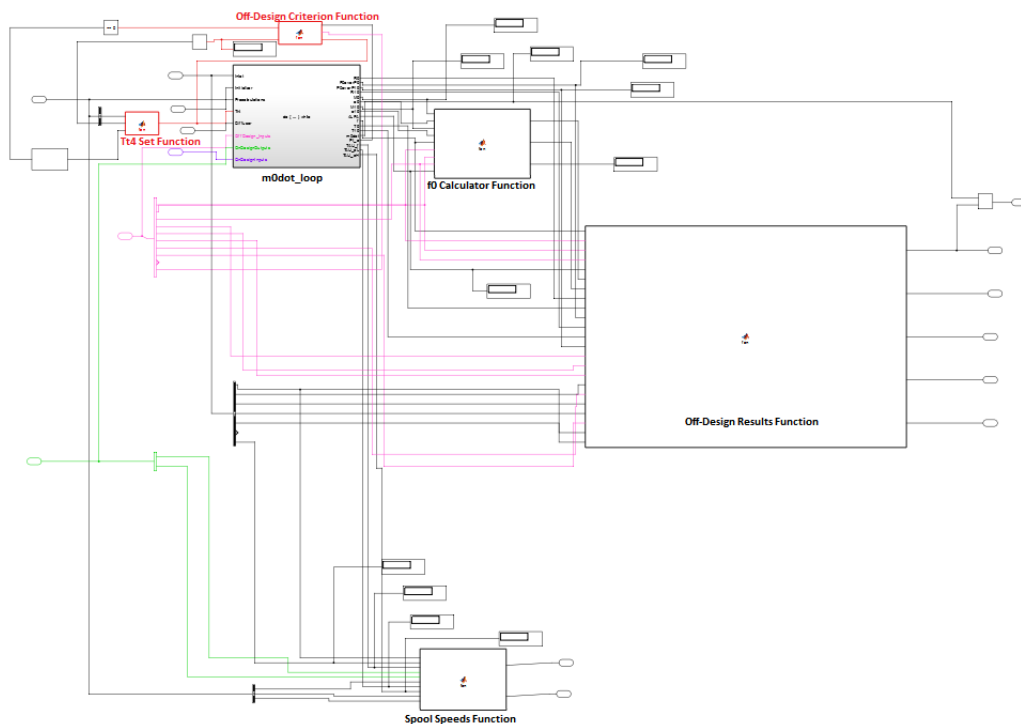


**Figure 76** Interior view of the Control Loop, off-design input signals are highlighted with pink, on-design output signals are highlighted with green, and the loop signals and the functions calculating them are highlighted with red

Off-Design Results Function uses Equation (56) for Specific Thrust calculation, and this value is then multiplied with the engine mass flow rate to obtain the Thrust value. Equation (67) is used to calculate the Thrust Specific Fuel Consumption and Equations (68), (69) and (70) are used to calculate the propulsive, thermal and overall efficiency in the Off-Design Results Function respectively. Aside, Spool Speeds Function calculates the  $\%N_L$  and  $\%N_H$  values by using Equations (154) and (155) respectively. The compressor pressure ratio, which is obtained from the multiplication of the pressure ratios of High and Low Pressure Compressors calculated by the design loops, is then compared with the limit given in the off-design input set at the Off-Design Criterion Function. If the new compressor pressure value is greater than the limit, then a new  $T_{t4}$  is calculated by reducing the recent value by  $2.78 \text{ }^0\text{K}$ . Then the whole loop is run again with the reduced  $T_{t4}$  and the process is repeated until the limit on compressor pressure ratio is satisfied.

### 3.4 Turbomachinery Design Model

The aim of the Turbomachinery Design Model is to make Fan, Low Pressure Compressor, High Pressure Compressor, High Pressure Turbine and Low Pressure Turbine aerothermodynamic design of a dual spool high by pass turbofan engine. The model takes on-design outputs to make necessary design calculations; therefore the design is based on on-design conditions. However, the Engine Design Model can easily be rearranged so that the off-design outputs can be connected as inputs to the Turbomachinery Design Model in order to make an off-design based aerothermodynamic design. The model view in Simulink is shown in Figure 77.

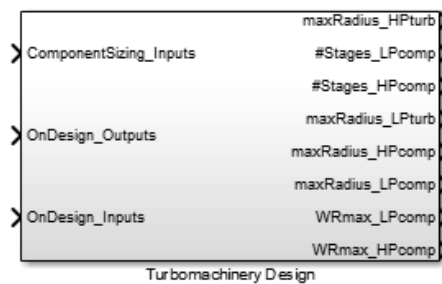


**Figure 77** Turbomachinery Design Model in the Engine Design Model

As stated in Section 2.3.1.1 according to Horlock [7] [8] and Mattingly et al. [3], there is not any precise design methodology for the design of axial flow compressors and turbines. In Turbomachinery Design Model, aerothermodynamic design algorithms are developed for compressors and turbines by using and combining the design methodologies and key points introduced in [6], [7], [8], [9] and [10]. The Turbomachinery Design Model starts calculations after the Parametric and Performance Cycle Models. This sequence is determined in order to make the model available to perform an off-design based aerothermodynamic design too.

Turbomachinery Design Model takes On-Design Outputs in addition to the component sizing inputs listed in Table 5. The component sizing inputs in the input m-file are the structural parameters and aerodynamic design limitations given in Section 2.3. Turbomachinery Design model takes parameters from the on-design input set which are by-pass ratio, total engine mass flow rate, on-design ambient conditions, bleed air fractions, High Pressure Turbine inlet temperature, and pressure ratios of compressors.

Because of the Turbomachinery Design Model is designed for dual spool systems, it includes two separate subsystems for the low and high pressure spool. The model can be extended to three shafted systems by removing the rotational speed signal connection between Low Pressure Turbine and Low Pressure Compressor.

In the model runtime, as being the inner loop, the Low Pressure Spool is executed first and the high pressure spool is executed at the end. After the convergence of both spools, the Turbomachinery Design calculations end and the outputs given in Table 6 are calculated. In addition to the output list given in Table 6, Turbomachinery Design Model calculates the stage velocity triangle angles, degree of reactions, areas, shaft rotational speeds, and rotor relative Mach numbers. The model is outlined in Figure 78.

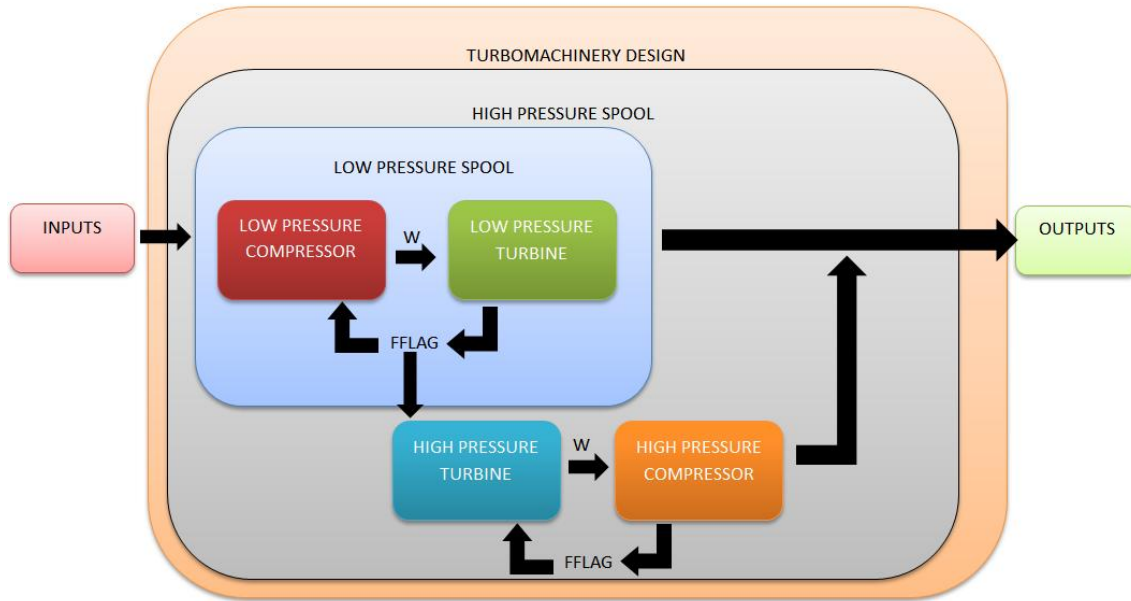


**Figure 78** A summarized view of the Turbomachinery Design Model

In Figure 78, both of the design loops are while-iterator loops which stop after the finish flag (FFLAG) is equal to a predetermined value. The finish flag is equated to the predetermined value if the calculated stage flow annulus area satisfies the mean line radius calculation. If the stopping criterion is not satisfied, FFLAG takes a different value and the spool rotational speed is decreased at the next iteration. The interior view of the model is shown in Figure 79.

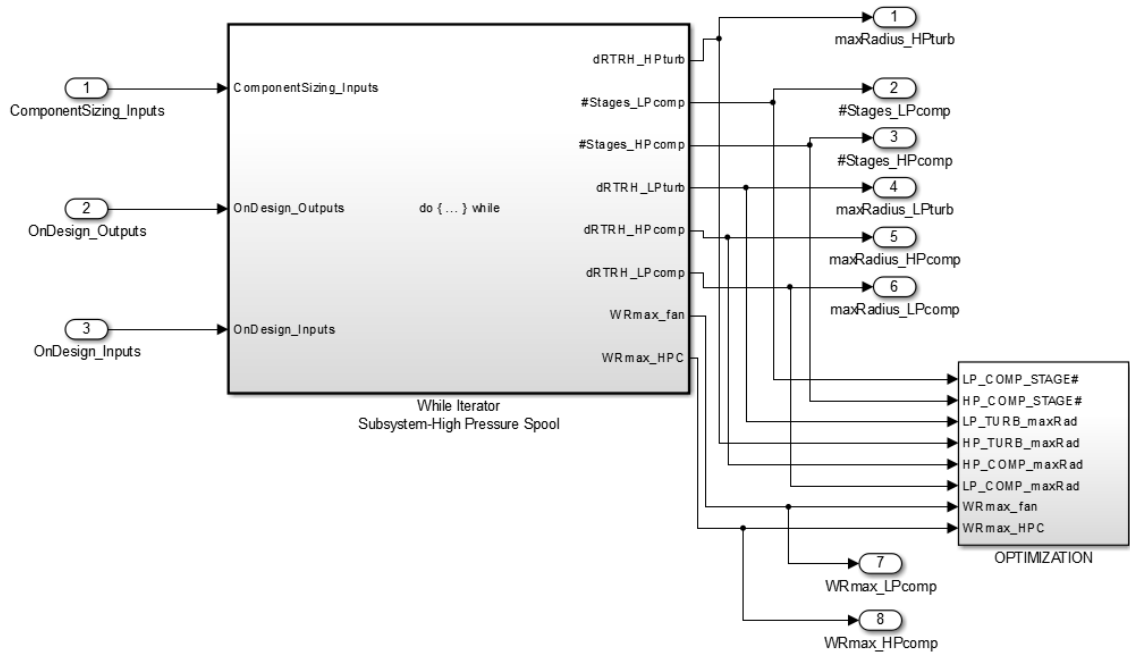


**Figure 79** Interior view of the Turbomachinery Design Model

In Figure 79, an Optimization block is added to the system as for the other models, in order to introduce the signal constraints on the predetermined optimization parameters to the Optimization Toolbox of Simulink. The sub-models used in aerothermodynamic turbomachinery design calculations are explained hereinafter.

### 3.4.6 Low Pressure Spool

The Low Pressure Spool while-iterator block includes the Low Pressure Compressor and Low Pressure Turbine subroutines which calculate the aerothermodynamic design parameters of the respective engine parts. Both subroutines are Embedded MATLAB Functions. The solution methodology design is based on the calculation methods given in [14]. The interior view of the model is shown in Figure 80.

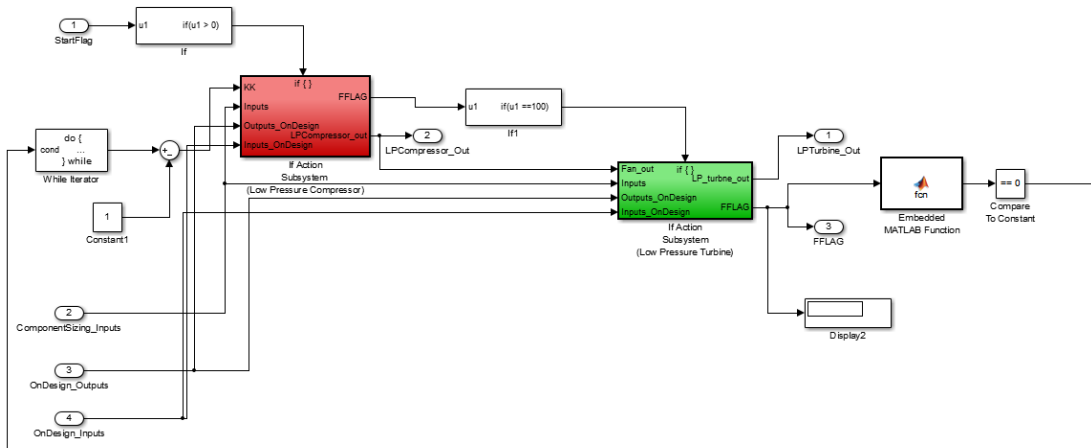


**Figure 80** Interior view of the Low Pressure Spool

The calculations start with the Low Pressure Compressor and Fan design which determines the shaft rotational speed ( $\omega$ ) and sends this value to the Low Pressure Turbine. The Low Pressure Turbine subroutine calculates the design parameters by using this rotational speed and compares the flow annulus area calculated by using the cascade angles with the mean line radius calculated by using the shaft rotational speed. If the mean line radius is not satisfied, then the blade tensile stress value is decreased by 0.689 MPa at the next iteration in the Low Pressure Compressor and the shaft rotational speed is decreased until the mean radius of Low Pressure Turbine stages satisfies the flow annulus area.

### 3.4.6.1 Low Pressure Compressor

The Low Pressure Compressor algorithm is based on the solution methodology given in Mattingly et al. [6] for the AAF engine case study and the key design points given in [8], [9] and [10]. The model including this subroutine in the Low Pressure Spool sub-model is shown in Figure 81.

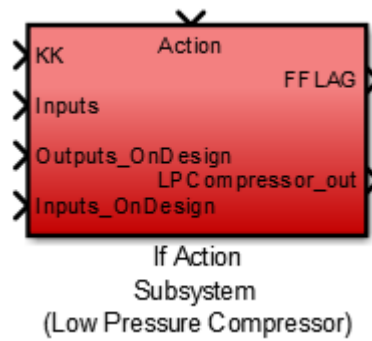


**Figure 81** Model including the Low Pressure Compressor subroutine

The algorithm for the Low Pressure Compressor includes fan design and it treats the first stage of the Low Pressure Compressor as the fan stage.

In the design algorithm illustration in Figure 82, the input parameter KK indicates the current number of iteration of the Low Pressure Spool. The specific heat ratio  $\gamma_C$  comes from the Low Pressure Compressor outputs of Parametric Cycle, total mass flow rate  $m_0$  and flight Mach number  $M_0$  comes from the on-design input set. The compressor blade tip to hub area ratio ( $A_t/A_h$ ) is taken as constant. Solidity (c/s) has an initial value of 1.1 but it may be changed if the degree of reaction criteria is not satisfied.

The design algorithm uses a for-loop to determine the total number of stages in the Low Pressure Compressor. It starts from single stage estimation and increases the number of stages if a design having stage entry angle ( $\alpha_1$ ) less than  $70^\circ$  (Mattingly et al. [6]) cannot be found. For each  $\alpha_1$  value the flow coefficient is estimated starting from 0.25 up to 0.8 (the limits are in accordance with the design suggestions given by Cumpsty [15]) and stage pressure ratio and rotor flow angle ( $\alpha_2$ ) are calculated. If the absolute difference between the calculated stage pressure ratio and the initial stage pressure ratio estimation (obtained by using on-design Low Pressure Compressor ratio) is less than 0.05 (tolerance given by Mattingly et al. [3]) then  $\alpha_2$  angle is found and degree of reaction is calculated. If the difference is greater than the tolerance value, then the stage entry angle  $\alpha_1$  is increased by  $1^\circ$  and the while loop runs until  $\alpha_1$  reaches to  $70^\circ$ . If  $\alpha_1$  reaches to the upper limit then the number of stages are increased,  $\alpha_1$  is set back to  $30^\circ$  and all of the iterative solution process is repeated with increased number of stages.

If the degree of reaction of compressor stage is greater than 0.2 and less than 0.8 (limits are in accordance with Horlock [8]) then the number of stages, cascade flow angles, and stage pressure ratio is found and the iterations are terminated. If the degree of reaction of the compressor stage is out of the given tolerance, a new solidity is calculated by using Equation (115) and the stage entry angle  $\alpha_1$  is increased by  $1^\circ$  and the while loop runs until  $\alpha_1$  reaches to  $70^\circ$ . If  $\alpha_1$  reaches to the upper limit then the number of stages are increased,  $\alpha_1$  is initialized and all of the process is repeated with increased number of stages.



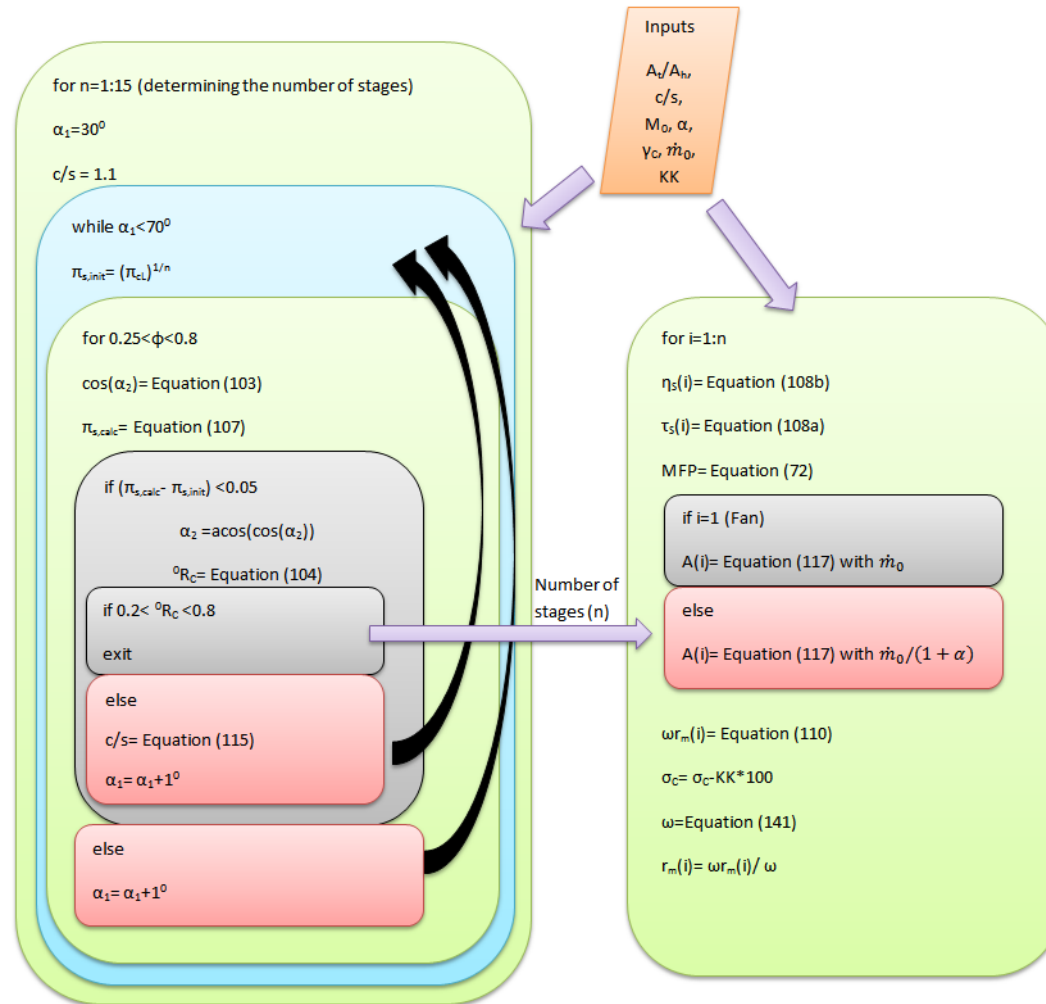


**Figure 82** Design algorithm in the Low Pressure Compressor subroutine

Once the number of stages and stage pressure ratio is found, another for-loop starting from the first stage up to the obtained number of stages is run for the dimensional calculations of each Low Pressure Compressor stage. The stage temperature ratio, throughflow annulus area and the tangential speed at the mean radius ( $\omega r_m$ ) are calculated with the Mass Flow Parameter at Low Pressure Compressor and stage total temperature and pressure values. In the Low Pressure Compressor, the first stage throughflow annulus area is calculated with the total mass flow rate and the area for the preceding stages are calculated with the core mass flow rate. If the Low Pressure Spool stopping criterion is not satisfied and the iteration is repeated, the blade tensile stress is reduced and shaft rotational speed is calculated by using Equation (141). By using the tangential speed and the shaft speed the mean line radius is calculated.

### 3.4.6.2 Low Pressure Turbine

The Low Pressure Turbine calculations start after the termination of the Low Pressure Compressor calculations. The algorithm is based on the solution methodology given in Mattingly et al. [6] for the AAF engine case study and the key design points given in [7], [9] and [10]. The model including this subroutine in the Low Pressure Spool sub-model is shown in Figure 83.

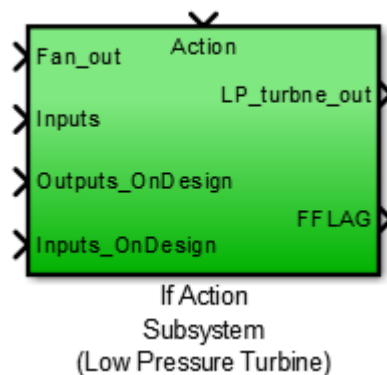


**Figure 83** Model including the Low Pressure Turbine subroutine

The design subroutine developed for the Low Pressure Turbine is illustrated in Figure 84.

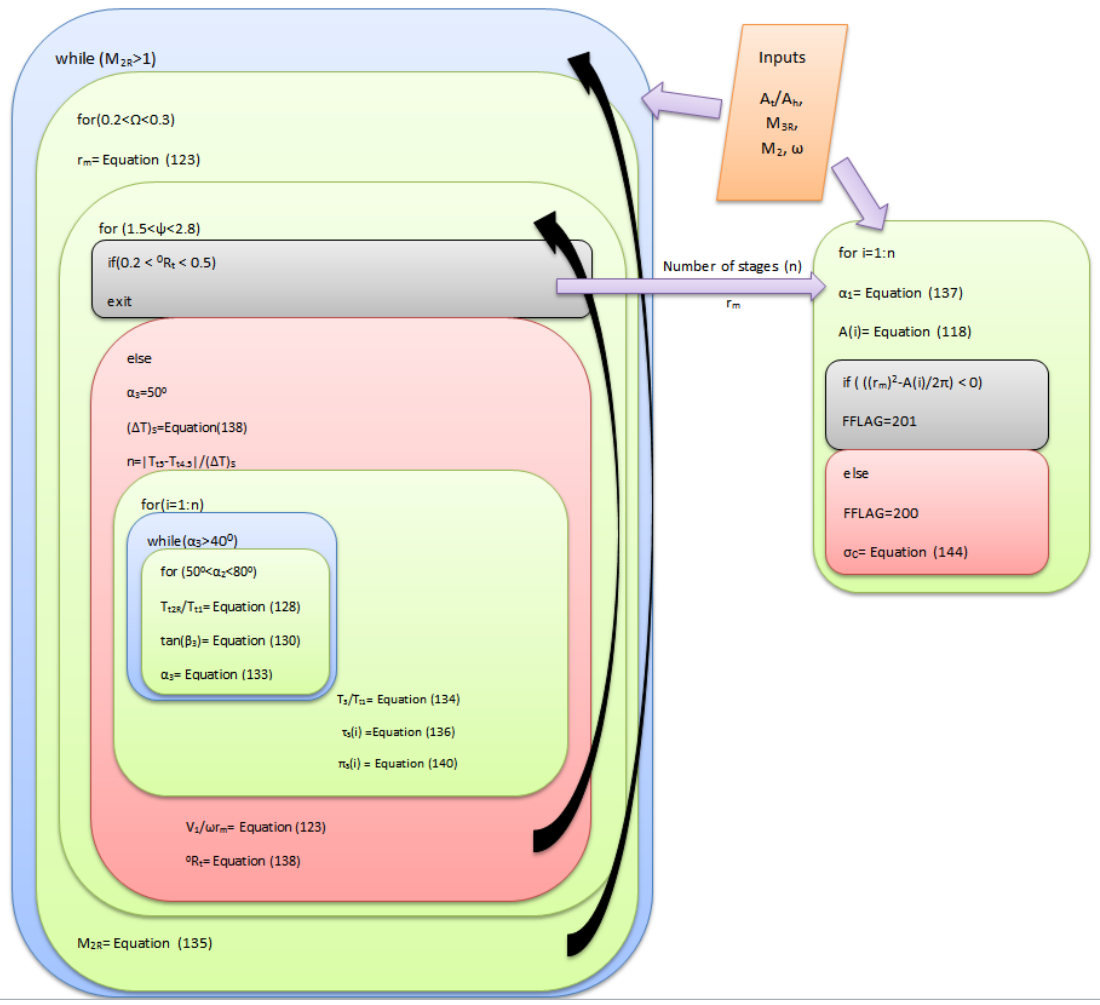


Figure 84 Design algorithm in the Low Pressure Turbine subroutine

The subroutine for Low Pressure Turbine design takes the tip to hub area ratio of turbine blades,  $M_{3R}$ ,  $M_2$  and  $\omega$  as inputs and  $M_{3R}$  is taken equal to 0.9 and  $M_2$  is taken as 1.1 for the first stage and 0.9 for the preceding stages according to the design suggestions given in Section 2.3.2 by Mattingly et al. [6]. The Low Pressure Spool shaft rotational speed  $\omega$  is determined by the Low Pressure Compressor subroutine.

The subroutine starts iterations with a for-loop which changes  $\Omega$  value (defined by Equation (121)) in order to calculate radius at the mean line ( $r_m$ ) by using shaft rotational speed. The range of the  $\Omega$  value is taken between 0.2 and 0.3, which is given in design considerations for a good turbine design in Section 2.3.2.

After determining the  $r_m$  value, the algorithm enters into the next nested for-loop which determines the Low Pressure Turbine stage loading value ( $\psi_{tL}$ ). The limits of this for-loop are determined according to the findings by Kacker and Okapuu [16]. The Stage Loading value is used to find the number of stages required by the Low Pressure Turbine in order to obtain the temperature rise determined by the on-design analysis. For this purpose, Equation (136) is used with the Low Pressure Turbine inlet and exit total temperatures determined in the Parametric Cycle Model.

After finding the number of stages, for each stage another nested for-loop iterates the  $\alpha_2$  angle starting from  $50^0$  up to  $80^0$ . The limits of this loop are determined according to the design suggestions given by Mattingly et al. [6] with a  $5^0$  tolerance on both sides. The innermost for-loop calculates the total velocity at Cascade Station 2, stage axial velocity, tangential velocity at Cascade Station 2, rotor relative tangential velocity at Cascade Station 2, rotor relative flow angle at Cascade Station 2, rotor relative total temperature, rotor relative flow angle at Cascade Station 3, tangential velocity at Cascade Station 3 by using Equations (122), (123), (124), (125), (126), (127), (128) and (130) respectively to calculate the stage exit flow angle ( $\alpha_3$ ) by using Equation (131) at the end. The calculated stage flow angle is controlled by the outer while loop and if this angle is smaller than  $40^0$  (this limit is given by Horlock J.H. [7] for multistage turbines to have reasonable exit swirl with reasonable efficiency) then the static temperature at Cascade

Station 3 and stage temperature and pressure ratios can be calculated, otherwise  $\alpha_2$  angle is increased and a new  $\alpha_3$  will be calculated.

After finding cascade designs having reasonable exit swirl conditions for each stage,  $V_1/\omega r_m$  is calculated by using Equation (121) and the degree of reaction of the turbine is calculated by using Equation (135). If the calculated degree of reaction is within 0.2 and 0.5 (limits given by Mattingly et al. [6]) then the for loop determining the stage loading and  $r_m$  value is terminated and rotor exit relative Mach number ( $M_{2R}$ ) is calculated by using Equation (133). If the calculated turbine degree of reaction is out of the limits then the stage loading is increased and the whole calculation process is repeated until a turbine design that satisfies the design limits on exit swirl angle, and the degree of reaction is found.

If the calculated rotor exit relative Mach number ( $M_{2R}$ ) is less than speed of sound, then the calculations are terminated and turbine flow field geometry design is completed. This limit on  $M_{2R}$  is put to prevent the boundary layer separation across the rotors. If the rotor exit relative Mach number ( $M_{2R}$ ) is equal or greater than the sonic speed then  $\Omega$  is increased and the whole flow field design procedure is repeated until this criterion is met.

After the finalization of the flow field geometry design, for each stage the stator exit flow angle ( $\alpha_1$ ), throughflow annulus area, and tip and hub radii are calculated by using  $r_m$  value determined in the flow field geometry design. If the calculated  $r_m$  satisfies the throughflow annulus area then the Low Pressure Spool is terminated by sending FFLAG signal equal to 201, else a new Low Pressure Spool design is made by decreasing the shaft speed at Low Pressure Compressor subroutine by sending the relevant FFLAG signal to the Low Pressure Spool while-iterator model.

### **3.4.7 High Pressure Spool**

The High Pressure Spool while-iterator block includes the Low Pressure Spool sub-model in addition to the High Pressure Turbine and High Pressure Compressor subroutines which calculate the aerothermodynamic design parameters of the respective

engine parts. Both subroutines are Embedded MATLAB Functions as for the Low Pressure Spool. The interior view of the model is shown in Figure 85.

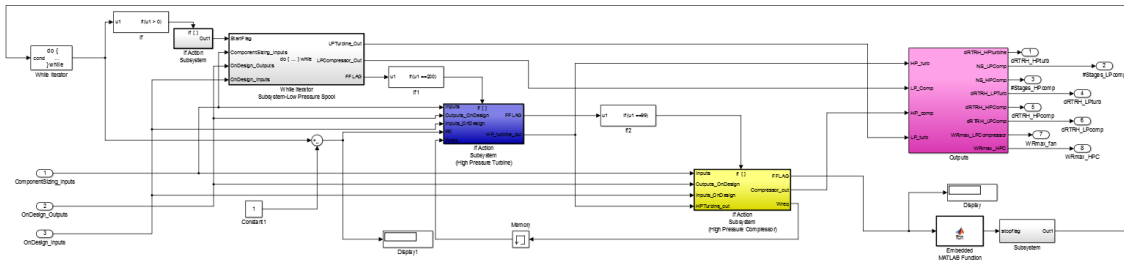


**Figure 85** Interior view of the High Pressure Spool

In the model runtime, the Low Pressure Spool aerothermodynamic design is run first before the calculations of the High Pressure Turbine design which determines the shaft rotational speed ( $\omega$ ) and sends this value to the High Pressure Compressor subroutine. The High Pressure Compressor subroutine calculates the flow field design parameters by using this rotational speed and checks for the compliance of the flow annulus area with the mean line radius calculated by using the shaft rotational speed. If the mean line radius is not suitable for the flow field design, then the blade tensile stress value is decreased by 0.689 MPa at the next iteration in the High Pressure Turbine and the shaft rotational speed is decreased until the mean radius of High Pressure Compressor stages satisfies the flow annulus area. The Engine Design Model completes its calculations by the finalization of the Turbomachinery Design Model with the completion of the High Pressure Spool design calculations, which is the end of the Rotating Turbomachinery Design calculations therewithal.

### 3.4.7.1 High Pressure Turbine

In the High Pressure Spool, High Pressure Turbine subroutine starts calculations after the completion of the Low Pressure Spool aerothermodynamic design. The algorithm is based on the solution methodology given in Mattingly et al. [6] and the key design points given in [7], [9] and [10]. The solution algorithm resembles the one introduced for the Low Pressure Turbine further it calculates the shaft speed for the High Pressure Spool. The model including this subroutine in the High Pressure Spool sub-model is shown in Figure 86.

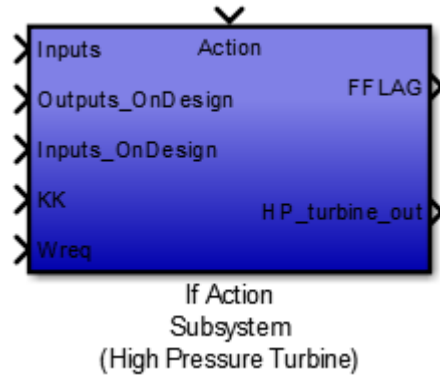


**Figure 86** Model including the High Pressure Turbine subroutine

In the design algorithm illustration in Figure 87, the input parameter  $KK$  indicates the current number of iteration of the High Pressure Spool. The subroutine for High Pressure Turbine design takes the tip to hub area ratio of turbine blades,  $M_1$ ,  $M_{3R}$ , and  $M_2$  as inputs and  $M_1$  is taken as 1.0,  $M_{3R}$  is taken equal to 0.9 and  $M_2$  is taken as 1.1 for the first stage and 0.9 for the preceding stages according to the design suggestions given in Section 2.3.2 by Mattingly et al. [6].

The specific heat ratio  $\gamma_T$  comes from the High Pressure Turbine outputs of Parametric Cycle. The compressor blade tip to hub area ratio ( $A_t/A_h$ ) is taken as constant. By the reason of calculating the shaft rotational speed for the High Pressure Spool, High Pressure Turbine subroutine does not have  $\Omega$  prediction as in Low Pressure Turbine subroutine. Instead, it starts with the for-loop which determines the High Pressure Turbine stage loading value ( $\psi_{tH}$ ).

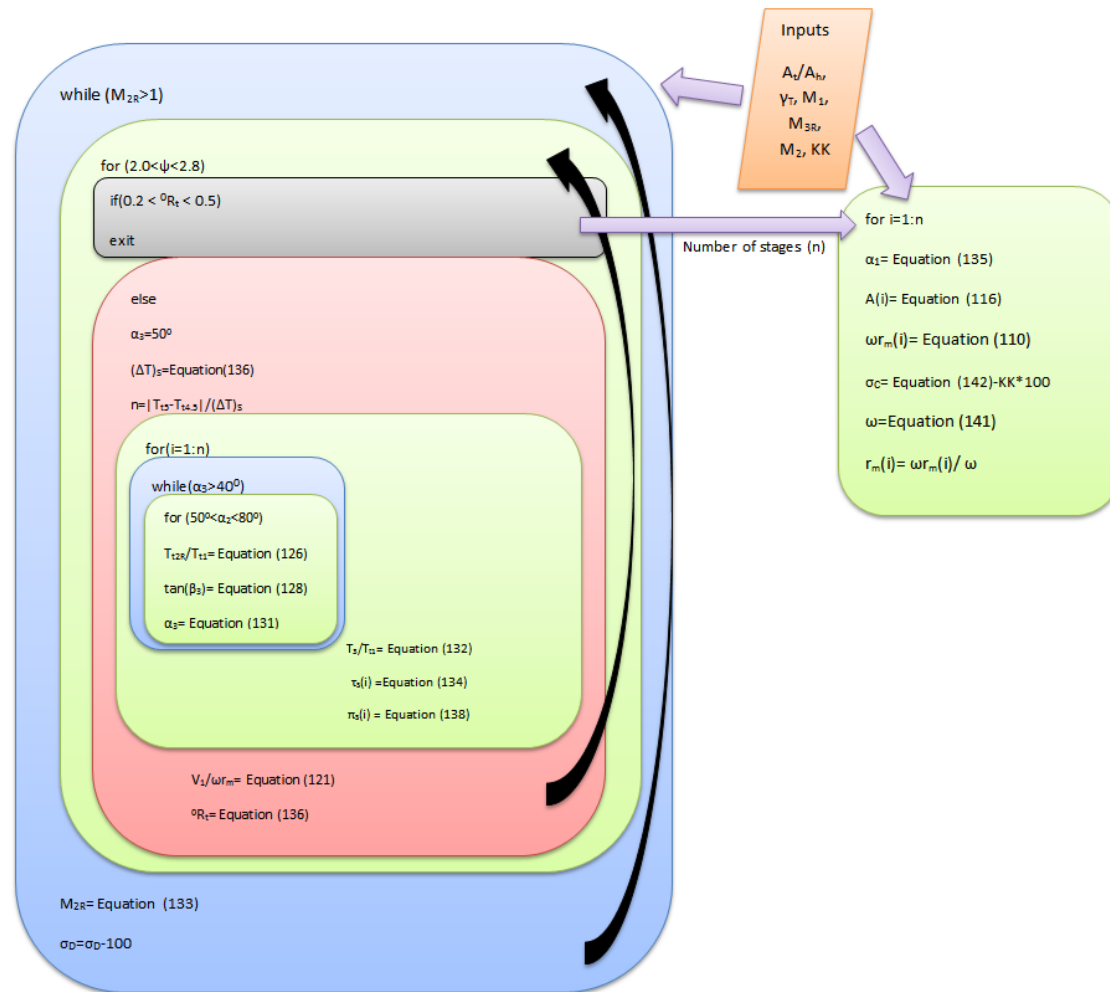


**Figure 87** Design algorithm in the High Pressure Turbine subroutine



The limits of the stage loading predictor for-loop are determined according to the findings by Kacker and Okapuu [16]. The Stage Loading value is used to find the number of stages required as in the Low Pressure Turbine in order to obtain the temperature rise determined by the on-design analysis. For this purpose, Equation (136) is used with the High Pressure Turbine inlet and exit total temperatures determined in the Parametric Cycle Model.

After finding the number of stages, for each stage another nested for-loop iterates the  $\alpha_2$  angle starting from  $50^\circ$  up to  $80^\circ$ . The limits of this loop are determined according to the same rationale with the Low Pressure Turbine. The innermost for-loop calculates the flow field velocities and flow angles by using Equations (122), (123), (124), (125), (126), (127), (128) and (130) to calculate the stage exit flow angle ( $\alpha_3$ ) by using Equation (131) at the end. The calculated stage flow angle is controlled by the outer while loop and if this angle is smaller than  $40^\circ$  (this limit is given by Horlock J.H. [7] for multistage turbines to have reasonable exit swirl with reasonable efficiency) then the static temperature at Cascade Station 3 and stage temperature and pressure ratios can be calculated, otherwise  $\alpha_2$  angle is increased and a new  $\alpha_3$  will be calculated.

After finding cascade designs having reasonable exit swirl conditions for each stage,  $V_1/\omega r_m$  is calculated by using Equation (121) and the degree of reaction of the turbine is calculated by using Equation (134). If the calculated degree of reaction is within 0.2 and 0.5 (limits given by Mattingly et al. [6]) then the for loop determining the stage loading value is terminated and rotor exit relative Mach number ( $M_{2R}$ ) is calculated by using Equation (133). If the calculated turbine degree of reaction is out of the limits then the stage loading is increased and the whole calculation process is repeated until a turbine design that satisfies the design limits on exit swirl angle, and the degree of reaction is found.

If the calculated rotor exit relative Mach number ( $M_{2R}$ ) is less than speed of sound, then the calculations are terminated and turbine flow field geometry design is completed. If the rotor exit relative Mach number ( $M_{2R}$ ) is equal or greater than the sonic speed, than

disk tensile stress ( $\sigma_D$ ) is decreased and the whole flow field design procedure is repeated until this criterion is met.

Once the number of stages and stage pressure ratio is found, another for-loop starting from the first stage up to the obtained number of stages is run for the dimensional calculations of each High Pressure Turbine stage. The stage temperature ratio, throughflow annulus area and the tangential speed at the mean radius ( $\omega r_m$ ) are calculated with the Mass Flow Parameter at High Pressure Turbine and stage total temperature and pressure values. If the High Pressure Spool stopping criterion is not satisfied and the iteration is repeated, the blade tensile stress is reduced and shaft rotational speed is calculated by using Equation (141). By using the tangential speed and the shaft speed the mean line radius is calculated.

### 3.4.7.2 High Pressure Compressor

The High Pressure Compressor algorithm is based on the solution methodology given in Mattingly et al. [6] and the key design points given in [8], [9] and [10]. The model including this subroutine in the High Pressure Spool sub-model is shown in Figure 88.

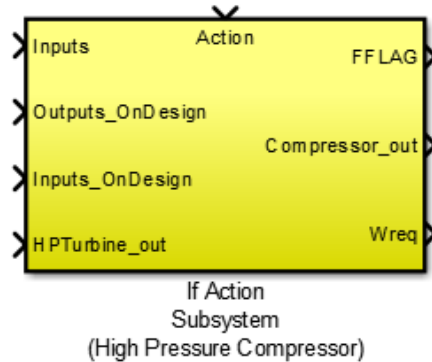


**Figure 88** Model including the High Pressure Compressor subroutine

The specific heat ratio  $\gamma_C$  comes from the High Pressure Compressor outputs of Parametric Cycle, total mass flow rate  $m_0$  and by-pass ratio ( $\alpha$ ) comes from the on-design input set. The compressor blade tip to hub area ratio ( $A_t/A_h$ ) is taken as constant. Solidity ( $c/s$ ) has an initial value of 1.0, which is an ideal value suggested by Mattingly et al.[3] for the compressor design, but it may be changed if the degree of reaction criteria is not satisfied.

The design algorithm uses a for-loop to determine the total number of stages in the Low Pressure Compressor. It starts from single stage estimation and increases the number of stages if a design having stage entry angle ( $\alpha_1$ ) less than  $70^\circ$  (Mattingly et al. [6]) cannot be found. For each  $\alpha_1$  value the flow coefficient is estimated starting from 0.45 up to 0.8 (the lower limit is increased for High Pressure Compressor case since it requires higher technology level than Low Pressure case) and stage pressure ratio and rotor flow angle ( $\alpha_2$ ) are calculated. If the absolute difference between the calculated stage pressure ratio and the initial stage pressure ratio estimations (obtained by using on-design High Pressure Compressor ratio) is less than 0.1 then  $\alpha_2$  angle is found and degree of reaction is calculated. If the difference is greater than the tolerance value, then the stage entry angle  $\alpha_1$  is increased by  $1^\circ$  and the while loop runs until  $\alpha_1$  reaches to  $70^\circ$ . If  $\alpha_1$  reaches

to the upper limit then the number of stages are increased,  $\alpha_1$  is set back to  $30^0$  and all of the iterative solution process is repeated with increased number of stages.

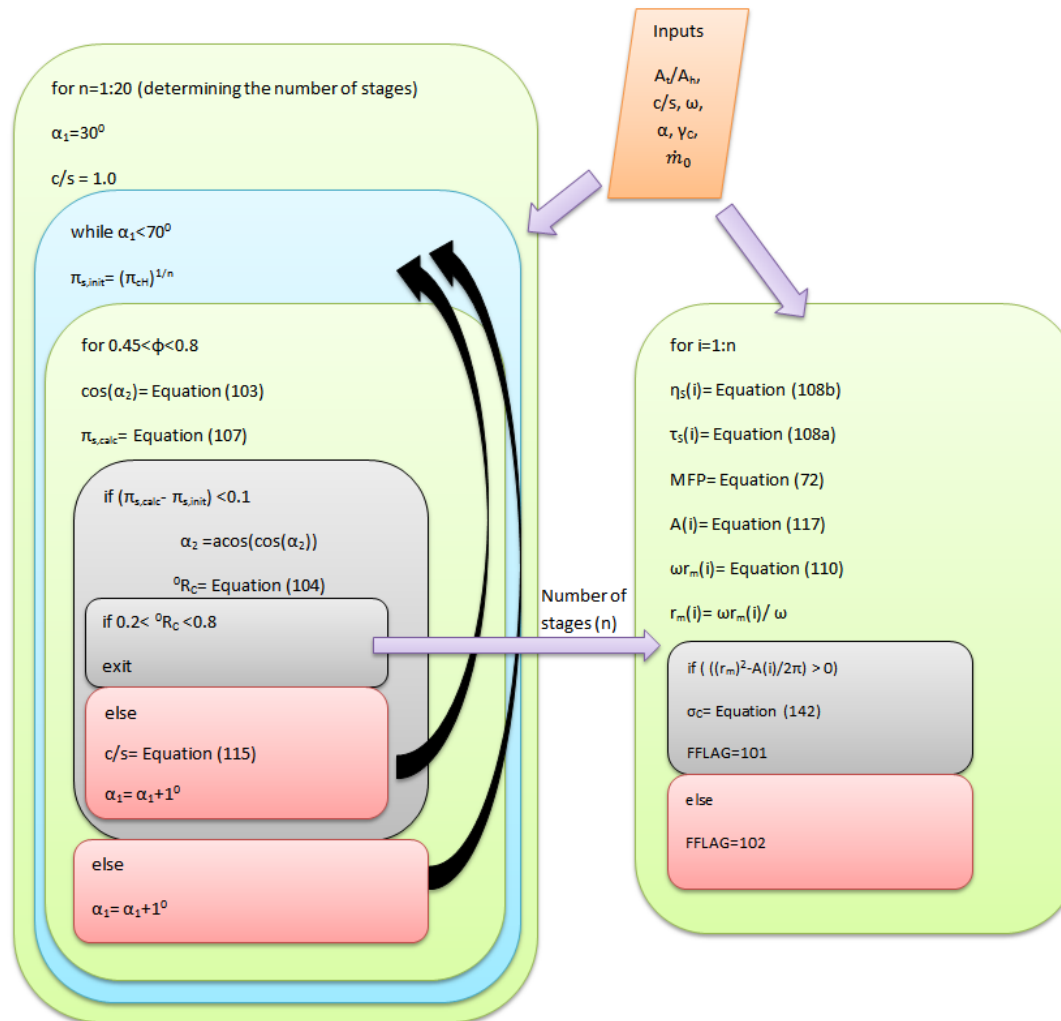


**Figure 89** Design algorithm in the High Pressure Compressor subroutine

If the degree of reaction of compressor stage is within the limits 0.2 and 0.8 (limits are in accordance with Horlock [8]) then the number of stages, cascade flow angles, and stage pressure ratio is found and the iterations are terminated.

If the degree of reaction of the compressor stage is out of the given tolerance, a new solidity is calculated by using Equation (115) and the stage entry angle  $\alpha_1$  is increased by  $1^\circ$  and the while loop runs until  $\alpha_1$  reaches to  $70^\circ$ . If  $\alpha_1$  reaches to the upper limit then the number of stages are increased,  $\alpha_1$  is initialized and all of the process is repeated with increased number of stages.

After determining the number of stages and stage pressure ratio, another for-loop starting from the first stage up to the obtained number of stages is run for the dimensional calculations of each High Pressure Compressor stage. The stage temperature ratio, throughflow annulus area and the tangential speed at the mean radius ( $\omega r_m$ ) are calculated with the Mass Flow Parameter at High Pressure Compressor and stage total temperature and pressure values. For each stage the stator exit flow angle ( $\alpha_1$ ), throughflow annulus area, and tip and hub radii are calculated by using  $r_m$  value determined in the flow field geometry design. If the calculated  $r_m$  satisfies the throughflow annulus area then the High Pressure Spool is terminated by sending FFLAG signal equal to 101, else a new High Pressure Spool design is made by decreasing the shaft speed at High Pressure Turbine subroutine by sending the relevant FFLAG signal to the High Pressure Spool while-iterator model.

## **CHAPTER 4**

### **VALIDATION**

The verification of the Engine Design Model is carried out for each sub-model separately. The validation of the Parametric Cycle Model and Performance Cycle Model is made with AEDsys Software by Mattingly et al. [3] and the Turbomachinery Design Model with engine data of CFM56-5A and GE90-94B engines.

#### **4.1 Parametric Cycle Model**

The validation of this model is carried out in two different test types. The first type of test is the case specific comparison test, in which the same input set is given to both AEDsys and EDM then their results are compared. The second type of test is a type of continuity tests, which checks for the coherency of the results for a wide input range. For this purpose, 3 different high by-pass ratio engine input cases are generated and the results are presented hereinafter.

##### **4.1.1 Case Specific Tests**

In this type of tests, a generic mid-by pass ratio engine, CFM56-5A engine and GE90-94B engine input data are given to AEDsys Software and EDM and their results are compared. The input set of the mid-by pass ratio generic engine is obtained from Mattingly et al. [3], GE90-94B engine from Cantwell Brian J. [18] and CFM56-5A engine from its Technical Training Manual [19].

#### 4.1.1.1 Mid By-Pass Ratio Generic Engine

The on-design input set of this engine is given for the cruise condition in Table 8. These inputs are entered to AEDsys Software through its user interface, and written into the input file, which is in the format given in Appendix A, to be used by EDM.

**Table 8** The list of on-design input parameters for the tests with Mid By-Pass Ratio Generic Engine

Name of the Parameter	Value of the Parameter
Flight Mach Number ( $M_0$ )	0.8
Flight Altitude [m]	12192
Ambient Temperature ( $T_0$ ) [°K]	216.823
Ambient Pressure ( $P_0$ ) [mBar]	188.227
Engine Mass Flow Rate ( $m_0$ ) [kg/s]	45.39
By-Pass Ratio ( $\alpha$ )	3.5
Bleed Air Fraction ( $\beta$ ) [%]	1.0
Coolant Mixer 1 Air Fraction ( $\varepsilon_1$ ) [%]	2.0
Coolant Mixer 2 Air Fraction ( $\varepsilon_2$ ) [%]	2.0
Fan Pressure Ratio ( $\pi_f$ )	3.5
Low Pressure Compressor Pressure Ratio ( $\pi_{cl}$ )	3.5
High Pressure Compressor Pressure Ratio ( $\pi_{ch}$ )	4.571
Diffuser Pressure Ratio ( $\pi_d$ )	0.97
Combustor Pressure Ratio ( $\pi_b$ )	0.97
Nozzle Pressure Ratio ( $\pi_n$ )	0.98
Fan Nozzle Pressure Ratio ( $\pi_{nf}$ )	0.98
Combustor Efficiency ( $\eta_b$ )	0.98
High Pressure Spool Mechanical Efficiency ( $\eta_{mH}$ )	0.98
Low Pressure Spool Mechanical Efficiency ( $\eta_{mL}$ )	0.99
High Pressure Spool Power Takeoff Efficiency ( $\eta_{mPH}$ )	0.98
Low Pressure Spool Power Takeoff Efficiency ( $\eta_{mPL}$ )	0.98
Fan Polytropic Efficiency ( $e_f$ )	0.89
Low Pressure Compressor Polytropic Efficiency ( $e_{cl}$ )	0.89
High Pressure Compressor Polytropic Efficiency ( $e_{ch}$ )	0.9
High Pressure Turbine Polytropic Efficiency ( $e_{tH}$ )	0.89
Low Pressure Turbine Polytropic Efficiency ( $e_{tL}$ )	0.91
Fuel Heating Value ( $h_{PR}$ ) [kJ/kg]	41868
High Pressure Turbine Inlet Temperature ( $T_{t4}$ ) [°K]	1779
CTO Low (CTOL)	0.01
CTO High (CTOH)	0.0



The comparison of the results obtained by using the input set in Table 8 from two Software, including the differences, are given in Table 9.

**Table 9** On-Design result comparison for Mid By-Pass Ratio Generic Engine

Parameter	ONX (AEDsys)	Parametric Cycle Model (EDM)	Difference%
Inlet Flow Speed ( $V_0$ ) [m/s]	236.4	236.1	0.13
Inlet Speed of Sound ( $a_0$ ) [m/s]	295.5	295.1	0.12
Inlet Temperature Ratio ( $\tau_r$ )	1.128	1.128	0
Inlet Pressure Ratio ( $\pi_r$ )	1.524	1.525	0.07
Fan Temperature Ratio ( $\tau_f$ )	1.496	1.498	0.15
Fan Exhaust Total Pressure Ratio ( $P_{t19}/P_{19}$ )	1.883	1.910	1.41
Low Pressure Compressor Temperature Ratio ( $\tau_{cL}$ )	1.496	1.498	0.15
High Pressure Compressor Temperature Ratio ( $\tau_{cH}$ )	1.621	1.619	0.15
High Pressure Turbine Pressure Ratio ( $\pi_{tH}$ )	0.578	0.584	1.00
High Pressure Turbine Temperature Ratio ( $\tau_{tH}$ )	0.888	0.888	0.07
Low Pressure Turbine Pressure Ratio ( $\pi_{tL}$ )	0.206	0.209	1.55
Low Pressure Turbine Temperature Ratio ( $\tau_{tL}$ )	0.696	0.696	0.01
Pressure Ratio $P_0/P_9$	0.688	0.674	2.05
Combustor fuel-to air ratio ( $f$ )	0.0386	0.0384	0.60
Overall fuel-to air ratio ( $f_0$ )	0.00815	0.0081	0.61

**Table 9 Continued**

<b>Parameter</b>	<b>ONX (AEDsys)</b>	<b>Parametric Cycle Model (EDM)</b>	<b>Difference%</b>
<b>Coolant Mixer 1 Temperature Ratio (<math>\tau_{m1}</math>)</b>	0.986	0.986	0
<b>Coolant Mixer 2 Temperature Ratio (<math>\tau_{m2}</math>)</b>	0.987	0.987	0.01
<b>Fan Exhaust Temperature Ratio (<math>T_{t19}/T_0</math>)</b>	1.686	1.688	0.09
<b>Fan Exhaust Pressure Ratio (<math>P_0/P_{19}</math>)</b>	0.372	0.377	1.37
<b>Fan Exhaust Speed Ratio (<math>V_{19}/V_0</math>)</b>	1.482	1.491	0.59
<b>Specific Thrust [N/(kg/s)]</b>	330.5	329.5	0.37
<b>Thrust Specific Fuel Consumption [(kg/hr)/N]</b>	0.0887	0.0884	0.24
<b>Primary Exhaust Temperature Ratio (<math>T_9/T_0</math>)</b>	4.529	4.536	0.17
<b>Primary Exhaust Speed Ratio (<math>V_9/V_0</math>)</b>	2.577	2.591	0.54
<b>M9/M0</b>	1.250	1.258	0.6

#### 4.1.1.2 CFM56-5A Engine

The inputs given for the cruise condition in Table 10 retrieved from the data given in [19] and [18] are entered to AEDsys and EDM through the interface and input file respectively.

**Table 10** The list of on-design input parameters for the tests with CFM56-5A Engine

<b>Name of the Parameter</b>	<b>Value of the Parameter</b>
<b>Flight Mach Number (<math>M_0</math>)</b>	0.8
<b>Flight Altitude [m]</b>	10058.4
<b>Ambient Temperature (<math>T_0</math>) [°K]</b>	223.43
<b>Ambient Pressure (<math>P_0</math>) [mBar]</b>	264.993
<b>Engine Mass Flow Rate (<math>m_0</math>) [kg/s]</b>	425.878

Table 10 Continued

Name of the Parameter	Value of the Parameter
By-Pass Ratio ( $\alpha$ )	6
Bleed Air Fraction ( $\beta$ ) [%]	3.0
Coolant Mixer 1 Air Fraction ( $\epsilon_1$ ) [%]	5.0
Coolant Mixer 2 Air Fraction ( $\epsilon_2$ ) [%]	5.0
Fan Pressure Ratio ( $\pi_f$ )	1.55
Low Pressure Compressor Pressure Ratio ( $\pi_{cl}$ )	1.55
High Pressure Compressor Pressure Ratio ( $\pi_{ch}$ )	17.097
Diffuser Pressure Ratio ( $\pi_d$ )	0.99
Combustor Pressure Ratio ( $\pi_b$ )	0.95
Nozzle Pressure Ratio ( $\pi_n$ )	0.99
Fan Nozzle Pressure Ratio ( $\pi_{nf}$ )	0.99
Combustor Efficiency ( $\eta_b$ )	0.99
High Pressure Spool Mechanical Efficiency ( $\eta_{mH}$ )	0.99
Low Pressure Spool Mechanical Efficiency ( $\eta_{mL}$ )	0.99
High Pressure Spool Power Takeoff Efficiency ( $\eta_{mPH}$ )	0.99
Low Pressure Spool Power Takeoff Efficiency ( $\eta_{mPL}$ )	1.0
Fan Polytropic Efficiency ( $e_f$ )	0.93
Low Pressure Compressor Polytropic Efficiency ( $e_{cl}$ )	0.91
High Pressure Compressor Polytropic Efficiency ( $e_{ch}$ )	0.91
High Pressure Turbine Polytropic Efficiency ( $e_{tH}$ )	0.93
Low Pressure Turbine Polytropic Efficiency ( $e_{tL}$ )	0.93
Fuel Heating Value ( $h_{PR}$ ) [kJ/kg]	42798
High Pressure Turbine Inlet Temperature ( $T_{t4}$ ) [°K]	1539.4
CTO Low (CTOL)	0.0
CTO High (CTOH)	0.005

The comparison of the results obtained by using the input set in Table 10 from two Software, including the differences, are given in Table 11.

Table 11 On-Design result comparison for CFM56-5A Engine

Parameter	ONX (AEDsys)	Parametric Cycle Model (EDM)	Difference%
Inlet Flow Speed ( $V_0$ ) [m/s]	239.8	239.5	0.13
Inlet Speed of Sound ( $a_0$ ) [m/s]	299.7	299.3	0.13
Inlet Temperature Ratio ( $\tau_r$ )	1.128	1.128	0

Table 11 Continued

Parameter	ONX (AEDsys)	Parametric Cycle Model (EDM)	Difference%
Inlet Pressure Ratio ( $\pi_r$ )	1.524	1.525	0.07
Fan Temperature Ratio ( $\tau_f$ )	1.144	1.145	0.11
Fan Exhaust Total Pressure Ratio ( $P_{t19}/P_{19}$ )	1.892	1.895	0.15
Low Pressure Compressor Temperature Ratio ( $\tau_{cL}$ )	1.147	1.149	0.17
High Pressure Compressor Temperature Ratio ( $\tau_{cH}$ )	2.440	2.436	0.15
High Pressure Turbine Pressure Ratio ( $\pi_{tH}$ )	0.270	0.272	0.93
High Pressure Turbine Temperature Ratio ( $\tau_{tH}$ )	0.730	0.731	0.14
Low Pressure Turbine Pressure Ratio ( $\pi_{tL}$ )	0.377	0.375	0.45
Low Pressure Turbine Temperature Ratio ( $\tau_{tL}$ )	0.785	0.783	0.2
Pressure Ratio $P_0/P_9$	0.485	0.491	1.2
Combustor fuel-to air ratio ( $f$ )	0.0257	0.0255	0.62
Overall fuel-to air ratio ( $f_0$ )	0.00319	0.00317	0.49
Coolant Mixer 1 Temperature Ratio ( $\tau_{m1}$ )	0.968	0.968	0
Coolant Mixer 2 Temperature Ratio ( $\tau_{m2}$ )	0.979	0.978	0.01
Fan Exhaust Temperature Ratio ( $T_{t19}/T_0$ )	1.290	1.292	0.16
Fan Exhaust Pressure Ratio ( $P_0/P_{19}$ )	0.818	0.818	0

Table 11 Continued

Parameter	ONX (AEDsys)	Parametric Cycle Model (EDM)	Difference%
Fan Exhaust Speed Ratio ( $V_{19}/V_0$ )	1.296	1.297	0.06
Specific Thrust [N/(kg/s)]	167.92	167.21	0.42
Thrust Specific Fuel Consumption [(kg/hr)/N]	0.0685	0.0683	0.16
Primary Exhaust Temperature Ratio ( $T_9/T_0$ )	3.419	3.408	0.32
Primary Exhaust Speed Ratio ( $V_9/V_0$ )	2.263	2.292	1.29
$M_9/M_0$	1.250	1.270	1.6

#### 4.1.1.3 GE90-94B Engine

The analysis given in [18] uses the data given for the cruise condition in Table 12 for GE90-94B engine, which is input to the AEDsys and EDM for on-design result comparison.

Table 12 The list of on-design input parameters for the tests with GE90-94B Engine

Name of the Parameter	Value of the Parameter
Flight Mach Number ( $M_0$ )	0.85
Flight Altitude [m]	9144
Ambient Temperature ( $T_0$ ) [°K]	228.98
Ambient Pressure ( $P_0$ ) [mBar]	301.508
Engine Mass Flow Rate ( $m_0$ ) [kg/s]	1350
By-Pass Ratio ( $\alpha$ )	8.4
Bleed Air Fraction ( $\beta$ ) [%]	3.0
Coolant Mixer 1 Air Fraction ( $\epsilon_1$ ) [%]	5.0
Coolant Mixer 2 Air Fraction ( $\epsilon_2$ ) [%]	5.0
Fan Pressure Ratio ( $\pi_f$ )	1.6
Low Pressure Compressor Pressure Ratio ( $\pi_{cl}$ )	1.6
High Pressure Compressor Pressure Ratio ( $\pi_{ch}$ )	15.625

Table 12 Continued

Name of the Parameter	Value of the Parameter
Diffuser Pressure Ratio ( $\pi_d$ )	0.99
Combustor Pressure Ratio ( $\pi_b$ )	0.95
Nozzle Pressure Ratio ( $\pi_n$ )	0.99
Fan Nozzle Pressure Ratio ( $\pi_{nf}$ )	0.99
Combustor Efficiency ( $\eta_b$ )	0.99
High Pressure Spool Mechanical Efficiency ( $\eta_{mH}$ )	0.99
Low Pressure Spool Mechanical Efficiency ( $\eta_{mL}$ )	0.99
High Pressure Spool Power Takeoff Efficiency ( $\eta_{mPH}$ )	0.99
Low Pressure Spool Power Takeoff Efficiency ( $\eta_{mPL}$ )	1.0
Fan Polytropic Efficiency ( $e_f$ )	0.93
Low Pressure Compressor Polytropic Efficiency ( $e_{cl}$ )	0.91
High Pressure Compressor Polytropic Efficiency ( $e_{ch}$ )	0.91
High Pressure Turbine Polytropic Efficiency ( $e_{tH}$ )	0.93
Low Pressure Turbine Polytropic Efficiency ( $e_{tL}$ )	0.93
Fuel Heating Value ( $h_{PR}$ ) [kJ/kg]	42798.4
High Pressure Turbine Inlet Temperature ( $T_{t4}$ ) [°K]	1381
CTO Low (CTOL)	0.0
CTO High (CTOH)	0.005

The comparison of the results obtained by using the input set in Table 12 from two Software, including the differences, are given in Table 13.

**Table 13** On-Design result comparison for GE90-94B Engine

<b>Parameter</b>	<b>ONX (AEDsys)</b>	<b>Parametric Model (EDM)</b>	<b>Cycle</b>	<b>Difference%</b>
<b>Inlet Flow Speed (<math>V_0</math>) [m/s]</b>	258.1	257.8		0.13
<b>Inlet Speed of Sound (<math>a_0</math>) [m/s]</b>	303.7	303.3		0.13
<b>Inlet Temperature Ratio (<math>\tau_r</math>)</b>	1.144	1.145		0.09
<b>Inlet Pressure Ratio (<math>\pi_r</math>)</b>	1.603	1.604		0.06
<b>Fan Temperature Ratio (<math>\tau_f</math>)</b>	1.155	1.156		0.09
<b>Fan Exhaust Total Pressure Ratio (<math>P_{t19}/P_{19}</math>)</b>	1.892	1.897		0.29
<b>Low Pressure Compressor Temperature Ratio (<math>\tau_{cL}</math>)</b>	1.159	1.160		0.11
<b>High Pressure Compressor Temperature Ratio (<math>\tau_{cH}</math>)</b>	2.371	2.368		0.13
<b>High Pressure Turbine Pressure Ratio (<math>\pi_{tH}</math>)</b>	0.221	0.223		1.13
<b>High Pressure Turbine Temperature Ratio (<math>\tau_{tH}</math>)</b>	0.690	0.691		0.16
<b>Low Pressure Turbine Pressure Ratio (<math>\pi_{tL}</math>)</b>	0.146	0.145		0.62
<b>Low Pressure Turbine Temperature Ratio (<math>\tau_{tL}</math>)</b>	0.612	0.610		0.26
<b>Pressure Ratio <math>P_0/P_9</math></b>	1	1		0
<b>Combustor fuel-to air ratio (<math>f</math>)</b>	0.01996	0.01986		0.55
<b>Overall fuel-to air ratio (<math>f_0</math>)</b>	0.00185	0.00184		0.64
<b>Coolant Mixer 1 Temperature Ratio (<math>\tau_{m1}</math>)</b>	0.972	0.972		0.01
<b>Coolant Mixer 2 Temperature Ratio (<math>\tau_{m2}</math>)</b>	0.985	0.985		0.02

**Table 13 Continued**

<b>Parameter</b>	<b>ONX (AEDsys)</b>	<b>Parametric Model (EDM)</b>	<b>Cycle</b>	<b>Difference%</b>
<b>Fan Exhaust Temperature Ratio (<math>T_{119}/T_0</math>)</b>	1.321	1.323		0.15
<b>Fan Exhaust Pressure Ratio (<math>P_0/P_{19}</math>)</b>	0.752	0.754		0.2
<b>Fan Exhaust Speed Ratio (<math>V_{19}/V_0</math>)</b>	1.235	1.237		0.15
<b>Specific Thrust [N/(kg/s)]</b>	103.53	103.46		0.07
<b>Thrust Specific Fuel Consumption [(kg/hr)/N]</b>	0.0642	0.0639		0.51
<b>Primary Exhaust Temperature Ratio (<math>T_9/T_0</math>)</b>	2.495	2.496		0.06
<b>Primary Exhaust Speed Ratio (<math>V_9/V_0</math>)</b>	0.972	0.984		1.25
<b><math>M_9/M_0</math></b>	0.623	0.631		1.26

#### **4.1.2 Continuity Tests**

In this type of tests, a predetermined input parameter from the input set given in Section 4.1.1.1 for the generic mid-by pass engine is changed within an interval and the response of two software according to the change in that parameter are compared.

In the first continuity test, the change in Thrust and Thrust Specific Fuel Consumption with respect to the change in engine by-pass ratio is tracked for the Parametric Cycle Model and compared with ONX results from AEDsys Software. The difference from the reference program outputs are 0.5% both in Thrust and Thrust Specific Fuel Consumption, which is coherent with the case specific tests. The change in Thrust and Thrust Specific Fuel Consumption with respect to engine by-pass ratio is given in Figure 90.



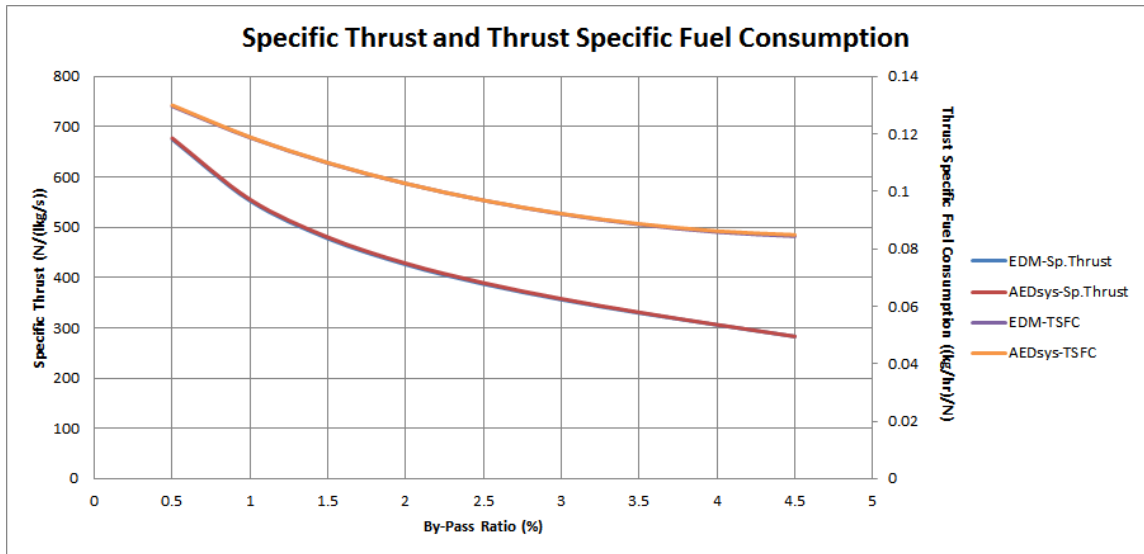


**Figure 90** Variation of On-Design Specific Thrust and Thrust Specific Fuel Consumption with respect to By-Pass ratio compared for Engine Design Model (EDM) and AEDsys program (ONX)

Another comparison is made for different High Pressure Compressor pressure ratios (Low Pressure Compressor pressure ratio retain constant) in order to observe the change in Thrust and Thrust Specific Fuel Consumption and the 0.5% difference from the reference program results is remaining the same as in the previous analysis and the comparisons in case specific tests. The change in Thrust and Thrust Specific Fuel Consumption with respect to compressor pressure ratio is given in Figure 91.

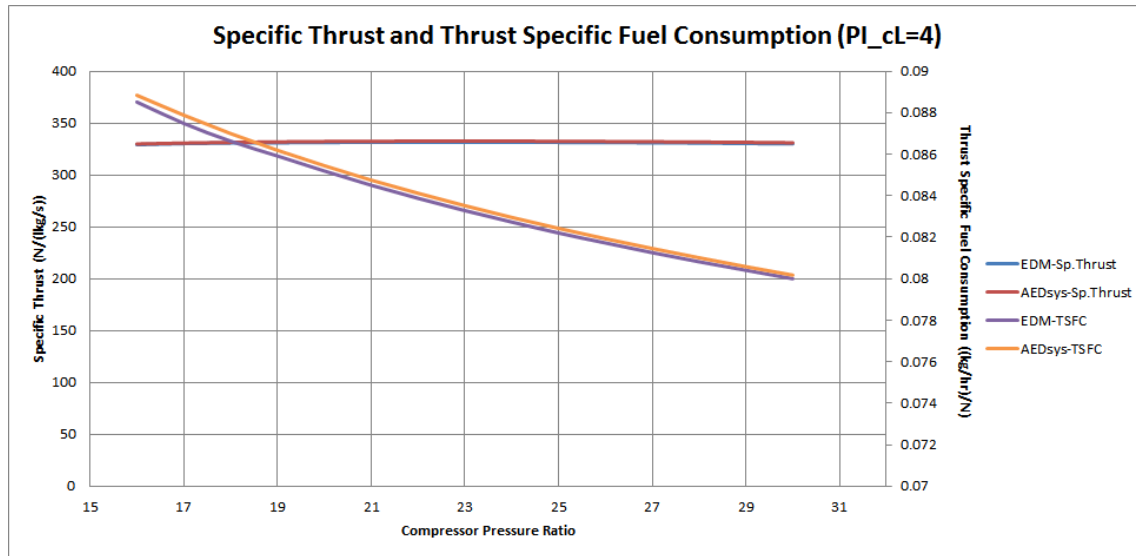


**Figure 91** Variation of On-Design Specific Thrust and Thrust Specific Fuel Consumption with respect to High Pressure Compressor pressure ratio compared for Engine Design Model (EDM) and AEDsys program (ONX)

Third comparison is made for the preferred design region estimation of Engine Design Model and AEDsys software. The preferred design region is the one that has minimum Thrust Specific Fuel Consumption change, whereas the thrust is increasing. In this comparison, High Pressure Turbine Inlet Temperature ( $T_{t4}$ ) is altered and the changes in Specific Thrust and Thrust Specific Fuel Consumption are observed. The difference between two predictions is 0.3% which is coherent with the previous analyses and case specific tests. This comparison is given in Figure 92.

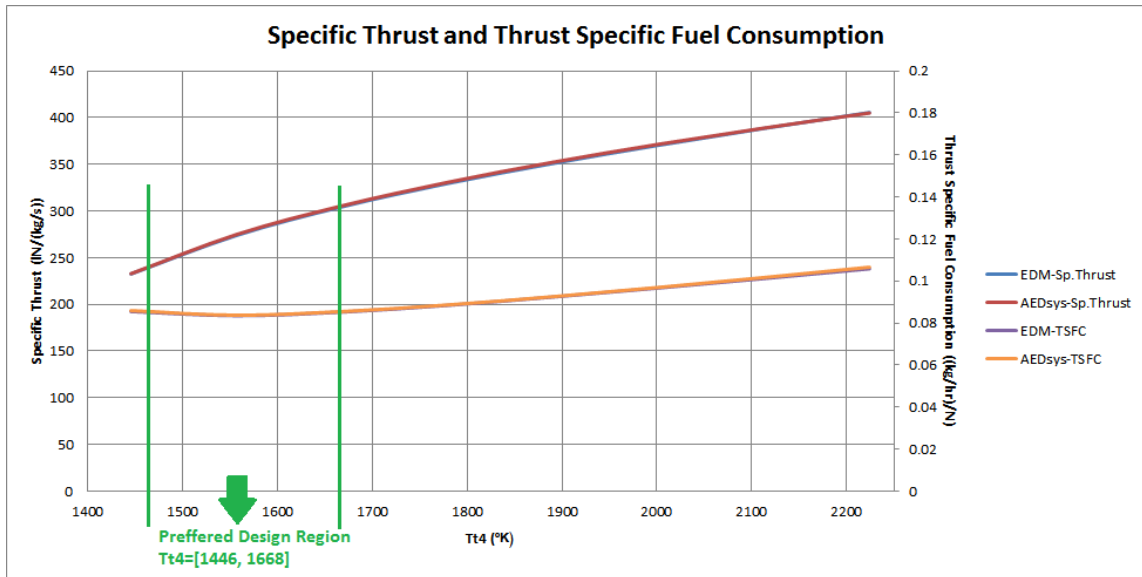


**Figure 92** Variation of On-Design Specific Thrust and Thrust Specific Fuel Consumption with respect to High Pressure Turbine Inlet Temperature compared for Engine Design Model (EDM) and AEDsys program (ONX)

From Figure 92, it can be deduced that the preferred design range estimations of EDM is coherent with the reference software.

In the comparisons made in Figures 90, 91 and 92 the constant differences between the predictions of Specific Thrust and Thrust Specific Fuel Consumption parameters of EDM and AEDsys stems from the fact that a different Variable Specific Heat model used in EDM than the AEDsys Software. The Variable Specific Heat Model (F-AIR blocks) calculates the thermodynamic properties throughout the cycle and the constant difference between the predictions of different heat models causes a constant difference in pressure ratios, hence giving constant differences in result parameters which are using them.

## 4.2 Performance Cycle Model

The validation of this model is carried out with the two different test types used for the Parametric Cycle Model. For this purpose, the 3 engines used in on-design validation are

used with the on-design outputs obtained in Section 4.1.1 and the results are presented hereinafter.

#### 4.2.1 Case Specific Tests

In this type of tests, a generic mid-by pass ratio engine, CFM56-5A engine and GE90-94B engine on-design output data are used in AEDsys Software and EDM and their results are compared. The Engine Test tool under Cycle Deck tool is used in AEDsys for the performance cycle calculations.

##### 4.1.2.1 Mid By-Pass Ratio Generic Engine

The off-design input set of this engine is given for the landing condition in Table 14. These inputs are entered to AEDsys Software through the user interface of Cycle Deck, and written into the input file, which is in the format given in Appendix A, to be used by EDM.

**Table 14** The list of off-design input parameters for the tests with Mid By-Pass Ratio generic engine

Name of the Parameter	Value of the Parameter
Flight Mach Number ( $M_0$ )	0.4
Flight Altitude [m]	0
Ambient Temperature ( $T_0$ ) [°K]	288.39
Ambient Pressure ( $P_0$ ) [mBar]	1013.253
Bleed Air Fraction ( $\beta$ ) [%]	1.0
Coolant Mixer 1 Air Fraction ( $\epsilon_1$ ) [%]	2.0
Coolant Mixer 2 Air Fraction ( $\epsilon_2$ ) [%]	2.0
Power Take Off (Low Pressure Spool) [kW]	99.4
Power Take Off (High Pressure Spool) [kW]	0
Fuel Heating Value ( $h_{PR}$ ) [kJ/kg]	41868
Max. High Pressure Turbine Inlet Temperature ( $T_{t4}$ ) [°K]	1590.16
Max. Compressor Pressure Ratio ( $\pi_c$ )	30

The comparison of the results obtained by using the input set in Table 8 from two Software, including the differences, are given in Table 15.

**Table 15** Off-Design result comparison for Mid By-Pass Ratio Generic Engine

<b>Parameter</b>	<b>OFFX (AEDsys)</b>	<b>Performance Cycle Model (EDM)</b>	<b>% Difference</b>
<b>Inlet Pressure Ratio (<math>\pi_r</math>)</b>	1.5204	1.525	0.30
<b>Inlet Temperature Ratio (<math>\tau_r</math>)</b>	1.1275	1.128	0.04
<b>Fan Pressure Ratio (<math>\pi_f</math>)</b>	2.1584	2.189	1.42
<b>Fan Temperature Ratio (<math>\tau_f</math>)</b>	1.2843	1.29	0.44
<b>Low Pressure Compressor Pressure Ratio (<math>\pi_{cL}</math>)</b>	2.1584	2.189	1.42
<b>Low Pressure Compressor Temperature Ratio (<math>\tau_{cL}</math>)</b>	1.2843	1.29	0.44
<b>High Pressure Compressor Pressure Ratio (<math>\pi_{cH}</math>)</b>	3.4511	3.046	11.74
<b>High Pressure Compressor Temperature Ratio (<math>\tau_{cH}</math>)</b>	1.4844	1.426	3.93
<b>High Pressure Turbine Pressure Ratio (<math>\pi_{tH}</math>)</b>	0.5778	0.6239	7.98
<b>High Pressure Turbine Temperature Ratio (<math>\tau_{tH}</math>)</b>	0.8845	0.9118	3.09
<b>Low Pressure Turbine Pressure Ratio (<math>\pi_{tL}</math>)</b>	0.2269	0.243	7.10
<b>Low Pressure Turbine Temperature Ratio (<math>\tau_{tL}</math>)</b>	0.705	0.7207	2.23

Table 15 Continued

Parameter	OFFX (AEDsys)	Performance Cycle Model (EDM)	% Difference
LP Spool RPM %	87.34%	87.97%	0.72
HP Spool RPM%	94.35%	88.81%	5.87
By-Pass Ratio ( $\alpha$ )	3.995	4.519	13.12
Fan Exhaust Total Pressure Ratio ( $P_{19}/P_{19}$ )	1.8829	1.553	17.52
Fan Exhaust Pressure Ratio ( $P_0/P_{19}$ )	0.6036	0.4896	18.89
Fan Exhaust Mach Number ( $M_{19}$ )	1	0.8195	18.05
Fan Exhaust Total Pressure Ratio ( $P_{19}/P_9$ )	1.3688	1.421	3.81
Primary Exhaust Pressure Ratio ( $P_0/P_9$ )	1	1	0
Primary Exhaust Mach Number ( $M_9$ )	0.7035	0.75	6.61
Engine Mass Flow Rate ( $m_0$ ) [kg/s]	134.93	135.71	0.58
Combustor fuel-to air ratio ( $f$ )	0.03076	0.03755	22.07
Overall fuel-to air ratio ( $f_0$ )	0.00585	0.006462	10.46
Specific Thrust [N/(kg/s)]	197.8	203.3	2.78
Thrust Specific Fuel Consumption [(kg/hr)/N]	0.1065	0.1144	7.43

According to the results presented in Table 15, maximum differences were occurred in fuel to air ratio, and the Fan Exhaust Pressure Ratio. EDM uses predetermined Mach numbers in certain engine stations and in this case, the difference in the predetermined Mach number values at Station 4 and 19 caused the differences in fuel to air ratio, and  $P_0/P_{19}$  and total Pressure Ratio at Station 19 respectively. This is due to the fact that the

theory that Engine Design Model is developed from, is derived only from mass conservation and energy conservation laws excluding the Momentum Conservation law. Therefore the Mach numbers in the combustor and the secondary exhaust cannot be calculated by EDM and they should be given as constants and the difference between these constant values in EDM and AEDsys causes the differences observed in Table 15.

#### 4.1.2.2 CFM 56-5A Engine

The on-design results obtained in Section 4.1.1.2 used as reference in the off-design analysis. The off-design input data given for the landing condition in Table 16 are entered to AEDsys and EDM through the interface and input file respectively.

**Table 16** The list of off-design input parameters for the tests with CFM56-5A Engine

Name of the Parameter	Value of the Parameter
Flight Mach Number ( $M_0$ )	0.4
Flight Altitude [m]	0
Ambient Temperature ( $T_0$ ) [°K]	288.39
Ambient Pressure ( $P_0$ ) [mBar]	1013.25
Bleed Air Fraction ( $\beta$ ) [%]	3.0
Coolant Mixer 1 Air Fraction ( $\varepsilon_1$ ) [%]	5.0
Coolant Mixer 2 Air Fraction ( $\varepsilon_2$ ) [%]	5.0
Power Take Off (Low Pressure Spool) [kW]	0
Power Take Off (High Pressure Spool) [kW]	133.8
Fuel Heating Value ( $h_{PR}$ ) [kJ/kg]	42798.4
Max. High Pressure Turbine Inlet Temperature ( $T_{t4}$ ) [°K]	1593.5
Max. Compressor Pressure Ratio ( $\pi_c$ )	30

The comparison of the results obtained by using off-design conditions given in Table 16 are given in Table 17.

**Table 17** Off-Design result comparison for CFM56-5A Engine

Parameter	OFFX (AEDsys)	Performance Cycle Model (EDM)	% Difference
Inlet Pressure Ratio ( $\pi_r$ )	1.117	1.117	0.05
Inlet Temperature Ratio ( $\tau_r$ )	1.032	1.032	0.01
Fan Pressure Ratio ( $\pi_f$ )	1.424	1.35	5.18

Table 17 Continued

Parameter	OFFX (AEDsys)	Performance Cycle Model (EDM)	% Difference
Fan Temperature Ratio ( $\tau_f$ )	1.115	1.1	1.64
Low Pressure Compressor Pressure Ratio ( $\pi_{cL}$ )	1.424	1.35	5.18
Low Pressure Compressor Temperature Ratio ( $\tau_{cL}$ )	1.118	1.1	1.62
High Pressure Compressor Pressure Ratio ( $\pi_{cH}$ )	14.258	14.86	4.22
High Pressure Compressor Temperature Ratio ( $\tau_{cH}$ )	2.306	2.33	1.05
High Pressure Turbine Pressure Ratio ( $\pi_{tH}$ )	0.271	0.261	3.59
High Pressure Turbine Temperature Ratio ( $\tau_{tH}$ )	0.732	0.741	1.19
Low Pressure Turbine Pressure Ratio ( $\pi_{tL}$ )	0.377	0.315	16.59
Low Pressure Turbine Temperature Ratio ( $\tau_{tL}$ )	0.786	0.749	4.68
LP Spool RPM %	97.45%	88.88%	8.8
HP Spool RPM%	102.27%	102.30%	0.03
By-Pass Ratio ( $\alpha$ )	6.665	6.719	0.81
Fan Exhaust Total Pressure Ratio ( $P_{t19}/P_{19}$ )	1.558	1.477	5.2
Fan Exhaust Pressure Ratio ( $P_0/P_{19}$ )	1	1	0
Fan Exhaust Mach Number ( $M_{19}$ )	0.825	0.768	6.92
Fan Exhaust Total Pressure Ratio ( $P_{t9}/P_9$ )	1.852	1.801	2.77
Primary Exhaust Pressure Ratio ( $P_0/P_9$ )	0.860	1	16.29
Primary Exhaust Mach Number ( $M_9$ )	1	1	0
Engine Mass Flow Rate ( $m_0$ ) [kg/s]	991.55	1000.6	0.91
Combustor fuel-to air ratio ( $f$ )	0.0259	0.0258	0.23



**Table 17 Continued**

<b>Parameter</b>	<b>OFFX (AEDsys)</b>	<b>Performance Cycle Model (EDM)</b>	<b>% Difference</b>
<b>Overall fuel-to air ratio (<math>f_0</math>)</b>	0.00294	0.00290	1.26
<b>Specific Thrust [N/(kg/s)]</b>	188.98	183.88	2.70
<b>Thrust Specific Fuel Consumption [(kg/hr)/N]</b>	0.056	0.056	0.66

The result comparison in Table 17 shows that the maximum difference occurred in Low Pressure Turbine Pressure Ratio ( $\pi_{L}$ ) and the  $P_0/P_9$  pressure ratio.  $P_0/P_9$  pressure ratio calculation methodology involves the usage of the total temperature at Station 5 ( $T_{t5}$ ) which is affected from the Mach number ratio  $M_{4.5}/M_5$ . The Mach numbers in Stations 4.5 and 5 are taken as constants in the on-design section and they are transferred to the off-design section for the TURB sub-model as well. Because of the non-existence of the Momentum Conservation Law in the EDM performance cycle theory, these values are taken as constants and the difference between these constant values in EDM and AEDsys caused the difference observed in Table 17.

#### **4.1.2.3 GE90-94B Engine**

The same off-design flight conditions are used in the off-design analysis of CFM 56-5A engine case given in Section 4.1.2.2. The input list for this case is given for the landing condition in Table 18.

**Table 18** The list of off-design input parameters for the tests with GE90-94B Engine

Name of the Parameter	Value of the Parameter
Flight Mach Number ( $M_0$ )	0.4
Flight Altitude [m]	0
Ambient Temperature ( $T_0$ ) [°K]	288.39
Ambient Pressure ( $P_0$ ) [psia]	1013.25
Bleed Air Fraction ( $\beta$ ) [%]	3.0
Coolant Mixer 1 Air Fraction ( $\epsilon_1$ ) [%]	5.0
Coolant Mixer 2 Air Fraction ( $\epsilon_2$ ) [%]	5.0
Power Take Off (Low Pressure Spool) [kW]	0
Power Take Off (High Pressure Spool) [kW]	1562.0
Fuel Heating Value ( $h_{PR}$ ) [kJ/kg]	42798.4
Max. High Pressure Turbine Inlet Temperature ( $T_{t4}$ ) [°K]	1593.5
Max. Compressor Pressure Ratio ( $\pi_c$ )	25

The comparison of the results obtained by using off-design conditions given in Table 18 are given in Table 19.

**Table 19** Off-Design result comparison for GE90-94B Engine

Parameter	OFFX (AEDsys)	Performance Cycle Model (EDM)	% Difference
Inlet Pressure Ratio ( $\pi_r$ )	1.117	1.117	0.05
Inlet Temperature Ratio ( $\tau_r$ )	1.032	1.032	0.01
Fan Pressure Ratio ( $\pi_f$ )	1.530	1.519	0.71
Fan Temperature Ratio ( $\tau_f$ )	1.140	1.138	0.21
Low Pressure Compressor Pressure Ratio ( $\pi_{cL}$ )	1.530	1.519	0.71
Low Pressure Compressor Temperature Ratio ( $\tau_{cL}$ )	1.143	1.141	0.24
High Pressure Compressor Pressure Ratio ( $\pi_{cH}$ )	16.17	16.41	1.47
High Pressure Compressor Temperature Ratio ( $\tau_{cH}$ )	2.391	2.397	0.24
High Pressure Turbine Pressure Ratio ( $\pi_{tH}$ )	0.222	0.226	1.80

**Table 19 Continued**

<b>Parameter</b>	<b>OFFX (AEDsys)</b>	<b>Performance Cycle Model (EDM)</b>	<b>% Difference</b>
<b>High Pressure Turbine Temperature Ratio (<math>\tau_{tH}</math>)</b>	0.695	0.716	3.08
<b>Low Pressure Turbine Pressure Ratio (<math>\pi_{tL}</math>)</b>	0.194	0.223	14.98
<b>Low Pressure Turbine Temperature Ratio (<math>\tau_{tL}</math>)</b>	0.661	0.685	3.68
<b>LP Spool RPM %</b>	101.42%	100.19%	1.21
<b>HP Spool RPM%</b>	106.66%	106.83%	0.16
<b>By-Pass Ratio (<math>\alpha</math>)</b>	8.161	8.251	1.10
<b>Fan Exhaust Total Pressure Ratio (<math>P_{t19}/P_{t9}</math>)</b>	1.674	1.662	0.72
<b>Fan Exhaust Pressure Ratio (<math>P_0/P_{t9}</math>)</b>	1	1	0
<b>Fan Exhaust Mach Number (<math>M_{19}</math>)</b>	0.894	0.884	1.13
<b>Fan Exhaust Total Pressure Ratio (<math>P_{t9}/P_9</math>)</b>	1.104	1.301	17.81
<b>Primary Exhaust Pressure Ratio (<math>P_0/P_9</math>)</b>	1	1	0
<b>Engine Mass Flow Rate (<math>\dot{m}_0</math>) [kg/s]</b>	2865.34	3152.92	10.04
<b>Combustor fuel-to air ratio (<math>f</math>)</b>	0.0229	0.0245	6.89
<b>Overall fuel-to air ratio (<math>f_0</math>)</b>	0.00218	0.00230	5.37
<b>Specific Thrust [N/(kg/s)]</b>	159.17	170.299	6.99
<b>Thrust Specific Fuel Consumption [(kg/hr)/N]</b>	0.0493	0.0485	1.37

The comparison given in Table 19 shows that, the maximum difference occurred in the Low Pressure Turbine Pressure Ratio ( $\pi_{tL}$ ) and Total Pressure Ratio at Station 9. The Total Pressure Ratio at Station 9 is directly related to the difference in the Low Pressure Turbine Pressure Ratio (Equation (97)). The difference in Low Pressure Turbine pressure ratio is explained with the same reasoning made in the CFM56-5A Engine Case Specific Comparison Test (Section 4.1.2.2).

### 4.2.2 Continuity Tests

In the validation with the continuity tests of the Performance Cycle Model, the variation in predicted mass flow rate, predicted by-pass ratio, Specific Thrust, and Thrust Specific Fuel Consumption with respect to Mach Number (for the same on-design output case) is tracked in order to observe the change in outputs of the Performance Cycle Model in a wider operational range.

The change in Mass Flow Rate predictions with respect to flight Mach number is given in Figure 93. The average difference between the outputs of the Engine Design Model and the AEDsys is constant for all flow Mach numbers and 1%.

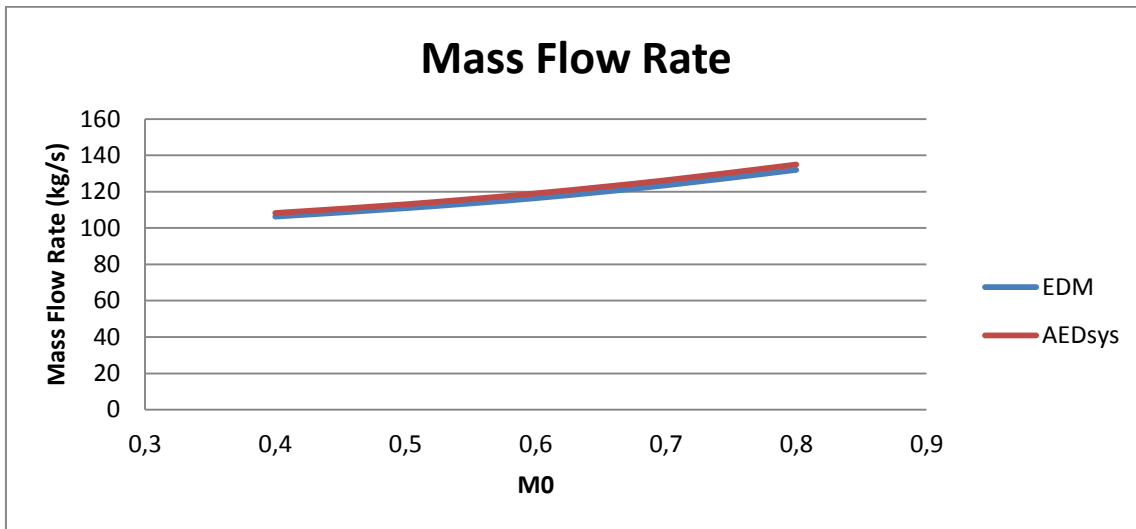


**Figure 93** Variation of Off-Design Mass Flow Rate prediction with respect to flight Mach number compared for Engine Design Model (EDM) and AEDsys program (OFFX)

The By-Pass ratio predicted after the convergence of the Alfa Loop is also compared for different off-design flight Mach number cases. The difference between the by-pass ratio outputs of EDM and AEDsys is 0.4% and constant for all cases as can be seen from Figure 94.

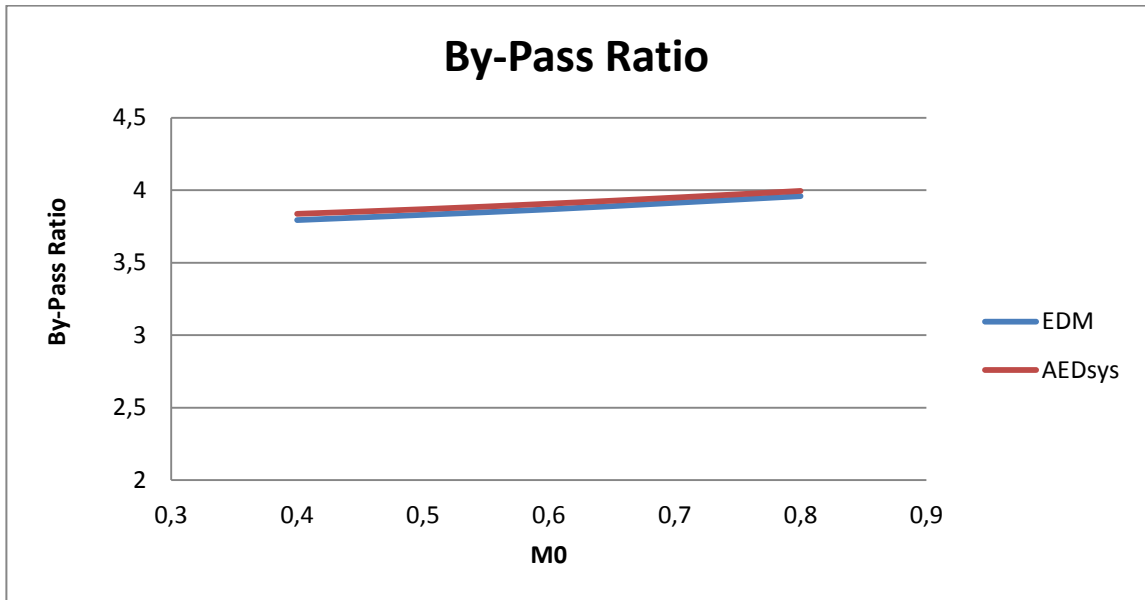


**Figure 94** Variation of Off-Design By-Pass ratio prediction with respect to flight Mach number compared for Engine Design Model (EDM) and AEDsys program (OFFX)

The change in the Specific Thrust is compared for the off-design flight Mach number cases given in the previous analyses. The difference between the outputs of EDM and AEDsys is constant and occurred as 5%. The comparison is illustrated in Figure 95.

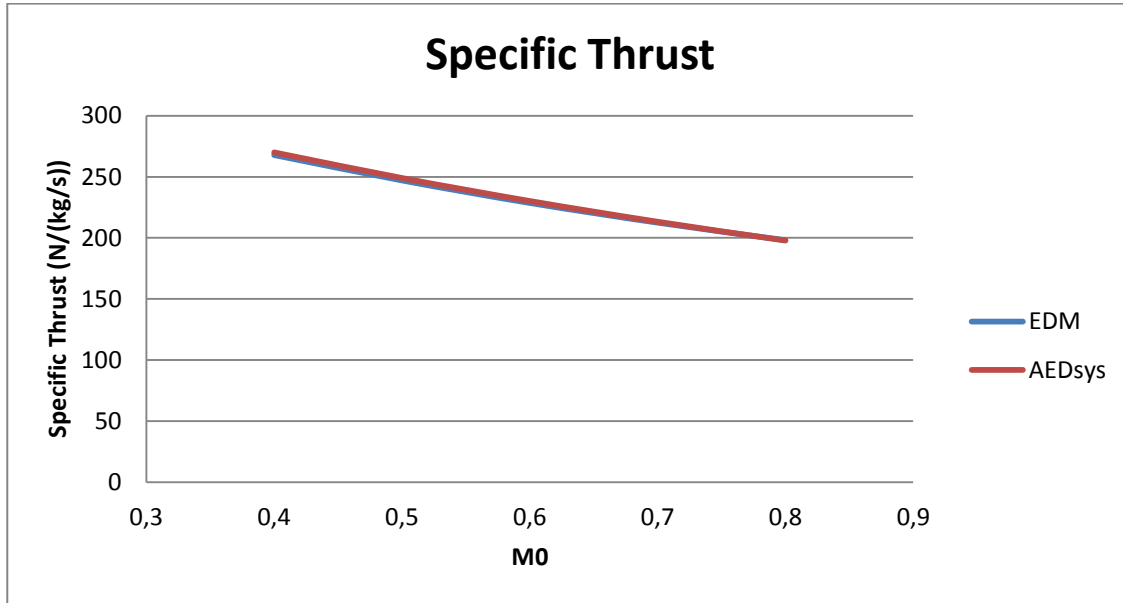


**Figure 95** Variation of Specific Thrust with respect to flight Mach number compared for Engine Design Model (EDM) and AEDsys program (OFFX)

The last comparison is made with the Thrust Specific Fuel Consumption. The change in this output is compared in Figure 96. The difference between the results of EDM and AEDsys is constant for all cases and 3%.

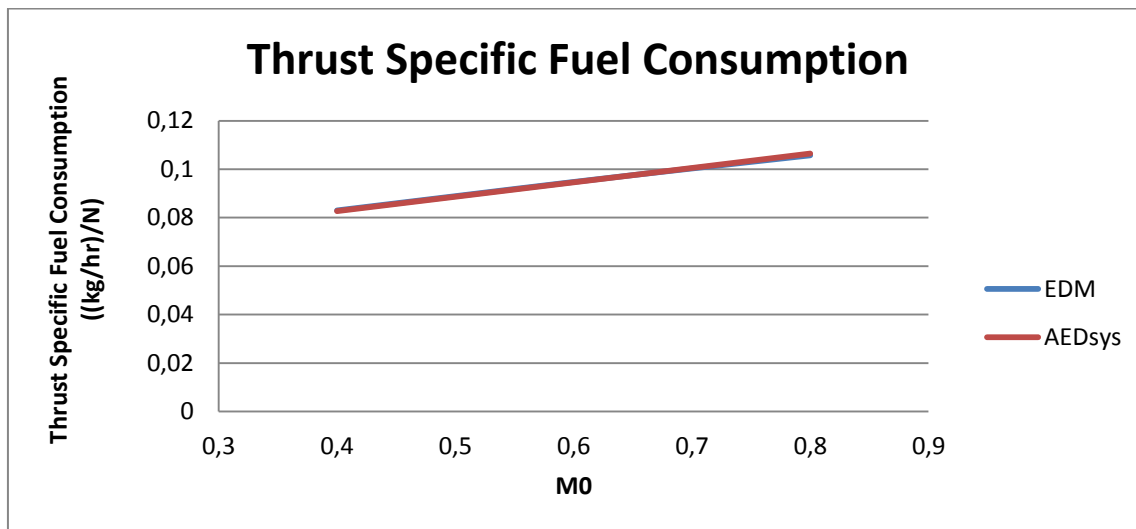


**Figure 96** Variation of Thrust Specific Fuel Consumption with respect to flight Mach number compared for Engine Design Model (EDM) and AEDsys program (OFFX)

In the continuity tests of Performance Cycle Model, the constant differences between the results are due to the different Variable Specific Heat Model usage and different convergence values of by-pass ratio and mass flow rate loops. The difference in computation environment in MATLAB may cause a difference in loop stopping criterion parameter values given in Sections 3.3.5.1 and 3.3.5.2. Stopping the design loops with different by-pass ratio and mass flow rate causes differences in predicted pressure and temperature ratios of components which results in differences at off-design cycle outputs.

### **4.3 Turbomachinery Design Model**

The validation of the Turbomachinery Design Model is carried out by using real engine data obtained from [4], [19], [20] and [21]. The dimensions of components are obtained by plot digitizing from the engine drawings given in [4] and [19] by using Plot Digitizer Software (v2.5.0) by Joseph A. Huwaldt. Number of Stages of each component, blade heights at each stage, and predicted  $N_1$  (Low Pressure Spool) and  $N_2$  (High Pressure Spool) wheel speeds are used in the validation. Because of the uncertainty in the dimension determination with plot digitizing, the presented real component dimensions in the following sections should not be considered as their exact values.

#### **4.3.1 CFM 56-5A Engine**

The validation of the Turbomachinery Design Model with CFM 56-5A Engine starts with the component dimension and number of stage comparison of Low Pressure Compressor and Fan. The required data for CFM56-5A Engine and the reference lengths for the plot digitizing are retrieved from [19]. The dimensional comparison for the Low Pressure Compressor and Fan of the real engine dimensions and the results obtained from Engine Design Model is illustrated in Figure 97.

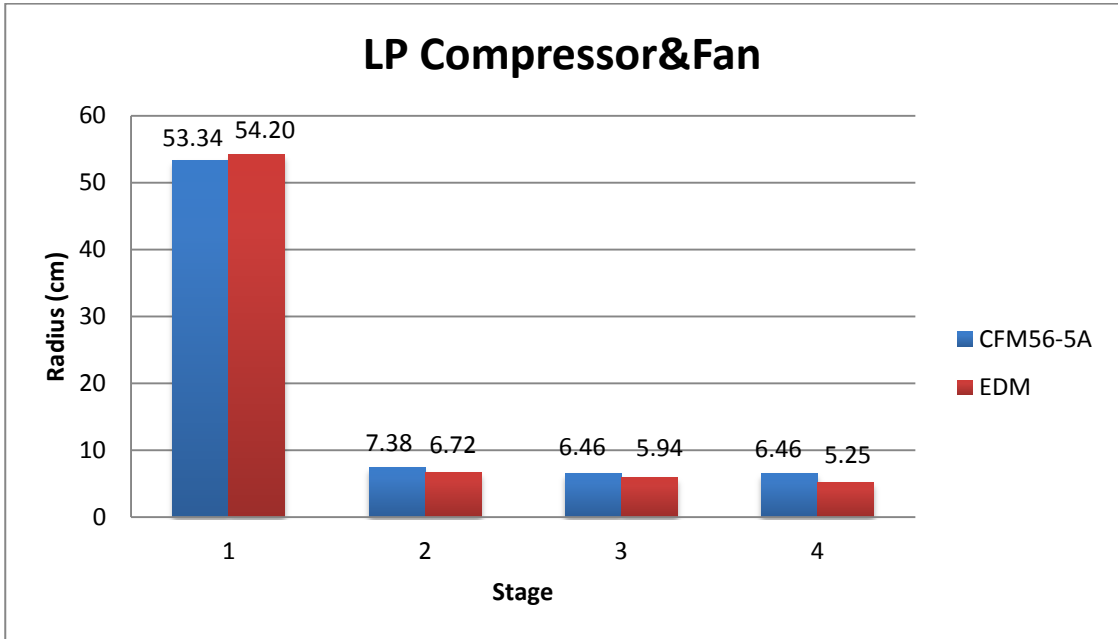


**Figure 97** Low Pressure Compressor and Fan dimensional comparison given for CFM56-5A Engine, the first stage is fan and the remaining stages are Low Pressure Compressor

Engine Design Model predicts the number of stages of Fan as 1, and Low Pressure Compressor as 3 which is coherent with the real engine data [19]. Fan dimension is coherent with the real data. A possible explanation to the differences in the Low Pressure Compressor radii can be the 3D flow field considerations and the difference in the material information used in those stages.

The comparison of the calculated High Pressure Compressor stage number and blade heights with the real engine dimensions are illustrated in Figure 98.



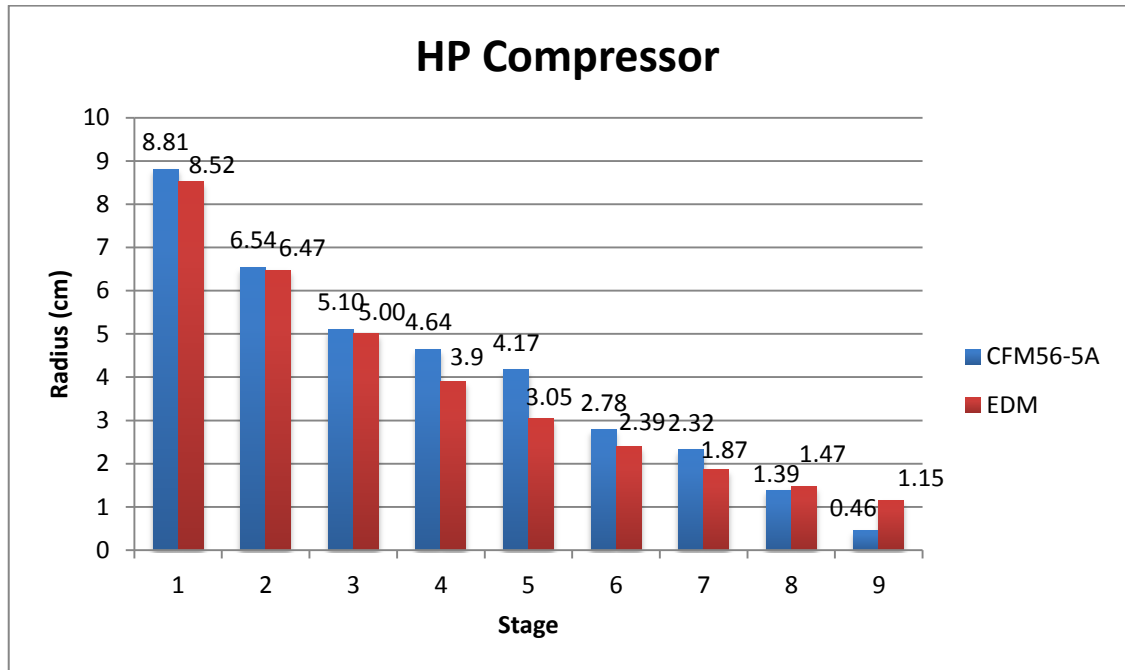


**Figure 98** High Pressure Compressor dimensional comparison is given for CFM56-5A Engine Engine Design Model predicts the number of stages of High Pressure Compressor as 9 which is coherent with the real engine data [19]. The dimensions obtained with EDM are in ideal conditions, whereas the real engine dimensions are determined by considering the non-ideal effects in the flow field and structural design limitations. Because of this fact, the compressor stage dimensions are predicted always smaller (except for the last two stages) by EDM. For the last two stages, a possible explanation to the difference can be the difference in the material information used in actual blade design at those stages.

When the last stage of Low Pressure Compressor in Figure 97 and the first stage of High Pressure Compressor in Figure 98 are compared, it can be shown that EDM considers the expansion difference between Low and High Pressure Compressors.

The comparison of the calculated High Pressure Turbine stage number and blade heights with the real engine dimensions are illustrated in Figure 99.

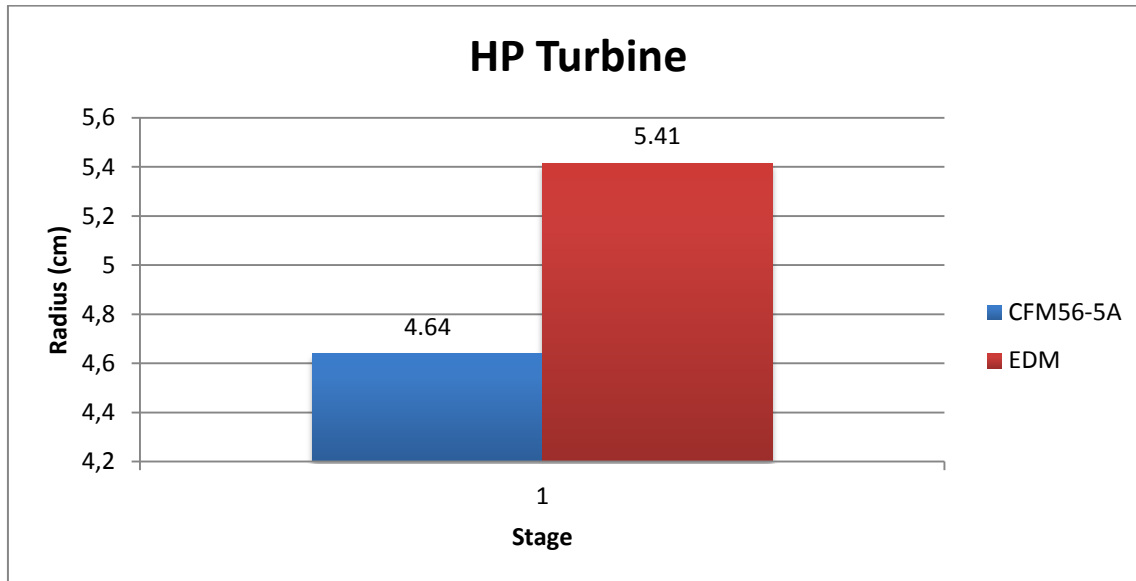


**Figure 99** High Pressure Turbine dimensional comparison is given for CFM56-5A Engine. Engine Design Model predicts the number of stages of High Pressure Turbine as 1 which is coherent with the real engine data [19]. A possible explanation to the difference can be the difference in the actual material information, and the structural design (thermal loads) in the actual High Pressure Turbine blade design.

The comparison of the calculated Low Pressure Turbine stage number and radii with the real engine dimensions are illustrated in Figure 100.

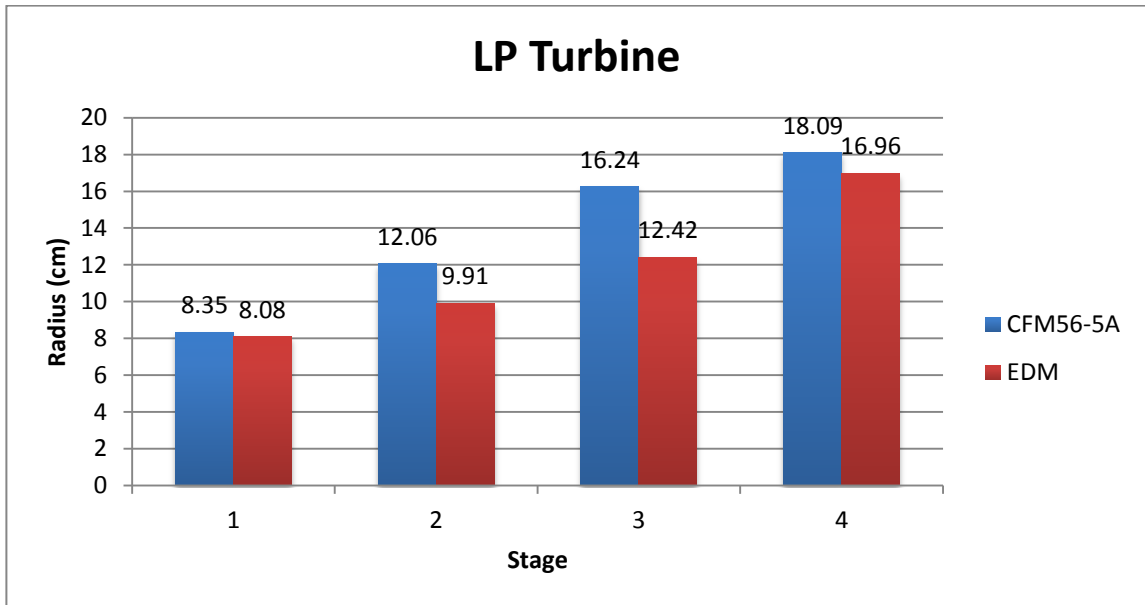


**Figure 100** Low Pressure Turbine dimensional comparison is given for CFM56-5A Engine Engine Design Model predicts the number of stages of Low Pressure Turbine as 4 which is coherent with the real engine data [19]. The dimensions obtained with EDM are smaller than the real engine dimensions. This can be explained with the ideal design conditions in EDM and possible flow field considerations in the actual Low Pressure Turbine blade design.

A summary view of comparison is shown in Figure 101, in which the hub dimensions are included and an engine map is drawn in order to show the comparisons of blade height calculations of EDM.

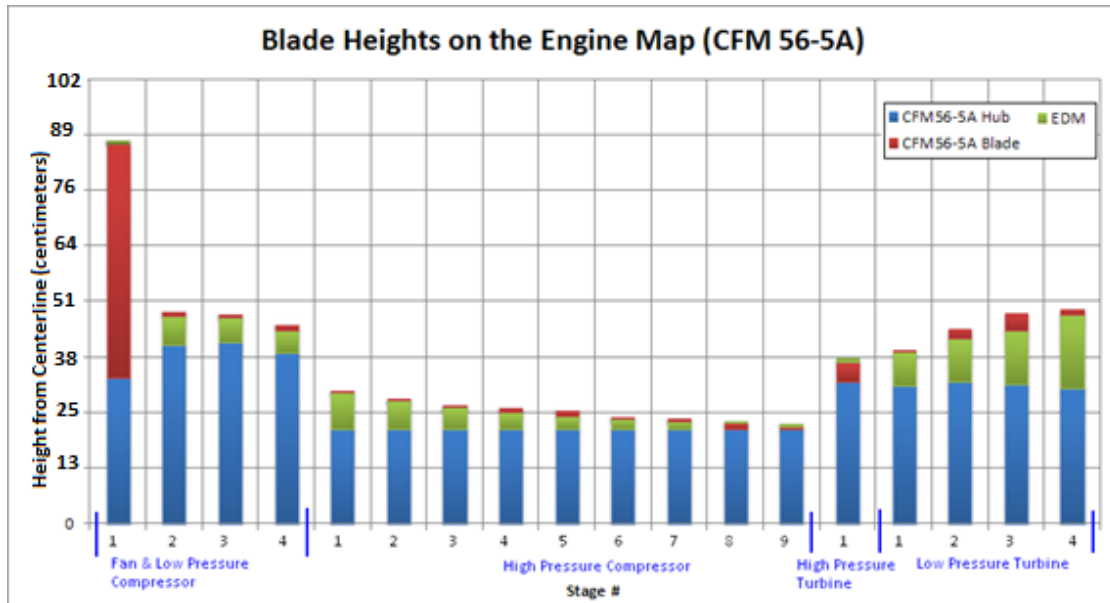


**Figure 101** The blade heights are given on the engine map for CFM56-5A Engine

The N1 and N2 wheel speeds obtained from [19] is compared with the relevant outputs of Turbomachinery Design Model in Figure 102. The wheel speeds are compared at the mean-line radii of Low Pressure Compressor and High Pressure Turbine for Low and High pressure spools respectively.

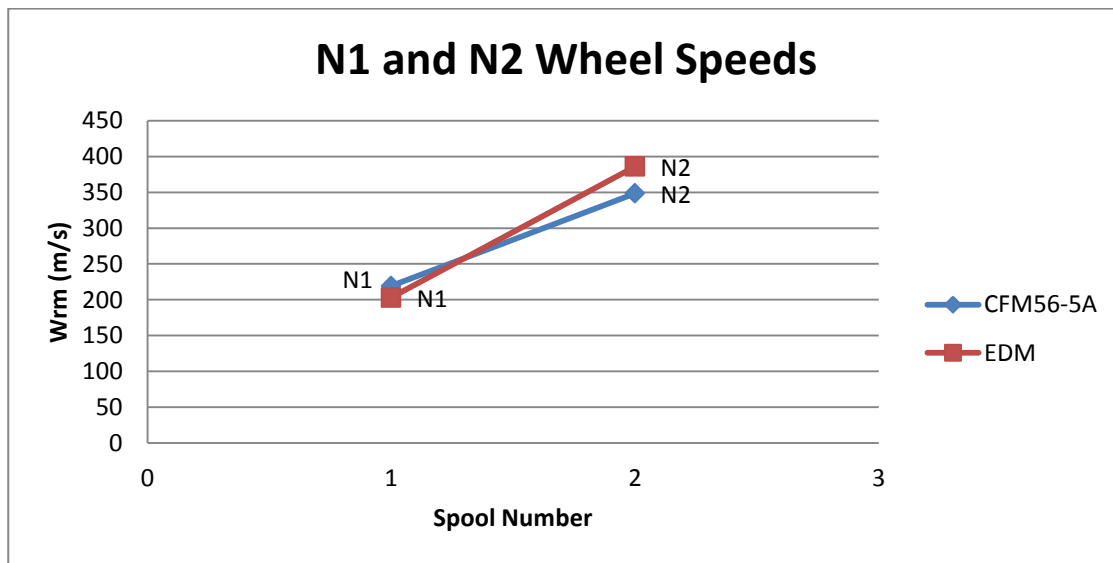


**Figure 102** The wheel speed at mean-line comparison is given for CFM56-5A Engine

The difference of the  $N_1$  wheel speed prediction of EDM is 7% and  $N_2$  wheel speed prediction is 10%, which are reasonable differences for aerothermodynamic (1D) turbomachinery design.

### 4.3.2 GE90-94B Engine

The required data for GE90-94B Engine and the reference lengths for the plot digitizing are retrieved from [4] and [21]. The wheel speed values of this engine are obtained from [20]. The dimensional comparison for the Low Pressure Compressor and Fan of the real engine dimensions and the results obtained from Engine Design Model is illustrated in Figure 103.

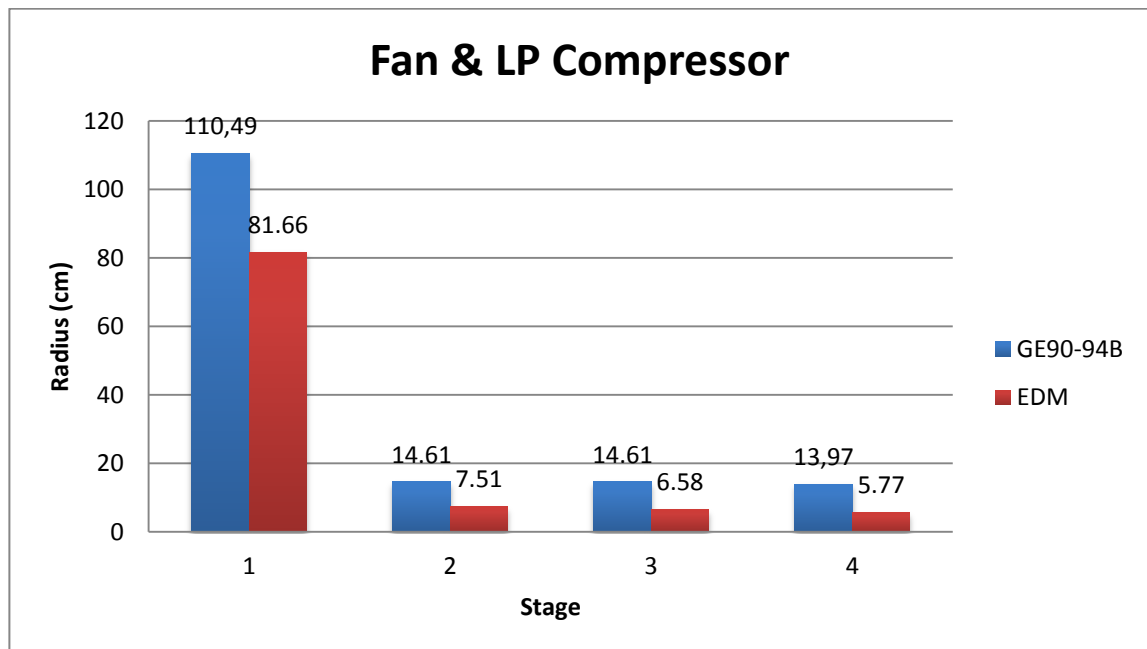


**Figure 103** Low Pressure Compressor and Fan dimensional comparison given for GE90-94B Engine, the first stage is fan and the remaining stages are Low Pressure Compressor

Engine Design Model predicts the number of stages of Fan as 1, and Low Pressure Compressor as 3 which is coherent with the real engine data [4]. The calculated component sizes for the Fan and Low Pressure Compressor are smaller than the sizes of actual engine dimensions for all stages. A possible explanation to this situation can be the ideal design considerations made in EDM, the differences in the material information

used in stress calculations in EDM and flow field related considerations in the actual design.

The comparison of the calculated High Pressure Compressor stage number and blade heights with the real engine dimensions are illustrated in Figure 104.

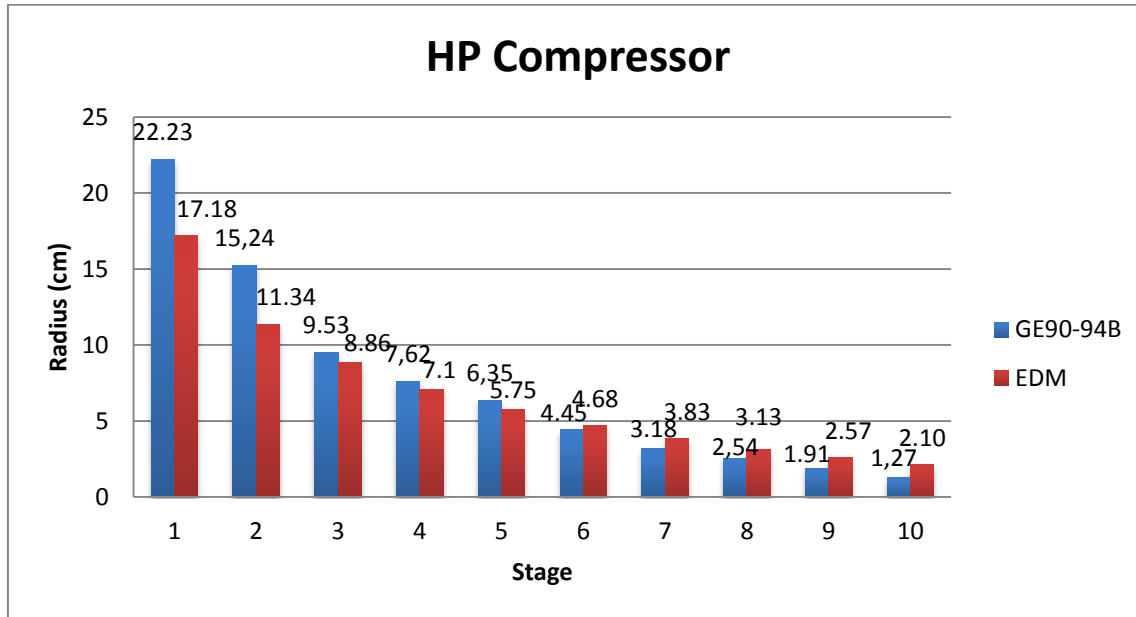


**Figure 104** High Pressure Compressor dimensional comparison is given for GE90-94B Engine Engine Design Model predicts the number of stages of High Pressure Compressor as 10 which is coherent with the real engine data given in [21] and [4]. The component dimensions at first 5 stages are calculated smaller than the actual engine data. A possible explanation to these differences in these stages can be the ideal design consideration and flow field related design considerations. Whereas for the remaining 5 stages, the dimensions obtained with EDM are bigger than the actual engine component sizes, which has a possible explanation with the difference in the material information used in stress calculations and/or structural analysis considerations in the actual High Pressure Compressor component design.

When the last stage of Low Pressure Compressor in Figure 103 and the first stage of High Pressure Compressor in Figure 104 are compared, it can be shown that EDM considers the expansion difference between Low and High Pressure Compressors.

The comparison of the calculated High Pressure Turbine stage number and radii with the real engine dimensions are illustrated in Figure 105.

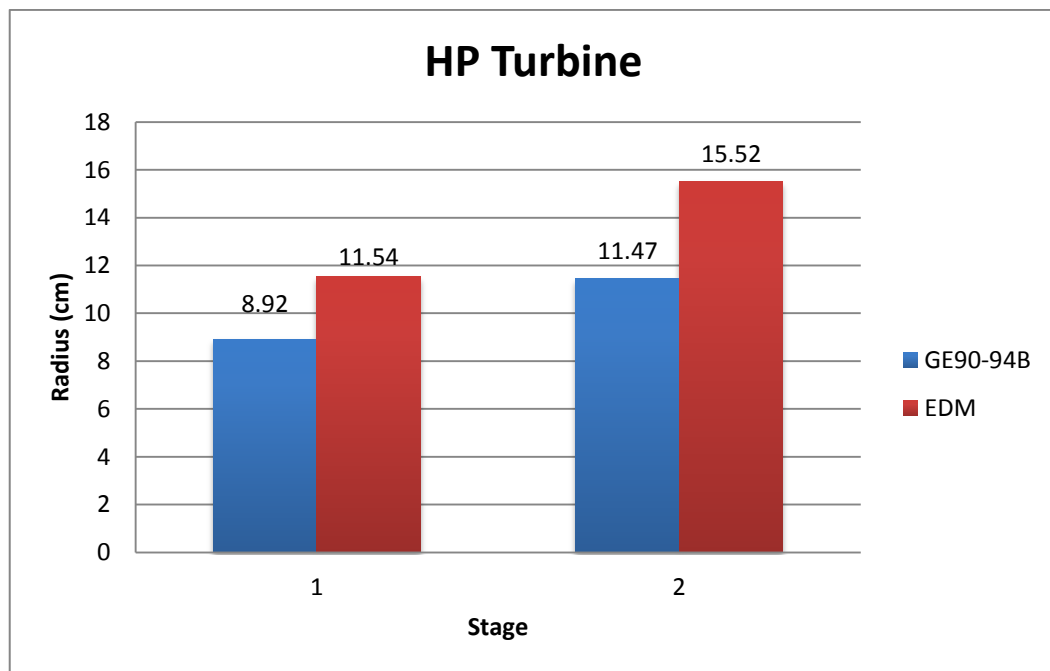


**Figure 105** High Pressure Turbine dimensional comparison is given for GE90-94B Engine. Engine Design Model predicts the number of stages of High Pressure Turbine as 2 which is coherent with the real engine data [4] and [21]. The dimensions obtained by EDM are bigger than the actual data. A possible explanation to the difference can be the difference in the actual material information, and the structural design (thermal loads) in the actual High Pressure Turbine blade design.

The comparison of the calculated Low Pressure Turbine stage number and blade heights with the real engine dimensions are illustrated in Figure 106.

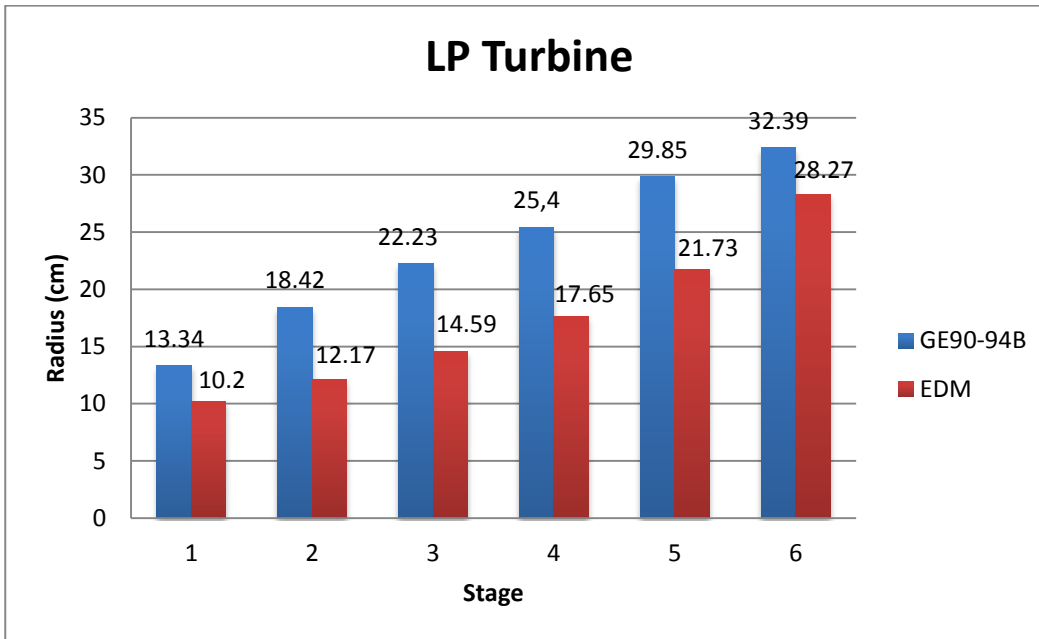


**Figure 106** Low Pressure Turbine dimensional comparison is given for GE90-94B Engine

Engine Design Model predicts the number of stages of Low Pressure Turbine as 6 which is coherent with the real engine data in [4] and [21]. The dimensions obtained with EDM are smaller than the real engine dimensions because of the ideal design conditions in EDM and possible flow field considerations in the actual Low Pressure Turbine blade design.

A summary view of comparison is shown in Figure 107, in which the hub dimensions are included and an engine map is drawn in order to show the comparisons of blade height calculations of EDM.



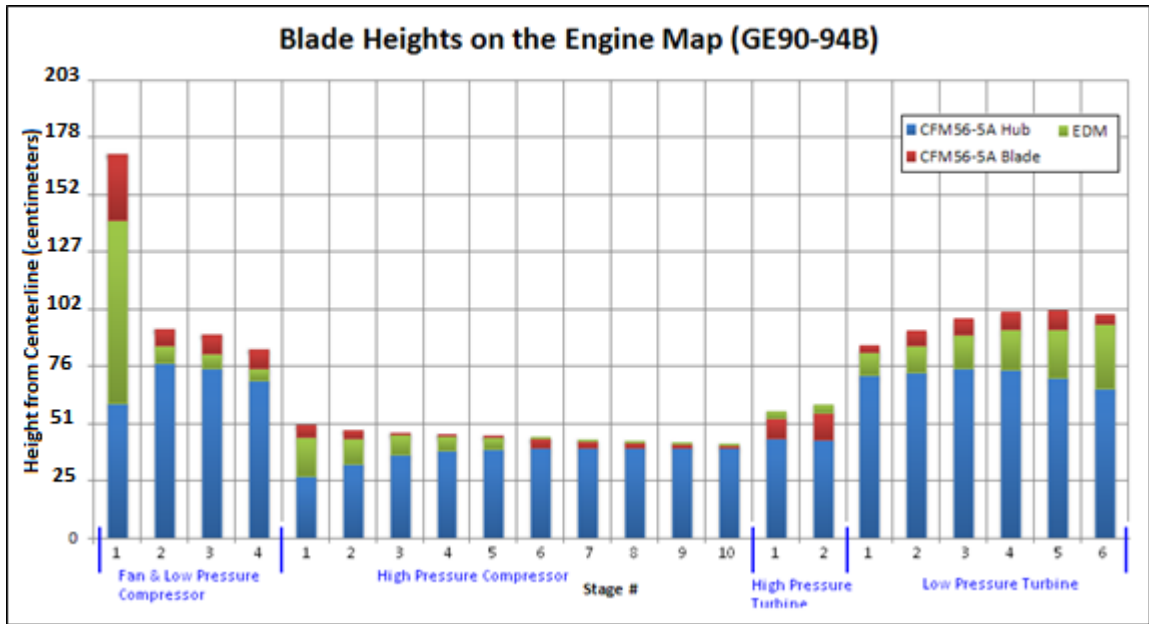


**Figure 107** The blade heights are given on the engine map for GE90-94B Engine

The  $N_1$  and  $N_2$  wheel speeds obtained from [20] is compared with the relevant outputs of Turbomachinery Design Model in Figure 108. The wheel speeds are compared at the mean-line radii of Low Pressure Compressor and High Pressure Turbine for Low and High pressure spools respectively.

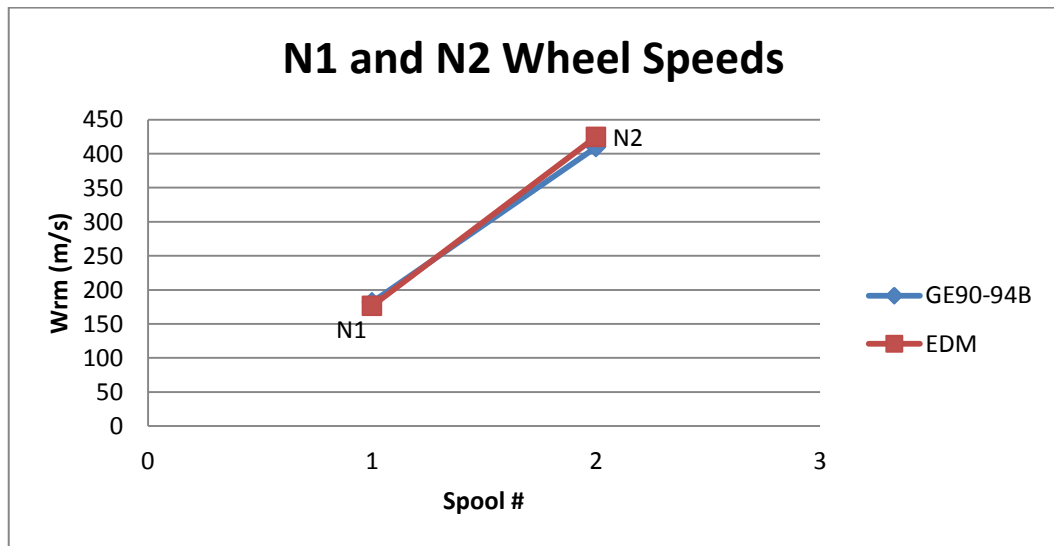


**Figure 108** The wheel speed at mean-line comparison is given for GE90-94B Engine

The difference of the  $N_1$  wheel speed prediction of EDM is 3% and  $N_2$  wheel speed prediction is 3.5%, which are reasonable differences for aerothermodynamic (1D) turbomachinery design.

As stated by Oates [22], the actual component design includes aerodynamic and aeromechanical design phases and the final shaping of the components are highly determined by these analyses. For the last stages of High Pressure Compressor and first stages of the High Pressure Turbine, aeromechanical effects due to high temperature and pressure is more dominant, whereas for the Fan, Low Pressure Compressor and the Low Pressure Turbine flow effects and flow stability are more dominant parameters in the design.

The aerothermodynamic design gives the designers only a starting point for the component design and Engine Design Model gives sufficient results for comparison of engine component dimension changes due to changes in on-design conditions.

## CHAPTER 5

### OPTIMIZATION

#### 5.1 Introduction

The definition given by Snyman [23] for optimization is that it is being the science of determining the best solutions to mathematically defined problems. Mathematical definition is given as it is the process of minimization of an objective function  $f(x)$  which may subject to equality or inequality constraints or may not subject to any constraints at all. The solution of the optimization problem is the optimum vector  $x^*$  that gives the optimum function value  $f(x^*)$ .

In order to obtain reliable solutions from an optimization method, the mathematical modelling and integration of the model with the optimization algorithm is important. An illustration of the process of the integration of the mathematical model with the optimization algorithm is given in [23] and shown in Figure 109.

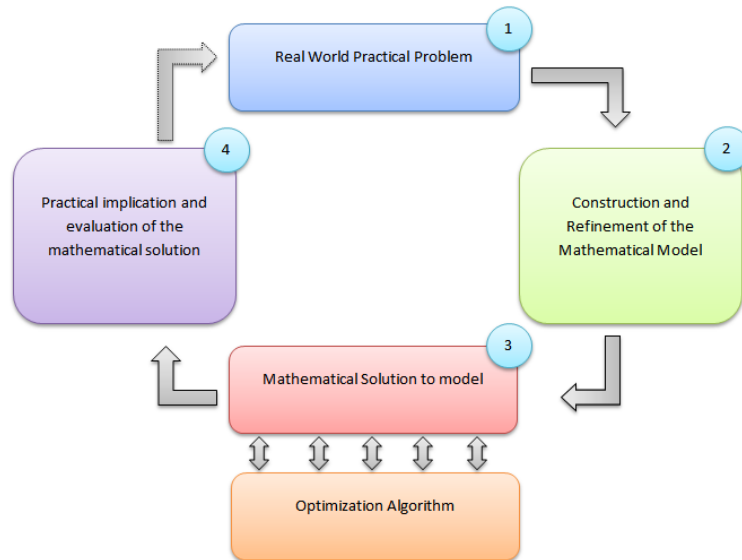


**Figure 109** The location of the optimization algorithm in a mathematical problem

As can be seen from Figure 109, the first step in the optimization problem is to define the real world practical problem. It follows with the abstraction of the problem by the construction of a mathematical model that is described in terms of preliminary fixed model parameters, and variables. After the construction of the model, an analytical or numerical parameter dependent solution can be obtained. The optimization algorithm calls the mathematical model repeatedly to find the optimum solution at this step. After finding an optimum solution to the problem, investigation of the results may lead to refinement of the mathematical model and the loop described in Figure 109 will be run once again.

The constraint functions defined at the beginning of the optimization problem defines the boundaries of the feasible solution region to the optimization algorithm. These functions help the optimization method to evaluate the feasibility of the found solution and in some cases they may also provide a starting point of optimization iterations. An illustration of the feasible region of solution and the constraints is given in Figure 110.

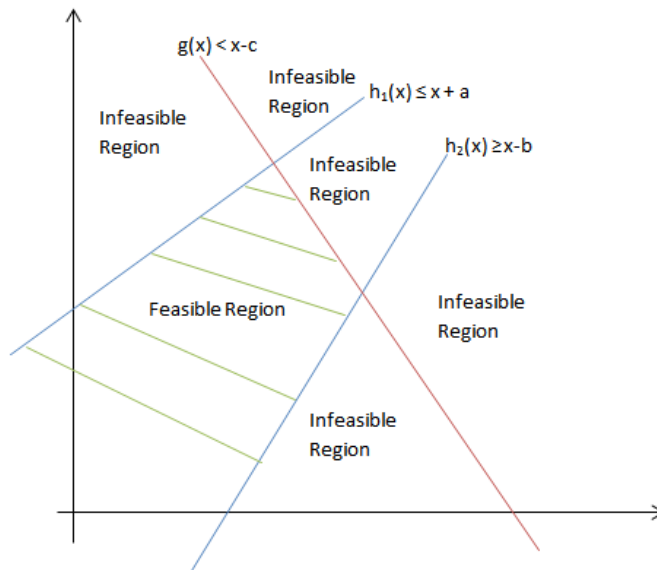


**Figure 110** The feasible region definition;  $g(x)$  is an inequality constraint and  $h(x)$ 's are equality constraints

Equality constraints are the lines of feasible solutions and they are included in the feasible region. Whereas for the inequality constraints, any solution that is on the inequality lines are infeasible solutions and these boundaries are not included in feasible region.

The design variables are the parameters that are allowed to be changed by the optimization algorithm while searching for the optimum solution. The initial conditions are defined with these parameters and great care must be taken to ensure that the scales of the variables are more or less of the same order. If not, the formulated problem will be insensitive to the variations and any optimization algorithm will encounter with excessive amount of iterations to converge to the true solution. The recommended practice by Snyman [23] is to scale the variables so that all the variables are dimensionless and vary between 0 and 1 by considering the minimum and maximum physical limits of each variable. Commonly most of the optimization software does the

scaling automatically after entering the design variable limits, but scaling may be changed later if the optimization does not converge after successive iterations.

Before starting to an optimization problem, the variation of the solution parameters (outputs) of the mathematical model with the design variables should be investigated as a first step. In some type of mathematical problems there may exist several local minima/or maxima and a global minimum/maximum point, or there may be a unique minimum/maximum point which is also being the global minimum/maximum. In these two types of cases, an optimization algorithm can converge and able to find a minimum/maximum point which may be a local minimum/maximum or the global minimum/maximum point. Whereas for the functions that are continuously decreasing or increasing to the infinity which have no minimum/maximum points, any optimization algorithm will fail to converge and a feasible solution cannot be found.

Optimization algorithms usually test their solutions during the iterations whether it is a local or global minimum or not. However, the global minimizer can be difficult to find since the knowledge of  $f(x)$  is usually only local. Most optimization methods therefore seek only a local minimum. An approximation to find the global solution is obtained in practice by multi-start application of a local minimizer from randomly selected different points in design variable domain. The lowest value obtained after a sufficient number of trials is then taken as a good approximation to the global solution. If, however, the function  $f(x)$  is known to be as strictly convex over the solution domain, then only one trial will give the solution. [23]

## **5.2 Optimization Algorithms**

The direct search method is the basic optimization method and forms the basis of many advanced optimization algorithms. Over the last 40 years from the introduction of early optimization algorithms, many powerful direct search algorithms have been developed. These algorithms require an initial estimate to the optimum point (denoted by  $x^0$ ). With this estimate as starting point, the algorithm generates a sequence of

estimates  $x^0, x^1, x^2, \dots$ , by successively searching directly from each point in a direction of descent to determine the next point. This process is illustrated in Figure 111.

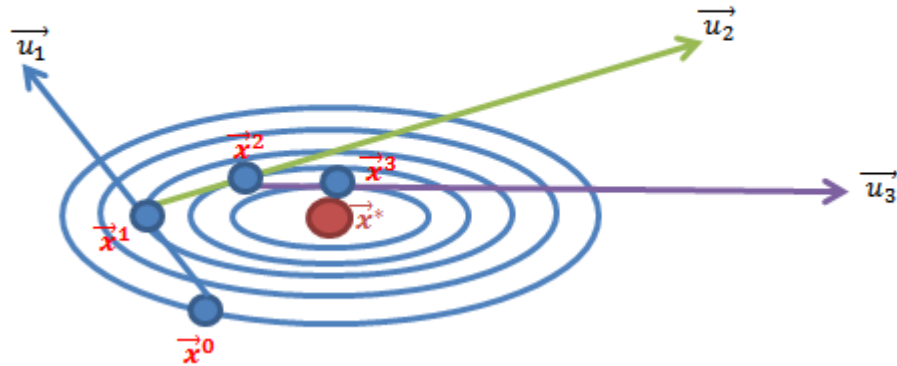


**Figure 111** The process of direct search method to find the optimum solution  $x^*$ .

The process is terminated if either no further progress is made, or if a point  $x^k$  is reached (for smooth functions) at which the gradient of the objective function ( $\nabla f(x)$ ) is equal to 0. In this case  $x^k$  is said to be an approximation to the optimum solution  $x^*$ . It is necessary, but not always, required that the function value at the new iterate  $x^{i+1}$  be lower than at  $x^i$ .

The direct search methods differ from each other by the selection of the descent direction  $u^{i+1}$  at each iteration  $x^i$ , that ensures descent at  $x^i$  in the direction of  $u^{i+1}$ , i.e. it is required that the directional derivative in the direction  $u^{i+1}$  be negative.

### 5.2.1 Unconstrained Optimization

This type of optimization methods can find the optimum solution even if the boundaries of the feasible region are not specified. The unconstrained optimization methods are given hereinafter.

### 5.2.1.1 1<sup>st</sup> Order Methods

The 1<sup>st</sup> Order direct search methods use the gradient vector ( $\nabla f(x)$ ) to determine the search direction at each iteration. The methods are classified according to the degree of the partial derivative taken to compute the search direction at the current iteration. Examples of the 1<sup>st</sup> Order Direct Search method algorithms are:

- The method of Steepest Descend
- Conjugate Gradient Methods (Formal Fletcher-Reeves Conjugate Gradient Algorithm)

### 5.2.1.2 2<sup>nd</sup> Order Methods

2<sup>nd</sup> Order Line Search Descent methods are based on Newton's Method for solving  $\nabla f(x)$  iteratively. Although it is a more advanced algorithm, the convergence is not always guaranteed and it may sometimes diverge even from close to the solution. However, if it converges, it converges very fast and it is quadratically convergent. The implementation of the method requires the evaluation of Hessian matrices at each step and these methods are computationally very expensive for large number of design variables. Examples of such algorithms are:

- Modified Newton's Method
- Quasi Newton's Methods (Davidon-Fletcher-Powell and BFGS methods)

### 5.2.1.3 0<sup>th</sup> Order Methods

These methods are called such because they do not use either first or second order derivative information but only function values, i.e. only zeroth order derivative information.

Although these methods are expected to be slower and computationally more expensive than the higher order methods, they are usually reliable and easily to program. Some examples are:

- SIMPLEX (by Nelder and Mead, 1965)
- Method of Powell (1964)



- Simulated Annealing (Genetic Algorithms)

The SIMPLEX method had many variations and modifications in order to increase its accuracy. Some of the types of SIMPLEX algorithms are given in Künzi H.P. et al. [24] which are:

- The basic SIMPLEX method
- Dual SIMPLEX method
- Revised SIMPLEX Method
- DUOPLEX Method
- Gomory Algorithm
- Beale's Algorithm
- The Wolfe's Algorithm

Most of computer software is commercially available for optimization. Examples are MATLAB Optimization Toolbox™, IMSL, NAG Mathematical Library, HEEDS, SHERPA, and IOSO. [23]

### **5.2.2 Constrained Optimization**

It is the process of optimizing the objective function with respect to design variables in the presence of constraints on those variables. [25] Some of the standard methods under this type of optimization are:

- Penalty Function Method
- Lagrangian Method
- Quadratic Programming (The method of Theil and Van de Panne)
- Gradient Projection Methods (Rosen, 1961)
- Augmented Lagrangian multiplier methods (Haftka and Gündel, 1992)
- Successive or Sequential Quadratic Programming (SQP) methods (Bazaraa et al., 1993) [23]

### **5.3 Using Optimization in Engine Design**

Optimization methods are frequently used in Engine Design in the determination of the geometry of certain turbomachinery parts such as in [26], or to find the engine design parameters that meets a predefined aim such as in the studies of Rifai H. [27], and Berton J. et al. [28].

In practice, the input parameters of aerothermodynamic design are determined as intervals rather than specific singular values. This is due to the fact that the Request for Proposal for a new engine design often avoids giving exact boundaries for certain parameters such as Thrust, Thrust Specific Fuel Consumption or maximum Fan diameter. An engine that has the maximum Thrust with minimum Thrust Specific Fuel Consumption and the lowest fan diameter would be the best design that will meet the proposal. According to the constraints set by the proposal, the design output parameters may be increased and finding such a design that meets all of the constraints cannot be found easily by manually searching the output data produced by varying certain input parameters.

In order to gain speed and increase the performance in finding the best engine design parameters that meets the design constraints, optimization methods can be used. A mathematical model that performs the aerothermodynamic engine design calculations such as Engine Design Model can be used as the mathematical model of such an optimization problem.

MATLAB Simulink Design Optimization Toolbox is used in the aerothermodynamic design optimization because of its wide variety of optimization algorithms. The Design Optimization Toolbox provides users the following optimization algorithms:

- Gradient Descent Algorithms
  - Active Set
  - Interior Point
  - Trust Region Reflective

- Sequential Quadratic Programming
- Pattern Search Algorithms
  - Positive Basis Np1
  - Positive Basis 2N
  - Latin Hypercube
  - Genetic Algorithm
  - Nelder-Mead
- SIMPLEX

Using an unconstrained optimization algorithm such as pattern search algorithms, may cause unphysical results when it sends design variable inputs regardless of the physical boundaries. In order to avoid this and because of the aerothermodynamic engine design problem is a non-linear constrained problem, Gradient Descent Algorithms are used. SIMPLEX is also used in order to make a comparison between different algorithms.

According to the MATLAB Documentation Center [29], the properties of the Gradient Descent Algorithms are given as follows:

- 1) *Active Set Algorithm*: This algorithm can take large steps, which adds speed. The algorithm is effective on some problems with non-smooth constraints. It is not a large scale algorithm<sup>†</sup>.
- 2) *Interior Point Algorithm*: This algorithm handles large, sparse problems, as well as small dense problems. The algorithm satisfies bounds at each iteration and can recover from NaN (Not a Number) and Infinite results. It is a large scale algorithm.

<sup>†</sup> An optimization algorithm is *large scale* when it uses linear algebra that does not need to store, nor operate on, full matrices. This may be done internally by storing sparse matrices, and by using sparse linear algebra for computations whenever possible. [29]

- 3) *Trust Region Reflective*: It requires the user to provide a gradient, and allows only bounds or linear equality constraints but not both. Within these limitations, the algorithm handles both large sparse problems and small dense problems efficiently. It is a large scale algorithm. The algorithm has special techniques to reduce the memory usage.
- 4) *Sequential Quadratic Programming*: It satisfies bounds at all iterations. It can recover from NaN (Not a Number) and Infinite results. It is not a large scale algorithm.

All of these algorithms are explained in detail by Abebe [30]. In the optimization studies with Engine Design Model the Active Set, and Trust Region Reflective algorithms are used in order to see the difference in the results from a large scale algorithm and verify the results with different algorithms.

#### **5.4 Results of an Example Optimization Problem with EDM**

An example optimization problem is generated for the Mid By-Pass Ratio Generic Engine given in Section 4.1.1.1. The on-design conditions are set to the cruise condition and the off-design flight conditions are set to landing conditions. The design variables of the optimization problem are determined to be as follows:

- By-Pass Ratio ( $\alpha$ )
- Fan Pressure Ratio ( $\pi_f$ )
- High Pressure Compressor Pressure Ratio ( $\pi_{cH}$ )
- Engine Mass Flow Rate ( $m_0$ )

The pressure ratio  $\pi_f$  is taken equal to  $\pi_{cL}$ , therefore by changing the  $\pi_{cH}$  and  $\pi_f$  in the optimization, (considering the  $\pi_c = \pi_{cL} \pi_{cH}$  relation) the overall compressor pressure ratio can also be said to be a design variable. The design constraints are put on the following Engine Design Model output parameters, which are the objective functions of the optimization problem:

- On-Design Specific Thrust
- On-Design Thrust Specific Fuel Consumption
- On-Design Overall Efficiency
- Off-Design Specific Thrust
- Off-Design Thrust Specific Fuel Consumption
- Low Pressure Compressor Number of Stages
- High Pressure Compressor Number of Stages
- Fan blade height
- High Pressure Compressor maximum blade height
- High Pressure Turbine maximum blade height
- Low Pressure Turbine maximum blade height
- Low Pressure Spool wheel speed
- High Pressure Spool wheel speed

In order to see the effect of the constraints on the optimization, 4 different optimization cases are generated. These cases differ from each other with the usage of the constraints given previously. The optimization cases are explained in Table 20.

**Table 20** Optimization Example Cases, the active constraints are shown with green and inactive ones are shown with red

Case	ON-DESIGN CONSTRAINTS			OFF-DESIGN CONSTRAINTS		TURBOMACHINERY CONSTRAINTS							
	$F/m_0$	TSFC	$\eta_o$	$F/m_0$	TSFC	LPC Stage #	HPC Stage #	Fan B.H.	HPC B.H.	HPT B.H.	LPT B.H.	$N_1$ wheel speed	$N_2$ wheel speed
1	✓	✓	✓	✓	✓	✓	✓	✗	✗	✗	✗	✗	✗
2	✓	✓	✓	✓	✓	✓	✓	✗	✗	✓	✓	✗	✗
3	✓	✓	✓	✓	✓	✓	✓	✓	✓	✓	✓	✗	✗
4	✓	✓	✓	✓	✓	✓	✓	✓	✓	✓	✓	✓	✓

The design variables limits are determined for Gradient Descent Algorithms as given in Table 21.

**Table 21** Design Variable limits defined for constrained optimization algorithms

Design Variable	Lower Limit	Upper Limit
By-Pass Ratio ( $\alpha$ )	1	5
Fan Pressure Ratio ( $\pi_f$ )	2	7
High Pressure Compressor Pressure Ratio ( $\pi_{cH}$ )	3	20
Mass Flow Rate ( $m_0$ ) [kg/s]	36.29	113.398

The signal constraints put on the chosen output variables of the Engine Design Model are given in Table 22.

**Table 22** Signal constraint values on output parameters

Section	Constraint	Lower Limit	Upper Limit
ON-DESIGN	$F/m_0$	294.21	441.32
	TSFC	0.0408	0.0918
	$\eta_o$	0.1	1
OFF-DESIGN	$F/m_0$	166.72	490.35
	TSFC	0.0408	0.112
TURBOMACHINERY	Stage Number (Low Pressure Compressor)	1	8
	Stage Number (High Pressure Compressor)	1	9
	Fan Blade Height	5.08	38.1
	High Pressure Compressor Maximum Blade Height	0.254	12.7
	High Pressure Turbine Maximum Blade Height	2.54	10.16
	Low Pressure Turbine Maximum Blade Height	2.54	15.24
	$N_1$ Wheel Speed	152.4	457.2
	$N_2$ Wheel Speed	152.4	457.2

Optimizations with the given conditions in Tables 20, 21 and 22 are executed by using “Response Optimization” from the “Analysis” tools of Simulink. Response Optimization uses MATLAB Optimization Toolbox and provides an interface, from which users can

choose and set limits of the design variables from the Simulink model, enable and disable constraints and change their values, decide on iteration plots, and choose an optimization method with specifying tolerances.

The results of optimizations are given for each case defined in Table 20 hereinafter. The optimizations with all of the Cases are accomplished by using two types of Gradient Descent algorithms and SIMPLEX. Since the Gradient Descent algorithms are prone to find local optimum points, one should not confine to the results of a single optimization run. Therefore according to the advices given in MATLAB Documentation [31], the optimizations are repeated three more times with new initial conditions on design variables and these conditions are taken from the results of previous optimization run. This method is called “Rerun Starting at Final Point” and it also follows running the model with different initial conditions advice.

#### 5.4.1 Results of Case 1

The design variables calculated for the four runs with Gradient Descent Active Set algorithm is given in Table 23, and the changes made by the optimization algorithm on the design variables for each optimization iteration is shown graphically in Appendix B. (Figure B1)

**Table 23** The changes in design variables for each optimization run

Run	Number of Iterations	F(x)	F-Count	Max. Constraint	By-Pass Ratio ( $\alpha$ )	Fan Pressure Ratio ( $\pi_f$ )	High Pressure Compressor Pressure Ratio ( $\pi_{ch}$ )	Mass Flow Rate ( $m_0$ ) [kg/s]
1	3	-0.0916	36	0.002	3.6688	4.2745	5.1825	36.2874
2	2	-0.1323	27	0.0017	3.4128	4.3454	7.4444	36.4588
3	2	-0.1479	27	8.65E-04	3.2613	4.419	8.956	36.4588
4	2	-0.1416	27	1.93E-04	3.0893	4.5095	9.0803	36.4588

The respective Engine Design Model outputs are calculated as given in Table 24 for each optimization run.

**Table 24** The results obtained at each run

Run	ON-DESIGN CONSTRAINTS			OFF-DESIGN CONSTRAINTS		TURBOMACHINERY CONSTRAINTS							
	$F/m_0$	TSFC	$\eta_o$	$F/m_0$	TSFC	LPC Stage #	HPC Stage #	Fan B.H. (cm)	HPC B.H. (cm)	HPT B.H. (cm)	LPT B.H. (cm)	$N_1$ wheel speed (m/s)	$N_2$ wheel speed (m/s)
1	320.6	0.084	11.60%	245.1	0.089	6	6	16.792	2.256	2.507	8.049	268.1	306.9
2	332.8	0.080	11.70%	322.4	0.089	6	7	14.679	1.941	2.253	6.993	278.7	363.0
3	337.7	0.078	11.90%	322.7	0.084	6	7	14.869	2.931	2.098	6.995	289.0	352.0
4	347.1	0.079	13.40%	371.7	0.082	6	7	16.101	5.471	0.734	6.441	299.0	94.3

The small changes in the results from second run to third run indicates that the results found in the third run is very close to the optimum point. The iterations are stopped after the fourth run because of having higher  $f(x)$  value than the third run, which indicates a further solution point to the optimum solution point. In addition, the results obtained in other Turbomachinery constraints gave lower  $N_2$  wheel speed than  $N_1$  wheel speed which indicates an inapplicable result. Therefore the results obtained in the third iteration are the closest results to the optimum for Case 1.

Another set of optimization runs are made with Gradient Descent Trust Region Reflective Algorithm. The design variables calculated for the four runs with this algorithm is given in Table 25, and the changes made by the optimization algorithm on the design variables for each optimization iteration is shown graphically in Appendix B. (Figure B2)



**Table 25** The changes in design variables for each optimization run

Run	Number of Iterations	F(x)	F-Count	Max. Constraint	By-Pass Ratio ( $\alpha$ )	Fan Pressure Ratio ( $\pi_f$ )	High Pressure Compressor Pressure Ratio ( $\pi_{cH}$ )	Mass Flow Rate ( $m_0$ ) [kg/s]
1	3	-0.0916	36	0.002	3.6688	4.2745	5.1825	36.2874
2	2	-0.1323	27	0.0017	3.4128	4.3454	7.4444	36.4588
3	2	-0.1479	27	8.65E-04	3.2613	4.419	8.956	36.4588
4	2	-0.1416	27	1.93E-04	3.0893	4.5095	9.0803	36.4588

The respective Engine Design Model outputs are calculated as given in Table 26 for each optimization run.

**Table 26** The results obtained at each run

Run	ON-DESIGN CONSTRAINTS			OFF-DESIGN CONSTRAINTS		TURBOMACHINERY CONSTRAINTS							
	$F/m_0$	TSFC	$\eta_o$	$F/m_0$	TSFC	LPC Stage #	HPC Stage #	Fan B.H. (cm)	HPC B.H. (cm)	HPT B.H. (cm)	LPT B.H. (cm)	$N_1$ wheel speed (m/s)	$N_2$ wheel speed (m/s)
1	320.6	0.084	11.60%	245.1	0.089	6	6	16.792	2.256	2.507	8.049	268.1	306.9
2	332.8	0.080	11.70%	322.4	0.089	6	7	14.679	1.941	2.253	6.993	278.7	363.0
3	337.7	0.078	11.90%	322.7	0.084	6	7	14.869	2.931	2.098	6.995	289.0	352.0
4	347.1	0.079	13.40%	371.7	0.082	6	7	16.101	5.471	0.734	6.441	299.0	94.3

As can be seen from Table 26, Trust Region Reflective algorithm gave the same results obtained with Active Set algorithm therefore differing the gradient descent algorithm did not changed the results.

The last optimization runs are made with SIMPLEX algorithm. . The design variables calculated for the three runs with SIMPLEX is given in Table 27, and the changes made by the optimization algorithm on the design variables for each optimization iteration is shown graphically in Appendix B. (Figure B3)

**Table 27** The changes in design variables for each optimization run

Run	Number of Iterations	F(x)	F-Count	By-Pass Ratio ( $\alpha$ )	Fan Pressure Ratio ( $\pi_f$ )	High Pressure Compressor Pressure Ratio ( $\pi_{cH}$ )	Mass Flow Rate ( $m_0$ ) [kg/s]
1	42	-0.0706	80	3.8055	3.3671	5.24	42.1553
2	56	-0.0993	118	3.2149	4.6871	6.0194	28.4084
3	65	-0.1343	127	3.1268	5.2481	8.5172	28.7315

The respective Engine Design Model outputs are calculated as given in Table 28 for each optimization run.

**Table 28** The results obtained at each run

Run	ON-DESIGN CONSTRAINTS			OFF-DESIGN CONSTRAINTS		TURBOMACHINERY CONSTRAINTS							
	F/ $m_0$	TSFC	$\eta_0$	F/ $m_0$	TSFC	LPC Stage #	HPC Stage #	Fan B.H. (cm)	HPC B.H. (cm)	HPT B.H. (cm)	LPT B.H. (cm)	N <sub>1</sub> wheel speed (m/s)	N <sub>2</sub> wheel speed (m/s)
1	315.0	0.085	11.60%	212.1	0.095	5	6	17.958	2.840	3.147	7.887	259.5	296.9
2	344.7	0.083	11.70%	394.2	0.099	6	6	13.208	2.012	2.159	5.979	318.2	359.1
3	334.5	0.079	11.90%	376.5	0.098	6	7	15.469	1.857	1.786	6.787	434.6	390.1

As can be seen from Table 27, the results obtained with SIMPLEX for Case 1 used lower Mass Flow Rates than the given lower limit. This is because of the fact that SIMPLEX is an unconstrained optimization algorithm and may use design parameter values out of the given ranges. Although the results of second and third runs given in Table 28 have higher specific thrust values both in on-design and off-design, they are not satisfactory since they are obtained with lower mass flow rates. Therefore the results obtained in the first run can be taken as the closest estimation of SIMPLEX to the optimum result.

When the results from different optimization algorithms are compared, Gradient Descent algorithms found higher thrust and lower thrust specific fuel consumptions with higher number of stages at Low and High Pressure Compressors., whereas SIMPLEX found lower thrust and higher thrust specific fuel consumptions with lower number of stages at

Low and High Pressure Compressors. A comparison with  $f(x)$  values given in Tables 23, 25 and 27 indicates that Gradient Descent algorithms found more optimum solution (lower the  $f(x)$ , closer to the optimum [31]).

#### 5.4.2 Results of Case 2

The design variables calculated for the four runs with Gradient Descent Active Set algorithm is given in Table 29, and the changes made by the optimization algorithm on the design variables for each optimization iteration is shown graphically in Appendix B. (Figure B4)

**Table 29** The changes in design variables for each optimization run

Run	Number of Iterations	F(x)	F-Count	Max. Constraint	By-Pass Ratio ( $\alpha$ )	Fan Pressure Ratio ( $\pi_f$ )	High Pressure Compressor Pressure Ratio ( $\pi_{ch}$ )	Mass Flow Rate ( $m_0$ ) [kg/s]
1	12	-0.1277	146	0.00010663	3.2647	4.483	7.533	59.238528
2	2	-0.132	27	2.45E-04	3.4138	4.294	7.568	59.514403
3	2	-0.1403	27	2.75E-04	3.3507	4.2482	8.3376	64.287238
4	3	-0.1461	38	1.08E-04	3.2795	4.2378	9.0391	68.375648

The respective Engine Design Model outputs are calculated as given in Table 30 for each optimization run.

**Table 30** The results obtained at each run

Run	ON-DESIGN CONSTRAINTS			OFF-DESIGN CONSTRAINTS		TURBOMACHINERY CONSTRAINTS							
	$F/m_0$	TSFC	$\eta_o$	$F/m_0$	TSFC	LPC Stage #	HPC Stage #	Fan B.H. (cm)	HPC B.H. (cm)	HPT B.H. (cm)	LPT B.H. (cm)	$N_1$ wheel speed (m/s)	$N_2$ wheel speed (m/s)
1	340.4	0.080	11.60%	327.0	0.084	6	6	20.526	2.477	2.865	8.821	299.0	370.0
2	332.9	0.080	11.70%	331.3	0.083	6	7	21.628	2.488	2.875	8.428	268.1	368.2
3	335.4	0.079	11.90%	311.5	0.083	6	7	22.476	2.847	2.898	8.479	268.1	382.5
4	338.3	0.078	13.40%	334.9	0.082	6	7	23.180	4.346	2.913	8.557	268.1	342.9

The small changes in the results from second run to fourth run indicates that the results found in the fourth run is very close to the optimum point. The iterations are stopped

after the fourth run because of having very low  $f(x)$  value change, which indicates a close estimation to the optimum solution. Therefore the results obtained in the fourth iteration are the closest results to the optimum for Case 2.

Another set of optimization runs are made with Gradient Descent Trust Region Reflective Algorithm. The design variables calculated for the four runs with this algorithm is given in Table 31, and the changes made by the optimization algorithm on the design variables for each optimization iteration is shown graphically in Appendix B. (Figure B5)

**Table 31** The changes in design variables for each optimization run

Run	Number of Iterations	F(x)	F-Count	Max. Constraint	By-Pass Ratio ( $\alpha$ )	Fan Pressure Ratio ( $\pi_f$ )	High Pressure Compressor Pressure Ratio ( $\pi_{cH}$ )	Mass Flow Rate ( $m_0$ ) [kg/s]
1	12	-0.1277	146	0.00010663	3.2647	4.483	7.533	59.238528
2	2	-0.132	27	2.45E-04	3.4138	4.294	7.568	59.514403
3	2	-0.1403	27	2.75E-04	3.3507	4.2482	8.3376	64.287238
4	3	-0.1461	38	1.08E-04	3.2795	4.2378	9.0391	68.375648

The respective Engine Design Model outputs are calculated as given in Table 32 for each optimization run.

**Table 32** The results obtained at each run

Run	ON-DESIGN CONSTRAINTS			OFF-DESIGN CONSTRAINTS		TURBOMACHINERY CONSTRAINTS							
	$F/m_0$	TSFC	$\eta_o$	$F/m_0$	TSFC	LPC Stage #	HPC Stage #	Fan B.H. (cm)	HPC B.H. (cm)	HPT B.H. (cm)	LPT B.H. (cm)	$N_1$ wheel speed (m/s)	$N_2$ wheel speed (m/s)
1	340.4	0.080	11.60%	327.0	0.084	6	7	20.526	2.477	2.865	8.821	299.0	370.0
2	332.9	0.080	11.70%	331.3	0.083	6	7	21.628	2.488	2.875	8.428	268.1	368.2
3	335.4	0.079	11.90%	311.5	0.083	6	7	22.476	2.847	2.898	8.479	268.1	382.5
4	338.3	0.078	13.40%	334.9	0.082	6	7	23.180	4.346	2.913	8.557	268.1	342.9

As can be seen from Table 32, Trust Region Reflective algorithm gave the same results obtained with Active Set algorithm therefore differing the gradient descent algorithm type did not changed the results.

The third optimization runs are made with SIMPLEX algorithm. . The design variables calculated for the three runs with SIMPLEX is given in Table 33, and the changes made by the optimization algorithm on the design variables for each optimization iteration is shown graphically in Appendix B. (Figure B6)

**Table 33** The changes in design variables for each optimization run

Run	Number of Iterations	F(x)	F-Count	By-Pass Ratio ( $\alpha$ )	Fan Pressure Ratio ( $\pi_f$ )	High Pressure Compressor Pressure Ratio ( $\pi_{ch}$ )	Mass Flow Rate ( $m_0$ ) [kg/s]
1	69	-0.0874	129	3.643	3.7083	5.6197	40.118975
2	47	-0.096	91	3.6848	3.7077	5.8753	43.755561
3	29	-0.1035	69	3.6079	3.912	6.0726	44.422206

The respective Engine Design Model outputs are calculated as given in Table 34 for each optimization run.

**Table 34** The results obtained at each run

Run	ON-DESIGN CONSTRAINTS			OFF-DESIGN CONSTRAINTS		TURBOMACHINERY CONSTRAINTS							
	$F/m_0$	TSFC	$\eta_o$	$F/m_0$	TSFC	LPC Stage #	HPC Stage #	Fan B.H. (cm)	HPC B.H. (cm)	HPT B.H. (cm)	LPT B.H. (cm)	$N_1$ wheel speed (m/s)	$N_2$ wheel speed (m/s)
1	324.7	0.084	11.60%	303.2	0.072	5	6	14.986	2.445	2.761	8.679	324.6	330.1
2	322.7	0.083	11.70%	332.2	0.072	5	6	15.651	2.588	2.850	8.110	324.6	342.9
3	326.2	0.082	11.90%	342.8	0.068	5	6	16.416	2.680	2.804	7.874	377.0	350.8

As can be seen from Table 34, the results obtained from second to third run are very close to each other and the change in the  $f(x)$  value is small. This indicates a closer solution to the optimum point is obtained as in the optimization with Gradient Descent. However, the third run resulted in lower  $N_2$  speed than  $N_1$  which is harder to realize in

an actual design. Therefore the results from the second iteration are accepted as the optimum results found by SIMPLEX for Case 2.

When the results from the Gradient Descent and SIMPLEX algorithms are compared, the results of the output parameters are close to each other but SIMPLEX found a solution having lower stage numbers. Therefore the solution found by SIMPLEX algorithm is a better solution for Case 2.

### 5.4.3 Results of Case 3

The design variables calculated for the three runs with Gradient Descent Active Set algorithm is given in Table 35, and the changes made by the optimization algorithm on the design variables for each optimization iteration is shown graphically in Appendix B. (Figure B7)

**Table 35** The changes in design variables for each optimization run

Run	Number of Iterations	F(x)	F-Count	Max. Constraint	By-Pass Ratio ( $\alpha$ )	Fan Pressure Ratio ( $\pi_f$ )	High Pressure Compressor Pressure Ratio ( $\pi_{cH}$ )	Mass Flow Rate ( $m_0$ ) [kg/s]
1	7	-0.127	72	0.000414	3.4731	4.1095	7.294	57.765623
2	4	-0.1318	59	9.75E-04	3.4353	3.9148	7.9841	57.55434
3	3	-0.1334	36	9.74E-05	3.4276	4.0273	7.9551	58.86622

The respective Engine Design Model outputs are calculated as given in Table 36 for each optimization run.

**Table 36** The results obtained at each run

Run	ON-DESIGN CONSTRAINTS			OFF-DESIGN CONSTRAINTS		TURBOMACHINERY CONSTRAINTS							
	F/ $m_0$	TSFC	$\eta_o$	F/ $m_0$	TSFC	LPC Stage #	HPC Stage #	Fan B.H. (cm)	HPC B.H. (cm)	HPT B.H. (cm)	LPT B.H. (cm)	N <sub>1</sub> wheel speed (m/s)	N <sub>2</sub> wheel speed (m/s)
1	331.5	0.080	11.60%	315.0	0.084	5	7	23.721	2.523	2.921	8.740	428.5	353.3
2	333.4	0.080	11.70%	303.6	0.082	5	7	19.530	2.583	2.878	8.725	377.0	375.5
3	333.4	0.080	11.90%	308.5	0.082	5	7	23.345	2.583	2.878	8.799	423.7	376.7

The small changes in the results from second run to third run indicates that the results found in the third run is very close to the optimum point. The iterations are stopped after the third run because of having very low  $f(x)$  value change, which indicates a close estimation to the optimum solution. Therefore the results obtained in the third iteration are the closest results to the optimum for Case 3.

Second set of optimization runs are made with Gradient Descent Trust Region Reflective Algorithm. The design variables calculated for the three runs with this algorithm is given in Table 37, and the changes made by the optimization algorithm on the design variables for each optimization iteration is shown graphically in Appendix B. (Figure B8)

**Table 37** The changes in design variables for each optimization run

Run	Number of Iterations	F(x)	F-Count	Max. Constraint	By-Pass Ratio ( $\alpha$ )	Fan Pressure Ratio ( $\pi_f$ )	High Pressure Compressor Pressure Ratio ( $\pi_{cH}$ )	Mass Flow Rate ( $m_0$ ) [kg/s]
1	7	-0.127	72	0.000414	3.4731	4.1095	7.294	57.765623
2	4	-0.1318	59	9.75E-04	3.4353	3.9148	7.9841	57.55434
3	3	-0.1334	36	9.74E-05	3.4276	4.0273	7.9551	58.86622

The respective Engine Design Model outputs are calculated as given in Table 38 for each optimization run.

**Table 38** The results obtained at each run

Run	ON-DESIGN CONSTRAINTS			OFF-DESIGN CONSTRAINTS		TURBOMACHINERY CONSTRAINTS							
	$F/m_0$	TSFC	$\eta_o$	$F/m_0$	TSFC	LPC Stage #	HPC Stage #	Fan B.H. (cm)	HPC B.H. (cm)	HPT B.H. (cm)	LPT B.H. (cm)	$N_1$ wheel speed (m/s)	$N_2$ wheel speed (m/s)
1	331.5	0.080	11.60%	315.0	0.084	5	7	23.721	2.523	2.921	8.740	428.5	353.3
2	333.4	0.080	11.70%	303.6	0.082	5	7	19.530	2.583	2.878	8.725	377.0	375.5
3	333.4	0.080	11.90%	308.5	0.082	5	7	23.345	2.583	2.878	8.799	423.7	376.7

As can be seen from Table 38, Trust Region Reflective algorithm gave the same results obtained with Active Set algorithm therefore differing the gradient descent algorithm type did not changed the results.

The last optimization runs are made with SIMPLEX algorithm. . The design variables calculated for the three runs with SIMPLEX is given in Table 39, and the changes made by the optimization algorithm on the design variables for each optimization iteration is shown graphically in Appendix B. (Figure B9)

**Table 39** The changes in design variables for each optimization run

Run	Number of Iterations	F(x)	F-Count	By-Pass Ratio ( $\alpha$ )	Fan Pressure Ratio ( $\pi_f$ )	High Pressure Compressor Pressure Ratio ( $\pi_{cH}$ )	Mass Flow Rate ( $m_0$ ) [kg/s]
1	69	-0.0874	129	3.643	3.7083	5.6197	40.118975
2	47	-0.096	91	3.6848	3.7077	5.8753	43.755561
3	29	-0.1035	69	3.6079	3.912	6.0726	44.422206

The respective Engine Design Model outputs are calculated as given in Table 40 for each optimization run.

**Table 40** The results obtained at each run

Run	ON-DESIGN CONSTRAINTS			OFF-DESIGN CONSTRAINTS		TURBOMACHINERY CONSTRAINTS							
	$F/m_0$	TSFC	$\eta_o$	$F/m_0$	TSFC	LPC Stage #	HPC Stage #	Fan B.H. (cm)	HPC B.H. (cm)	HPT B.H. (cm)	LPT B.H. (cm)	$N_1$ wheel speed (m/s)	$N_2$ wheel speed (m/s)
1	324.7	0.084	11.60%	303.2	0.072	5	6	14.986	2.445	2.761	8.679	324.6	330.1
2	322.7	0.083	11.70%	332.2	0.072	5	6	15.651	2.588	2.850	8.110	324.6	342.9
3	326.2	0.082	11.90%	342.8	0.068	5	6	16.416	2.680	2.804	7.874	377.0	350.8

As can be seen from a comparison between Tables 34 and 40, SIMPLEX gives the same results with Case 2. This indicates that the solution given by SIMPLEX is no longer affected by the active set of constraints and the iterations stopped after the third iteration as for Case 2 due to having same results with Case 2 and obtaining small differences in



$f(x)$  values at respective iterations. With the same reasoning with Case 2, the solution obtained at the second run will be taken as the optimum solution for Case 3.

When the results from the optimum solutions provided by using Gradient Descent and SIMPLEX algorithms are compared, all of the output constraint results are very close to each other. However, SIMPLEX found a solution with lower number of High Pressure Compressor stages and lower wheel speed value at  $N_1$  than  $N_2$  spool which is a better and more applicable design suggestion. Therefore the results from the second iteration of SIMPLEX can be said as the optimum solution for Case 3.

#### 5.4.4 Results of Case 4

The design variables calculated for the three runs with Gradient Descent Active Set algorithm is given in Table 41, and the changes made by the optimization algorithm on the design variables for each optimization iteration is shown graphically in Appendix B. (Figure B10)

**Table 41** The changes in design variables for each optimization run

Run	Number of Iterations	F(x)	F-Count	Max. Constraint	By-Pass Ratio ( $\alpha$ )	Fan Pressure Ratio ( $\pi_f$ )	High Pressure Compressor Pressure Ratio ( $\pi_{cH}$ )	Mass Flow Rate ( $m_0$ ) [kg/s]
1	10	-0.1178	101	3.1943E-04	3.5235	4.2045	6.6115	52.317843
2	4	-0.131	59	5.53E-04	3.4455	4.0657	7.679	57.505443
3	5	-0.132	96	1.93E-04	3.435	4.0937	7.7382	58.277774

The respective Engine Design Model outputs are calculated as given in Table 42 for each optimization run.

**Table 42** The results obtained at each run

Run	ON-DESIGN CONSTRAINTS			OFF-DESIGN CONSTRAINTS		TURBOMACHINERY CONSTRAINTS							
	$F/m_0$	TSFC	$\eta_o$	$F/m_0$	TSFC	LPC Stage #	HPC Stage #	Fan B.H. (cm)	HPC B.H. (cm)	HPT B.H. (cm)	LPT B.H. (cm)	$N_1$ wheel speed (m/s)	$N_2$ wheel speed (m/s)
1	328.9	0.081	11.60%	396.9	0.063	6	6	20.251	4.397	2.855	7.996	257.2	316.4
2	332.8	0.080	11.70%	295.4	0.084	5	7	23.076	2.510	2.870	8.776	423.7	370.0
3	333.0	0.080	11.90%	307.5	0.083	5	7	23.231	2.511	2.875	8.694	423.7	370.9

The small changes in the results from second run to third run indicates that the results found in the third run is very close to the optimum point. The iterations are stopped after the third run because of having very low  $f(x)$  value change, which indicates a close estimation to the optimum solution. However, even if the second and the third run solutions are closer to the optimal value, the wheel speeds at Low Pressure Spool are higher than the High Pressure Spool which is an unwanted design condition. Therefore the result from the first run will be taken as the solution suggested by Gradient Descent Active Set algorithm for Case 4.

The next set of optimization runs are made with Gradient Descent Trust Region Reflective Algorithm. The design variables calculated for the three runs with this algorithm is given in Table 43, and the changes made by the optimization algorithm on the design variables for each optimization iteration is shown graphically in Appendix B. (Figure B11)

**Table 43** The changes in design variables for each optimization run

Run	Number of Iterations	F(x)	F-Count	Max. Constraint	By-Pass Ratio ( $\alpha$ )	Fan Pressure Ratio ( $\pi_f$ )	High Pressure Compressor Pressure Ratio ( $\pi_{cH}$ )	Mass Flow Rate ( $m_0$ ) [kg/s]
1	10	-0.1178	101	3.1943E-04	3.5235	4.2045	6.6115	52.317843
2	4	-0.131	59	5.53E-04	3.4455	4.0657	7.679	57.505443
3	2	-0.1333	27	4.50E-04	3.4241	4.1007	7.8423	59.028152

The respective Engine Design Model outputs are calculated as given in Table 44 for each optimization run.

**Table 44** The results obtained at each run

Run	ON-DESIGN CONSTRAINTS			OFF-DESIGN CONSTRAINTS		TURBOMACHINERY CONSTRAINTS							
	$F/m_0$	TSFC	$\eta_o$	$F/m_0$	TSFC	LPC Stage #	HPC Stage #	Fan B.H. (cm)	HPC B.H. (cm)	HPT B.H. (cm)	LPT B.H. (cm)	N <sub>1</sub> wheel speed (m/s)	N <sub>2</sub> wheel speed (m/s)
1	328.9	0.081	11.60%	396.9	0.063	6	6	20.251	4.397	2.855	7.996	257.2	316.4
2	332.8	0.080	11.70%	295.4	0.084	5	7	23.076	2.510	2.870	8.776	423.7	370.0
3	333.4	0.080	11.90%	310.1	0.083	5	7	23.381	2.543	2.878	8.656	423.7	374.6

As can be seen from Table 44, Trust Region Reflective algorithm gave the same results obtained with Active Set algorithm except for the last run. However, this result is an inapplicable result due to the same reasoning made for Active Set for wheel speeds. Therefore the result from the first run will be taken as the solution as in Active Set for Case 4.

The third optimization runs are made with SIMPLEX algorithm. . The design variables calculated for the three runs with SIMPLEX is given in Table 45, and the changes made by the optimization algorithm on the design variables for each optimization iteration is shown graphically in Appendix B. (Figure B12)

**Table 45** The changes in design variables for each optimization run

Run	Number of Iterations	F(x)	F-Count	By-Pass Ratio ( $\alpha$ )	Fan Pressure Ratio ( $\pi_f$ )	High Pressure Compressor Pressure Ratio ( $\pi_{ch}$ )	Mass Flow Rate ( $m_0$ ) [kg/s]
1	69	-0.0874	129	3.643	3.7083	5.6197	40.118975
2	47	-0.096	91	3.6848	3.7077	5.8753	43.755561
3	29	-0.1035	69	3.6079	3.912	6.0726	44.422206

The respective Engine Design Model outputs are calculated as given in Table 40 for each optimization run.

**Table 46** The results obtained at each run

Run	ON-DESIGN CONSTRAINTS			OFF-DESIGN CONSTRAINTS		TURBOMACHINERY CONSTRAINTS							
	$F/m_0$	TSFC	$\eta_o$	$F/m_0$	TSFC	LPC Stage #	HPC Stage #	Fan B.H. (cm)	HPC B.H. (cm)	HPT B.H. (cm)	LPT B.H. (cm)	$N_1$ wheel speed (m/s)	$N_2$ wheel speed (m/s)
1	324.7	0.084	11.60%	303.2	0.072	5	6	14.986	2.445	2.761	8.679	324.6	330.1
2	322.7	0.083	11.70%	332.2	0.072	5	6	15.651	2.588	2.850	8.110	324.6	342.9
3	326.2	0.082	11.90%	342.8	0.068	5	6	16.416	2.680	2.804	7.874	377.0	350.8

As can be seen from a comparison between Tables 34, 40 and 46, SIMPLEX gives the same results with Case 2 and 3. This indicates that the solution given by SIMPLEX is no longer affected by the active set of constraints and the iterations stopped after the third iteration. With the same reasoning with Case 2 or 3, the solution obtained at the second run will be taken as the optimum solution for Case 4.

When the results produced by Gradient Descent and SIMPLEX algorithms are compared, the solutions found by Gradient Descent have higher specific thrust, lower thrust specific fuel consumption and higher efficiency in on-design outputs. The same situation is also valid for the off-design outputs. The solution found by SIMPLEX has lower number of stages at the Low Pressure Compressor but it has higher wheel speeds which may cause more complex flow field and structural design when compared to the design found by Gradient Descent having lower wheel speeds at both spools. The only drawback of the solution from Gradient Descent is one additional Low Pressure Compressor stage but other advantages of this solution compensates this situation and results from the first iteration of Gradient Descent can be said as the optimum solution for Case 4.

## CHAPTER 6

### CONCLUSION AND FUTURE WORK

The Aerothermodynamic Design of an Engine is the first step in the Engine Design process of a real engine. It includes Parametric and Performance cycle analyses and turbomachinery design subsections. The results obtained from this analysis are then used in structural and aerodynamic design of the engine components.

In order to perform the cycle and turbomachinery design calculations a design tool named “Engine Design Model” is developed according to the cycle design theory in [3] with Variable Specific Heat Model and a turbomachinery design algorithm, which uses the results of the cycle calculations, is developed for the calculations of the aerothermodynamic component design. MATLAB Simulink is chosen as the development platform because of its high integrity with optimization methods and advantages of evading from possible difficulties in programming.

The verification of Engine Design Model (EDM) is carried out with two different types of tests for cycle calculations which are case specific tests and continuity tests. In the first test type, selected output parameters from EDM are compared with the relevant output parameters obtained by AEDsys Software. In the second type of tests, the change in the outputs of EDM with respect to chosen input parameters are compared with the AEDsys Software. For the turbomachinery design calculations, the validations are carried out with real engine component data obtained for CFM 56-5A and GE90-94B engines.

Optimization methods can be used to find the most feasible value in a solution set determined by the constraints. Such methods use several algorithms which determine the

inputs of the mathematical model and modify them according to the aloofness of the outputs to the optimum point. In order to find such a design point, an optimization study which is using EDM as the mathematical model is accomplished by using MATLAB Simulink Response Optimization tool. Four different cases formed with different active set of constraints on on-design, off-design and turbomachinery design outputs. Gradient Descent and SIMPLEX algorithms are used in the study. It is found out that the mathematical optimum is not always being the best applicable solution and the results from an optimization study in engine design should be investigated whether it is physically reasonable or not. With the existence of a turbomachinery design model together with the cycle calculations in EDM, this reasoning can be made easily.

The flexibility of the EDM to add different calculation blocks or to modify the loop structures provides the ability to model different engine configurations and even to model different thermodynamic cycles. By using this feature and its integrity with the Optimization Toolbox of MATLAB, new trends in engine design can be used and investigated with EDM. The turbomachinery design section can be modified with different swirl distribution models and the effects of thermal and torsional stresses may also be added to increase the effect of structural design parameters on turbomachinery design.

## BIBLIOGRAPHY

1. Mattingly Jack D. (2006), "Elements of Propulsion: Gas Turbines and Rockets / Jack D. Mattingly foreword by Hans von Ohain", American Institute of Aeronautics and Astronautics Inc., Reston, Virginia, USA
2. Bräunling W.J.G. (2009), "Flugzeugtriebwerke: Grundlagen, Aero-Thermodynamik, ideale und reale Kreisprozesse, Thermische-Turbomaschinen, Komponenten, Emissionen und Systeme", Springer, Hamburg, Germany
3. Mattingly Jack D., Heiser William H., and Pratt David T. (2002), "Aircraft Engine Design Second Edition", American Institute of Aeronautics and Astronautics Inc., Reston, Virginia, USA
4. Kyohei Horibe, Kawahira Kouji, Sakai Jun, and Sakaki Junichi (2004), "Development of GE90-115B Engine", IHI Engineering Review, Vol.37, No. 1, pp. 1-8
5. Liew, Ka Heng (2006), "Aerothermodynamic Cycle Analysis of a Dual-Spool, Separate Exhaust Turbofan Engine with an Interstage Turbine Burner", PhD Thesis(Dissertation) in Mechanical Engineering-Engineering Mechanics submitted to Michigan Technological University, USA
6. Mattingly Jack D., Heiser William H., and Pratt David T. (1987), "Aircraft Engine Design", American Institute of Aeronautics and Astronautics Inc., Reston, Virginia, USA
7. Horlock J.H. (1966), "Axial Flow Turbines", Butterworth & Co. (Publishers), Belfast, Ireland
8. Horlock J.H. (1973), "Axial Flow Compressors", Robert E. Krieger Publishing Company, Huntington, New York, USA
9. Korpela Seppo A. (2011), "Principles of Turbomachinery", John Wiley and Sons Inc., Hoboken, New Jersey, USA
10. Dixon Sydney L. and Hall Cesare A. (2010), "Fluid Mechanics and Thermodynamics of Turbomachinery Sixth Edition", Elsevier Inc., USA
11. Oates G.C. (1997), "The Aerothermodynamics of Gas Turbine and Rocket Propulsion", 3<sup>rd</sup> Ed., AIAA Education Series, AIAA, Reston, Virginia, USA
12. Guha Abhijit (2001), "An Efficient Generic Method for Calculating the Properties of Combustion Products", IMechE, Proc. Inst. of Mechanical Engineers, Vol. 215, Part A, pp.375-387
13. Moran Michael J., Shapiro Howard N. (2006), "Fundamentals of Engineering Thermodynamics 5<sup>th</sup> Edition", John Wiley and Sons Inc., East Lothian, United Kingdom

14. Göre S., (1994), "Conceptual Overall Rotating Turbomachinery Design of a Medium By-Pass Ratio, Separated Flow, Nonafterburning, Fixed Nozzle Turbofan Engine Vol. 1", Aircraft Engine Design Term Project, Aerospace Engineering Department, Middle East Technical University
15. Cumpsty Nicholas A. (2004), "Compressor Aerodynamics", 2<sup>nd</sup> Revised Edition, Krieger Publishing Company
16. Kacker S.C., Okapuu U. (1982), "A Mean Line Prediction Method for Axial Turbines", Journal for Engineering for Power, 104(1), ASME, pp.111-119
17. Cengel Yunus A., Boles Michael A. (2002), "Thermodynamics: An Engineering Approach", Mc Graw Hill, Boston, pp.91-93
18. Cantwell Brian J., (2010), "GE90- An Introduction", AA283 Aircraft and Rocket Propulsion Course Material, Department of Aeronautics and Astronautics, Stanford University
19. Lufthansa Technical Training GmbH, (1999), "Training Manual A319/A320/A321 ATA 71-80 Engine CFM56-5A", Lufthansa Base Frankfurt, Germany (retrieved from [http://atconsortium-indonesia.com/wp-content/uploads/2012/06/Airbus\\_A320\\_CFM56-Wartungs-Manual\\_71-80-30-20-CFM56-5A-L3-e.pdf](http://atconsortium-indonesia.com/wp-content/uploads/2012/06/Airbus_A320_CFM56-Wartungs-Manual_71-80-30-20-CFM56-5A-L3-e.pdf) )
20. European Aviation Safety Agency (2004), "Engine Type Certificate Data Sheet EASA.IM.E.002, GE Aircraft Engines, GE90 Series Engines", Issue 2
21. Lironi Paolo (2010), "The Engine Yearbook 2010", UBM Aviation Publications Inc., United Kingdom, pp. 20-27
22. Oates Gordon C. (1985), "Aerothermodynamics of Aircraft Engine Components", Second Printing, American Institute of Aeronautics and Astronautics Inc., New York, USA
23. Snyman, Jan A. (2005), "Practical Mathematical Optimization: An Introduction to Basic Optimization Theory and Classical and New Gradient Based Algorithms", Applied Optimization, Vol. 97, Springer Science + Business Media Inc., USA
24. Dechter, Rina (2003), "Constrained Processing", Morgan Kaufmann, ISBN 1-55860-890-7
25. Künzi H.P., Tzschach H.G., and Zehnder C.A., (1968), "Numerical Methods of Mathematical Optimization with ALGOL and FORTRAN Programs", Ed. Werner Rheinboldt, Academic Press Inc., London, pp. 84-154
26. Öksüz Ö., (2007), "Multiploid Genetic Algorithms for Multi-Objective Turbine Blade Aerodynamic Optimization", Doctor of Philosophy Thesis, Aerospace Engineering Department, Middle East Technical University
27. Rifai, Hicham (2005), "Turbojet Engine Performance Modelling Using Multi-Objective Optimization Algorithms", Master's Thesis, Department of Mathematics, Chalmers University of Technology Göteborg University, Sweden



28. Berton Jeffrey J., and Guynn Mark D. (2010), "Multi-Objective Optimization of Turbofan Design Parameters for an Advanced, Single Aisle Transport", 10th AIAA Aviation Technology, Integration, and Operations (ATIO) Conference, AIAA 2010-9168
29. "Choosing a Solver- MATLAB & Simulink" , < <http://www.mathworks.com/help/optim/ug/choosing-a-solver.html#bsbqd7i>> , retrieved on 19.12.2013
30. Geletu Abebe, (2007), "Solving Optimization Problems using the MATLAB Optimization Toolbox- a Tutorial", Technische Universität Ilmenau, Fakultät für Mathematik und Naturwissenschaften, retrieved on 19.12.2013 from <<http://www.tu-ilmenau.de/simulation/mitarbeiter/dr-rer-nat-abebe-geletu-w-selassie/>>
31. "When the Solver might have succeeded-MATLAB & Simulink", < <http://www.mathworks.com/help/optim/ug/when-the-solver-might-have-succeeded.html>>, retrieved on 20.12.2013



# APPENDICES

## APPENDIX A

### EXAMPLE INPUT FILE FOR EDM

An example input file is given below for the Engine Design Model for the CFM-56/5A Engine case. (All inputs are in BE Units)

```
%Parametric Cycle Inputs
%Flight Conditions
M0=0.8; %Mach Number
P0=3.8434; %Ambient Pressure (psia)
T0=401.85; %Ambient Temperature (R)

CTOL=0.0;
CTOH=0.005;

%Fuel Properties
hPR=18400; %Fuel Heating Value (Btu/lbm)
%Bleed Air and Coolant Air Ratios
BETA=0.03;
EPS1=0.05;
EPS2=0.05;

%Pressure Ratios
PI_B=0.95;
PI_Dmax=0.99;
PI_n=0.99;
PI_F=1.55;
PI_nF=0.99;
PI_cL=PI_F;
PI_c=26.5;
PI_cH=PI_c/PI_cL;

%Polytropic Efficiencies
e_f=0.93;
e_cL=0.91;
e_cH=0.91;
e_tH=0.93;
e_tL=0.93;

%Component Efficiencies
n_b=0.99;
```

```

n_mL=0.99;
n_mH=0.99;
n_mPL=1.0;
n_mPH=0.99;

%Others
ALFA=6;
Tt4=2768.7; % (R)

m0dot=938.904; % (lbm/s)

%%
%PerformanceCycleInputs
%Flight Conditions
M0p=0.4;
T0p=518.69; %Ambient Temperature (R)
P0p=14.696; %Ambient Pressure (psia)
PTOL=0;
PTOH=133.8; % (kW)
CTOLp=0.0;
CTOHP=0.005;

%Fuel Properties

hPRp=18400; %Fuel Heating Value (Btu/lbm)

%Bleed Air and Coolant Air Ratios
BETAp=0.03;
EPS1p=0.05;
EPS2p=0.05;

%Pressure Ratios
PI_dmaxp=0.99;
PI_bp=0.95;
PI_np=0.99;
PI_nfp=0.99;

%Component Efficiencies

n_fp=0.9252;
n_cLp=0.9039;
n_cHp=0.8721;
n_tHp=0.9407;
n_tLp=0.9438;
n_bp=0.99;
n_mLp=0.99;
n_mHp=0.99;

```

```

n_mPLp=1.00;
n_mPHp=0.99;

%Limiting Condition

Tt4p=2866; %(R)
PI_cMAXp=30;
%%
%%Component Sizing Inputs
R0_HPC=8.5; %density of High Pressure Compressor Blade
[slug/ft^2]
R0C=8.5; %density of Low Pressure Compressor Blade
[slug/ft^2]
SIGMAC_HPC=55000; %Stress Coefficient of High Pressure
Compressor Blade [psi]
SIGMAC_F=55000; %Stress Coefficient of Low Pressure
Compressor Blade [psi]
R0_F=8.5; %density of Low Pressure Compressor Blade
[slug/ft^2]

SIGMAD_LP=60000; % Stress Coefficient of Low Pressure
Turbine Disk psi
R0D_LP=16.0; %density of low pressure turbine disk
[slug/ft^2]
SIGMAC_LP=41000; %Stress Coefficient of Low Pressure
Turbine Blade [psi]
R0C_LP=15.0; %density of low pressure turbine blade
[slug/ft^2]
SIGMAD_HP=60000; %Stress Coefficient of High Pressure
Turbine Disk [psi]
R0D_HP=16.0; %density of High Pressure Turbine Disk
[slug/ft^2]
SIGMAC_HP=41000; %Stress Coefficient of High Pressure
Turbine Blade [psi]
R0C_HP=15.0; %density of High Pressure Turbine Blade
[slug/ft^2]

FI_val=0.065; %loss coefficient
D=0.5; %diffusion factor
ES=e_tL; %polytropic efficiency of low pressure turbine
ES1=e_tH-0.05; %polytropic efficiency of high pressure
turbine stage1
ES2=e_tH; %polytropic efficiency of high pressure turbine
stage2

```



## APPENDIX B

### CHANGE OF DESIGN VARIABLES DURING OPTIMIZATION PROCESS BY SIMULINK

#### 1. Case 1

The change of the design variables with the Gradient Descent Active Set algorithm for Case 1 in different runs are given in Figure B1.

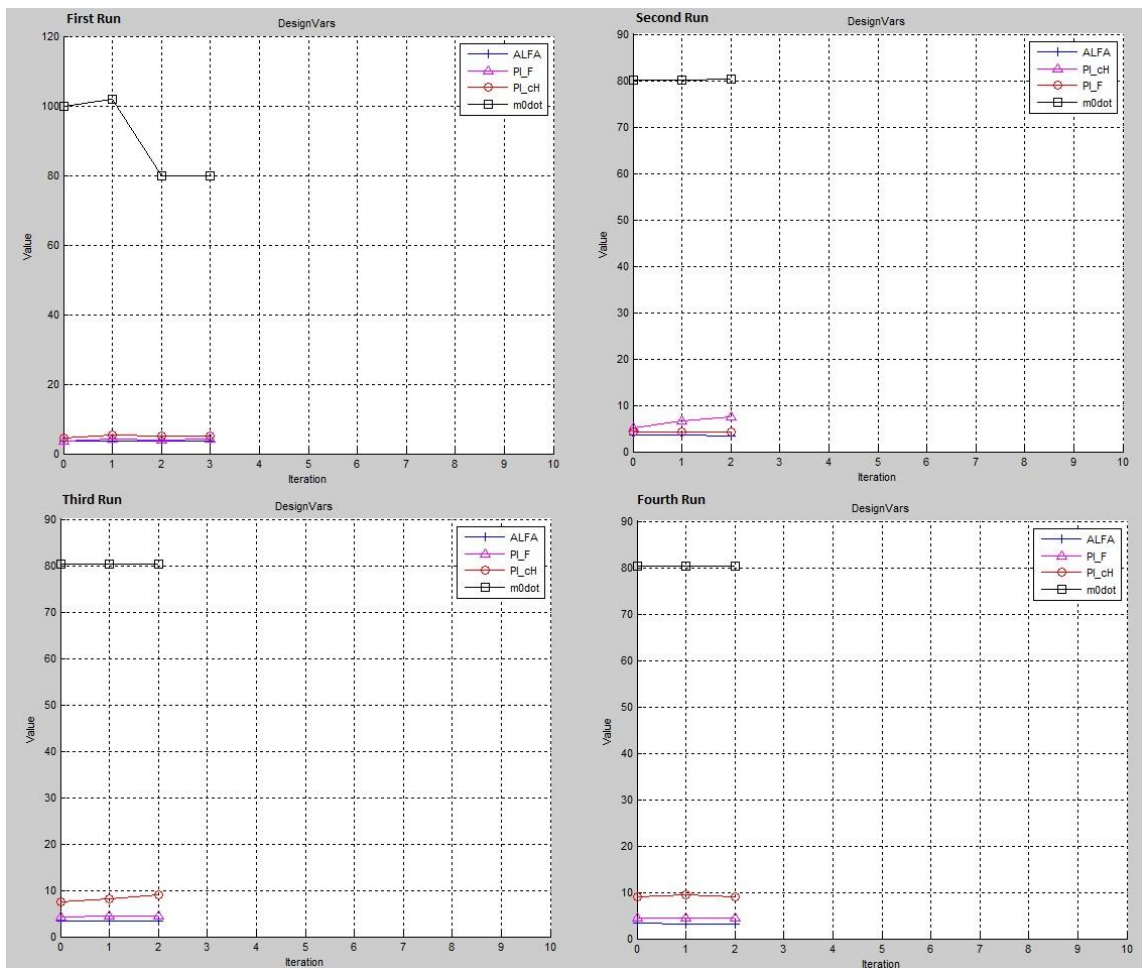


**Figure B 1** The change of design variables with iterations for Case 1 (Gradient Descent Active Set)

The change of the design variables with the Gradient Descent Trust Region Reflective algorithm for Case 1 in different runs are given in Figure B2.

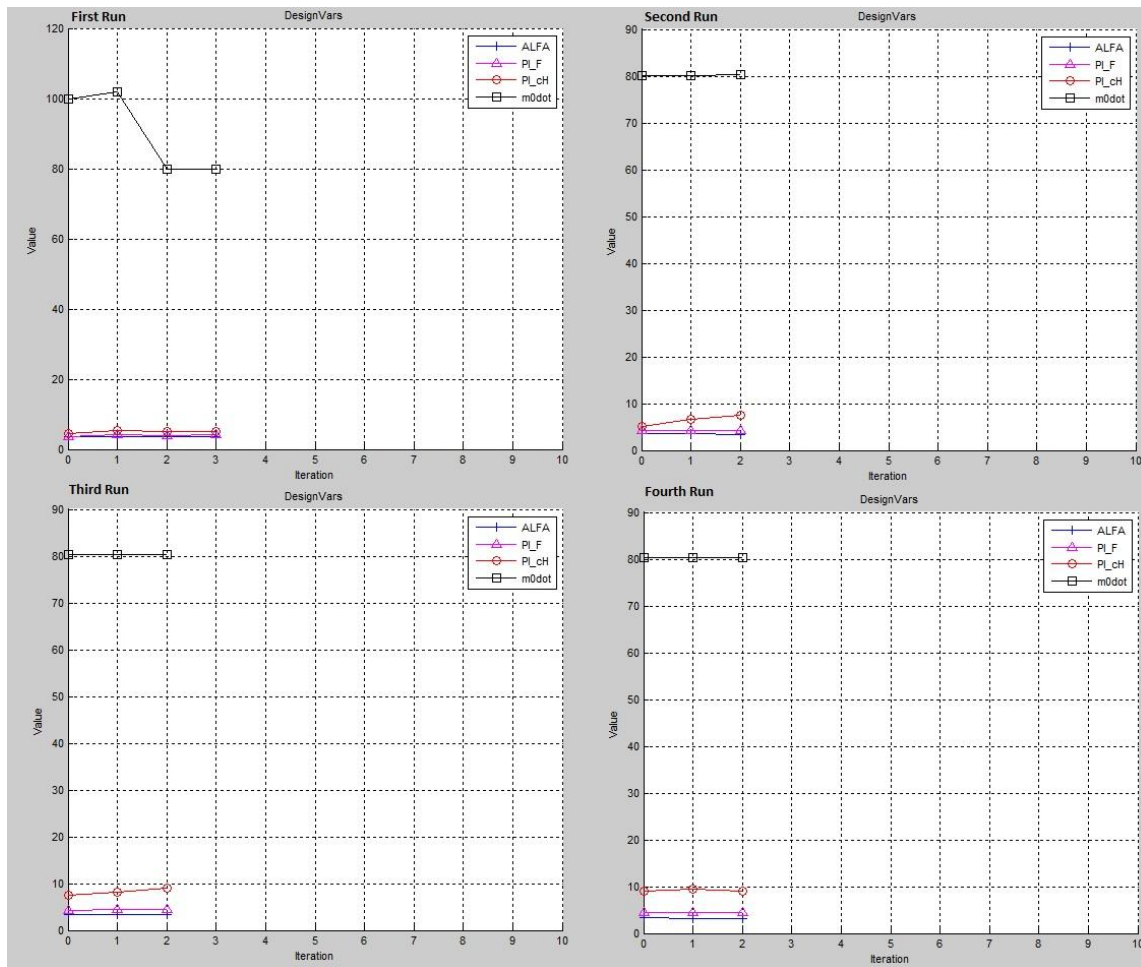


**Figure B 2** The change of design variables with iterations for Case 1 (Gradient Descent Trust Region Reflective)

The change of the design variables with the SIMPLEX algorithm for Case 1 in different runs are given in Figure B3.



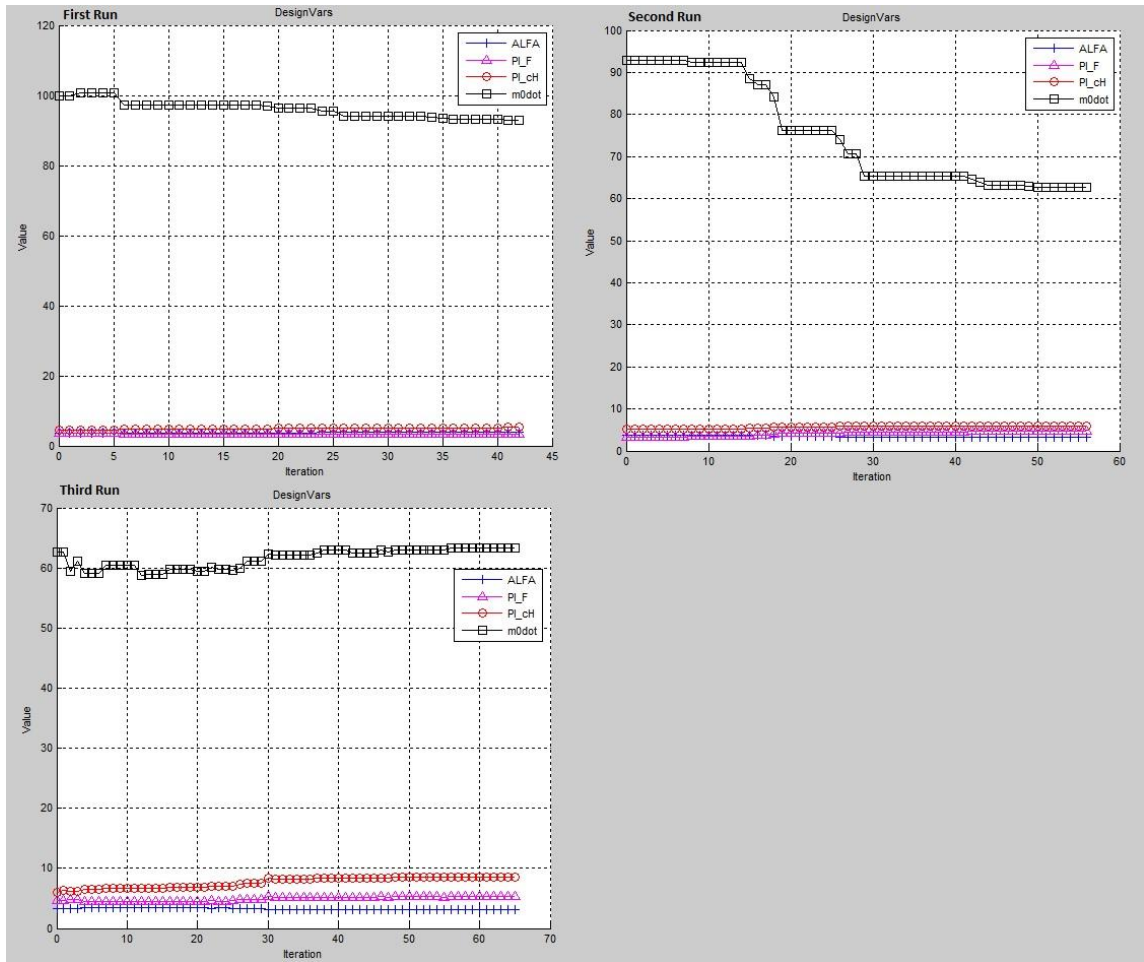


**Figure B 3** The change of design variables with iterations for Case 1 (SIMPLEX)

## 2. Case 2

The change of the design variables with the Gradient Descent Active Set algorithm for Case 1 in different runs are given in Figure B4.

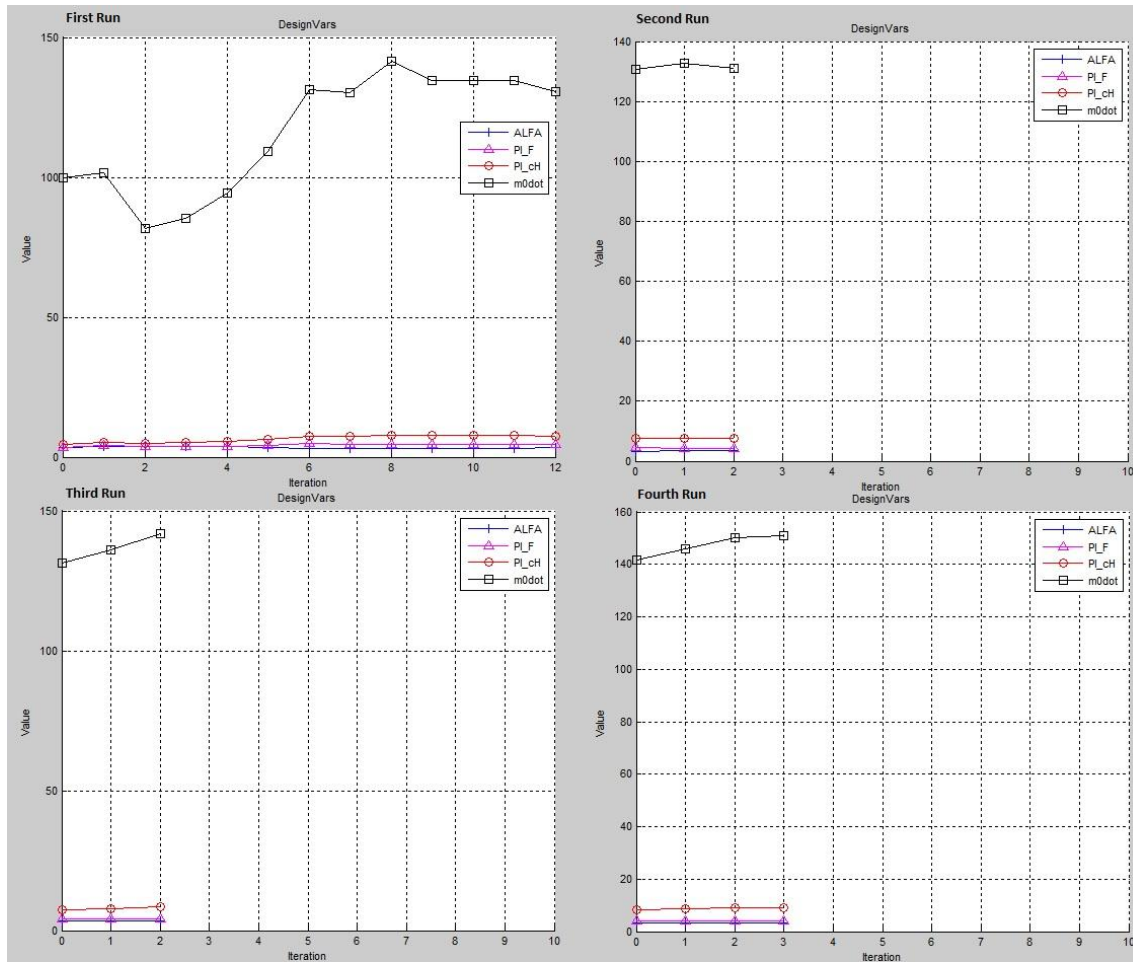


**Figure B 4** The change of design variables with iterations for Case 2 (Gradient Descent Active Set)

The change of the design variables with the Gradient Descent Trust Region Reflective algorithm for Case 1 in different runs are given in Figure B5.

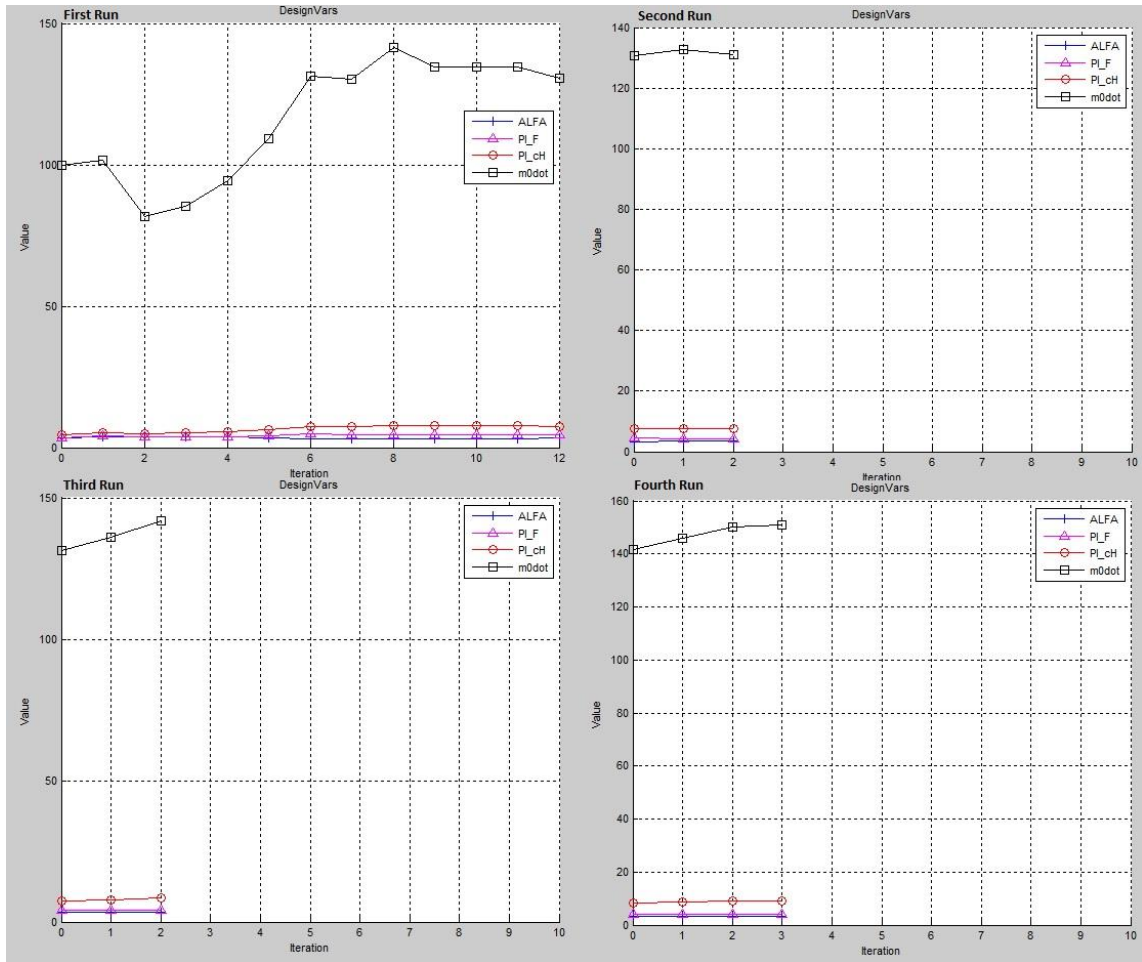


**Figure B 5** The change of design variables with iterations for Case 2 (Gradient Descent Trust Region Reflective)

The change of the design variables with the SIMPLEX algorithm for Case 1 in different runs are given in Figure B6.

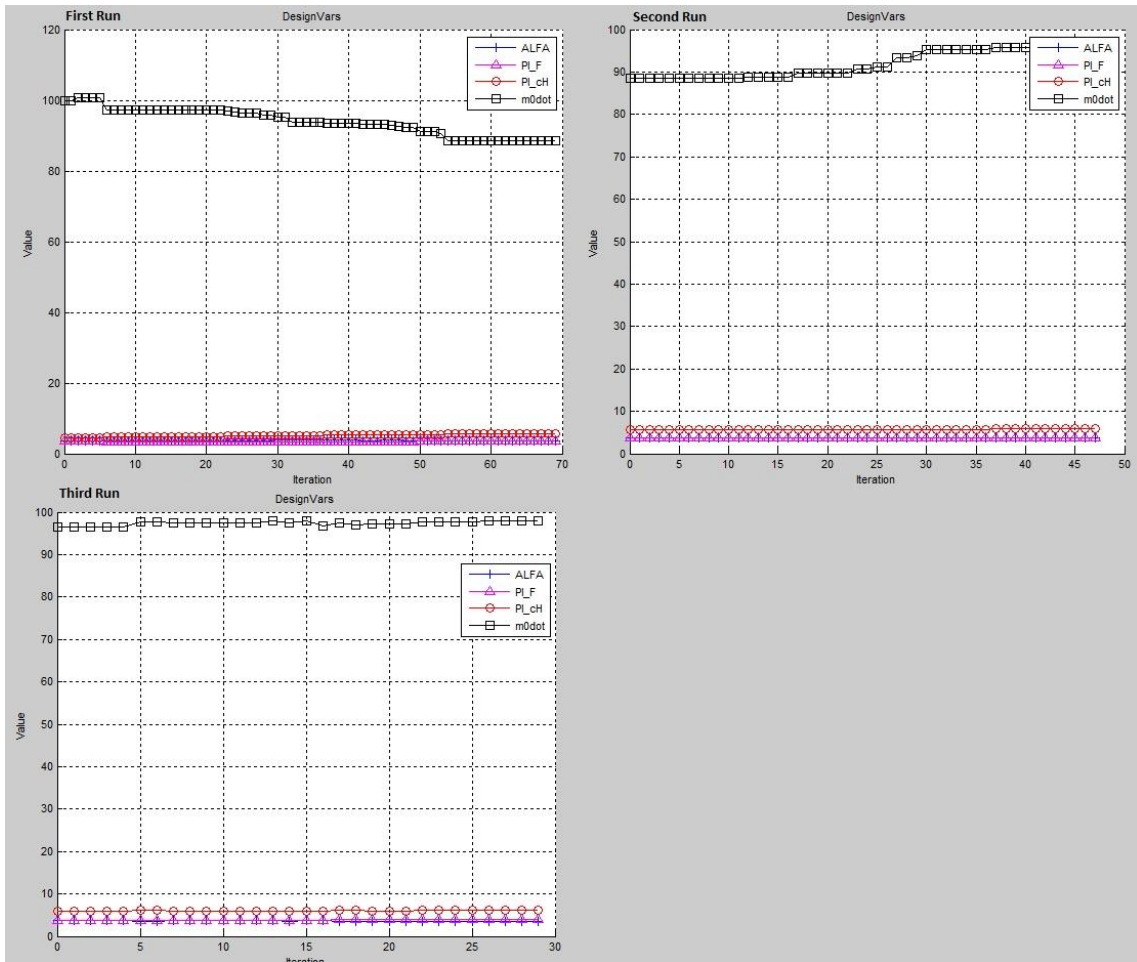


**Figure B 6** The change of design variables with iterations for Case 2 (SIMPLEX)

### 3. Case 3

The change of the design variables with the Gradient Descent Active Set algorithm for Case 1 in different runs are given in Figure B7.

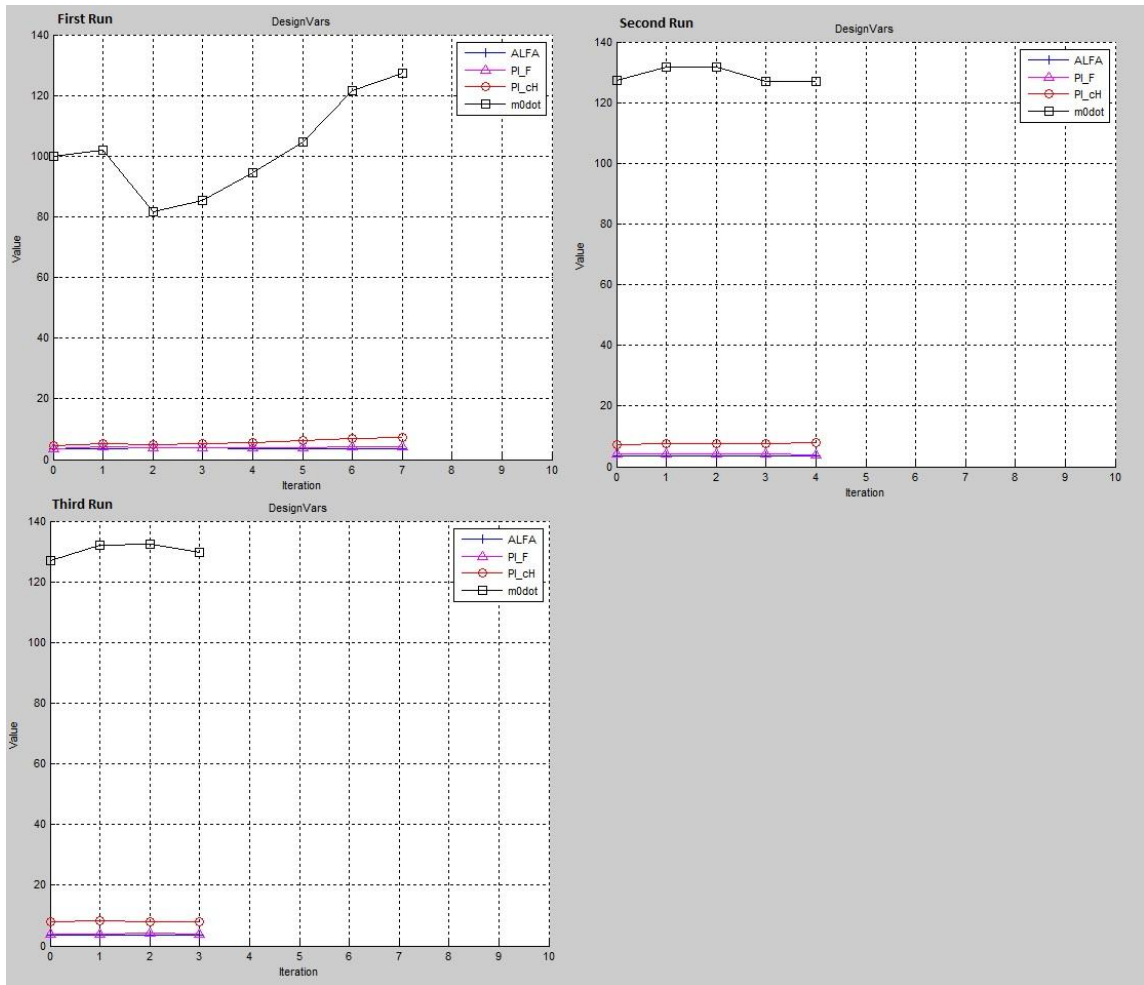


**Figure B 7** The change of design variables with iterations for Case 3 (Gradient Descent Active Set)

The change of the design variables with the Gradient Descent Trust Region Reflective algorithm for Case 1 in different runs are given in Figure B8.

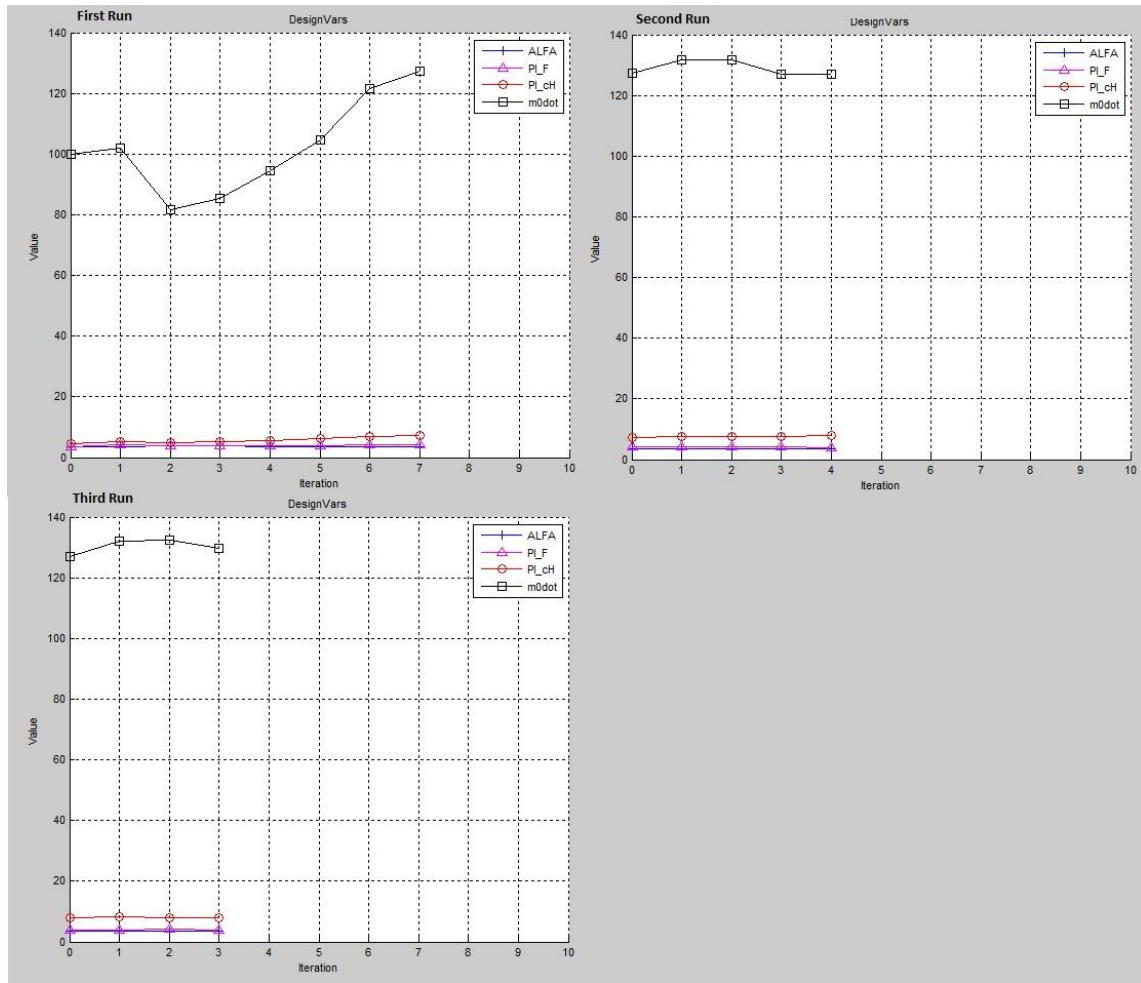


**Figure B 8** The change of design variables with iterations for Case 3 (Gradient Descent Trust Region Reflective)

The change of the design variables with the SIMPLEX algorithm for Case 1 in different runs are given in Figure B9.

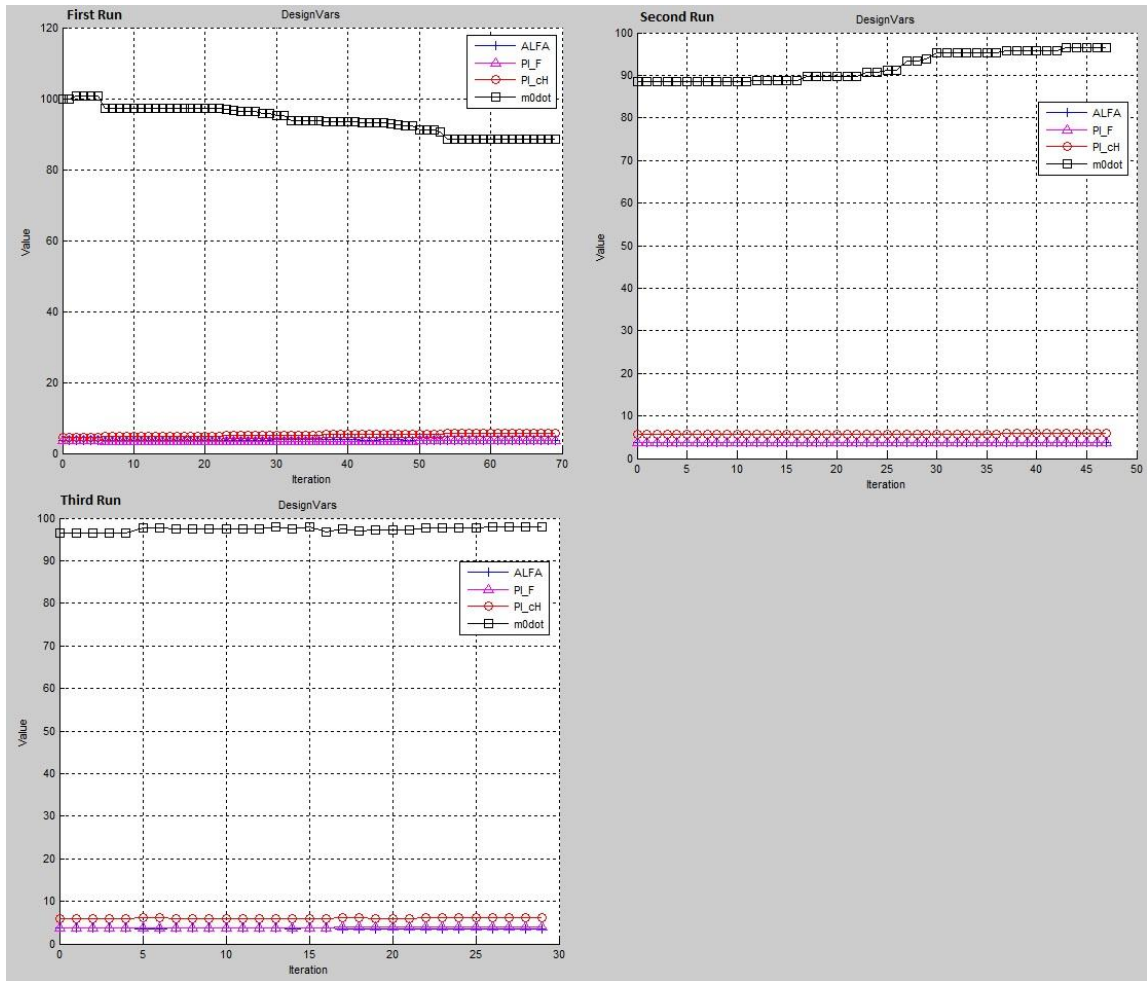


**Figure B 9** The change of design variables with iterations for Case 3 (SIMPLEX)

#### 4. Case 4

The change of the design variables with the Gradient Descent Active Set algorithm for Case 1 in different runs are given in Figure B10.



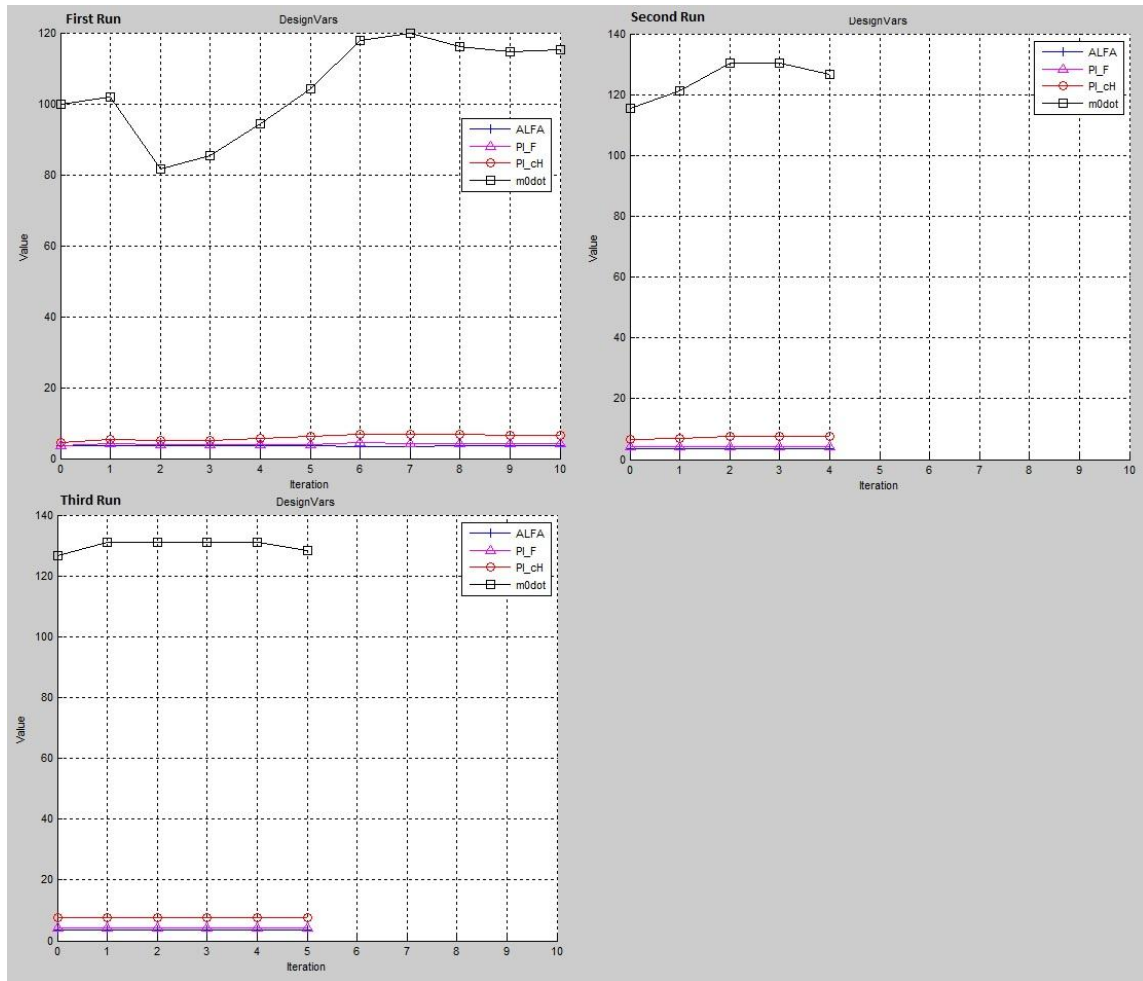


**Figure B 10** The change of design variables with iterations for Case 4 (Gradient Descent Active Set)

The change of the design variables with the Gradient Descent Trust Region Reflective algorithm for Case 1 in different runs are given in Figure B11.



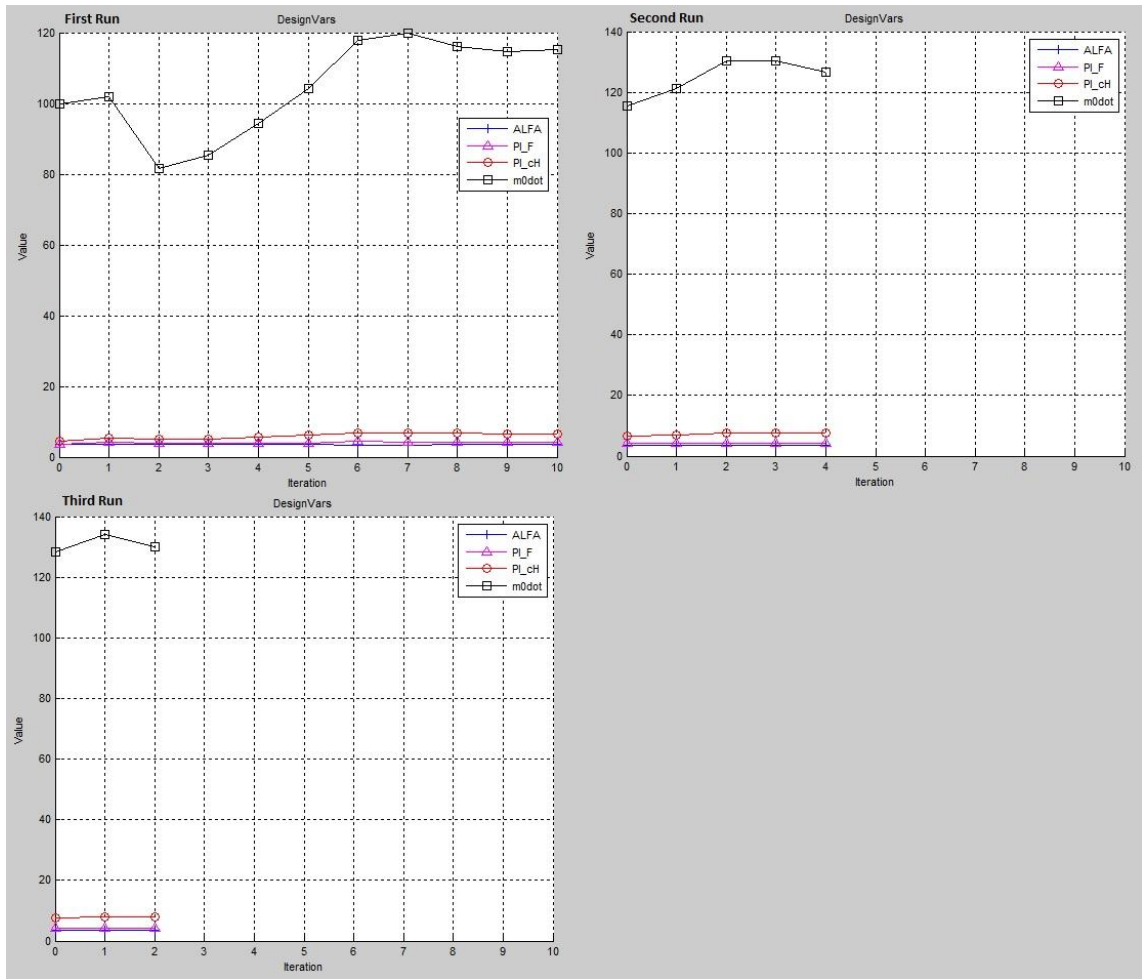


**Figure B 11** The change of design variables with iterations for Case 4 (Gradient Descent Trust Region Reflective)

The change of the design variables with the SIMPLEX algorithm for Case 1 in different runs are given in Figure B12.

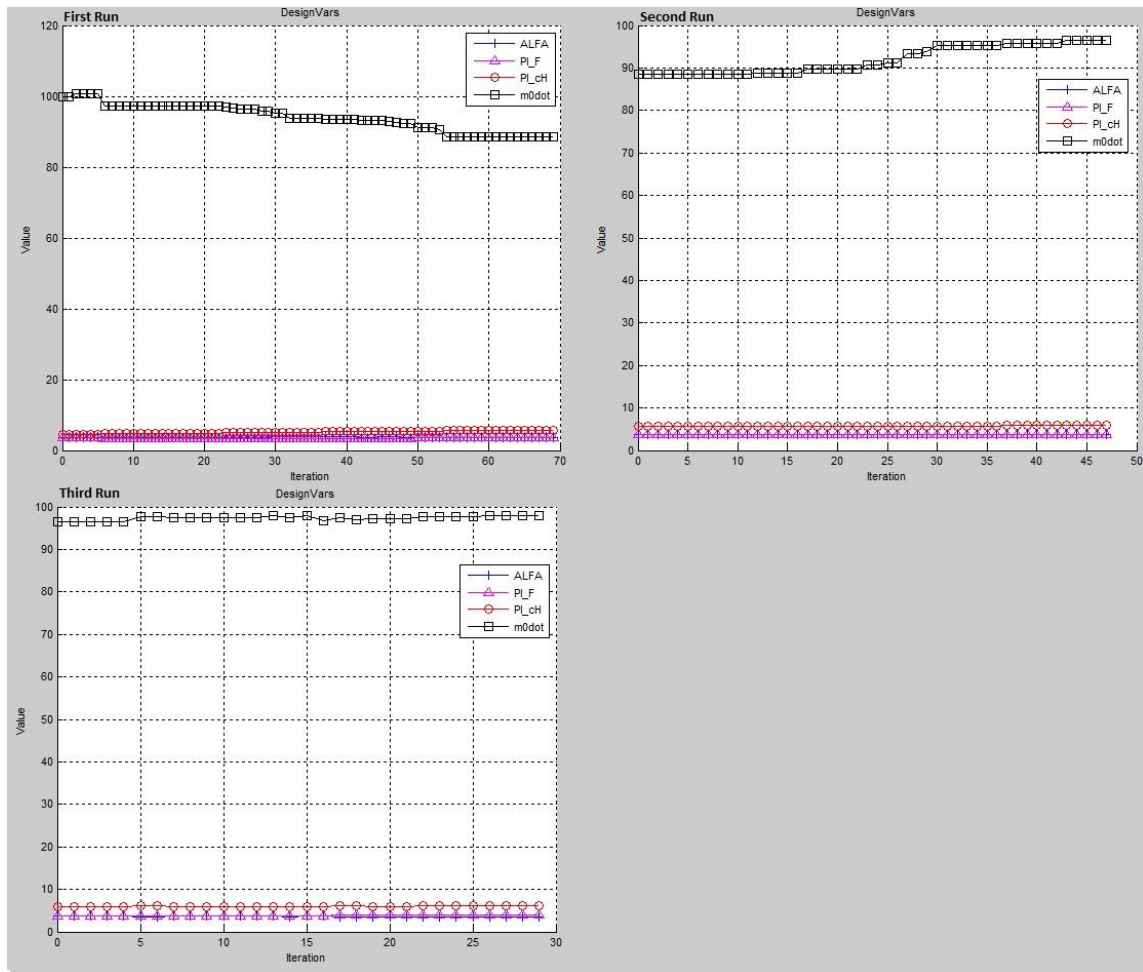


**Figure B 12** The change of design variables with iterations for Case 4 (SIMPLEX)